Effects of natural processes and human activity on North Sea sediment biogeochemistry

Emil De Borger
PhD Thesis

Emil De Borger

Effects of natural processes and human activity on North Sea sediment biogeochemistry

Promotors:

Prof. Dr. Karline Soetaert

Dr. Ulrike Braeckman

Ph.D. Thesis, Faculty of Sciences, Ghent University, Ghent, Belgium

TABLE OF CONTENTS

ABBREVIATIONS

AIC   : Akaike information criterion

BP_c : Community Bioturbation Potential

BPNS : Belgian Part of the North Sea

Chl *a* : Chlorophyll *a*

CoIA : Coinertia analysis

DCM : Deep chlorophyll maximum

DIC   : Dissolved inorganic carbon

DIN   : Dissolved inorganic nitrogen

DIP   : Dissolved inorganic phosphorus

DNRA : Dissimilatory nitrate reduction to ammonium

FDET : Fast (degrading) detritus

GLS   : Generalized least-squares (model)

IP_c : Community Irrigation Potential

MFA   : Multiple Factor Analysis

MGS : Median grainsize

OC   : Organic carbon

OM   : Organic matter

OPD   : Oxygen penetration depth

OWF   : Offshore windfarm

PCA   : Principle component analysis

PCO   : Principle coordinate analysis

POC   : Particulate organic carbon

SCOC : Sediment community oxygen consumption

SDET : Slow (degrading) detritus

SST   : Sea surface temperature

SWI   : Sediment-water interface

TOC   : Total organic carbon

Definitions

Advective flow : The transport of a substance or quantity by bulk motion. Pressure gradients on the sediment-water interface generate advective flows (of water) through the sediment.

Boundary conditions : A condition that is required to be satisfied at all or part of the boundary of a modelling domain in which a set of differential equations is to be solved. Concretely, they describe what happens to substances or other modelling units at the model boundaries.

Benthic-pelagic coupling : Those processes which connect the bottom substrate and the water column habitats through the exchange of mass and energy.

Benthos : The community of organisms living on, in, or near the bottom of fresh or salt water bodies.

Biogeochemistry : The study of the cycles of chemical elements that make up the composition of the natural environment, and the chemical, physical, geological, and biological processes and reactions that govern them.

Bioirrigation : The exchange of water between the porewater in sediments and the water column as a result of the activities of fauna inhabiting the sediment.

Bioturbation : The mixing and translocation of particles in the sediment matrix as a result of the activities of fauna inhabiting the sediment.

Boxcorer : A device used to sample sediments from the seafloor. This device uses gravity to push some type of container into the sediment, and a mechanism is in place that encloses the sediment volume in the container upon retraction out of the sediment. A boxcore in turn, is a sample taken with a boxcorer.

Coarsening : An increase in median grainsize of the upper sediment layers, or the introduction of hard substrates in an otherwise soft sediment matrix.

Denitrification : The microbially mediated mineralization of organic matter using nitrate (NO_3^-) as the oxidant, producing dinitrogen gas (N_2) in the process.

Diagenesis (early) : The sum total of biological, chemical, and physical processes that occur in the sediment matrix or in sedimentary rock, following the arrival of a particle at the sediment-water interface.

Diffusive transport : Transport of solutes driven by concentration gradients.

Domain (of a model) : Model equations are usually only valid within a set of spatial, temporal, or conceptual boundaries. This is the domain of a model.

Eutrophication : When an aquatic environment becomes enriched with nutrients and minerals, inducing excessive growth of algae (sediments become **eutrophied** as this escessive algae growth is deposited).

Fining : A decrease in median grainsize of the upper sediment layers.

Fluxes : In the context of biogeochemistry, a flux is the mass of a substance that crosses a surface (usually the sediment-water interface) per unit of time, and is expressed in units of $M\ L^{-2}\ T^{-1}$.

Incubation (of a sample) : Keeping an experimental unit in a controlled environment with the goal of collecting measurements, or following its evolution over time.

Mechanistic model : A model that represents a functional mimic of a system (e.g. organic matter mineralisation). In these models mathematical descriptions of real-life processes (e.g. nitrification, bioirrigation) are used to couple state variables (e.g. nitrate, organic detritus) to oneanother.

Mineralisation : The microbially mediated degradation (i.e. oxidation) of organic matter to inorganic nutrients.

Nitrification : The microbially mediated oxidation of ammonia to nitrite (NO_2^-) followed by the oxidation of the nitrite to nitrate (NO_3^-).

Permeability : The capacity of a sediment matrix to transmit a fluid.

Porewater : Water contained within the pores of a sediment matrix.

Porosity : The volume of pore-space relative to the bulk sediment volume.

Shelf sea : (The part of) a sea or ocean that is on the continental shelf.

State variable : Variables whose behaviour is described by a (set of) model equation(s). E.g. concentrations of nutrients or population sizes.

Tortuosity : The mean additional distance that solutes travel from point to point in a sediment matrix because of the shape and size of sediment grains.

Trait (biological) : Characteristics or features exhibited by an organism (e.g. eye color, fecundity, feeding stategy).

Chapter 1.   GENERAL INTRODUCTION

1.1.   Benthic-pelagic coupling in the North Sea

1.1.1.   The North Sea

1.1.1.1. Bathymetry and circulation

The North sea is a shallow shelf sea with a total area of 575 000 km^2. The bathymetry can be summarized by two depth gradients. The first is a S – N gradient of increasing depth, with shallow waters in the South (~ 40 m) making way for deeper waters in the north (> 80 m). With the exception of the Norwegian trench (725 m), depths do not exceed 250 m. A second gradient from E – W mostly shows deepest waters in the center, except for the Dogger Bank, a feature in the middle of the North Sea where depths decrease again to 10 m (Fig. 1-1).
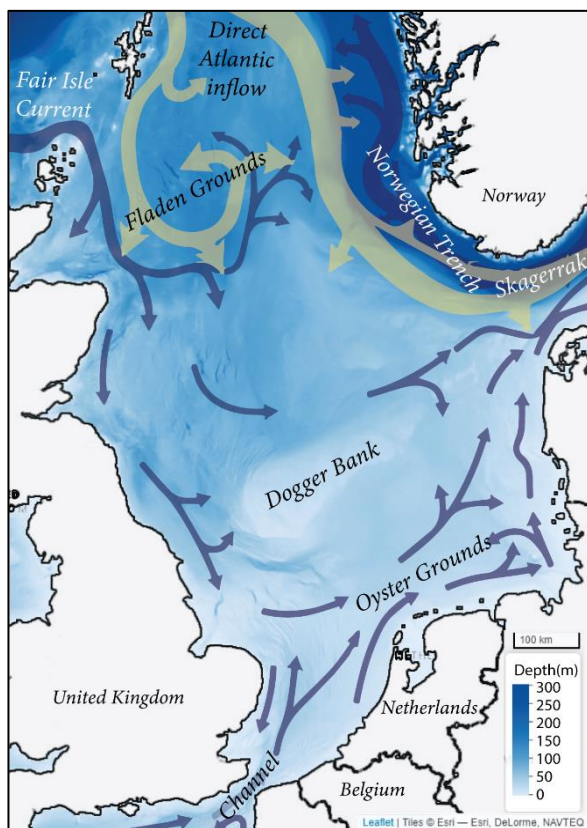
Fig. 1-1: Bathymetry and main water circulation pattern in the North Sea (arrows). Yellow arrows indicate the direct inflow of Atlantic water, as opposed to coastal currents (blue). Width of the arrows indicates relative volume transported. Figure adapted from Quante et al. (2016).

The North Sea is characterized by a strong connection to the Atlantic ocean, and continental riverine inputs. The dominant current pattern in the North Sea is an anti-clockwise circulation, in which Atlantic water enters from the Fair Isle Current, through the Channel, and exits along the deep Norwegian Trench. Water from the Baltic enters the North Sea through the Skagerrak. Very little inflow from the northern connection with the Atlantic reaches areas south of the Dogger Bank, and this feature thus effectively divides the North Sea in a southern and a northern part (Fig. 1-1) (Thomas et al., 2005). The combination of strong tidal currents, and shallow bathymetry makes the water column of the southern North Sea generally well mixed, but thermal stratification during the summer months, and haline stratification due to riverine freshwater inputs takes place in more central areas and coastal regions respectively (van Leeuwen et al., 2015). In the deeper northern North Sea, stratification occurs from mid-April until autumn (van Leeuwen et al., 2015).
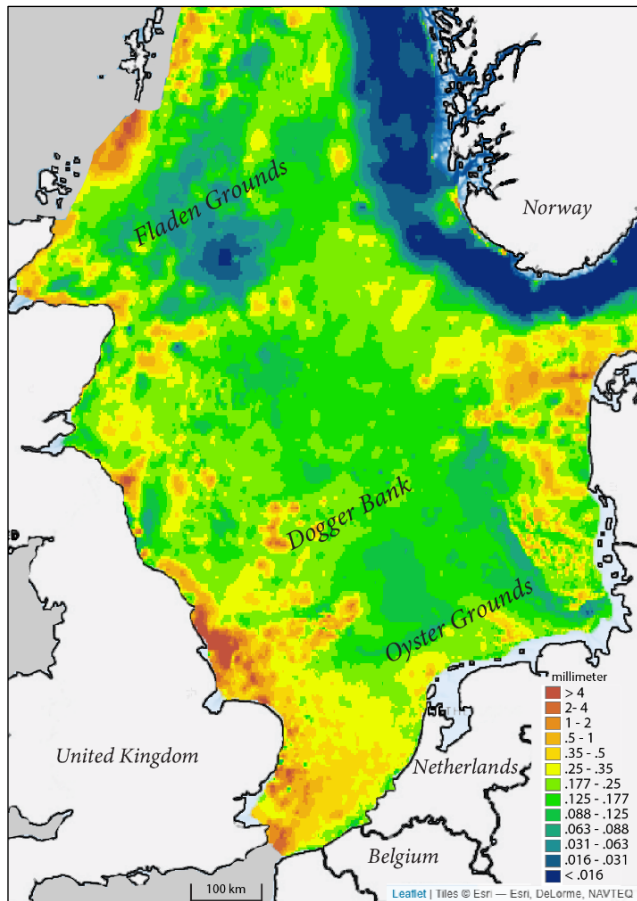
Fig. 1-2: Median grainsize of sediments in the North Sea (in mm). Grainsize raster © Helmholtz-Zentrum Geesthacht.

1.1.1.2. Seafloor physico-chemical characteristics

The bottom of the North Sea is dominated by soft sediments, with the majority consisting of medium to coarse sands (Fig. 1-2). Bathymetry and hydrodynamics are determining factors in sediment sorting (Bockelmann et al., 2018). Strong bed shear stress in the shallow waters of the Strait of Dover leave behind coarse sands or larger materials, and keep finer sediments in suspension, to be sequentially transported along the eastern border further northward, where the remainder is eventually deposited in the deep of the Skagerrak (Eisma and Kalf, 1987). Deposition of these finer materials also takes place in areas of reduced current speed, such as the Oyster Grounds, and the Fladen Grounds more to the west (Eisma and Kalf, 1987; De Haas et al., 1997). These variations in sediment sorting lead to predictable patterns of grainsize-derived properties: sediment porosity, and permeability. The sediment porosity, a measure of the amount of pore space (voids in between sediment grains, filled with pore water) present in stacked grains, is inversely related to the median grain size (Wilson et al., 2018). Permeability on the other hand, the capacity of sediment to transmit a fluid, increases directly with increasing median grain size, and with decreasing silt content (particles < 63 µm; Wilson et al., 2018). In coarse grained, permeable sediments the pore spaces are well connected, which allows porewater to move freely. When the silt content increases, sediment grains cohere more to each other (= cohesive sediments), and porewater moves slower. As a result of this, the gradient from coarse grained sediments (e.g. Southern North Sea) to silty sediments (e.g. Oyster Grounds, Fladen Grounds, Norwegian Trench - Skaggerak) also represents a gradient of increasing porosity, and decreasing permeability (Wilson et al., 2018).

1.1.2. Organic matter production

In biological systems, the conversion of inorganic carbon to organic matter (OM) occurs during primary production. In the marine realm, primary production is predominantly performed by photosynthetic algae: phytoplankton. These organisms live in the euphotic zone (i.e. where there is light) of the water column, and use light energy and free carbon and other nutrients to build biomass. In the North Sea, the main phytoplankton bloom occurs in April – May, and is strongest in the nutrient rich, well mixed waters of the southern North Sea, and along the eastern boundary (Fig. 1-1). Where waters are stratified

in summer, deep chlorophyll maxima (DCM) form near the thermocline if nutrients are still available. In areas with a long-lasting DCM, this secondary primary productivity can represent up to 37% of net annual primary production (Richardson, 2000; Weston et al., 2005). The first autumn storms mix the waters again and a second, smaller algae bloom forms in the northern areas of the North Sea. While this bimodal pattern was present also in the southern regions, it has largely disappeared since the mid-1980's. The combined effects of increasing sea surface temperature (SST), and the decrease in terrestrial nutrient inputs lead to relatively high chl *a* concentrations instead persisting longer throughout the growing season (Raitsos et al., 2014; Nohe, 2019).

The organic matter is predominantly deposited in the vicinity of the sites where it is produced, but it is also transported through successive deposition-resuspension events (transient deposition, Van Raaphorst et al. (1998)). The dominant counter-clockwise residual currents transport fine-grained, organic matter rich material from the Southern Bight along the eastern boundaries, towards the Skagerrak. As a consequence, the lability or "freshness" of deposited organic matter decreases towards the site of final deposition, the Skagerrak, relative to the initial production site, the Southern Bight of the North Sea (Dauwe and Middelburg, 1998). Organic matter sorbs to the sediment surface, and smaller particles have a larger surface area for a given bulk volume. Additionally, the tight geometry of pore spaces in silt or clay effectively keeps the OM in place (Mayer, 1994). In contrast, OM in permeable sediments can be transported with the currents that flow through the grains. A further consequence of the transient deposition is that older, more refractory organic matter makes up the bulk of the carbon pool in most sediments, with fresh organic matter predominantly present in the sediment surface layers (Boudreau and Ruddick, 1991; Dauwe and Middelburg, 1998).

1.1.3.   Early diagenesis

Once organic matter settles on the sediment, temporarily or permanently, itself and its byproducts will be transformed by a set of biological, chemical, and physical processes collected under the term "diagenesis" (Fig. 1-3). When the transformations of organic matter in the upper layers of the sediment are described (centimeters – meter scale), the term *early* diagenesis is used (Boudreau, 2000). Organic matter is degraded (= mineralized) to CO_2 and other inorganic compounds through a set of microbially mediated oxidation-reduction reactions, starting with the oxidant (= electron acceptor) which yields the highest free energy (i.e. is the most efficient). When this oxidant is consumed, oxidation of the remaining OM will continue with the next most efficient oxidant available, and so on until either all oxidants are consumed, or the organic matter has been fully oxidized to CO_2 (Froelich et al., 1979; Soetaert et al., 1996a). This principle results in a well-defined sequence of reactions, which can be identified by a zonation of reactants in sediment porewater profiles (Fig. 1-3). The primary electron acceptor is oxygen (O_2), and the associated mineralization process that consumes it is called oxic mineralization or aerobic respiration. Nitrate (NO_3^-) and nitrite (NO_2^-) are the electron acceptors in the nitrate reduction process, known as denitrification. Oxidation reactions with other electron acceptors (MnO_2, FeOOH, SO_4^{2-}, CO_2) can be aggregated with the term anoxic mineralization, entailing manganese, iron and sulfate reduction and finally fermentation (Soetaert et al., 1996a). Early diagenesis in sediments can thus be seen as the
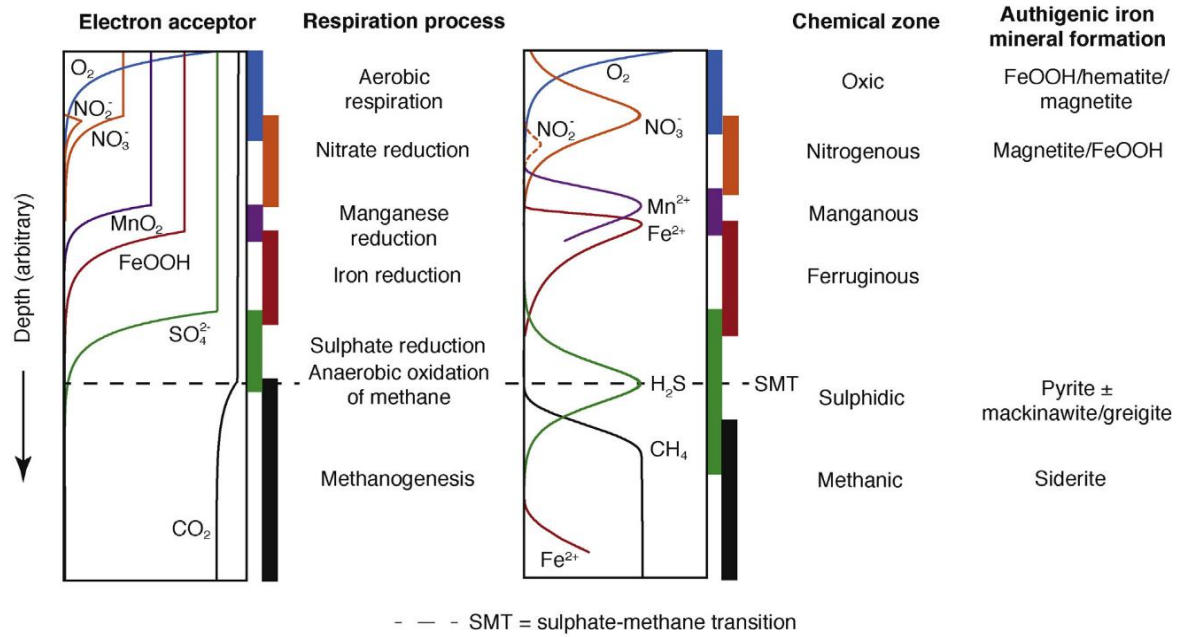
Fig. 1-3: An idealized representation of the distribution of biogeochemical reaction processes in the sediment (Adapted from Canfield and Thamdrup, 2009).

recycling mechanism that converts fixed organic matter back to free nutrients, available to be taken up by processes in the water column. This benthic-pelagic coupling (pelagic = the water column) is of great importance to the carrying capacity in shallow coastal seas, where primary production is strongly dependent on the amount of regenerated nutrients in the sediment (Soetaert and Middelburg, 2009; Provoost et al., 2013).

1.1.3.1. Porewater transport

In the early diagenesis scenario described above, depth in the sediment can be seen as a measure of time since deposition (Berner 1980). However, such a neat vertical succession of oxidation processes (Fig. 1-3) is usually reserved for little disturbed, muddy sediments of the deep sea (Soetaert et al., 1996a), and it is less clear-cut in more dynamic sediments of, for example, the North Sea. Different transport mechanisms, both of physical and biological origin, can strongly impact the zonation of diagenetic reactions. Due to the high permeability of sandy sediments, even small pressure gradients at the sediment-water interface (SWI) drive porewater flows through the interstitial space (= advective flows). In permeable sediments these advective flows can
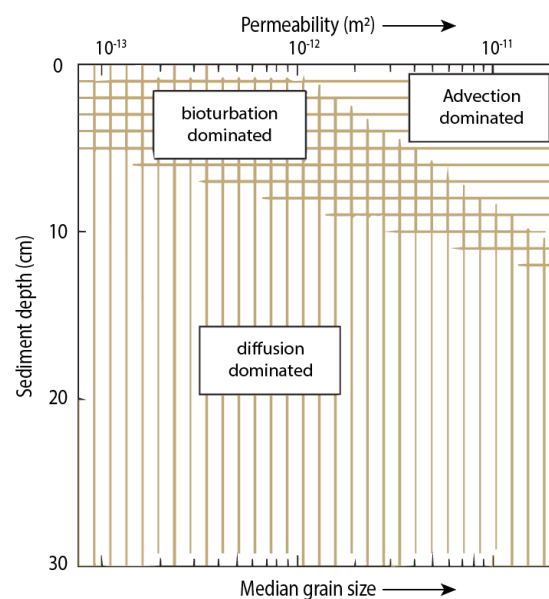
Fig. 1-4: The permeability spectrum. From diffusion, to advection dominated sediments (Huettel and Gust, 1992).

penetrate deep into the sediment (decimeters), and porewater is rapidly exchanged with the water column. This part of the permeability spectrum is characterized as advection dominated (Fig. 1-4). Pore spaces in cohesive sediments are smaller, and advective flows penetrate less deep (mm – cm) or even not at all. Here, porewater transport is dominated by molecular diffusion, based on concentration gradients (Fig. 1-4; Huettel and Gust, 1992). Many benthic organisms (fauna living on or in the sediment) also contribute to porewater transport through bioirrigation: they passively or actively exchange sediment porewater with the overlying water column as a result of burrowing, pumping, ventilation and feeding activities (Kristensen et al., 2012). Bioirrigation enables sediment dwelling organisms to forage and live in the otherwise anoxic deeper sediment layers (Olaffson, 2003; Braeckman et al., 2011). As a result, bioirrigation plays an important role in aquatic sediment biogeochemistry (see section 1.1.4).

1.1.3.2. Particle transport

Benthic organisms also redistribute the particles in the sediment matrix itself through bioturbation activities: burrow construction and maintenance, ingestion and defecation of substratum, or movement through the sediment (Kristensen et al., 2012). During these activities, detritus and microorganisms are displaced vertically and laterally within the sediment matrix. Functionally, the reworking modes of benthos are classified as downward conveyors, upward conveyors, biodiffusors, and regenerators (François et al., 1997). Up- and downward conveyors are vertically oriented organisms which ingest sediment in deeper layers, or near the sediment surface respectively, and expel this material at the opposite end. Biodiffusors randomly mix sediment over short distances, usually through body movements. Regenerators dig up sediment from deeper layers, and transport it to the surface (François et al., 1997).

1.1.4. Faunal controls on early diagenesis

Faunal activities exert strong controls on the cycles of different nutrients. The microbial respiration rate of organic matter is a function of the quantity and reactivity of the deposited organic matter (see LaRowe et al. (2020) for an extensive overview of factors affecting reactivity). Additionally the availability of different reactants determines the sequence of degradation processes through which degradation occurs in the sediment. In turn, these concentrations are affected by the benthos mediated transport regime (Aller and Aller, 1998; Vasquez-Cardenas et al., 2016). Organisms bring partially reduced, refractory organic matter to oxygen rich areas near the sediment surface (bioturbation), and conversely pump oxygen, and nitrate rich water into reduced environments (Fig. 1-5). This increased exposure to oxidants allows for increased mineralization rates, as well as the reoxidation of reduced
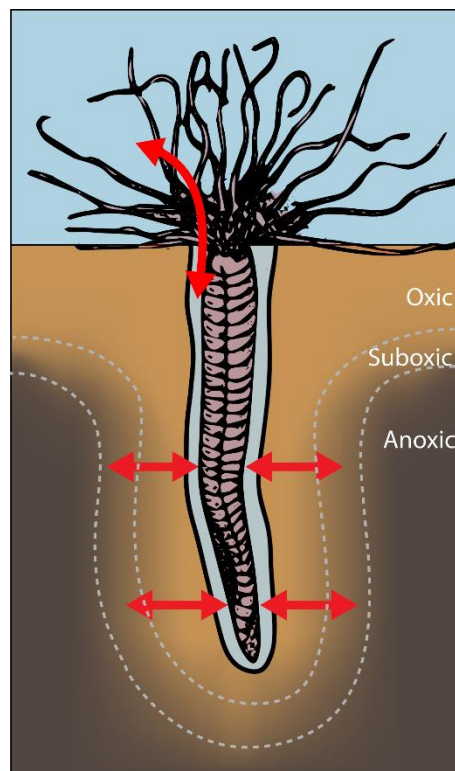
Fig. 1-5: The effect of bioirrigation on the sediment surrounding an organismal burrow. Red arrows show the exchange of solutes between the water column, and the sediment. © Emil De Borger

substances to take place well below the sediment-water interface (Aller and Aller, 1998; Kristensen, 2001).

Faunal activities affect the nitrogen cycle in different ways. Denitrification is one of the most important nitrogen sinks in coastal environments, and is of societal relevance in nitrogen - eutrophied waters with an overabundance of ammonium and nitrate. Denitrification encompasses the reduction of nitrate (NO_3^-) to dinitrogen gas (N_2), which is mostly biologically unavailable and diffuses to the atmosphere (Galloway et al., 2004; Seitzinger et al., 2006). In marine sediments, this process is carried out by facultative anaerobic bacteria. Since denitrification is inhibited by oxygen, it is confined to sediments where the aerobic degradation of organic matter has consumed most of the oxygen. Nitrate is supplied from the overlying water, and through sedimentary nitrification, the microbially mediated oxidation of NH_4^+ to NO_3^- coupled to oxygen consumption. This coupled nitrification-denitrification thus occurs when oxic and suboxic zones occur in close proximity (spatially or temporally) in sediments (Seitzinger, 1988; Galloway et al., 2004), often a consequence of the burrowing or ventilation activities of many organisms (Fig. 1-5; Huettel, 1990; Nielsen et al., 2004; Polerecky et al., 2006; D'Andrea and DeWitt, 2009; Dornhoffer et al., 2015). Alternatively, the majority of nitrate produced by nitrification can diffuse to the overlying water column when ambient nitrate concentrations are low.

Besides the carbon and nitrogen cycles, bioturbation and bioirrigation exhibit strong controls on the redox state of substances such as iron (Fe), which in turn affects the phosphorus (P) and sulphur (S) cycles. Phosphorus, like nitrogen, is one of the nutrients limiting primary production in aquatic systems. Human activity has roughly quadrupled the input of phosphorus to the marine realm, predominantly in the form of wastewater discharge, detergents, and fertilizers, relative to the natural production of P through weathering of rock (Harrison et al., 2010). As such, excessive inputs of P, but also N (Billen et al., 2005; Lenhart et al., 2010) have for decades altered primary productivity patterns and subsequent mineralization in coastal waters (Desmit et al., 2019; Nohe et al., 2020).

In oxic conditions iron is present in the sediment in an oxidized form (Fe^{3+}), which forms iron (oxyhydr)oxides, or can bind to free phosphate (PO_4^{3-}) to form (quasi-)stable forms of iron-bound phosphorus (Fe-P, vivianite). When brought in anoxic sediment (e.g. through downward bioturbation) the iron (oxyhydr)oxides are reduced (Fe^{2+}), releasing phosphate in the process (Isaev et al., 2017; Norkko et al., 2012). In what is called "sink switching" (Ruttenberg and Berner, 1993), phosphate can further precipitate with calcium ions to Ca-P minerals (apatite), and together with Fe-P, this authigenic Ca-P is the main phosphorus sink in marine sediments (Slomp, 2011).

This Fe^{3+} - Fe^{2+} redox shuttle also affects the sulphur cycle. Fe-oxides may be used to oxidize H_2S to SO_4^{2-} in deeper sediment layers, again producing reduced iron (Fe^{2+}). This can be transported upward again through diffusion or faunal activity, or alternatively precipitate with H_2S to iron sulphides FeS (Vasquez-Cardenas et al., 2016; van de Velde and Meysman, 2016). In turn, sulfate reduction thus exerts a control on the P-cycle, as produced sulfides may reductively dissolve Fe-oxides and release associated P. For example, because of the dominance of sulfate reduction in organic matter mineralization in some sediments, and subsequent scavenging of most dissolved Fe2+ in porewaters by produced sulfides, Fe2+
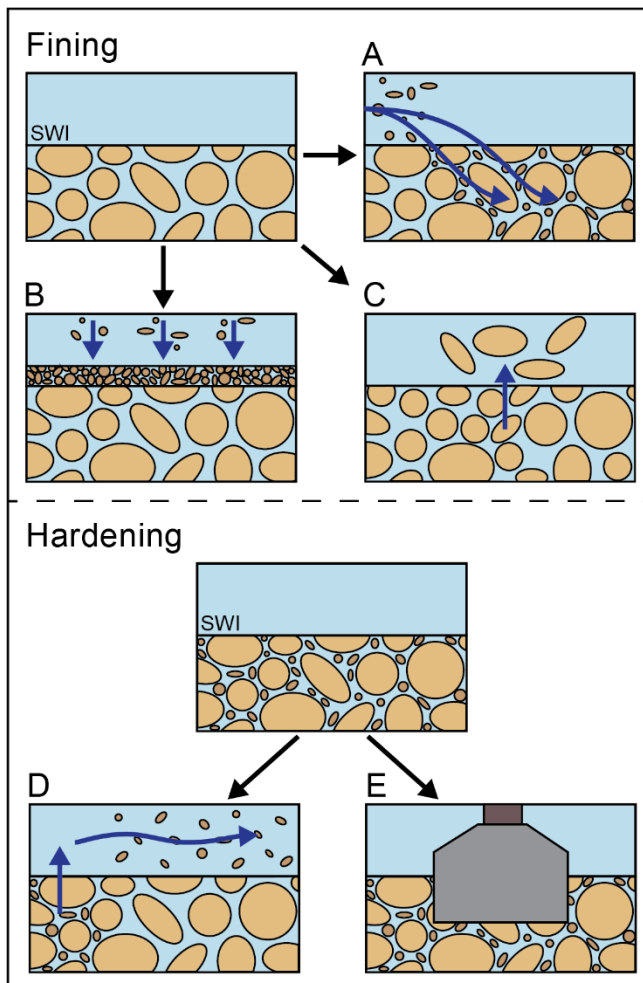
Fig. 1-6: Mechanisms of fining (top) and hardening (bottom). (A) entrainment of fine sediment in the sediment matrix; (B) deposition of fines on the sediment surface; (C) Removal of intermediate grainsize by dredging; (D) removal of resuspended fines after a disturbance event; (E) placement of hard structures in, or on the sediment matrix.

available for the formation of vivianite only after all sulfate has been converted to Fe sulfides (Slomp, 2011).

1.2. Natural and anthropogenic changes to sediments.

1.2.1. Sedimentary dynamics

Sediments of dynamic coastal areas are in constant motion. Tidal energy, residual currents, wave-energy, and sediment characteristics all contribute to the resuspension, transport, and redeposition of sediment in a given location (Cataño-Lopera and García, 2006; Stide, 1982). It is this interplay that generates phenomena such as longshore drift, sand- or mudbanks, or migrating bedforms (sand ripples to waves) (Elliott et al., 1998; Holland and Elmore, 2008; Stide, 1982). So although the dominant grainsize class is generally constant over decadal timescales, natural processes generate continuous dynamism in the surface sediments. This dynamism sustains a range of habitats, as sediment characteristics, and linked to it the distribution of organic matter may differ over relatively small spatial scales (10's – 100's of meters). Sandwaves for example, are bedform structures that form in shallow, sandy coastal regions dominated by tidal energy . Individual waves of 100 to 1000 m in length, and up to 10 m high, may be classified in zones with differing sediment characteristics (through, slope, crest), with separate species adapted to the conditions in each zone (Baptist et al., 2006; Cheng et al., 2020; Degraer et al., 2003). All while the sandwaves themselves move up to several meters per year (Besio et al., 2004; Németh et al., 2002).

1.2.2. Fining and coarsening

Multiple pressures cause sediment fining, and sediment coarsening in the North Sea (see **2.2.**). Sediment fining is the decrease in median grain size of (surface) sediments. The dominant mechanisms of sediment fining are the entrainment of an elevated concentration of suspended fine particles ("fines") into a coarser seabed sediment layer (Fig. 1-6 A), while also a layer of fines can be deposited on top of the sediment matrix that may subsequently be incorporated in the sediment, for example by bioturbation (Fig. 1-6 B). Water column suspended particulate matter (SPM) concentrations become

elevated during storm events. 'Storminess' in general is an important contributor to bed shear stress throughout the North Sea (Stanev et al., 2009), and in nearshore areas with finer sediments, SPM concentrations near the bottom have been seen to double or triple during storms of regular intensity (Fettweis et al., 2010; Green et al., 1995). Lastly, sand extraction industry targets intermediate sediment classes, resulting in the removal of this class, and a finer sediment matrix as a result (Fig. 1-6 C). Sediment coarsening is the opposite process: the increase in median grain size of surface sediments. This occurs when fine sediments are resuspended during a disturbance event (Fig. 1-6 D). Coarsening also includes all activities which introduce temporary or permanent hard structures on, or into an otherwise mobile sediment layer (Fig. 1-6 E). Sediment fining of sufficient magnitude provokes a decrease in permeability, and may thus induce a shift from advection-dominated to diffusion-dominated habitats (Fig. 1-4). This shift affects sediment biogeochemistry twofold: firstly the entrainment of fines increases the available surface area for OM to bind to, hence, the amount of organic carbon available for mineralization, which may induce intense bacterial activity in sediments and increase the demand for oxygen (Huettel and Rusch, 2000; Navel et al., 2012). As advective flows can increase solute exchange 20 – 50 times relative to diffusive transport (Huettel et al., 2003a; Precht and Huettel, 2003), solute exchange between the sediment and the water column will decrease as advection lowers. In permeable sediments, advective flows provide ample dissolved oxygen for rapid organic matter mineralization (Ehrenhauss et al., 2004a), and rapidly remove the metabolites, while in more diffusion dominated sediments, the solute exchange is lower and metabolites and solutes build up in the sediment matrix. As the availability of oxygen in diffusion-dominated sediments decreases with respect to the presence of other electron acceptors, the proportion of anaerobic mineralization increases (Volkenborn et al., 2007; Cardenas et al., 2008; van de Velde and Meysman, 2016).

Sediment coarsening brings an additional variety of changes, which are explained below within the context of anthropogenic activity.

1.2.3. Multiple anthropogenic pressures

1.2.3.1. Trawling activities

Commercial bottom trawling activities increase suspended particulate matter (SPM) concentrations in the water column through direct or turbulence-mediated agitation of the upper centimeters of the seafloor with towed fishing gears (Palanques et al., 2001; O'Neill and Summerbell, 2011; Depestele et al., 2016; Mengual et al., 2019). With recent estimates of annual bottom trawling intensities between 1 – 10 trawls y^{-1} in large parts of the North Sea (Eigaard et al., 2017), this is a major contributor to sediment resuspension for these waters (Rijnsdorp et al., 2020a). A shift towards sediment fining has also been described in certain trawled areas, with expected consequences for sediment biogeochemistry, such as an increased rate of sulphate reduction (Trimmer et al., 2005). Interestingly, sediment resuspension may also cause coarsening (Depestele et al., 2019; Mengual et al., 2019; Tiano et al., 2019). In these cases resuspended silt is exported away from the trawling site, leaving a coarsened trawling track.

1.2.3.2. Sand extraction and dredging

Sand extraction activities physically disturb the sediment with the draghead, the vacuum-like apparatus that sucks sediment aboard the dredging vessel, where the targeted grain size is selected. The finest sediments (< 125 µm) are often not targeted and are thus discarded, since they have little industrial applications (Laxton, 1992). This results in an increased fraction of very fine sands and silt in areas of sand extraction (De Backer et al., 2014). Secondly, overflow tanks on the vessels discard excess material of coarser and finer particles as plumes into the water column (Todd et al., 2014). Increased suspended fines concentrations do not only have local effects: currents can distribute them to other areas where deposition is possible, or they can be kept in suspension for longer periods (Le Bot et al., 2010; Robinson et al., 2005). This transport over longer distances has been observed in cases of sand extraction, but also when dredged material is dumped (Fettweis et al., 2011).

1.2.3.3. Offshore wind construction

Offshore windfarm construction is rapidly accelerating. The North Sea currently holds wind turbines with a production capacity of 18.5 GW, and by 2030 this is expected to rise to 60 - 70 GW in order to meet the EU's 30 % of renewable energy target (Nghiem and Pineda, 2017; Selot et al., 2019; European Commission, 2020a). An offshore windfarm (OWF) is a collection of grouped wind turbines, and the associated network of power cables, placed onto submerged substrates in the marine environment. Given the unique nature, novelty, and scale of these developments, many of the effects OWFs have on their environment are only just becoming clear to scientists and policy makers. In addition, construction methods are evolving rapidly, allowing a shift of OWF construction from shallow areas to deeper stratified waters in the coming years, which is likely to affect the surroundings differently (Ramirez et al., 2020).

During the construction of OWFs, sediments are resuspended, as this involves preparatory work on the seabed supported by dredging vessels, and the placement of the turbine base itself, with a jack-up vessel. During the operational phase sediment plumes can be seen in the wake of the turbines under certain hydrodynamic conditions ("turbid wake plumes", Baeye and Fettweis, 2015). The presence of a wind turbine in the water column locally alters hydrodynamics, reducing current speeds within its wake (Rivier et al., 2016; Legrand et al., 2018), which is one mechanism by which wind turbines increase fine sediment deposition. These turbulent effects further redistribute suspended particles in the water column nearer to the surface, forming a wake plume (Forster, 2018). It is yet unknown whether the large biomass of filter feeding organisms on the turbine and the erosion protection layer around it contributes to this plume by producing aggregates of suspended materials (faecal pellets and pseodofaeces). However, it is known that these settle locally and as such cause sediment fining (Baeye and Fettweis, 2015). These are currently the leading hypotheses used to explain the observed decrease of grain size, and organic enrichment found near wind turbines (Coates et al., 2014; De Backer et al., 2014).

1.3.   Measuring biogeochemistry

Through direct changes of the sediment structure, the species community, or ambient nutrient concentrations, anthropogenic activities affect the biogeochemistry of aquatic sediments. To study these changes, a variety of techniques is used. Below is a discussion of common methods that are used in the field of sediment biogeochemistry, limited to those used in this thesis.

1.3.1.   Sample collection

The first step to studying aquatic sediment biogeochemistry is often collecting samples, in which the various mineralization processes and the influencing faunal activities can be deduced. To sample sediments in submerged locations, usually a shipboard sampling device is used, such as a multi-corer, or a boxcorer (Flanders Marine Institute, 2020), which is lowered to the seafloor to retrieve a sediment sample (Fig. 1-7 A). These devices use gravity to push some type of container into the sediment, and a mechanism is in place that encloses the sediment volume in the container upon retraction out of the sediment. Ideally, this delivers a relatively undisturbed sediment sample back on deck of the sampling vessel, so that the redox zonation and locations of organisms in the sediment, can be assumed to be the same as they were on the seafloor. In reality, there is usually some disturbance of the surface during impact of the sampling device. Analogous to geological studies, where coring devices are used to collect samples that are often meters in length, samples in cylindrical containers are called "cores". In locations
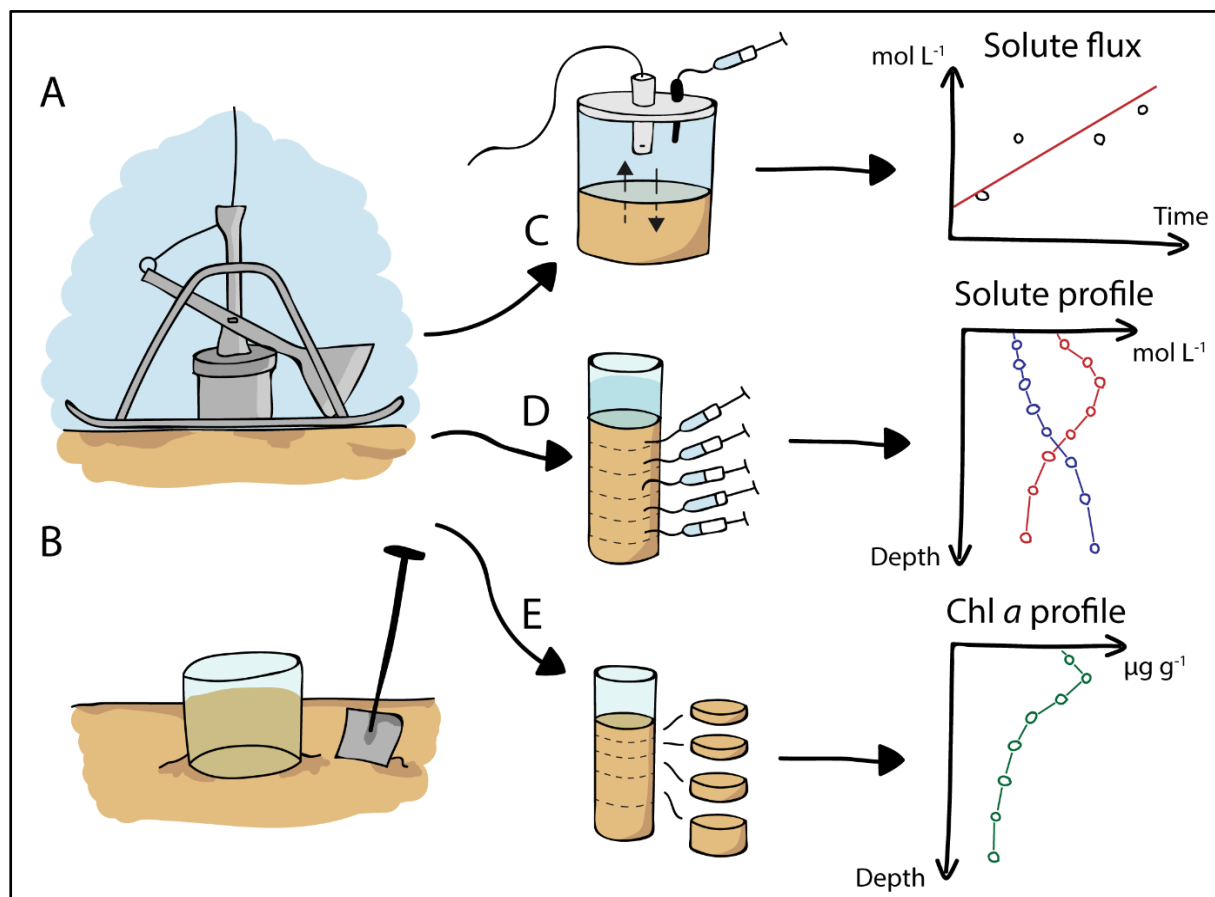
Fig. 1-7: Samples taken with shipboard instruments (A), or on intertidal sites (B). Samples subsequently used to determine (C) solute fluxes, (D) solute profiles, or (E) chl a profiles. © Emil De Borger

accessible by foot, such as intertidal mudflats, sediment can be collected by pushing sampling cores into the sediment by hand, and digging these out carefully with a shovel (e.g., Mestdagh et al., 2018; De Borger et al., 2020; Fig. 1-7 B).

Once a sediment sample is obtained, subsamples ("subcores") of several shapes and sizes may be taken to study different aspects of the sediment ecosystem. Depending on the goal of the study, core incubations are performed (Fig. 1-7 C), or pore water or solids (e.g. chl *a*, grain size distribution) are extracted from the sediment to establish depth profiles (Fig. 1-7 D-E).

1.3.2. Nutrient cycling

In the best-case scenario, in-situ measurements are performed on the seafloor. In the North Sea however, this is often logistically impossible, and then ex situ measurements are a more flexible way to cover larger study areas. Core incubations are used to estimate the exchange rates of solutes (nutrients and tracer substances) across the sediment water interface (i.e. the fluxes). During incubations, sediment cores are kept in a buffer tank (either in a laboratory, or aboard a vessel) to prevent temperature fluctuations, which affect mineralization process rates and faunal metabolism (Brey, 2010; Klump and Martens, 1989). Changes in solute concentrations are measured in the water column overlying the sediments. To attain representative water column samples, the water column overlying the incubated sediment is also mixed using a stirrer. During the incubation, concentrations of solutes of interest are monitored for a given time period, either by taking water samples in discrete intervals, or in the case of oxygen or uranine (a tracer for irrigation, see 1.3.3), with a continuous logging device that measures concentrations in the overlying water directly. For oxygen consumption measurements, the cores need to be closed airtight, to prevent replenishment of oxygen in the water column. Assuming that production or consumption of the substances in the overlying water is negligible, the changes induced are ascribed to uptake or release through the sediment-water interface. Thus, a linear regression is fitted through the sampled concentrations over time, and multiplied with the height of the overlying water to retrieve a flux in units of mass per surface area, per unit of time (Fig. 1-7 C). From fluxes, valuable information about nutrient cycling can be derived. The oxygen demand of the sediment may be compared to the amount of dissolved inorganic carbon (DIC, the sum of CO_2, HCO_3^-, and CO_3^{2-}, the end-product of organic matter mineralization) produced, often by expressing DIC over O_2 consumption as a ratio (the respiratory quotient RQ; Brenner et al., 2016; Therkildsen and Lomstein, 1993). This can indicate the relative importance of oxic and anoxic mineralization processes, the composition of the degraded material, or point to addition processes such as calcite formation in which CO_2 is immobilized as $CaCO_3$ (Paulmier et al., 2009). Influx and efflux rates of nitrogen and phosphorus can inform about whether sediments are a source, or a sink for certain nutrients (whether or not the nutrient is recycled to a form available to consumers in the ecosystem; Nedwell et al., 1994; van Raaphorst et al., 1992; Rao et al., 2016).

Other subcores (usually with smaller diameter) are used to examine profiles of nutrients in the porewater (Fig. 1-7 D), or of solids in the sediment (such as chl *a*, organic carbon, or solid forms of phosphorus; Fig. 1-7 E). Porewater nutrients can be extracted from the sediment by slicing the sediment core into layers of a certain thickness, and subsequently extracting the porewater from each slice through centrifugation (Clavero et al., 1991; Lohse et al., 1995; Van De Velde et al., 2018). Alternatively, the

porewater may be extracted with the use of rhizon samplers; small tubes with microscopic pores that extract porewater through capillary force, and suction applied with a syringe (Seeberg-Elverfeldt et al., 2005; Shotbolt, 2010). Both methods have advantages and disadvantages: whereas slicing makes it possible to generate profiles of a higher resolution (5 mm in slicing, 10 mm with rhizons), the possibility of experimentally altering the porewater structure in the sediment is larger. The main disadvantage of the rhizon method is the fragility of the rhizons themselves, but it causes less disturbance to the sediment, and requires less processing steps (Shotbolt, 2010). Based on the nutrient profiles, the stock of nutrients in the sediment can be calculated (Magni and Montani, 2006; Legge et al., 2020), and the importance of different biogeochemical processes can be derived from (relative) concentrations of nutrients (Rao et al., 2016; Berg et al., 2003; Lohse et al., 1995; Navel et al., 2012).

1.3.3. Faunal activities

Incubation studies are equally useful to study organismal behaviours, such as bioturbation and bioirrigation. Bioirrigation is measured using a tracer substance, that is preferably chemically inert (e.g., Br⁻) and added to the overlying water in the core (a 'spike'). Additionally, it is important that the tracer is distributed equally through the water column to prevent a density gradient from forming. Similar to nutrient fluxes, the concentration of the tracer in the water is followed over time, and the "irrigation flux" is determined through linear regression. Though useful to compare experimental replicates, this method is sensitive to the height of the incubated sediment, and the timeframe over which the incubation took place (See De Borger et al., 2020, **Chapter 6**). For a time-independent rate, it is more accurate to analyse a concentration time series using a mechanistic model which mimics the continuous exchange of 'spiked' overlying water with 'clean' porewater, until both are in equilibrium. For this, a fluorescent tracer such as uranine may be used, which can be measured continuously with a spectrofluorometer (Na et al., 2008; De Borger et al., 2020).

Bioturbation rates can be derived from sediment depth profiles of chl *a*, generated by slicing a sediment core into subsections (Fig. 1-7 E), or of small (chemically inert) fluorescent particles (luminophores) which are added experimentally on the sediment surface. The idea is that organisms distribute new particles added to the sediment surface throughout the sediment matrix, as a result of their movements, and burrowing and feeding activities. These depth profiles can then be modelled with either a diffusive or a non-local biodiffusion model, to derive a biodiffusion coefficient that quantifies the intensity of mixing. A model is called 'non-local', when –in addition to diffusive mixing, it also includes the exchange of particles between non-adjacent sediment layers (e.g., mimicking conveyor-like feeding modes, Boudreau (1986)). In the 'diffusive' model, the assumption is made that the faunal activities over time redistribute particles in a way that resembles Fickian diffusion (Fick, 1855; Wheatcroft et al., 1990). In such cases, a biodiffusion coefficient quantifies the strength of this mixing process. For a more complete overview of techniques to determine bioirrigation and bioturbation rates, see Volkenborn et al. (2016) and Maire et al. (2008) respectively.

1.4. Modelling of biogeochemistry

1.4.1. Model descriptions

Mathematical models of sediment diagenesis are often used to understand the processes that affect the mineralization of organic matter. In general one or more substances are described in such a model, these substances are called "state variables" (e.g. organic matter concentration, oxygen concentration), and very often they relate to quantities that can be observed in field measurements, or experiments (see section **3**). Consequently, observations can be used to constrain several processes in the model (e.g. oxic mineralization, denitrification, bioturbation) and that are of interest to understand the system's functioning. Once the model is sufficiently capturing the observational data, the model may then be used to better understand the system and predict how changes to environmental conditions could affect nutrient cycling in the sediment.

The type of model depends on the questions that need answering, the data that is available to constrain the model, and (historically) the available computational power. For example, diagenetic models have been used in studies of North Sea sediments to derive bioturbation rates from chlorophyll *a* profiles (Boon and Duineveld, 1998), and to describe the effects of anthropogenic sediment reworking on organic matter remineralization of a muddy coastal sediment (Van De Velde et al., 2018). In more regional studies, simplified diagenetic models were dynamically coupled to pelagic ecosystem models such as ERSEM (Baretta et al., 1995; Ruardij and Van Raaphorst, 1995), or ECOHAM1 (Luff and Moll, 2004; Moll, 2000), to describe seasonal dynamics in benthic pelagic coupling.

Several types of models can be used to represent the biogeochemical functioning in the sediment. The main assumption for all these models is conservation of mass, a cornerstone for reliable models. No mass is created or destroyed in the sediment, so at all times the fluxes out of the sediment should be matched by the incoming fluxes, and whatever reactions and burial processes that happen within the sediment. In so-called *steady state* models, a second important assumption is that the concentrations of the state variables are in equilibrium[1] with the fluxes and biogeochemical processes, i.e. the rate of change of the state variables is balanced with the sources and sinks of that variable. This means that there is no build-up of organic matter, or reaction products in the sediments through time.

In *dynamic* model simulations (section 1.4.1.3.), the conditions that are at play at the model boundaries (forcings, or boundary conditions) need to be prescribed[2]. These conditions are for instance bottom water concentrations, temperature, carbon deposition rates, and they may change over time, due to disturbance events, the uptake of tracer substances, or the annual cycles of OM deposition rates, faunal activity, temperature, and bottom water nutrient concentrations. As a result, process rates and solute fluxes are not always in equilibrium, and over time there can be a buildup, or depletion of solids and solutes in the sediment.

---

[1] Or quasi-equilibrium, in which the rate of change of state variables is multiple orders of magnitude lower than the individual process rates, so that it can be ignored.

[2] From a mathematical point of view, boundary conditions are needed to solve a system of differential equations,

A

0D Mass budget

OM

Mineralization products

Mineralization processes
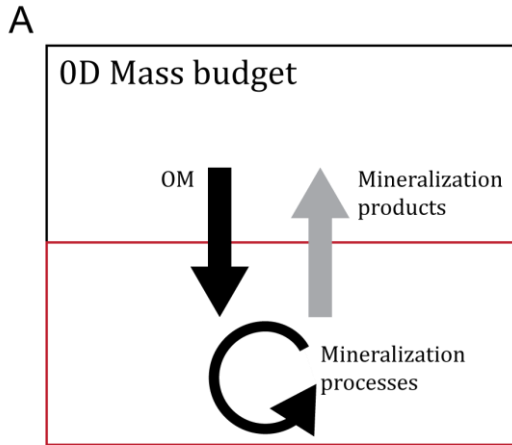
Rate of change of *i* state variables:

$$\frac{dC_i}{dt} = Flux_i + \sum Sources_i - \sum Sinks_i \qquad \text{Eq. 1}$$

Solved as a system of quadratic equations:

$$min(\|Ax - b\|^2), \qquad \text{Eq. 2}$$

with *A* the numeric matrix containing the coefficients of the quadratic function to be minimized, x the unknown to be solved, and *b* the right hand-side of the quadratic function to be minimized.

B

1D Steady state

OM

Mineralization products

Transport processes

Mineralization processes

Depth (z)
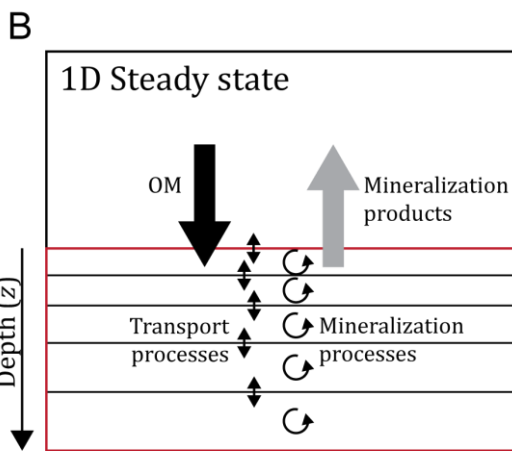
Rate of change of *i* state variables, with separate equations for solutes C, and solids S, subject to a different porosity and modes of transport (Boudreau, 1997; Meysman et al., 2005b):

$$\varphi \frac{\partial C_i}{\partial t} = \frac{\partial}{\partial z}\left(\varphi D_i \frac{\partial C_i}{\partial z} - \varphi v C_i\right) + \varphi \alpha(z)\left(C_{i,\,ow} - C_i(z)\right)$$
$$+ \sum_k v_{i,k} R_k \qquad \text{Eq. 3}$$

$$(1 - \varphi)\frac{\partial S_i}{\partial t} = \frac{\partial}{\partial z}\left((1 - \varphi)D_B(z)\frac{\partial S_i}{\partial z} - (1 - \varphi)w S_i\right)$$
$$+ \sum_k v_{i,k} R_k \qquad \text{Eq. 4}$$

Solved for 0 as the rate of change:

$$C_i = f(C_i) = \frac{\partial C_i}{\partial t} = 0 \qquad \text{Eq. 5}$$

C

1D Dynamic

Depth (z)

t_0 Time (t) t_{end}
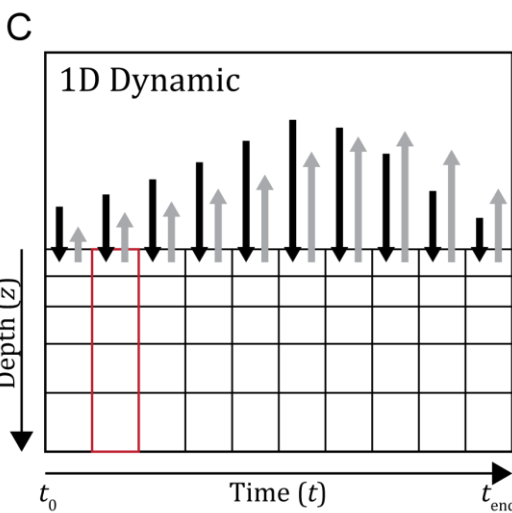
Rate of change of *i* state variables is the same as in the steady state model:

$$\varphi \frac{\partial C_i}{\partial t} = \frac{\partial}{\partial z}\left(\varphi D_i \frac{\partial C_i}{\partial z} - \varphi v C_i\right) + \varphi \alpha(z)\left(C_{i,\,ow} - C_i(z)\right) \qquad \text{Eq. 6}$$
$$+ \sum_k v_{i,k} R_k$$

$$(1 - \varphi)\frac{\partial S_i}{\partial t} = \frac{\partial}{\partial z}\left((1 - \varphi)D_B(z)\frac{\partial S_i}{\partial z} - (1 - \varphi)w S_i\right) \qquad \text{Eq. 7}$$
$$+ \sum_k v_{i,k} R_k$$

Integrated over a given amount of time:

$$C_i = \int_{t_0}^{t_{end}} \frac{dC_i}{dt} dt \qquad \text{Eq. 8}$$

Fig. 1-8: Schematic representations and main theoretical differences between the model descriptions used to model sediment biogeochemistry in this thesis. Red lines indicate equivalent zones of sediment modelled between figures A, B and C.

1.4.1.1. Mass budget model

In a 0D mass budget interpretation of early diagenesis, the sediment column is considered as a whole, and all concentrations and rates are vertically integrated. The model thus becomes a dimensionless box (the model domain is said to be 0D) in which organic matter and reactants enter from the surface at a certain rate, and mineralization products exit at a certain rate (Fig. 1-8 A; Soetaert et al., 2000). These models consist of a set of balance equations that are constructed for the rate of change of all state variables in the sediment. This rate of change equates to the flux of the state variable across the sediment water interface (SWI) and its summed production (sources) or consumption (sinks) processes (Fig. 1-8 A, Eq. 1). By measuring the fluxes of the state variables, incorporating the stoichiometric relations between state variables in the source and sink terms, and using the equilibrium assumption, a system of equations can be constructed where the number of unknowns (the process rates) matches the number of equations. The unique solution of this system of equations is then found by minimizing the sum of squares between the measured fluxes, and the modelled fluxes (Fig. 1-8 A, Eq. 2). This approach has been used to describe the main biogeochemical processes in the Belgian Part of the North Sea (Braeckman et al., 2010, 2014).

1.4.1.2. 1D steady state model

When considering the depth-averaged concentrations (as in the mass budget models), one disregards any information that can be deduced from the spatial distribution of the biogeochemical constituents. While our environment is inherently 3-dimensional, fortunately, in sediments the constituents change much more drastically (over a few mm) in the vertical extent than in the horizontal extent (metres). Thus, in line with a typical sampling where the vertical gradient will be assessed, and the horizontal gradient ignored, diagenetic models typically only consider the vertical extent. In these so-called 1D diagenetic models, the sediment is subdivided into multiple vertical layers, and different mineralization processes occur in specific zones of the sediment, regulated by the concentrations of reactants in each layer (Fig. 1-8 B). This means for instance, that the concentrations of organic carbon entering from the surface, and its mineralization products are simulated in each depth layer. The sediment also has physical properties, such as porosity (φ) and tortuosity (the mean additional distance that solutes travel from point to point because of the shape and size of sediment grains), which affect solutes and solids differently, and which may (or may not) change with sediment depth. Processes affecting solutes are expressed in the liquid fraction of the sediment (*porosity, φ*), whereas solids are described for the solid sediment fraction ($1 - \varphi$). Because solutes and solids are also subject to different transport mechanisms, their rate of change is described by separate equations (Fig. 1-8 B: Eq. 3 & 4). In general the equations of 1D model are much more complex than the mass balance equations, because they also include transport between several layers, and because the processes are described by mechanistic equations. The concentration of a solute in a layer at depth z (Eq. 3) is affected by molecular diffusion (diffusion coefficient D), burial due to sediment accretion on the surface (advection rate, v), and depth-dependent nonlocal bioirrigation (irrigation rate $\alpha(z)$). Whereas solids (Eq. 4) are also affected by advection (w) similar to solutes, the bioturbation D_B causes sediment mixing (diffusion), which is usually modelled as

a depth-dependent process. Each reactive solute or solid species i takes part in a certain amount (k) of biogeochemical processes (R), with stoichiometric equivalents ($v_{i,k}$).

Similar to the mass budget models, the rate of change in 1D diagenetic models can be set equal to 0 in order to solve the model at equilibrium conditions (Fig. 1-8: Eq. 5). Finding a solution requires initial conditions and boundary conditions. Initial conditions are an initial guess for the solution, prescribing the concentrations at t_0; in the case of the diagenetic model, this means a distribution of the state variable concentrations along the depth gradient. Boundary conditions stipulate the concentrations of the state variables at the boundaries of the model domain, in this case the SWI is the upper boundary, and the specified maximum depth of the sediment is the lower boundary. Boundary conditions need to be specified so that transport processes, which are based on concentration gradients between two layers, can be calculated at the edges of the model domain (for a full explanation see Soetaert and Herman (2009), pages 179-180). For solid substances such as organic matter, a constant flux is typically imposed across the sediment water interface (e.g. deposition of OM, sediment accumulation rate). Boundary conditions for solutes (e.g. oxygen, nitrate) are usually specified by the respective concentrations in the overlying water.

1.4.1.3. 1D dynamic models

In dynamic model solutions, the boundary conditions are not constant (Fig. 1-8 C). Bottom water concentrations of nutrients change throughout the year, as does primary productivity, the main source of organic carbon for the sediment. Additionally, abiotic conditions, such as the temperature can change with time, which also affects the system, e.g. via the molecular diffusion rates, or process rates. If the behaviour of a system over a given period of time (e.g. a tidal cycle, or a 12 hour lab experiment, or an annual cycle) is of interest, the varying boundary conditions need to be included. Because the boundary conditions, or environmental settings continuously change, the model will rarely be in equilibrium, instead always adapting to the new situation. Therefore, the equations are not solved for steady-state, but integrated over a given amount of time over which we want to understand the behaviour of the state variables, or the process rates.

1.5.   Structure of the thesis

1.5.1.   Objectives

Understanding a changing environment such as the North Sea encompasses many aspects, starting with an understanding of the current state of the system. As described, sediment biogeochemistry is subject to an array of controlling factors. The complex interplay between these drivers of sediment biogeochemistry is not yet fully understood, and therefor observations of biogeochemical functioning in conjunction with descriptions of the faunal component, and of the abiotic context remain needed (Chapter 2, 3, and 4). Secondly, model descriptions may be used to estimate how new developments or environmental changes could affect the current state. By simulating the response of organic matter mineralization in sediments to anthropogenic activities, we gain insight in past and future changes to nutrient cycling, and learn where steps may be taken to manage these impacts (Chapters 5 and 6).

In **Chapter 2** the aim was to determine how much of the variation seen in the mineralization processes in the BPNS can be attributed to either the activities of the fauna, or the physical properties of the sediment. This was achieved by first sampling the benthic fauna, the sediment characteristics, and measuring biogeochemical processes in 7 locations in the BPNS. Subsequently a mass budget model was applied to derive mineralization rates from flux measurements. The patterns in mineralization rates were analyzed using variance partitioning, to elucidate to which degree mineralization processes could be explained by the benthic fauna, or the sediment characteristics. Statistical models for the mineralization rates were constructed, for use in future predictive endeavours.

In **Chapter 3** we characterized the sediment biogeochemistry on a 670 km long S-N transect in the North Sea (Dutch and British parts). During a research cruise, on-board incubations were performed to quantify nutrient exchange rates, and collect porewater nutrient profiles. These data were used to constrain a 1D steady state diagenetic model, from which mineralization rates were derived. This technique allowed us to compare the biogeochemical functioning in several distinct zones in the North Sea (Oyster Grounds, Dogger Bank, central North Sea, Fladen Grounds), and describe general patterns along the longitudinal gradient.

In **Chapter 4** a new method to measure bioirrigation is presented, which makes a distinction between the rate of solute exchange in the sediment, and the depth over which this occurs. This was a necessary methodological study to further advance the inclusion of biological processes into models of sediment biogeochemistry. The technique was used to quantify bioirrigation rates in samples collected in the Oosterschelde estuary over a full year, revealing differences in bioirrigation characteristics between subtidal and intertidal species communities.

Chapter 5 is a modelling study on the effects of bottom trawl fisheries on organic matter mineralization, in a variety of sediment types. 1D Diagenetic models were calibrated using data collected in the previous chapters, and a dynamic solution of this model was then used to acquire mineralization patterns over an annual cycle. Subsequently, trawling events ($1 - 5$ y^{-1}) were imposed on random days during the simulation, as an instantaneous removal of the top layer of sediment, and a subsequent mixing of a layer below. We then described the changes to organic matter mineralization caused by trawling, and identified mechanistic drivers to explain these changes.

In **Chapter 6** a dynamic diagenetic model solution was coupled to the output of a hydrodynamic transport model of the BPNS, to investigate how filtration by the blue mussel (*M. edulis*) on wind turbine substructures affects nutrient cycling in surrounding sediments. This was implemented as a transformation of suspended particulate matter, to fast-sinking faecal pellets in zones in the hydrodynamic model containing OWFs.

This thesis ends with a general discussion (**Chapter 7**) in which the coupling of the sediment characteristics, species composition, and the sediment biogeochemistry in the BPNS (**Chapter 2**), and the greater North Sea (**Chapter 3**) is compared. Subsequently, the impacts of both anthropogenic activities discussed in this thesis (bottom trawling (**Chapter 5**) and OWF development (**Chapter 6**)) are discussed in the context of a changing North Sea.
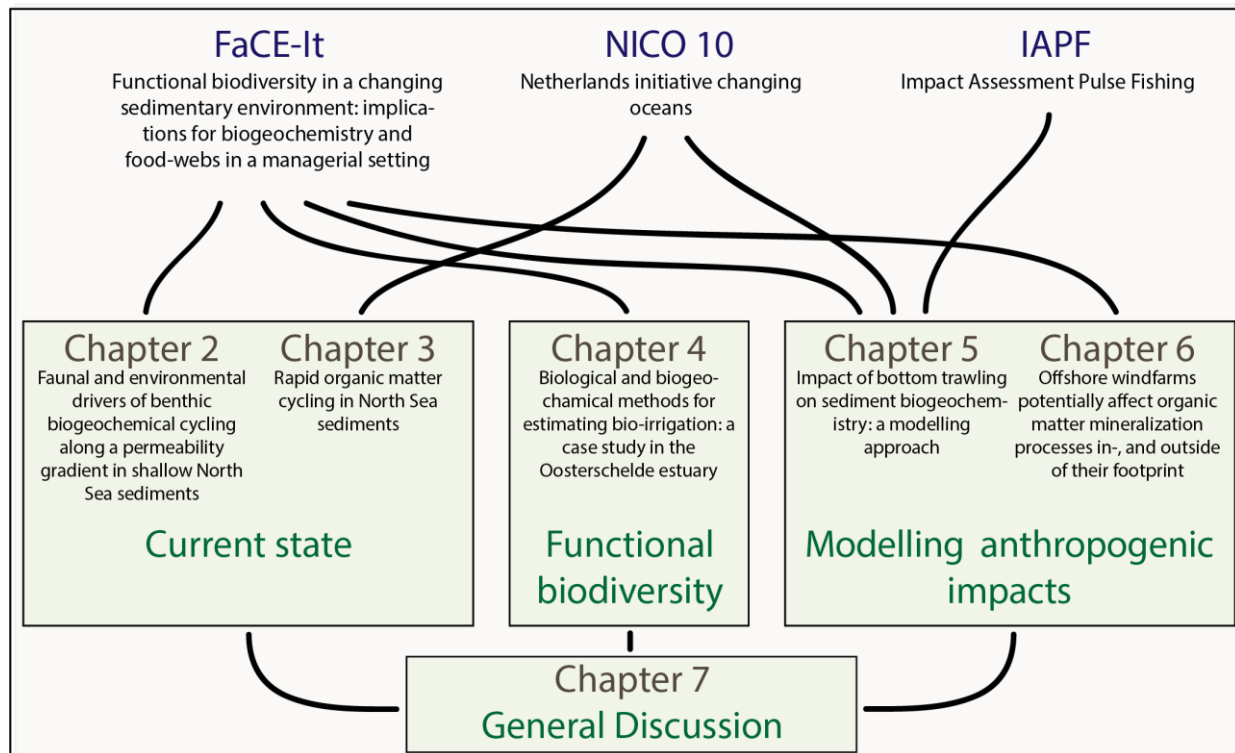
Fig. 1-9: The chapters in this thesis, and associated research projects.

1.5.2. Research projects

This thesis combines research from different research projects, which fit together under the overarching theme of sediment biogeochemistry in a changing environment.

The majority of the work was performed within the framework of the FaCE-It project: Functional biodiversity in a changing sedimentary environment: implications for biogeochemistry and food-webs in a managerial setting (Fig. 1-9). As the name implies, this project focussed on investigating the links between sedimentary changes (fining - coarsening) on ecosystem functioning, i.e., the changes in energy and matter over time and space through biological activity (Snelgrove et al., 2014). Whereas the focus here is on sediment biogeochemistry, FaCE-It also investigated food-web dynamics throughout the Belgian Part of the North Sea (BPNS), with an emphasis on novel food-webs developing around wind turbine foundations (Mavraki et al., 2020a, 2020b), on the link between biogeochemistry and biology (Toussaint et al., subm.; this work), and on developing a hydrodynamic model of the Southern Bight in which to simulate changes (Ivanov et al., 2020).

While FaCE-It focussed on the BPNS / Southern Bight, here the work was complemented by measurements of sediment biogeochemistry performed in Dutch and British waters, during Leg 10 of the expedition of the Netherlands Initiative Changing Oceans (NICO, NWO (2019)). This cruise focussed on biodiversity in the North Sea, both in the water column and in the sediment, which offered the opportunity to sample the sediment biogeochemistry alongside of benthic fauna.

The studies undertaken for FaCE-It, and during NICO 10 enabled us to link to the Impact Assessment Pulse Fishing project through a modelling study (IAPF, Fig. 1-9), in which the impacts of pulse fishing on different components of the benthic ecosystem were investigated (Rijnsdorp et al., 2020a).

Chapter 2. FAUNAL AND ENVIRONMENTAL DRIVERS OF CARBON AND NITROGEN CYCLING ALONG A PERMEABILITY GRADIENT IN SHALLOW NORTH SEA SEDIMENTS

Elise Toussaint*, Emil De Borger*, Ulrike Braeckman, Annelies De Backer, Karline Soetaert, Jan Vanaverbeke

*Joint co-authorship: Emil De Borger took part in fieldwork, assisted in performing incubations, performed multiple factor analysis, performed variance partitioning, created figures for the manuscript, and co-wrote manuscript.

Abstract

Ecosystem functions are driven by abiotic and biotic factors, but due to high collinearity of both, it is often difficult to disentangle the drivers of these ecosystem functions. We studied sedimentological and faunal controls of benthic organic matter mineralization, a crucial ecosystem process provided for by sediments of shelf seas. Subtidal benthic habitats representative of the wide permeability gradient found in the Belgian Part of the North Sea (Northeast Atlantic Shelf) were characterized in terms of sediment descriptors, macrofauna, and sediment biogeochemistry was estimated. Our results confirmed a strong correlation between sediment characteristics and macrofauna, and estimated sediment biogeochemical processes rates were clearly linked to both. Results of variance partitioning and statistical modelling showed that oxic mineralization and nitrification were mainly regulated by faunal activities whereas anoxic mineralization was controlled by sediment properties, with permeability as a decisive factor. Both biotic and abiotic factors were needed to explain variability in oxygen consumption and total mineralization estimates, suggesting that macrofaunal activities have different effects across habitats. The statistical models were a useful tool to interpret the impact of anthropogenic activities in the study area and represent a step towards predicting the effects of human activities on crucial ecosystem functions.

2.1. Introduction

It is well accepted that ecosystem functions, i.e. changes in energy and matter over time and space through biological activity (Snelgrove et al., 2014), are driven by biodiversity interacting with abiotic and anthropogenic drivers (Duncan et al., 2015). Species assemblages, in turn, are shaped by adaptations

to the prevailing environmental conditions in theirhabitat (Díaz and Cabido, 2001; Violle et al., 2007), the so-called functional response traits (Lavorel and Garnier, 2002). At the same time, species are characterised by a set of functional effect traits, having a direct or indirect role in ecosystem functioning (Lavorel and Garnier, 2002). This spatial pairing of species functional response and effect traits often generates a strong collinearity, which makes it difficult to disentangle the relative importance of biotic and abiotic drivers of ecosystem functions (Godbold and Solan, 2009a).

In marine sediments, the mineralisation of organic matter to free nutrients is an important ecosystem process, as this recycling mechanism drives biogeochemical cycling, which drives primary production in the water column (Soetaert and Middelburg, 2009; Provoost et al., 2013) and many important element cycles (Jørgensen, 2000). Typically, organic matter mineralization occurs through various processes, which are regulated by organic matter concentrations, the availability of oxygen (oxic vs. anoxic mineralization), and other electron acceptors such as nitrate (denitrification) (Froelich et al., 1979). Shelf seas are especially important as they account for up to 80 % of global carbon mineralization, despite covering only 7 % of the marine surface (Wollast, 1998). Organic matter mineralization and other ecosystem functions are the result of the functional effect of the organisms present, and habitat structuring forces such as hydrodynamics, and the natural and anthropogenic disturbance regime. The highly dynamic nature of coastal areas, combined with the high degree of anthropogenic disturbances (Eigaard et al., 2017; Fettweis et al., 2009; Van De Velde et al., 2018), leads to a heterogeneous patchwork of habitats with strongly differing mineralization regimes, despite occurring in close proximity to one another (Braeckman et al., 2014; Neumann et al., 2017; Gogina et al., 2018).

Local sediment characteristics such as grain size distribution, permeability (the capacity to transmit fluid), and porosity (the water content), influence the redox zonation patterns in which microbially mediated mineralization processes occur (Böttcher et al., 2000; Llobet-Brossa et al., 2002; Probandt et al., 2017), by providing binding sites for organic matter (Mayer, 1994) and by regulating the exchange of oxygen, organic matter and other reactants between the sediment and the overlying water (De Beer et al., 2005; Huettel et al., 2014). Large, connected pore-spaces in coarse grained, permeable sediments allow for advective flows, resulting in high organic matter turnover rates fuelled by a high oxygen supply (Huettel and Rusch, 2000; Ehrenhauss et al., 2004). In contrast, cohesive sediments are characterised by smaller and less connected interstitial spaces, so that diffusive processes, molecular diffusion or local transport stimulated by benthic fauna, dominate solute and particle transport (Aller, 1980; Gust and Harrison, 1981; Aller and Yingst, 1985; Aller and Aller, 1992; Huettel and Gust, 1992).

Organic matter mineralization processes are also affected by the fauna inhabiting this sediment gradient. Bioturbation, the faunal behaviour that results in particle displacement and increased exchange of solutes across the sediment-water interface (Aller and Yingst, 1985; Kristensen et al., 2012; Gogina et al., 2017), affects the vertical and horizontal distribution of organic matter, oxygen, and other electron acceptors involved in the mineralisation processes (Kristensen, 2001; Na et al., 2008; Tous Rius et al., 2018). Recently, functional indices, in which functional effect traits are used to approximate bioturbation activities, have been applied to relate benthic communities to benthic ecosystem processes (Van Colen et al., 2012; Braeckman et al., 2014; Wrede et al., 2019; De Borger et al., 2020).

Benthic communities are closely linked to specific habitat types because of adaptations to hydrodynamic conditions, and sedimentological variables (Van Hoey et al., 2004; Degraer et al., 2008). As a result, the expression of functional effect traits affecting ecosystem functions, such as biological particle mixing (bio-mixing), or burrow ventilation is inherently coupled to the habitat in which the species occur (Snelgrove and Butman, 1994; Bremner et al., 2003; Breine et al., 2018).

Empirical information on how fauna and the physical environment drive ecosystem functions across environmental settings is needed to improve our understanding of coastal marine ecosystems and to evaluate how the quantity and quality of the delivery of ecosystem services, and the benefits that humans obtain from ecosystems, could be affected in scenarios of future change (Snelgrove et al., 2014; Hillman et al., 2020).

To quantify the degree to which faunal activities and the physico-chemical sediment characteristics regulate specific mineralization processes, we investigated the sediment biogeochemistry and associated physico-chemical and biological characteristics, in contrasting environments in the Belgian Part of the North Sea (BPNS). This is a shallow coastal region where a wide gradient of permeable to cohesive sediments is found in close proximity (Braeckman et al., 2014), and where the distribution of benthic communities has been mapped extensively (Van Hoey et al., 2004; Degraer et al., 2008; Breine et al., 2018). More so, the small size of the BPNS (3462 km^2) ensures that temperature variations, light regime, and the magnitude of the phytoplankton bloom are relatively uniform throughout the study area (Rousseau et al., 2006).

Specific aims in the presented research were (1) to determine which mineralization processes are influenced predominantly by the abiotic components and which ones by the biotic components, and (2) to investigate which descriptor of the faunal activities (bioturbation potential or bioirrigation potential) is most suited as a predictor of individual biogeochemical processes, oxic mineralization (including nitrification, denitrification, and dissimilatory nitrate reduction or DNRA), and anoxic mineralization (investigated as the collection of individual anoxic processes). Our hypotheses were that total mineralization of organic material would correlate to abiotic factors mostly, given the linkage between fine particle structures and organic matter content; and secondly that faunal activities would be noticed most in sediments with intermediate grainsize, outside of the extreme advective flow or cohesive molecular diffusion dominated sediments.

2.2. Materials and Methods

2.2.1. Field sampling

In September 2016 and 2017, sediment, water column and benthic communities were sampled along a gradient of sediment permeability in the Belgian Part of the North Sea on board of *RV* Simon Stevin. Samples were collected at 5 stations (St. 130, St. 780, St. BRN11, St. 330, St. BBEG) in 2016 and at 7 stations (St. 130, St. 780, St. 120, St. BRN11, St. D6N, St. 330, St. D6S) in 2017 (Fig. 2-1, Appendix A in supplementary material). Amongst those stations, some are heavily impacted by human activities: BRN11 is located in a former aggregate extraction site that is abandoned since January 2015; BBEG is

located in close proximity to an offshore wind farm under construction, and D6N and D6S are located 200 m north and south respectively from a wind turbine in the C-Power wind farm, operational since 2008 (Coates et al., 2014). All samples were collected at the end of summer to target the period with the highest benthic mineralization rates in the study area (Provoost et al. 2013, Braeckman et al. 2014).

At each station, a CTD-cast was performed to determine bottom water temperature. Bottom water (± 1 m above the seafloor) was sampled with a 5L Niskin bottle to determine nutrient concentrations. Additional NISKIN bottles were closed at depth to collect bottom water used during incubation experiments. This water was stored in sealed vats, until further use in the laboratory.
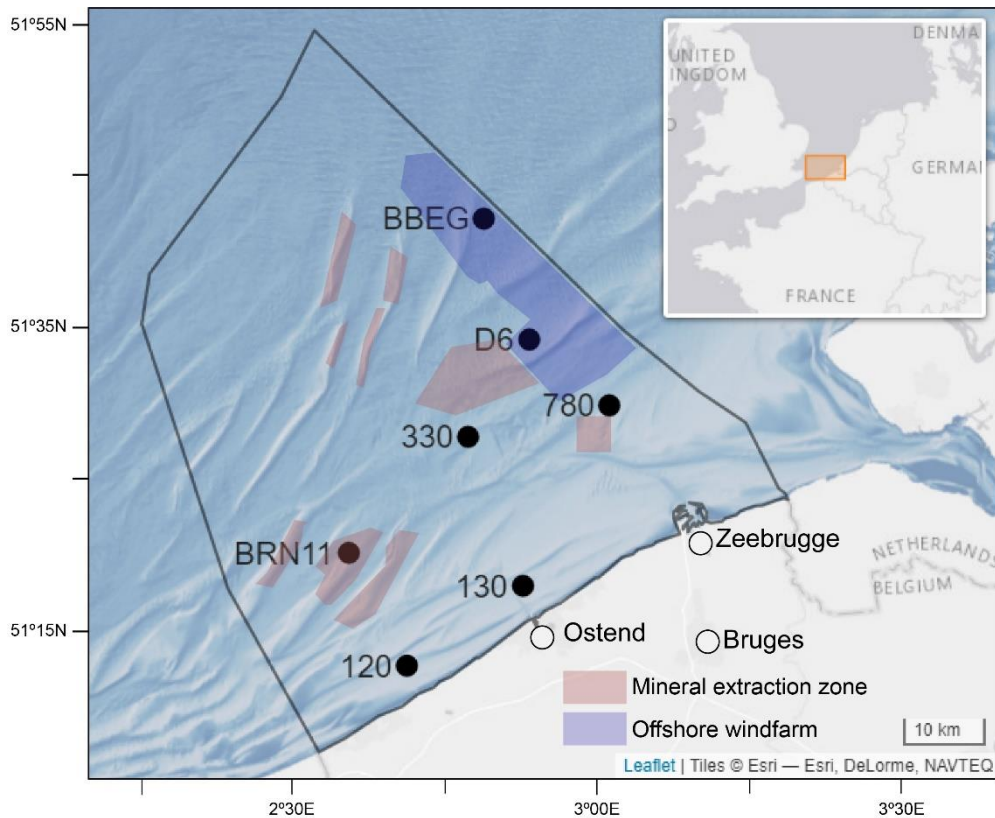
Fig. 2-1: Sampling sites (dots) in the Belgian Exclusive Economic Zone (EEZ, black outline) Basemap: © Esri, depth raster by (GEBCO Compilation Group, 2020), polygons by RBINS (MUMM scientific service, 2015).

A NIOZ box corer (0.028 m²) was deployed three times at each station to collect undisturbed sediments, from which three subsamples were taken to characterize the sediment in terms of (1) permeability (plexiglass core, inner diameter, i.Ø: 3.6 cm; length: ± 25 cm), (2) granulometry and porosity, and (3) pigments, total organic carbon, total nitrogen and total organic matter (TOC, TN and TOM) (cut off syringe, upper 3 cm). Porosity, TOC/TN and TOM samples were stored at -20°C and pigments samples were stored in liquid nitrogen onboard and transferred to the -80°C freezer in the lab.

Within each box core, one plexiglass core (cohesive sediment: i.Ø: 10 cm, height: 25 cm; permeable sediment: i.Ø: 19 cm to allow for advective porewater flow later, H: 30cm) was inserted into the sediment to a depth of 10 to 15 cm, enclosing ± 10 cm of overlying water. The cores were excavated from the box core, closed with a lid at the bottom, carefully filled up with *in situ* sea water without disturbing the sediment surface and placed in a tank of sea water at ambient temperature. Within 10 h, the cores were

transported to a climate room set at 19.3°C in the laboratory (*in situ* bottom water temperature for all stations was between 19 and 20°C for both years, see Table A.1., Appendix A for incubation volumes, temperature, and salinity).

2.2.2. Core incubations

For the cohesive sediments, Teflon-coated magnet rings (~ 2.5 cm) were placed in the small cores, 5 cm above the sediment-water interface. A homogeneous mixing of the water column was ensured with a rotating central magnet. The rotation speed was kept below the resuspension rate and did not induce an advection flow in the sediment. For permeable sediment, the lids were equipped with a flat stirring disk which was placed at 5.4 cm above the sediment surface. The rotation speed was set at 40 rpm, allowing an advection porewater flow in the permeable sediment (Huettel and Rusch, 2000). With these settings, an advective porewater flow corresponding to the lower end of *in situ* conditions was simulated (Oldham et al., 2004; Van den Eynde 2017). The overlying water was kept aerated until the start of the incubation. After 36h of acclimatization in the temperature-controlled room, the overlying water in the cores was replaced by freshly oxygenated *in situ* sea water.

Bio-irrigation was measured following the decrease of a tracer in the water overlying the sediment in the experimental units (Glud et al., 1996; De Smet et al., 2016; De Borger et al., 2020). In 2016, the overlying sea water was mixed with sodium bromide ($[NaBr]_{final} = 0.01$ mol L^{-1}) while in 2017, the newly replaced sea water was spiked with a uranine solution $C_{20}H_{14}Na_2O_7$; ($[uranine]_{final} = 10\text{-}15$ µg L^{-1}), a tracer that is cheaper and easier to analyse.

The cores were then sealed air-tight with lids equipped with gas-tight sampling ports and incubated in the dark. The incubations lasted for 2 to 8 h depending on the oxygen concentration in the overlying water which was not allowed to decrease below 50% of the initial saturation. The overlying water was subsampled at the beginning (T_0) and at the end (T_{end}) of the incubation and, depending on the length of the incubation, at one (T_1) or two (T_2) moments in between, always *in duplo*. Using a glass syringe, subsamples were collected for O_2 (only in 2016: 10 mL), dissolved inorganic carbon (DIC) (2 x 6 mL), dissolved inorganic nitrogen (DIN – NO_x, NH_x) (2 x 10 mL) and the irrigation tracer (Br⁻ or Uranine) (2 x 3 mL).

When a water sample was collected, the same volume of sea water collected from the field was simultaneously inserted into the core through the second sampling port to prevent aeration. This replacing sea water will be referred to as tank water. Subsamples of the tank water were taken at each sampling time for O_2, DIC, DIN, phosphate, silicate, and irrigation tracer. Sampling volumes were similar as described above. In total, 36 cores were incubated following this procedure, two of them were lost due to experimental errors.

DIC samples were transferred to exetainers which were directly closed hermetically and fixed with mercury chloride ($HgCl_2$: 10 µL, 3 %). DIC, bromide and uranine samples were stored at 4°C until analysis. Nutrient samples were filtered through WhatmanTM GF/F filters and stored at -20 °C until further analysis.

After the incubation, the remaining sediment was sieved on a 1 mm mesh to collect the macrofauna, which was fixed on 70% ethanol until processing (following Gaston et al. (1996) and Wetzel et al. (2005)).

2.2.3. Sample processing

2.2.3.1. Sediment parameters

Sediment grain size was determined by laser diffraction on freeze dried and sieved sediment samples in a Malvern Mastersizer 2000 (McCave et al., 1986). Grain size fractions were determined as volume percentages according to the Wentworth scale (Wentworth, 1922): clay/silt (< 63 μm), very fine sand (vfines: 63 – 125 μm), fine sand (fines: 125 – 250 μm), medium sand (250 – 500 μm), and coarse sand (500 μm – 1 mm). The median grain size (MGS) was calculated on the fraction < 1 mm.

Water content (weight %) was determined as the volume of water removed by freeze drying wet sediment samples. Sediment porosity was determined from water content and solid phase density measurements (determined by measuring the mass of sediment needed to displace 1 mL of water), accounting for the salt content of the porewater.

The % of total organic matter (TOM) was calculated by weighing the sediment before and after burning (2h at 500°C) all organic material in dried (min 48 h at 60°C) sediment.

The molar C/N ratio was calculated from the percentages of total organic carbon (TOC) and total N (TN), determined using an Interscience Flash 2000 organic element analyser (uncertainty: 0.01 %, standard used: sulphanilamide). The permeability of sediment in the i.Ø 3.6 cm sampling cores was determined with a permeameter (Buchanan, 1984) in 2017. In 2016, sediment permeability was calculated after Hazen in Eggleston and Rojstaczer (1998) (Eq. 1), using the first decile of the grainsize distribution (d_{10}) and the kinematic viscosity (v):

$$Permeability = 1.1019 \cdot 10^3 \, m^{-2}s \cdot d_{10}^2 \cdot v \qquad \text{(Eq. 1)}$$

2.2.3.2. Solute concentrations and fluxes

Sediment community oxygen consumption (SCOC)

In 2016, the oxygen concentration of the water in the incubation cores was determined discretely by inserting an oxygen microsensor (Unisense, 100 μm tip, 2-point calibration) into a subsample of the overlying water. In 2017, the oxygen concentration was continuously monitored using a robust oxygen miniprobe (Firesting, 3 mm Ø, 10 cm long, 2-point calibration). In both sampling campaigns, SCOC was determined from the linear decrease of oxygen concentration in the overlying water between T_{end} and T_1, standardized for overlying water volume and fluid exchange surface and correcting for concentration changes due to the water replacement.

DIN and DIC

After thawing, DIN samples were analyzed by automated colorimetric techniques (San++ SKALAR). DIC analysis was performed using a segmented flow analyzer (San++ SKALAR) according to the method of Stoll et al. (2001). DIC and nutrient fluxes were calculated from the linear change in concentration in the overlying water between T_{end} and T_1, standardized for overlying water volume and fluid exchange surface, and correcting for concentration changes due to the water replacement.

Irrigation tracer

Bromide anions (in 2016) were separated by ion chromatography (Dionex Ionpac AS14 column), using a 3.5mM Na_2CO_3/1mM $NaHCO_3$ eluent. They were then detected by an UV spectrophotometer (Thermo Ultimate-3000) and an electrochemical detector (Dionex ED40). Uranine samples (in 2017) were analysed using a spectrophotometer ($\lambda_{excitation}$ = 494 μm, $\lambda_{mission}$ = 515 μm).

The irrigation rate Q (L d^{-1}) (Meysman et al., 2007) was estimated as

$$Q = -\frac{V_{OW}}{(C_{T0} - C_{T\ refence})} \cdot \frac{dC}{dt} \tag{Eq. 2}$$

with V_{OW} the volume of overlying water, C_{T0} the tracer concentration at the beginning of the incubation, $C_{T\ reference}$ the ambient tracer concentration of seawater, and dC/dt the slope of the decreasing tracer concentration over time. The slope between T_0 and T_1 was selected since this represents best the actual irrigation rate rather than the depth of the irrigation (De Borger et al., 2020). The irrigation rates were standardized by dividing Q by the surface of the core (L m^{-2} d^{-1}).

2.2.3.3.   Biological samples

The benthic organisms were identified to the lowest possible taxonomic level, typically to species level, counted, and the blotted wet weight determined. The abundance and biomass data, standardized to m^{-2}, were used to calculate two functional indices of the benthic community: the bioturbation potential (BP_c, Eq. 3) (Solan et al., 2004) and the irrigation potential (IP_c, Eq. 4) (Wrede et al., 2018). For each species i in a sample, the abundance and biomass (resp. A_i and B_i) were scaled, and multiplied with either its mobility score M_i and reworking score R_i (for the BP_c; Queirós et al., 2013), or its burrow type BT_i, feeding type FT_i, and injection pocket depth ID_i (for IP_c; Wrede et al., 2018).

$$BP_c = \sum_{i=1}^{n} \left(\frac{B_i}{A_i}\right)^{0.5} \cdot A_i \cdot M_i \cdot R_i \tag{Eq. 3}$$

$$IP_c = \sum_{i=1}^{n} \left(\frac{B_i}{A_i}\right)^{0.75} \cdot A_i \cdot BT_i \cdot FT_i \cdot ID_i \tag{Eq. 4}$$

2.2.4.   Mass balance modelling

Biogeochemical process rates were estimated based on measured fluxes of O_2, DIC, NH_x and NO_x and an integrated mass balance of oxygen, carbon, nitrate and ammonium in the sediment, which is an extension of the model developed in Soetaert et al. (2001). This model contains the following processes: organic carbon can be oxidized aerobically (oxic mineralization - OxicMin), anaerobically (anoxic mineralization – AnoxicMin) or by denitrification (Denitr). Anoxic mineralization in this model consists of the collected anoxic mineralization sub-processes (e.g. Mn and Fe reduction, and methanogenesis as per Soetaert et al. (1996)). Reduced substances, also called Oxygen Demanding Units (ODU), produced by anoxic mineralization can be deposited in the sediment and remain buried (ODUdeposition), or be re-oxidized (Reoxidation – Reoxi). Oxygen can be used to oxidize organic carbon (OxicMin), to re-oxidize ODU (Reoxi) and to oxidize ammonium to nitrate (Nitrification – Nitr) which requires two moles of oxygen for each mole of ammonium (Eq. 5). On the other hand, dissolved inorganic carbon (DIC) is produced by organic carbon mineralization (OxicMin, AnoxicMin, Denitr) (Eq. 6). Ammonium is produced by the mineralization of organic nitrogen (Total N mineralization - Nmin) and the dissimilatory nitrate reduction to ammonium (DNRA), whilst it is consumed by

nitrification (Eq. 7). Nitrate is produced by nitrification and consumed by denitrification (0.8 moles of NO_3/mole of carbon denitrified) and DNRA (Eq. 8). Oxygen, DIC, nitrate, and ammonium are further exchanged through the sediment-water interface (O2influx, CO2efflux, NOxinflux, NHxinflux), while the lower boundary of the sediment is assumed to be a no flux boundary. The resulting balances are summarized below.

$$\frac{dO_2}{dt} = O_2influx - OxicMin - Reoxidation - Nitrification * 2 \qquad \text{(Eq. 5)}$$

$$\frac{dCO_2}{dt} = CO_2efflux - OxicMin - AnoxicMin - Denitrification \qquad \text{(Eq. 6)}$$

$$\frac{dNH_x}{dt} = NH_xinflux + Nmineralization + DNRA - Nitrification \qquad \text{(Eq. 7)}$$

$$\frac{dNO_x}{dt} = NO_xinflux + Nitrification - 0.8 * Denitrification - DNRA \qquad \text{(Eq. 8)}$$

The fluxes across the sediment-water interface (O2influx, CO_2efflux, NH_xinflux, NO_xinflux) were estimated during the incubation experiments, while the rates of change of oxygen, carbon dioxide, nitrate and ammonium fluxes were assumed to be zero (geochemical steady state). Two extra equations were added to solved the unmeasured quantities (OxicMin, AnoxicMin, ODUdeposition, Reoxi, Nmin, Nitr, Denitr, DNRA): the reoxidation of reduced substances equals the anoxic mineralization minus the ODU that remains buried (Eq. 9), and the total N mineralization equals the sum of all mineralization processes (OxicMin, AnoxicMin, Denitr) with a relationship between nitrogen and carbon mineralization using the Redfield N/C ratio (0.156) (Eq. 10).

$$Reoxi = AnoxicMin - ODUdeposition \qquad \text{(Eq. 9)}$$

$$Nmineralisation = (OxicMin + AnoxicMin + Denitrification) * N/C \; ratio \qquad \text{(Eq. 10)}$$

All unknows should be equal to or above 0. The mass balance model is based on two assumptions: the system reached a geochemical steady state and there was no carbonate dissolution or formation.

With 6 equations and 8 unknows, the model was underdetermined and the R package limSolve (Soetaert et al., 2009) was used to solve a Least Squares with Equality and Inequality Constraints inverse problem (lsei, type 2).

2.2.5.   Statistical analysis

2.2.5.1.   Multiple factor analysis

To visualize common patterns between the environmental parameters, species composition and biogeochemical characteristics, a Multiple Factor Analysis (MFA) was applied (Escofier and Pagès, 1994). MFA is a multivariate analysis performed in two steps: in a first step, principle component analyses (PCA) on separate tables of variables (environment, fauna, biogeochemistry) are performed, and the components of the PCA's are then normalized by dividing all elements by the total inertia obtained from the respective PCA's. In the second step the weighted PCA tables are combined and again

subjected to PCA to generate the reference structure; the common structure of all the data. For the initial PCA's in step one, environmental parameters (permeability, sediment granulometry, TOC, TOM, chl a) and biogeochemical parameters (process rates modelled in section 2.4) were subjected to correlation matrix PCA; species biomass was log-transformed and subjected to a centred PCA (Dray and Dufour, 2007).

2.2.5.2.   Variance partitioning

Variance partitioning was used to determine which biogeochemical processes are predominantly influenced by the sediment variables or by faunal components. This technique allows parts of the explained variance of a response variable to be attributed to individual subsets of potentially correlated explanatory variables (Borcard et al., 2011). In this case, the explanatory variables combined all environmental variables as one subset (T. 2-1), and the biological variables as the other (T. 2-2); the response variables were the modelled biogeochemical process rates. Since variance partitioning is based on linear relationships, linearity between the sets of the explanatory variables and each individual response variable was assessed through linear regression testing, assuming a *p*-value of 0.05 for significance. Explanatory variables (and in one case the response variable) were square root, or log transformed to resolve issues of non-linearity. If linearity could not be achieved, the variable was left out of the subset entirely (modelled variable and removed variables were for Oxic min: TOM, TOC, irrigation rate; for Anoxic min.: fines, all species variables; for Denitr: fines, vfines, BP_c, IP_c, species richness; for Nmin: fines, vfines; for Nitr: TOC, TOM, permeability, porosity, MGS, silt; SCOC: irrigation rate, species richness). Explanatory variables were centred on their means, and standardized to control for the different scales of the response variables in the subsets (Legendre and Legendre, 1998). A forward selection procedure was applied on the subsets of explanatory variables to remove redundancy (Blanchet et al., 2008). After the variance partitioning, the significance of each partition of explained variance was assessed using a permutation test, assuming a *p*-value of 0.05 (Borcard et al., 2011).

2.2.5.3.   Statistical modelling

To statistically correlate SCOC, estimated oxic and anoxic mineralization, denitrification, nitrification and total N mineralization to environmental and biological explanatory variables, a multiple linear regression approach was used. The factor "year" was also included to test for the importance of year-to-year variability. Prior to the model construction, collinear predictors were excluded from the full set of predictors until all the variance inflation factor (VIF) values were lower than 5 (Zuur et al., 2007). The full linear models included permeability, % of Total Organic Matter (TOM), % of fines (125–250 μm), BP_c, IP_c, irrigation rate and species richness as predictors. Model selection was performed through a stepwise procedure based on the Akaike Information Criterium (AIC). After selection of the best model, the assumptions were checked with graphical techniques. No violation of the assumptions was noticed for the SCOC and denitrification models. However, heterogeneity of variance in the residuals was detected for the other models. Linear regression with a generalized least-squares extension was then performed for the oxic, anoxic and total mineralization models (Chapter 4 in Zuur et al., 2009). The variance structure used for each model is summarized in T. 2-4. To model nitrification, a generalized

linear model (GLM) with a gamma distribution was adopted as this response variable is continuous and larger than zero. Finally, the relative consumption of nitrate by denitrification (denitrification / (denitrification + DNRA)) was modelled using a GLM with a quasibinomial distribution.

Data analysis and modelling was performed in R (R Core Team, 2020), using the software packages "ade4" for the MFA (Dray and Dufour, 2007), the "vegan" package for the variance partitioning (Oksanen et al., 2019), the "limSolve" package for the mass balance model (van den Meersche et al., 2009) and the "lmne" (Pinheiro et al., 2020) and "MASS" (Ripley et al., 2020) packages for linear models.

2.3. Results

2.3.1. Measurement results

2.3.1.1. Sediment

Sediments ranged from silty sediments with a high total organic matter (TOM) content and a low permeability nearshore (st. 130: median grain size (MGS) = 19 ± 2 μm, TOM = 5.4 ± 2.4 %, permeability = 0.12 10^{-12} ± 0.13 10^{-12} m^2, values as average ± sd), to highly permeable, coarse grained sediments with lower total organic matter contents further offshore (D6S: MGS = 524 ± 203 μm, TOM = 0.91 ± 0.37 %, permeability = 53.9 10^{-12} ± 19.7 10^{-12} m^2) (T. 2-1, Fig. 2-2 A). Stations BRN11, 120, and 780 represented fine sandy sediments of intermediate grainsize (169 ± 3 – 253 ± 6 μm), characterized by a high percentage of fine sands (45 ± 0 – 58 ± 2 %), low to intermediate permeability (0.18 10^{-12} ± 0.03 10^{-12} – 13.10 10^{-12} ± 4.25 10^{-12} m^2), and a TOM content varying from 0.52 ± 0.01 % to 1.58 ± 0.23%. Sediments were classified as permeable (D6, BBEG, BRN11, 330), or cohesive (120, 130, 780), depending on whether their permeability was above (permeable), or below (cohesive) 2.5*10^{-12} m^2 (Forster et al., 2003; Wilson et al., 2008).

T. 2-1: Sediment characteristics. Values are expressed as average ± sd (*n* = 3).

Year	Station	Permeab. · $10^{-12}\,m^2$	MGS μm	Silt %	Fine sand %	Very fine sand %	Porosity -	TOC %	TOM %	Chl *a* μg g^{-1}
2016	130	1.98 10^{-3} ± 0.12 10^{-3}	14 ± 1	87 ± 8	6 ± 6	4 ± 1	0.8 ± 0.02	1.67 ± 0.22	8.81 ± 0.94	95 ± 33.8
	780	0.18 ± 0.03	176 ± 1	12 ± 0	66 ± 3	9 ± 0	0.49 ± 0.05	0.23 ± 0.05	1.14 ± 0.34	3.2 ± 0.9
	BRN11	10.2 ± 0.45	294 ± 6	0 ± 0	31 ± 2	0 ± 0	0.41 ± 0.08	0.07 ± 0.01	0.52 ± 0.01	0.3 ± 0.1
	330	14.4 ± 0.79	349 ± 10	0 ± 0	15 ± 2	0 ± 0	0.35 ± 0.09	0.1 ± 0	0.55 ± 0.01	0.1 ± 0
	BBEG	41.10 ± 3.75	574 ± 32	0 ± 0	0 ± 0	0 ± 0	0.22 ± 0.14	0.03 ± 0.01	0.32 ± 0.1	0.1 ± 0
2017	130	0.12 ± 0.13	19 ± 2	75 ± 5	14 ± 4	5 ± 1	0.75 ± 0.03	0.74 ± 0.25	5.4 ± 2.39	31.5 ± 10
	780	0.37 ± 0.32	169 ± 3	19 ± 2	58 ± 2	9 ± 1	0.51 ± 0.05	0.24 ± 0.06	1.58 ± 0.23	9.6 ± 0.4
	120	5.29 ± 4.12	221 ± 9	9 ± 5	47 ± 8	5 ± 3	0.42 ± 0.03	0.13 ± 0.04	1.07 ± 0.18	2.7 ± 0.3
	BRN11	13.1 ± 4.25	253 ± 6	3 ± 3	45 ± 0	1 ± 0	0.39 ± 0.02	0.09 ± 0.03	0.73 ± 0.01	0.9 ± 0.2
	D6N	18.7 ± 7.00	353 ± 12	0 ± 0	16 ± 4	0 ± 0	0.36 ± 0.02	0.07 ± 0.01	0.43 ± 0.04	0.2 ± 0.1
	330	42.5 ± 1.83	434 ± 43	0 ± 0	5 ± 4	0 ± 0	0.33 ± 0.01	0.06 ± 0.01	0.82 ± 0.1	0.2 ± 0
	D6S	53.9 ± 19.7	524 ± 203	0 ± 0	5 ± 5	0 ± 0	0.35 ± 0.1	0.04 ± 0.01	0.91 ± 0.37	0.1 ± 0

2.3.1.2. Fauna

Species abundance and biomass were highest in the cohesive sediments (sts. 120, 130, 780) in both years, with up to 6196 ± 3184 ind. m^{-2} representing 772 ± 440 g WW m^{-2} at st. 780 (T. 2-2). The species communities in sts. 120 and 780 were representative of the *Abra alba* community (Breine et al., 2018; Van Hoey et al., 2004), with the bivalve *Abra alba* present in nearly every sample in combination with other bivalve species such as *Kurtiella bidentata, Fabulina fabula,* and the tube building polychaete *Owenia fusiformis* (Fig. 2-2 B). Station 130, in turn, was representative of the *Limecola balthica* community (Degraer et al., 2003). In the permeable sediments (sts. 330, D6, BBEG, BRN11) values for the species metrics were lower, with abundances and biomasses between 24 ± 20 and 1317 ± 283 ind. m^{-2}, and between 1 ± 1 and 157 ± 207 g WW m^{-2} respectively. As a result, values of the functional indices BP_c (21 ± 25 - 1294 ± 689 gWW$^{0.5}$ m^{-2}) and IP_c (5 ± 5 - 2760 ± 3980 gWW$^{0.75}$ m^{-2}) were low in the permeable sediments (with the exception of BRN11 in 2017 (IP_c: 2760 ± 3980 gWW$^{0.75}$ m^{-2}, BPc: 1294 ± 689 gWW$^{0.5}$ m^{-2}), and high in the cohesive sediments (BP_c: 212 ± 186 - 6299 ± 2891 gWW$^{0.5}$ m^{-2}; IP_c: 125 ± 130 - 6014 ± 1981 gWW$^{0.75}$ m^{-2}, T. 2-2). Species in the permeable sediments generally belonged to the *Nephtys cirrosa* community (Van Hoey et al., 2004), with *Nephtys cirrosa* dominating the biomass in every sample except for the BBEG samples (Fig. 2-2 B). The amphipod species *Urothoe brevicornis* and *U. poseidonis* were present in all samples besides the BBEG and D6S samples. The amphipod species *Bathyporeia elegans* and *B. guilliamsoniana* were also absent from the latter samples, as well as from st. 330 in 2017. Macrofauna communities at D6S were poor in species, in contrast to D6N, where additional species such as the sea urchin *Echinocardium cordatum,* the hermit crab species *Diogenes pugilator,* and the polychaete species *Eteone* sp. and *Spiophanes bombyx* were recorded.

T. 2-2: Variables used for describing the biological functioning in the different stations, for successive years. Values are expressed as average ± sd, for three replicates (n = 3).

Year	Station	Irrigation Rate $L\ m^{-2}\ d^{-1}$	IP_c $gWW^{0.75}\ m^{-2}$	BP_c $gWW^{0.5}\ m^{-2}$	Abundance $ind.\ m^{-2}$	Biomass $gWW\ m^{-2}$
2016	130	3.31 ± 2.79	125 ± 130	212 ± 186	297 ± 194	10 ± 11
	780	1.17 ± 0.09	6014 ± 1981	4017 ± 1190	1443 ± 482	1035 ± 130
	BRN11	24.92	112 ± 81	269 ± 78	270 ± 178	6 ± 2
	330	2.12 ± 0.8	282 ± 132	390 ± 110	788 ± 489	9 ± 7
	BBEG	6.7 ± 3.21	5 ± 6	21 ± 25	24 ± 20	1 ± 1
2017	130	15.64 ± 2.31	2341 ± 1845	2834 ± 1678	2716 ± 2617	387 ± 267
	780	6.42 ± 0.82	4106 ± 2381	6299 ± 2891	6196 ± 3184	772 ± 440
	120	0.62 ± 0.65	1340 ± 1279	2021 ± 1192	4923 ± 701	451 ± 593
	BRN11	7.76 ± 0.33	2760 ± 3980	1294 ± 689	811 ± 106	157 ± 207
	D6N	4.98 ± 2.08	715 ± 547	831 ± 205	1317 ± 283	23 ± 14
	330	10.91 ± 8.93	24 ± 12	163 ± 119	200 ± 81	2 ± 1
	D6S	3.95 ± 1.04	40 ± 55	175 ± 215	435 ± 181	3 ± 5

2.3.1.3. Fluxes and mineralization processes

The total modelled C mineralization decreased with the permeability gradient, ranging from 168 ± 74 mmol C m^{-2} d^{-1} in muddy sediment (st. 130) to 0.21 ± 0.19 mmol C m^{-2} d^{-1} in the coarsest and most permeable sediment (st. D6S) (Fig. 2-3 A). The same pattern was observed for the estimated anoxic mineralization that exhibited large and strongly variable rates in muddy sediments (St. 130, 135 ± 75 mmol C m^{-2} d^{-1}) and extremely low rates in coarse sediment from station D6S (0.1 ± 0.1 mmol C m^{-2} d^{-1}) (Fig. 2-3 D, Table A 2 Appendix A).

The measured SCOC and the estimated oxic mineralization rates were higher in all sediments with low permeability (Fig. 2-3 B & C). The SCOC showed the highest rates in the fine sandy station 780 in both years (SCOC: 48.7 ± 2.2 mmol O2 m^{-2} d^{-1} in 2016, 57.3 ± 15.1 mmol O2 m^{-2} d^{-1} in 2017) while the oxic mineralization showed the highest rates at 780 in 2016 (35.2 ± 7.5 mmol C m^{-2} d^{-1}) and at the muddy station 130 in 2017 (43.1 ± 19.3 mmol C m^{-2} d^{-1}) (Table A 2 Appendix A).

No clear pattern along the permeability gradient was found for estimated denitrification, nitrification nor for DNRA (Fig. 2-4). In general, denitrification rates ranged between 0 ± 0 and 14.3 ± 2.6 mmol N m^{-2} d^{-1}, indicating almost no denitrification in the coarsest sediments from stations D6N and BBEG (0 ± 0 – 0.4 ± 0.6 mmol C m^{-2} d^{-1}). Nitrification and DNRA rates revealed high interannual variation, especially at the muddy station 130, where both the lowest modelled rates (Nitr: 1.3 ± 2.2 N m^{-2} d^{-1} in 2017, DNRA: 0 ± 0 N m^{-2} d^{-1} in 2016) and the highest modelled rates (Nitr: 15.3 ± 2.4 mmol N m^{-2} d^{-1} in 2016, DNRA: 12.3 ± 7 N m^{-2} d^{-1} in 2017) were estimated (Table A 2 Appendix A).

The first two components of the MFA explained 60% of the variance in the combined dataset (Fig. 2-2 D, E). The sediment variables were the dominant contributor to the first component, followed by the mineralization processes, and the species community matrix (Fig. 2-2 E). The second component was mostly related to the community structure in terms of species biomass and the mineralization processes, with a lower contribution of the sediment variables.

2.3.2. Variance partitioning

Variance partitioning indicated that the biological component ([bio] column, T. 2-3) was a significant explanatory variable of the oxic mineralization, denitrification and SCOC. The sediment subset ([sed] column, T. 2-3) was significant in explaining the estimated anoxic mineralization, denitrification, and the (log transformed) N mineralization. Except for denitrification, a substantial part (6 –49 %) of variance was explained by both the biology and the sediment as shared variance([co] column, T. 2-3). The forward selection procedure did not select any significant explanatory variables from the biological component for anoxic mineralization. Similarly, none of the sediment-related components were selected as a significant explanatory variable for nitrification. In these instances, the variable with the highest significance was chosen to run the analysis with (T. 2-3). As a result, the model for anoxic mineralization was fully composed of the sediment parameters while the model for nitrification only comprised the species component (T. 2-3).
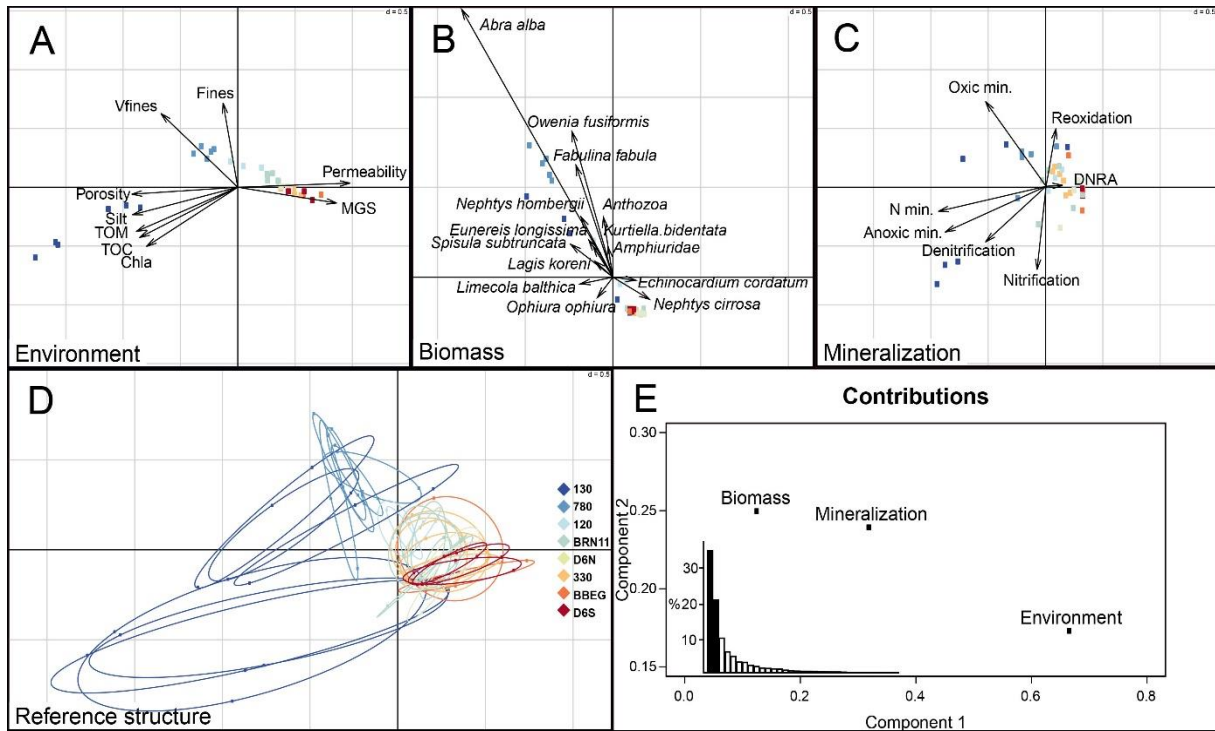
Fig. 2-2: Multiple factor analysis (MFA). A-C: Ordination of the samples based on sediment parameters (A), species biomass (B), and modelled process rates (C). D: Position of the samples for all parameter tables grouped per set of samples. A star and ellipse represent one set of samples. Ellipses are a graphical summary of the means (the reference structure), variances and the covariance of the three coordinates of the sample. Figures A-D share their coordinate system and are directionally compatible for interpretation. E: Relative influence of each table (red text) to first and second MFA components (axes); the histogram shows the relative importance of the first and second axes (black) relative to additional axes.

T. 2-3: Results of the variance partitioning procedure for the two methodologies: use of stepwise variable selection from the subset of variables selected through variance inflation testing (VIF), and the stepwise variable selection from all variables (All). [bio] and [sed] are the conditional effects of the species component and the sediment component respectively, [co] represents the jointly explained variance, and [res] the residuals of the full model [bio+co+sed]. Numbers show the adjusted R^2 for the model fractions and are in bold when significant as determined by the permutation test. (*) denotes variables that were not statistically significant ($p < 0.05$) according to the forward selection procedure but were most significant out of the set of variables.

	Variables	[bio+co]	[co+sed]	[bio+co+sed]	[bio]	[co]	[sed]	[res]
SCOC	[bio] $\sqrt{BP_c}$ [sed] Permeability, Fine	**0.50**	**0.34**	**0.53**	**0.19**	0.31	0.03	0.47
Oxic mineralization	[bio] BP_c, Species Richness [sed] Permeability, Fine	**0.64**	**0.30**	**0.64**	**0.33**	0.30	**0**	0.36
Anoxic mineralization	[bio] $\sqrt{SpRichness}$* [sed] Perm., TOM, Fine	0.06	**0.89**	**0.90**	0.0	0.05	**0.84**	0.1
Nitrification	[bio] IP_c [sed] Fine*	**0.15**	0.04	**0.12**	0.08	0.06	0	0.88
Denitrification	[bio] IrrigationRate [sed] Permeability	0.07	**0.24**	**0.32**	**0.07**	0	**0.25**	0.68
Log N mineralization	[bio] $\sqrt{BP_c}$ [sed] Permeability	0.13	**0.73**	**0.72**	0	0.13	**0.60**	0.28
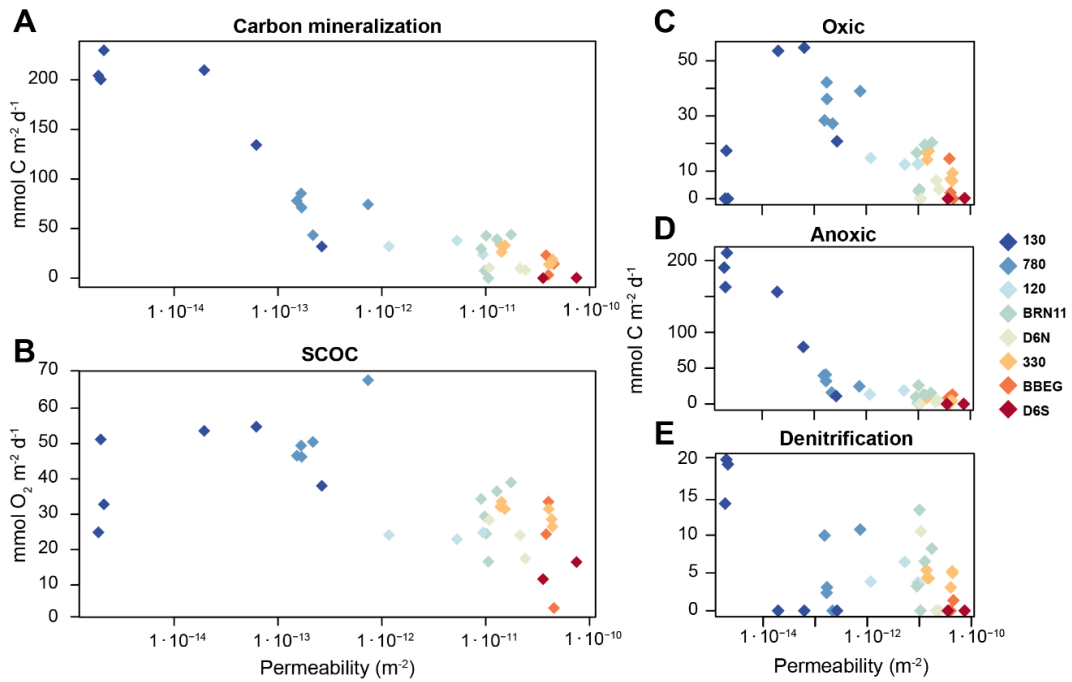
Fig. 2-3: Carbon mineralization processes: (A) Total organic carbon mineralization (mmol C m^{-2} d^{-1}); (B) Sediment community oxygen consumption (mmol O$_2$ m^{-2} d^{-1}); (C) - (E) Rate of carbon mineralization allocated to oxic or anoxic mineralization, or denitrification (mmol C m^{-2} d^{-1}). Values represented as a function of log transformed permeability (x-axis). Permeability gradient indicated by different colours (see legend).
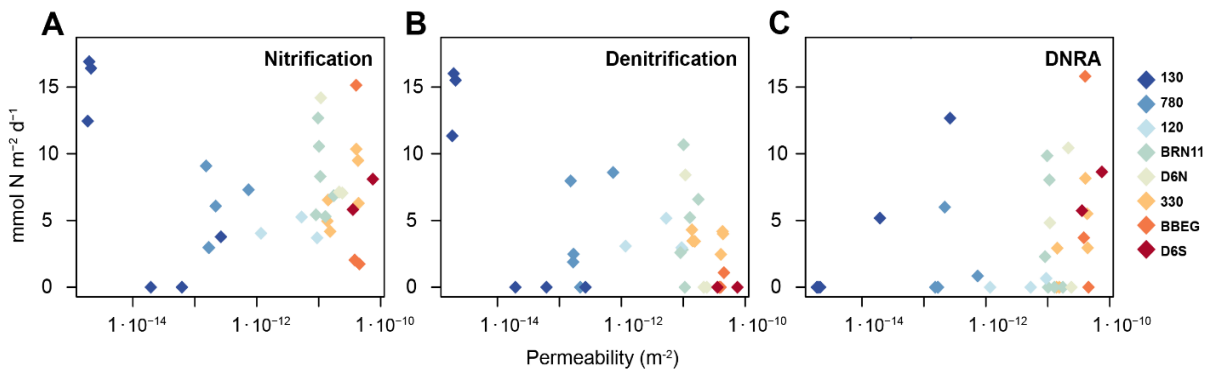
Fig. 2-4: Nitrogen cycling processes: (A) Nitrification; (B) Denitrification; (C) Dissimilatory nitrate reduction to ammonium (DNRA). Values as mmol N m^{-2} d^{-1} and represented as a function of log transformed permeability (x-axis). Permeability gradient indicated by different colours (see legend).

2.3.3. Statistical modelling

The results of the statistical models confirm that the sediment variables were particularly important in explaining anoxic processes while biological variables were particularly important in the models for oxic processes (T. 2-4). Year-to-year variability was deemed not significant during testing. Anoxic mineralization increased with TOM content while it decreased with permeability. TOM and fines were positively related to denitrification. Our models show that an increased irrigation rate had a negative effect on denitrification and anoxic mineralization and on the probability of nitrate to be consumed by denitrification rather than by DNRA.

T. 2-4: Summary of the significant (p < 0.05) predictive models for SCOC, oxic mineralization, anoxic mineralization, total N mineralization, nitrification and the probability of nitrate being transformed into nitrogen gas through denitrification. For each model, the distribution and the variance structure when applicable are detailed. The AIC and the adjusted R-squared or explained deviance when available are provided, when available.

Model	Distribution	Variance structure	AIC	Standard error
SCOC = 32.73*** -2.23 · 10^{11} Permeability* + 5.41 · 10^{-3} BP_c*** - 0.59 SpeciesRichness	Gaussian (LM)		AIC = 160 Adj R^2 = 58%	Intercept: 3.91 Perm.: 9.94 · 10^{10} BP_c: 1.12 · 10^{-3} Sp. richness: 0.32
Oxic mineralization = 4.08*** + 7 · 10^{-3} BP_c*** - 1.29 10^{11} Permeability – 0.42 SpeciesRichness	Gaussian (GLS)	Power of variance covariate ~ Permeability	AIC = 276	Intercept: 2.71 BP_c: 1 · 10^{-3}
Anoxic mineralization = 7.72 *** - 3.37 · 10^{11} Permeability*** + 14.64 TOM*** - 0.16 IrrigationRate***	Gaussian (GLS)	Exponential of variance covariate ~ TOM | Station	AIC = 265	Intercept: 1.25 Perm.: 0.03 TOM: 1.88 Irr.: 0.02
N mineralization = 3.96*** - 7. 66 · 10^{10} Permeability*** + 3.01 TOM*** + 8.25 · 10^{-4} BP_c * - 7.89 · 10^{-2} IrrigationRate*	Gaussian (GLS)	Different standard deviation ~ Station	AIC = 214	Intercept: 0.53 Perm.: 1.66 · 10^{10} TOM: 0.49 BP_c: 3.34 · 10^{-4} Irr.: 3.39 · 10^{-2}
Nitrification = 0.11*** + 3.13 · 10^{-5} BP_c*	Gamma (GLM)		AIC = 210 Explained Deviance = 6%	Intercept: 0.02 BP_c: 1.20 · 10^{-5}
Denitrification = 2.71 + 1.40 TOM*** + 0.10 Fines* - 0.27 IrrigationRate* - 1.08 · 10^{-3} IP_c*	Gaussian (LM)		AIC = 105 Adj R^2 = 46%	Intercept: 1.54 TOM: 0.28 Fines: 0.04 Irr.: 0.12 IP_c: 0.41 · 10^{-3}
Den / Den + DNRA = 1.25* - 0.17 IrrigationRate*	Binomial (GLM)		AIC = 46 Explained Deviance= 16%	Intercept: 0.5 Irr.: 0.07

Significance of terms (* P < 0.05, ** P < 0.01, *** P < 0.001)

The sediment reworking activity of the macrobenthos, estimated by BP_c, enhanced all three modelled oxic processes: SCOC, oxic mineralization and nitrification. The SCOC was also negatively correlated to the permeability. Finally, the variance in total N mineralization was explained both by sediment variables (permeability and TOM) and by biological variables (BP_c and irrigation rate).

2.4.   Discussion

2.4.1.   Spatial patterns

Our results indicated a clear link between the sedimentary environment, the sediment-inhabiting fauna and the estimated biogeochemical rates. All these properties varied substantially within the study area, notably changing along a gradient from cohesive sediments with high mineralization rates (sts. 120, 130, 780), to permeable sediments with low mineralization rates (D6, BBEG, 330, Fig. 2-2).

The reported oxygen consumption rates (14 – 57 mmol O_2 m^{-2} d^{-1}), nitrification (1 – 15 mmol N m^{-2} d^{-1}), and denitrification (0 – 14 mmol N m^{-2} d^{-1}) were generally in line with those found previously in the area (Braeckman et al. 2014) and other coastal North Sea stations (Bratek et al., 2020; Marchant et al., 2016). Nitrification and denitrification rates reported from the German Bight, a nearby coastal environment characterized by a high deposition rate, were also in line with the values obtained during the present study (Neumann et al., 2017).

The high estimated total mineralization rates in cohesive sediments (31–213 mmol C m^{-2} d^{-1}) were not matched by similar oxygen consumption rates (Fig. 2-3 A). Especially in St. 130, DIC fluxes were exceptionally high, opening up the possibility that the steady state assumption for the mass balance model was not met for these samples, given these high fluxes could result from increased respiration stimulated by high temperatures during transport. The steady-state assumption does not imply that nothing is changing in the sediment at all, but that changes in time of solid and liquid constituents (nutrient fluxes, the porewater concentrations, and solid substances in the sediment) are much smaller than the process rates themselves, so that they can be ignored. Given the otherwise acceptable agreement between the SCOC and DIC fluxes, and time elapsed since the peak organic matter deposition, we expect this assumption to have been fulfilled in the other stations.

In permeable sediments on the other hand, often more oxygen was consumed (13 – 32 mmol O_2 m^{-2} d^{-1}) than needed for mineralization alone (0.2 – 31 mmol C m^{-2} d^{-1}), with a larger allocation of the SCOC to nitrification, and the reoxidation of reduced products of anoxic mineralization.

We observed a shift from denitrification to DNRA as the main NO_3^- consuming process (up to 100 %) towards more irrigated sediments (Table A 2, Appendix A). This is consistent with previous studies, where maximal rates for DNRA in permeable sediments were 50 % and 77 % of the total NO_3^- consumption based on field cores (Hellemann et al., 2020) and slurry experiments (Behrendt et al., 2013) respectively. DNRA is performed by many anaerobic prokaryotes, but has been shown to occur in eukaryotes as well (Kamp et al., 2015). In permeable sands, advective flows can rapidly transport algal cells such as diatoms deep in the sediments (Huettel and Rusch, 2000), where temporary anoxia, or dark conditions, along with sufficient concentrations of NO_3^- could induce nitrate reduction by diatoms, to survive dark conditions (Kamp et al., 2011). With denitrification strongly dependent on the organic matter content of the sediment (T. 2-4), our observations suggest that DNRA increases in importance relative to denitrification when high nitrate concentrations are available (e.g. by ventilation activity, which favors both DNRA and denitrification), but where concentrations of organic matter to mineralize are lower (disfavoring denitrification, since this is strictly heterotrophic).

Alternatively, it is possible that the increasing irrigation rate promotes nitrogen fixation by bringing N_2 rich water deeper in the sediment. Nitrogen fixation transforms N_2 into NH_4^+, and appears to be more important than previously believed in marine sediments (Bertics et al., 2010; Newell et al., 2016a). Fan et al. (2015) showed that N_2 fixation occurs in Southern North Sea sediments, and exhibits similar rates as denitrification, with highest N_2 fixation rates observed in permeable sediments. N_2 fixed in the sediment would end up in both measurable NH_4^+ effluxes from the sediment and in biomass (and through biomass degradation to NH_4^+ concentrations) (Newell et al., 2016b). Hence, part of the NH_4^+

production in the model may be due to N_2 fixation, and part of the NO_3^- consumption by denitrification, as opposed to DNRA. However, additional measurements (e.g. of the N_2 flux), would have been needed to constrain the N_2 fixation process in the mass balance model. As is, the inclusion of DNRA, and the differentiation between oxic and anoxic mineralization are already useful improvements over previous applications of the mass balance approach (Soetaert et al., 1996; Braeckman et al., 2010, 2014). Given that only a few studies exist which describe DNRA, nitrogen fixation and anammox (anoxic ammonium oxidation) for the southern North Sea (e.g. Bale et al., 2014; Fan et al., 2015; Lipsewers et al., 2014), it would be of high interest to perform dedicated microbial and ^{15}N stable isotope research, to better understand the abiotic and biotic factors regulating the relative occurrence of these N-cycling processes in temperate coastal areas.

2.4.2.   Respective roles of macrobenthos and sediment characteristics in C and N cycling

Variance partitioning and multiple linear regression both showed that oxic processes were mainly related to faunal activities, whereas anoxic processes were more determined by sediment characteristics. Denitrification was significantly linked to both components. Moreover, the interaction between faunal and abiotic components was of prime importance for all modelled processes except denitrification.

2.4.2.1.   Faunal activities play a major role in C and N cycling

The key role that macrobenthos activity plays in benthic mineralization processes is well described (e.g. Braeckman et al., 2014; Kristensen, 2001; Volkenborn et al., 2016). In our study, we used the Bioturbation Potential (BP_c) and the Irrigation Potential (IP_c) of the community as proxies for two types of faunal activity, respectively particle reworking and burrow ventilation. Variance partitioning showed that BP_c explained a considerable amount of variance in oxic processes, and BP_c was selected in regression models for SCOC, oxic mineralization, total N mineralization, and nitrification (T. 2-4). Particle reworking enhances SCOC, by mixing buried reduced compounds back into the oxic zone of the sediment, where they are reoxidized (Aller, 1977). At the same time, bioturbators fragment organic matter and disperse it from the sediment-water interface where it originally settled, to a larger volume of sediment. This makes it more accessible to micro-organisms, and results in increased mineralization rates, both oxic and anoxic (van Nugteren et al., 2009; Canfield et al. 1993; Thamdrup et al. 1994).

While burrow ventilation fuels oxic mineralization and nitrification by bringing electron acceptors (e.g. O_2, NO_3^-) deeper in the sediment (Aller and Aller, 1998; Banta et al., 1999), the IP_c index was *not* selected as an explanatory variable, despite previous findings that stressed the importance of burrow ventilation (Mermillod-Blondin et al., 2004; Braeckman et al., 2010; Wrede et al., 2018). We suspect this could be due to different reasons. First, the IP_c index might not be an accurate estimation of the burrow ventilation rate. De Borger et al. (2020) indeed showed that IP_c correlates more strongly to the burrow ventilation depth than to the ventilation rate and our results do not indicate any correlation between the IP_c index and the measured irrigation rate (Appendix A). Second, BP_c and IP_c represent faunal activities that affect sediments at different timescales. Both functional indices represent the *potential* to express an activity, but they do not include the temporal dynamics of the activity. Temporal variation is strongly pronounced for ventilation as animals do not ventilate constantly (Volkenborn et al., 2016), and the

downward transported electron acceptors (e.g. oxygen) are rapidly consumed, leading to anoxic sediment again. As such, the stimulation of oxic mineralization processes takes place at short temporal scales, which is not taken into account in the IP_c formulation. Temporal dynamics are less pronounced for particle transport. Though organisms do not move constantly either, bioturbation displaces particulate organic matter to deeper layers, where it is mineralized over a much longer timeframe relative to the quasi-instantaneous consumption of oxygen, thus generating a longer lasting effect. We believe that IP_c could be more useful in predicting biogeochemical processes if a metric for temporal dynamics were included in the index.

Our results do not support the common idea that ventilation increases rates of coupled nitrification-denitrification (Pelegri et al. 1994; Rysgaard et al., 1995; Na et al., 2008; Volkenborn et al., 2016). Indeed, nitrification rates were strongly and positively related to faunal activities, but denitrification rates were negatively correlated to the irrigation rate and to IP_c (T. 2-4). Irrigation brings both nitrate and oxygen in the pore water at depth. Nitrification is then enhanced as oxygen serves as an electron acceptor but the high oxygen concentration or the low OM availability might inhibit denitrification (Bergaust et al. 2012). Similar patterns have been observed before. For example, *Trypaea australiensis* (a marine ghost shrimp) which constructs deep burrow systems and exhibits high particle transport and ventilation rates has been shown to stimulate nitrification, without affecting rates of denitrification. This uncoupling of nitrification and denitrification was probably due to larger spatial separation between nitrification and denitrification zones (Jordan et al., 2009).

Unlike denitrification, the importance of DNRA increased in well-irrigated sediments (Model of Denitrification / (Denitrification + DNRA), T 2-4) which results in the retention of reactive nitrogen in the marine environment. It is unclear why the ventilation rate would influence the balance between DNRA and denitrification in this way. We speculate that DNRA is more efficient to deal with oxic conditions than denitrification. Indeed, Roberts et al. (2014) showed that the contribution of DNRA to nitrate reduction increased from <1% in anoxic conditions to 18% in oxic conditions.

2.4.2.2.   Permeability, an important environmental variable for C and N cycling

At first sight, the high importance of permeability in our study is in contrast with the well-established idea that fauna plays an important role in the benthic biogeochemistry. Other studies using variance partitioning techniques have reported a more balanced importance of biotic and abiotic variables in ecosystem functioning (Godbold and Solan, 2009; Belley and Snelgrove, 2016; Mestdagh et al., 2020). However, these studies focused on a narrow part of the permeability gradient (MGS 20 – 332 µm), where faunal activities play a more important role in mineralization processes than in truly permeable sediment (Braeckman et al., 2014). The importance of permeability in explaining biogeochemical processes in permeable sediments has been highlighted before (Huettel et al. 2014), but our study is the first to show the importance of permeabilty for total carbon and nitrogen mineralization along such a wide gradient of permeability.

Permeability alone explained 60% of the variability in total N mineralization (T. 2-3). The oxic part of mineralization was mainly related to faunal activities, but the variability in anoxic mineralization and

denitrification, which together account for more than half of the total mineralization in most stations, was mainly explained by sediment characteristics (respectively 84% and 25%), with permeability as the main selected variable (T. 2-3). Permeability is a key factor for ecosystem functioning as it affects oxygen and food availability in the sediment, but it is also a structuring factor of the habitats and microbial communities (Seitzinger et al., 2006; Probandt et al., 2017). Indeed, sediments characterized by low permeability, high percentage of TOM and a high percentage of fine sands (125 – 250 µm) create a favourable environment for denitrifiers and in particular sulphate reducers (Seitzinger et al., 2006; Al-Raei et al., 2009; Probandt et al., 2017).

In addition to permeability, the total organic matter content was an important environmental variable for anoxic mineralization, denitrification and the total N mineralization (T. 2-4). This is not unexpected, since a higher OM content will trigger higher mineralization rates, hence lead to oxygen depletion. Despite similar bottom water chl *a* concentrations in the study area at the end of summer (Braeckman et al., 2014), the OM content tends to be lower in coarse permeable sediment, which probably indicates that most of the OM is already recycled at the end of summer in those highly active sediments (Huettel et al., 2003; Rasheed et al., 2003), or is less efficiently retained by sediment particles. Therefore, it would be interesting to investigate the relationship between permeability and mineralization processes in different seasons, to be able to determine the impact of permeability throughout the year.

2.4.3. Sediment – fauna interactions

The sediment properties and the inhabiting benthic fauna are closely related, as variance partitioning showed considerable covariance between both in the models for SCOC, oxic mineralization, and total N mineralization (T. 2-3). This is in line with results of other studies using variance partitioning (Godbold and Solan, 2009; Belley and Snelgrove, 2016; Mestdagh et al., 2020), where shared variability between biotic and abiotic factors remained present as a predictor for benthic biogeochemistry.

Benthic communities are strongly associated to certain ranges of sediment characteristics, such as median grain size, and the mud content, which are linked to water column processes that govern food availability and hydrodynamic stress (e.g. Llobet-Brossa et al., 1998, 2002; Degraer et al., 1999; Van Hoey et al., 2004; Vanaverbeke et al., 2011). Moreover, different sediment types impose different constraints on the fauna, resulting in a variable expression of effect traits along a range of habitats. We found high values for both BP_c and IP_c in fine sandy – muddy sediments, and lowest values in the most permeable, coarse sediments (T. 2-1, T. 2-2). Braeckman et al. (2014) similarly demonstrated that BP_c was a major predictor of SCOC and NH_x exchange in fine sandy sediments, and to a lesser extent in muddy and permeable sediments. While the higher values of the functional indices in finer sediment are partly attributed to higher faunal biomass, the functional traits of only few species in permeable sediments (e.g. the sea urchins *Echinocardium sp.* and the polychaetes *Nephtys sp.*, Appendix A) attain high values which contribute markedly to the index scores.

In permeable sediments, macrofauna tend to have response traits that make them more adapted to stronger hydrodynamic pressures, while they are less constrained by low oxygen availability than species in cohesive sediments (Vanaverbeke et al., 2011). Whereas ventilation rates were of similar magnitude

in permeable and cohesive sediments (T. 2-2), our measurements do not separate faunal burrow ventilation from physical ventilation. In permeable sediments, local hydrodynamics induce advective porewater flows that overwhelm animal pumping activities (Kristensen and Kostka, 2013; Huettel et al., 2014). It is thus difficult to provide statements about the actual ventilation rates in permeable sediments, based on organism trait scores alone. In cohesive sediments however, solute exchange with the overlying water is limited to the scale of a few millimetres by diffusive transport, which makes burrow ventilation and particle transport interesting processes from the organismal point of view to replenish oxygen and food supply, and remove metabolites (Aller and Aller, 1998; Meysman et al., 2006; Volkenborn et al., 2016).

As such, our results show the usefulness of using effect traits as predictors for ecosystem processes, but similarly highlight the caveat of interpreting them when calculated without proper consideration of environmental steering. This again shows that the use of functional trait indices is likely of little use without associated investigation of metrics of ecosystem functionality (Bolam and Eggleton, 2014).

2.4.4. Understanding the impact of anthropogenic activities on mineralization processes

Three of the studied stations were more strongly impacted by human activities. Station BRN11 is located in an abandoned sand extraction area, and stations D6N and D6S are situated 200 m north and south from an offshorewind turbine (Fig. 2-1). In this section, we discuss how environmental changes triggered by anthropogenic activities impact estimated mineralization rates and how the models that we applied could be a useful tool to understand those impacts.

We observed that stations experiencing anthropogenic impact were highly variable in time (BRN11) and in space (D6N & D6S). Compared to the situation in 2016, sediment from BRN11 in 2017 had higher fine sand and silt fractions, lower permeability and higher chl a content (T. 2-1). In addition, the macrobenthic community was much more diverse; and associated BP_c and IP_c were higher (T. 2-2). The irrigation rates were quite similar. Comparable differences were observed between D6N (finer sediment, richer in chl a and fauna) and D6S, although only 400 meters apart.

The reasons for the observed sedimentary and biological changes are unclear. At BRN11, the temporal changes following the closure of the site could be attributed to ongoing sand extraction activity in the vicinity, to the migration of sand dunes, or a combination of both, that contribute to fining of the sediment in the extraction pit (Degrendele & Vandenreyken, 2017; De Backer, pers. obs.). The spatial differences observed around wind turbine D6 could be due to altered local hydrodynamics linked to the presence of the turbine (Rivier et al., 2016; Legrand et al., 2018) or to the position on the sand wave (Cheng et al., 2020), in combination with the deposition of (pseudo)faeces by filter feeders living abundantly on the turbine (Coates et al., 2013; Baeye & Fettweis, 2015).

Regardless of the exact causes, these results tend to suggest that sediment fining causes a shift in the macrobenthos community, and enhances the estimated mineralization processes, as shown by higher oxic and anoxic mineralization rates in the finer-grained stations (Fig. 2-3). Our regression models (T. 2-4) have proven to be useful in understanding these impacts. For instance, the increased potential of

the community to rework particles along with the lower permeability in the finer-grained stations explain their enhanced oxic mineralization rates (Oxic mineralization model, T. 2-4).

The models developed here are a major step forward towards predicting and scaling up the effects of anthropogenic activities on different ecosystem functions in shallow North Sea sediments, which is crucial to support scientifically sound ecosystem management.

2.5.   Conclusions

In this study, we disentangled biotic and abiotic driving forces of benthic biogeochemical processes by applying variance partitioning on biogeochemical rates obtained via a mass balance model. While oxic processes were mainly regulated by faunal activities and advective processes in permeable sediments, anoxic mineralization was controlled by sediment characteristics. However, for processes such as denitrification, the sediment and its inhabiting fauna were too strongly linked to be separated. As a result, we showed that organism traits are useful to predict biogeochemical processes but should be interpreted in the right ecological context. Regression models were derived to estimate biogeochemical processes as a function of biotic and abiotic variables. They may prove to be a useful tool to understand the impact of anthropogenic activities and provide a step towards predicting and scaling up their impact on ecosystem functions.

Acknowledgements

Chapter 3. Rapid organic matter cycling in North Sea sediments

Emil De Borger, Ulrike Braeckman, Karline Soetaert

Abstract

Coastal shelf seas are zones of intense nutrient cycling, where a strong coupling between the sediment and the water column enhances primary productivity. To identify factors that control the strength of this benthic-pelagic coupling we measured sediment characteristics, solute fluxes, and porewater nutrient profiles in spring along a south - north transect in the North Sea crossing distinct regions: the shallow Oyster Grounds closest to the Dutch shore, the shallow Dogger Bank, the 80-m deep central North Sea, and the 150-m deep Fladen Grounds between the north of Scotland and Norway. The data were used to constrain rates of different mineralization processes (e.g. denitrification, oxic mineralization) and bioturbation with the 1-D diagenetic model (OMEXDIA). Surprisingly, we found smaller differences in the biogeochemical signature along the 670 km long North Sea transect than expected, as sediments ranged in median grainsize from 25 to 217 μm, and permeability ranged > 3 orders of magnitude. Total carbon mineralization ranged between 4 - 13.5 mmol C m^{-2} d^{-1}, and decreased significantly towards the north. Oxic mineralization was the dominant mineralization process in all studied sites. Finest, least permeable sediments were found in the Fladen Grounds where highest denitrification rates were recorded, linked to high nitrate concentrations in the overlying water. The coarsest, most permeable sediments of the shallow Dogger Bank represented a transition area between the Oyster Grounds, where oxic mineralization was highest (75 - 90 %), and the central North Sea samples, where anoxic mineralization increased relative to oxic mineralization due to higher bioturbation rates (oxic: 59 - 72 %, anoxic: 27 - 39 %). Overall, denitrification rates increased, while phosphorus removal tended to decrease towards the north. This contrasting behaviour in nitrogen and phosphorus removal was identified as a possible cause for decreasing DIN:DIP ratios in the water column towards the north.

3.1. Introduction.

Every spring, when irradiance and temperatures increase in the surface waters of coastal seas in temperate and higher latitudes, inorganic carbon and free nutrients are captured as organic matter in vast algae blooms. Part of this organic matter settles on sediments, where it is remineralized into free

nutrients, or buried in deeper sedimentary layers by a set of chemical, physical, and biological processes, collected under the term "early diagenesis" (Boudreau, 2000). Shelf seas account for up to 80 % of global benthic mineralization, despite covering only 7 % of the seafloor (Wollast, 1998). More so, shelf sediments account for an estimated third of all nitrogen loss from the global ocean through denitrification (Middelburg et al., 1996) and for 50 - 84 % of total phosphorus burial, making these regions crucial in the regulation of eutrophication (Galloway et al., 2004; Seitzinger et al., 2006; Slomp, 2011).

The North Sea is a shelf sea bordering the NE Atlantic, with a surface area of about 575 000 km^2, where shallow waters in the south (~ 40 m) make way for deeper waters towards the north (> 80 m). With the exception of the Norwegian trench (725 m), depths do not exceed 250 m (Fig. 3-1). Bordered by several industrialized nations, the North Sea receives considerable nutrient input through river discharge and, though on the decline, this input heavily affects nutrient levels in the coastal zone (Burson et al., 2016; Lenhart et al., 2010). Further offshore, nutrient levels are more regulated by input of Atlantic waters (Lenhart et al., 2010).

Organic matter deposition is strongly dependent on algae blooms, which are estimated to produce on average 180 g C m^{-2} y^{-1} of organic matter (van Leeuwen et al., 2013). The main phytoplankton bloom occurs in April - May, and is strongest in the nutrient rich, well mixed waters of the southern part of the North Sea, and along the eastern boundary (Fig. 3-1). In the more central and northern, stratified, regions of the North Sea, surface nutrients are rapidly consumed during the initial phytoplankton bloom, and are not replenished until autumn when waters get mixed again through advective overturning and storm events (Van Haren et al., 2003; Tijssen and Wetsteyn, 1984). A deep chlorophyll maximum (DCM) then forms near the thermocline, on the condition that this is within the euphotic zone. Here together with light, nutrients from the deeper, mixed water column are accessible to fuel primary productivity throughout the summer (Weston et al., 2005; van Leeuwen et al., 2013).

This primary production is predominantly deposited near the production sites, but it also gets transported through successive deposition-resuspension events (Van Raaphorst et al., 1998). The dominant counterclockwise residual currents transport fine-grained, organic matter rich material from the highly dynamic Southern Bight, along the eastern boundaries, towards the Skagerrak. As a consequence of this water circulation pattern, the reactivity, or "freshness" of deposited organic matter decreases towards the site of final deposition, the Skagerrak, relative to the initial production site (Dauwe and Middelburg, 1998). These patterns of deposition broadly correspond to the sediment composition. Recently published synthetic maps of several sediment-related variables (Wilson et al., 2018), highlighted the general shift in particle size when moving from the highly dynamic southern North Sea, where finer sediments are resuspended, towards the deeper northern North Sea.

The sediment composition and its resulting permeability (among others) regulate the magnitude of solute transport processes, the oxygen penetration depth, and the structure of microbial communities (Probandt et al., 2017; Ahmerkamp et al., 2020). In coarse grained sediments, organic matter is rapidly mineralized, because of the high availability of oxygen, the most efficient electron acceptor, penetrating deeply in the sediment matrix (Glud, 2008; Huettel et al., 2014). These sediments are characterized by

relatively high oxygen consumption rates, but low stocks of organic carbon (Braeckman et al., 2014; Brenner et al., 2016). In fine-grained cohesive sediments on the other hand, organic matter is trapped between sediment grains, and oxygen penetrates mere millimetres, resulting in a higher proportion of anoxic mineralization and a build-up of organic carbon (Jørgensen, 1982; Canfield et al., 1993). At the same time however, decomposition in the water column is expected to decrease the deposition of organic matter with increasing water depth (Brenner et al., 2016; Middelburg et al., 1997).

Denitrification is similarly regulated by deposition rates for the most part, with highest rates of denitrification expected where intermediate (4 - 9 mmol C m^{-2} d^{-1}) mineralization rates occur (Soetaert et al., 2000), due to the balance between sufficiently low oxygen availability to prevent inhibition of denitrification, but high enough to have nitrate available, and sufficient carbon availability to allow mineralization to proceed (Cardenas et al., 2008).

In recent decades, phytoplankton blooms in the North Sea occur earlier in the year, and phytoplankton production has decreased notably in areas under riverine influence. While this is likely due to de-eutrophication, decreasing trends are also seen for areas further away from the coast (Capuzzo et al., 2018; Desmit et al., 2019). North Sea sea surface temperature (SST) has increased by 1.6 °C between 1971 and 2014, and warming of surface waters affects the stratified regions further away from shore such as the central North Sea, with declines in phytoplankton biomass as a result (Holt et al., 2016; Desmit et al., 2019).

Given this range of controls on mineralization processes, a thorough understanding is needed to anticipate future changes to benthic nutrient cycling, for example caused by decreased carbon inputs or human induced changes to sediment characteristics. However, the sediment biogeochemistry is poorly characterised for large areas of the North Sea, such as the central North Sea northwest of the Dogger Bank, or the Fladen Grounds, where only a handful of studies have reported measurements (Fig. 3-1) (Upton et al., 1993; de Wilde et al., 1986; Brenner et al., 2016; Rosales Villa et al., 2019).

The aims of the study were to characterize the *in situ* response of regions with differing sedimentological, characteristics in the North Sea to the deposition of fresh organic matter, and to isolate potential driving factors behind observed differences in biogeochemical functioning. Shipboard incubations of sediment cores were performed to derive solute fluxes, and porewater profiles were established. A diagenetic model was subsequently used to derive rates of organic matter mineralization processes.

3.2. Materials and Methods

3.2.1. Study area

During the NICO-10 research expedition (Netherlands Initiative Changing Oceans, leg 10, 25th of May 2018 - 5th of June 2018) sediments were sampled from aboard the RV Pelagia at 11 stations along a 670 km long transect, from station "Oyster Grounds 100" (54.1494° N, 4.3419° E) near the Dutch coast, to station "Fladen Grounds 770" (59.4167° N, 0.4222° E) in the NW of the North Sea (Fig. 3-1, T. 3-1). In what follows, numbers in the station names indicate the distance travelled away from shore along the transect. This transect crossed multiple zones of interest: the Oyster grounds (OG, sts. O.100, O.135,

O.190), the Dogger Bank (DB, D.240), the central area from the north of the Dogger Bank up to the deepest station, Devils Hole (sts. C.300, C.380, C.450, C.545), and the Fladen Grounds in the north (sts. F.640, F.695 and F.770). The Oyster Grounds is an area with maximal water depths of 50 m, with well mixed water in winter, and stratified conditions in summer (Greenwood et al., 2010). The Dogger Bank is a 260 km long shallow sand bank with water depths of 20 - 40 m. Northward from this area the seabed slopes down to a more or less constant depth of 80 m, except for the > 260 m deep depression called "Devils Hole". In this area and further northward, waters are stratified from spring onwards, with continuously mixed conditions in winter (van Leeuwen et al., 2015). Towards the Fladen Grounds there is a further increase in depth (100 - 150 m), where seasonal variations in temperature of these deeper bottom waters are small. Published estimates for primary productivity in these regions are fairly similar, and range between 100 – 250 gC m^{-2} y^{-1} on the Oyster Grounds (Gieskes and Kraay, 1984; Joint and Pomroy, 1993), 270 gC m^{-2} y^{-1} for a stratified site in the central North Sea (Weston et al., 2005), and 150 – 200 gC m^{-2} y^{-1} for the Northern North Sea (Reid et al., 1990).
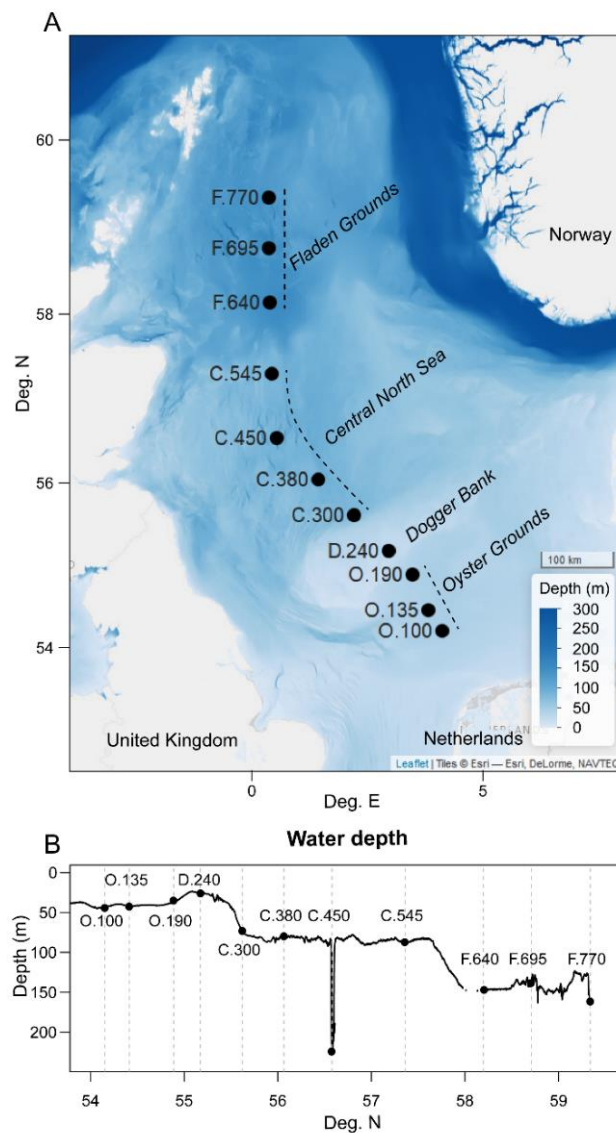
Fig. 3-1: (A) Stations sampled in the North Sea during the NICO 10 research campaign. (B) Water depth along the transect in latitudinal direction.

T. 3-1: Sampling dates (2018) and locations of stations, and bottom water concentrations.

Station	Sampling date	Latitude (Deg. N)	Longitude (Deg. E)	Depth (m)	PO_4^{3-} (mmol m^{-3})	NH_4^+ (mmol m^{-3})	NO_3^- (mmol m^{-3})	O_2 (mmol m^{-3})
O.100	June 5	54.14938	4.341914	45	0.6	3.0	1.5	230
O.135	June 4	54.41973	4.046748	43	0.4	1.5	0.9	253
O.190	June 3	54.87539	3.686554	41	1.0	5.7	3.6	281
D.240	May 25	55.17374	3.161264	26	0.3	6.8	0.7	290
C.300	June 2	55.62316	2.384164	72	0.7	4.4	1.1	201
C.380	June 1	56.06932	1.599237	79	1.3	5.7	3.7	255
C.450	May 26	56.58769	0.685672	224	1.1	32.8	5.2	294
C.545	May 31	57.36059	0.579088	84	1.1	5.4	5.5	253
F.640	May 27	58.20097	0.525871	148	1.8	6.0	11.1	251
F.695	May 29	58.83913	0.511693	135	1.5	6.0	8.5	248
F.770	May 30	59.41514	0.509838	135	3.1	3.8	8.8	237

3.2.2. On-board incubations

Sediments were sampled using a stainless steel NIOZ boxcorer (30 cm ID, 50 cm height), specially designed for on-board sediment measurements as the entire sediment sample can be incubated. At each location three intact boxcores were collected. The sediment surface in the boxcores was inspected for intactness, and subsequently covered with a Plexiglas lid with sampling ports and a built-in Teflon coated magnetic stirring motor that kept the overlying water homogenized. Bottom water (±5 m above the bottom) collected from NISKIN bottles was added to each boxcore to seal the sample airtight. The samples were then placed into large buffer tanks that maintained constant temperature (~ bottom water temperature of 11 °C) and were kept in the dark to prevent photosynthetic activity. To determine the sediment oxygen consumption rates, the oxygen concentration in the water overlying the sediment was monitored (1 Hz) with optode sensors (FireStingO2, Pyroscience). A two-point calibration of the sensors was conducted prior to measurements, using 100 and 0 % oxygen saturated seawater to represent water column and anoxic O_2 concentrations, respectively.

The samples were left to acclimatize for a period of two hours, before starting nutrient flux measurements. Five water samples were collected for flux measurements over a period of 48 hours. Nutrient samples were collected by extracting a volume of 50 mL from the overlying water, while simultaneously injecting the same amount of bottom water through a second sampling port to prevent air intrusion. Five mL of this volume was used for nutrients (ammonium (NH_4^+), nitrate (NO_3^-), nitrite (NO_2^-), phosphate (PO_4^{3-}), filtered through a 0.45 µm syringe filter), and 10 mL for dissolved inorganic carbon (DIC, 10 mL headspace vials). Nutrient samples were stored at -20 °C, DIC samples were poisoned with 1 µL of saturated $HgCl_2$ per mL sample for preservation, and placed into a 4 °C refrigerator. Upon thawing, nutrient samples were analysed in the lab, by a SEAL QuAAtro segmented flow analyser (Jodo et al., 1992). DIC analysis was performed using a segmented flow analyser (San++ SKALAR) following Stoll et al. (2001). Quality control of output from the flow analyzers is routinely performed with reference material from Osil and Quasimem (nutrients) and University of California

San Diego (DIC). Fluxes (in mmol m^{-2} d^{-1}) were calculated by fitting a linear regression through the concentration time series, and multiplying the regression coefficient by the height of the overlying water to convert from volumetric to surface standardized rates. If the regression was not significant (i.e. $p > 0.1$), the flux was interpreted as 'zero'. For oxygen fluxes the same method was applied to a consistently decreasing section of the oxygen concentration data.

At the end of the incubation period, several subsamples were collected from each boxcore to determine: sediment porosity and grainsize (2 cm of top sediment, Ø 2 cm), sediment organic carbon and nitrogen (2 cm of top sediment, Ø 2 cm), sediment permeability ($\sim$ 15 cm of sediment, Ø 3.6 cm), porewater nutrient profiles ($\sim$ 20 cm of sediment, Ø 10 cm Plexiglass sampling core), and oxygen microprofiles (Ø 5 cm Plexiglass sampling core).

3.2.3. Water column nutrient and chl *a* samples

To determine chlorophyll a (chl *a*) concentrations in the water column, NISKIN bottles were closed 3 m below the water surface, at the deep chlorophyll maximum (observed from CTD casts), and 5 m above the seafloor. Water samples were vacuum filtered over GF/F filters, and flash-frozen in liquid nitrogen before storage at -80 °C. In the laboratory, photosynthetic pigments were extracted from the filters using a 90 % acetone dilution (Wright, 1991), and quantified through high performance liquid chromatography (HPLC; Zapata et al., 2000). Only chl *a* concentrations are discussed in this work. From the sea floor NISKIN samples, subsamples for DIC and nutrients were taken to characterize bottom water concentrations.

3.2.4. Subsample processing

Porewater nutrients were extracted from the sediment subsamples using rhizon samplers (0.15 µm pore size, Rhizosphere Research Products) at 1 cm depth intervals for the first 8 cm, and then at 2 cm intervals down to 12 cm. The rhizons were inserted into the sediment core through pre-drilled holes in the core wall, and a maximum of 4 mL of porewater was extracted from each interval by connecting a 5 mL syringe and creating a vacuum (Seeberg-Elverfeldt et al., 2005; Dickens et al., 2007; Shotbolt, 2010). Porewater nutrient samples were stored and analysed in the same way as the water nutrient samples.

Sediment grain size was determined by laser diffraction on freeze-dried and sieved (< 1 mm) sediment samples in a Malvern Mastersizer 2000 (McCave et al., 1986). Water content was determined as the volume of water removed by freeze drying wet sediment samples. The sediment density was determined by measuring the water displacement of a given weight of dried sediment. Sediment porosity was determined from water content and solid phase density measurements, accounting for the salt content of the pore water. The Corg/N ratio was calculated from total Corg and N concentrations, determined using an Interscience Flash 2000 organic element analyser. Sediment permeability was determined using a permeameter (Buchanan, 1984).

Clark-type O_2 micro-electrodes (50 µm tip diameter, Unisense) were used to measure oxygen-depth profiles in the sediment (Revsbech, 1989). In each sediment core, up to three replicate profiles were taken from different areas of the sediment. For each profile, readings were taken at 100 µm intervals, starting 2000 µm (2 mm) above the sediment-water interface (water aerated to 100% O_2 saturation before

the experiment) down to the depth in the sediment at which all oxygen was depleted, the maximum oxygen penetration depth (OPD). A two-point calibration was conducted prior to measurements using 100 and 0 % oxygen saturated seawater to represent water column and anoxic O_2 concentrations, respectively. Note that profiles were only measured up to 1 mm for the coarse sandy station D.240.

3.2.5.   Biogeochemical modelling

3.2.5.1.   Model structure

Modelling of steady state sediment biogeochemistry was conducted with the OMEXDIA diagenetic modelling framework (Soetaert et al., 1996a), extended to include simplified phosphorus dynamics (Ait Ballagh et al., 2020) in line with the model of Slomp et al. (1996). This diagenetic model describes the dynamics of organic matter degradation on a 1D grid down to 100 cm deep, consisting of 100 layers, and with increasing layer thickness starting at 0.01 cm near the sediment water interface (SWI). Two classes of organic matter (detritus) with differing reactivity (fast decaying FDET, slow decaying SDET) are mineralized sequentially in oxic mineralization, followed by denitrification, and anoxic mineralization (T. 3-2). Consumption of oxygen and nitrate is explicitly modelled (Eqs. 1.1, 1.2), mineralization is limited by carbon availability (first order kinetics), and oxidant availability (Michaelis-Menten type kinetics), and inhibited by concentrations of inhibiting solutes. The anoxic mineralization with oxidants other than oxygen and nitrate (manganese oxides, iron oxides, sulfate, organic matter) are collected into one process in which so-called oxygen demand units (ODU's) are generated (Eq. 1.3). The reoxidation of these ODU's, as well as the nitrification are two additional processes that consume O_2 (Eqs. 1.4, 1.5). Phosphorus dynamics include the formation and release of Fe-bound phosphorus (FeP), as well as the formation and dissolution of Ca-bound P, apatite (CaP) (Ait Ballagh et al., 2020). Including the two classes of organic matter and dissolved organic carbon (DIC), this makes for 11 species, each defined in the 100 sediment layers.

State variables are transported in the sediment through advection, molecular diffusion (for solutes) and bioturbation (solids). The solute flux due to molecular diffusion and advection is described by Fick's first law (Fick, 1855),

$$J_D = \varphi D_i \frac{\partial C}{\partial z} + \varphi v C \qquad \text{(Eq. 1)}$$

where the effective diffusion coefficient is written as $D_i = D_0 / \theta^2$, with D_0 the molecular diffusivity of the solute, $\theta^2 = 1 - 2 \ln(\varphi)$ the correction factor for sediment tortuosity (Boudreau, 1996), and φ the sediment porosity, which was kept constant with depth. Bioturbation is depth-dependent (z), and was set as a constant biodiffusivity value Db_0 in a surficial layer with thickness L_{mix}. Below this depth, bioturbation decreases rapidly to zero, determined by the attenuation coefficient for bioturbation (Db_{coeff}, Eq. 2).

$$Db_z = Db_0 e^{-\frac{(z - L_{mix})}{Db_{coeff}}} \qquad \text{(Eq. 2)}$$

Deposition fluxes and bottom water concentrations were imposed for the upper boundaries of solid and liquid substances respectively, while a zero-gradient was assumed at the lower boundary.

T. 3-2: Diagenetic reactions used in OMEXDIA. x denotes the molar C:P ratio, y the molar N:P ratio in organic matter per mole of phosphorus (for Redfield Stoichiometry, x = 106, y = 16).

Process	Reaction	
Oxic mineralization	$(CH_2O)x\ (NH_3)y\ (H_3PO_4) + xO_2 \rightarrow xCO_2 + yNH_3 + H_3PO_4 + xH_2O$	(1)
Denitrification	$(CH_2O)x\ (NH_3)y\ (H_3PO_4) + 0.8\ x\ HNO_3 \rightarrow xCO_2 + yNH_3 + 0.4\ x\ N_2 + H_3PO_4 + 1.4\ x\ H_2O$	(2)
Anoxic mineralization	$(CH_2O)x\ (NH_3)y\ (H_3PO_4) + an\ oxidant \rightarrow xCO_2 + yNH_3 + H_3PO_4 + xODU + xH_2O$	(3)
Nitrification	$2NH_3 + 2O_2 \rightarrow HNO_3^- + H_2O$	(4)
ODU oxidation	$ODU + O_2 \rightarrow an\ oxidant$	(5)

Boundary conditions and parameters for the model obtained from measurements were temperature, salinity, solute bottom water concentrations (NO_3^-, NH_4^+, PO_4^{3-}, O_2, DIC), and the sediment porosity φ. The model was implemented in R (R Core Team, 2020), the transport of simulated species was calculated using the R-package ReacTran (Soetaert and Meysman, 2012), while steady state was estimated using the R-package rootSolve (Soetaert, 2009). Molecular diffusion coefficients were calculated using R-package marelac (Soetaert and Petzoldt, 2018).

3.2.5.2. Model fitting

Fitting of the diagenetic model to the data was done in two steps. Using the measured DIC flux as the upper boundary carbon input flux, profiles were first manually fitted. Measured fluxes of O_2, and porewater profiles of NH_4^+, NO_3^-, and PO_4^{3-} were approximated by manually tweaking a limited set of parameters (see T. 3-3). The degradation rate of slow degrading material (*rSlow*), and the biodiffusivity constant *Db* were constrained by fitting the NH_4^+, and O_2 profiles. Parameters affecting the NO_3^- and NH_4^+ profiles were then tuned, starting with the nitrification rate *rnit*, followed by the denitrification constants *ksNO3denit*, and *kinO2denit*. The shape of the oxygen profiles further constrained the oxidation rate of oxygen demanding units (ODU's), and reaction constants for anoxic mineralization *kinO2anox* and *kinNO3anox*. In the last manual fitting step, the modeled phosphate profiles were adjusted by changing the parameters for the processes affecting FeP and CaP. This could be done in the last step, as the phosphate dynamics do not impact the other model constituents. The manual fitting was followed by a constrained parameter fitting using an optimization algorithm. In this second step, the fitted parameters were allowed to vary in a range ±10% around the manually fitted parameters. Also the DIC fluxes were refitted within a narrow range (0.98 -1.02 of measured value), to allow freedom to the fitting algorithm. A random-based minimization algorithm (Price, 1977) implemented in the R package FME (Soetaert and Petzoldt, 2010) was used. This algorithm pseudo-randomly samples the parameter space, until the parameter set was found which returned the minimal model cost, the latter defined as the sum of variable costs (modeled - measured values), scaled using the mean - standard deviation relation determined for each nutrient.

3.2.5.3.   Post-processing

Based on the model results, the total stock of particulate organic carbon (POC) in the top 0.1 m of the sediment was calculated as the sum of both reactive classes of carbon (FDET, SDET), and the fraction of nonreactive carbon. The former was estimated from the model results, the latter was derived by subtracting the reactive carbon from the measured sediment organic carbon content C_{org} (top 2 cm, T. 3-4). Net P release/scavenging rates were calculated for the oxic and anoxic zones in the sediment by summing release processes (FeP and CaP release) and subtracting the scavenging processes (FeP and CaP formation). Trends between the model output (process rates, carbon stock), model parameters; and the sampling depth, and latitude were explored through Pearson's correlation (*r*) tests with 9 degrees of freedom, with a significance level (*p*-value) of 0.05. Analyses were performed in R (R Core Team, 2020).

T. 3-3: Definition of the parameters, and values.

Parameter	Parameter meaning	Unit	Type	Value (range)
Φ	Porosity	-	Measured	0.45 - 0.71
wSed	Solid phase advection rate	cm yr^{-1}	Fixed	0.0365
pFast	Fast degrading fraction organic matter	-	Fixed	0.95
pSlow	Slow degrading fraction organic matter	-	Fixed	0.05
rFast	Decay rate FDET	d^{-1}	Fixed	0.05
rSlow	Decay rate SDET	d^{-1}	Fitted	$0.11 \cdot 10^{-3}$ - $0.53 \cdot 10^{-3}$
Db	Biodiffusivity coefficient	cm^2 d^{-1}	Fitted	0.001 - 0.019
biotdepth	Mixed layer depth	cm	Fixed	2
rnit	Max. nitrification rate	d^{-1}	Fitted	2 - 34.7
rODUox	Max. ODU oxidation rate	d^{-1}	Fitted	4 - 70
ksO2oduox	Half saturation, O$_2$ in ODU oxidation	mmol O$_2$ m^{-3}	Fitted	1 - 8
ksNO3denit	Half saturation, NO$_3$ in denitrification	mmol NO$_3$ m^{-3}	Fitted	15 - 100
kinO2denit	Half saturation, O$_2$ inhibition of denitrification	mmol O$_2$ m^{-3}	Fitted	20 - 100
kinNO3anox	Half saturation, NO$_3$ inhibition anoxic mineralization	mmol NO$_3$ m^{-3}	Fitted	1 - 8
kinO2anox	Half saturation, O$_2$ inhibition anoxic mineralization	mmol O$_2$ m^{-3}	Fitted	35 - 97
rCaPprod	Rate of CaP production	d^{-1}	Fitted	0 - 0.06
rCaPdiss	Rate of CaP dissolution	d^{-1}	Fitted	0 - 0.001
rFePadsorp	Rate of FeP adsorption	d^{-1}	Fitted	0.1 - 2.7
rFePdesorp	Rate of FeP desorption	d^{-1}	Fitted	0 - 0.0066

3.3. Results

3.3.1. Description of the sampling sites.

The sampling stations differed in their sediment characteristics (T. 3-4). The sediment median grain size ranged between 25 ± 1 µm and 217 ± 2 µm, the differences mostly due to the relative contributions of fine (125 - 250 µm) and very fine sand (63 - 125 µm), and the silt content (< 63 µm). Deeper stations (C.450, F.640, F.695, F.770) had the lowest median grain size (25 ± 1 to 70 ± 8 µm), due to a high proportion of silt (40 ± 4 to 88 ± 2 %), the lowest permeability ($1.0 \cdot 10^{-16} \pm 0$ m^2 to $1.6 \cdot 10^{-14} \pm 0.40 \cdot 10^{-14}$), and the highest organic carbon (0.45 ± 0.06 to 1.12 ± 0.03 %) and nitrogen content (0.05 ± 0.01 to 0.14 ± 0.01 %). The shallowest station (D.240), and stations C.380 and C.545 had sediments with the highest median grain size (192 ± 1 to 217 ± 2 µm), fine sand content (48 ± 2 to 63 ± 2 %), and of the studied locations were the only to classify as permeable, instead of cohesive sediments (according to the threshold of 10^{-12} m^2 of Huettel at al., (2014); $1.0 \cdot 10^{-12} \pm 0.09 \cdot 10^{-12}$ to $7.4 \cdot 10^{-12} \pm 0.42 \cdot 10^{-12}$ m^2). Additionally, these stations had lower contents of organic carbon (0.06 ± 0.01 to 0.23 ± 0.02 %) and total nitrogen (0.01 ± 0 to 0.03 ± 0 %). The stations on either slope of the Dogger Bank (O.100 - O.190, and C.300) contained the highest fraction of very fine sands (36 ± 1 to 55 ± 1 %), intermediate contents of organic carbon and nitrogen (resp. 0.17 ± 0.01 to 0.28 ± 0.09 % and 0.02 ± 0 to 0.03 ± 0.01 %), and an intermediate permeability relative to the other zones ($3.1 \cdot 10^{-14} \pm 2.58 \cdot 10^{-14}$ to $7.2 \cdot 10^{-13} \pm 6.02 \cdot 10^{-13}$ m^2).

Along the transect, bottom water concentrations of NO_3^- (1.5 mmol m^{-3} at O.100 to 8.8 mmol m^{-3} at F.770) and PO_4^{3-} (0.6 mmol m^{-3} at O.100 to 3.1 mmol m^{-3} at F.770) increased northward (T. 3-1). Values for bottom water NH_4^+ (7.4 ± 8.6 mmol m^{-3}) and O_2 (253.9 ± 27.1 mmol m^{-3}) displayed no systematic pattern.

Water column chl a concentration was highest in the DCM of station O.100 (11.1 µg L^{-1}, Fig. 3-2). Other stations with noticeably higher chl a concentrations in the DCM compared to bottom or surface values were stations C.300, C.545, and F.640 (resp. 2.0, 1.2, and 3.9 µg L^{-1}). Surface and bottom water chl a concentrations were generally similar for the same station, and were highest at O.100 (2.2 - 2.6 µg L^{-1}), decreased towards the Dogger Bank (0.4 - 0.6 µg L^{-1}), and from then on ranged between 0.2 and 0.4 µg L^{-1} for surface concentrations, and 0.1 to 0.3 µg L^{-1} for bottom water concentrations, increasing northward. No clear patterns were found in the sediment surface chl a concentrations (µg chl a per g dry sediment), which ranged from 2.9 ± 2.6 µg g^{-1} at O.100 to 0.3 ± 0.3 µg g^{-1} at C.545 (Fig. 3-2).

3.3.2. Sediment profiles

In general, the gradients in nutrient concentrations were only pronounced within the top 3 - 6 cm of the sediment. At greater depths, solute concentrations stayed relatively constant (Fig. 3-3). Only ammonium profiles of D.240, F.640 and F.770 suggest a further build-up below the sampling horizon of 12 cm. Deep porewater concentrations (> 8 cm) of NH_4^+ were lowest in the Oyster Grounds (O.135: 44.5 ± 15.1 mmol m^{-3}) and the Dogger Bank (53.4 ± 6.9 mmol m^{-3}), and reached highest concentrations in the central North Sea (C.380: 64.1 ± 8.6 mmol m^{-3}), and Devils Hole (C.450, 87.6 ± 7.6 mmol m^{-3}). Values then decreased again in the Fladen Ground stations (F.695: $NH_4^+ = 49.2 \pm 21.0$ mmol m^{-3}), with the exception

of F.770 (NH$_4^+$ = 62.4 ± 21.0 mmol m^{-3}), where two out of three profiles did show a further increase in concentrations below 6 cm (Fig. 3-3). Phosphate profiles displayed a similar trend as the ammonium profiles. Deep concentrations of PO$_4^{3-}$ were highest in the central North Sea (e.g. C.380: 19.2 ± 5.6 mmol m^{-3}), and in station F.770 in the Fladen Grounds (20.1 ± 10.8 mmol m^{-3}). Deep PO$_4^{3-}$ concentrations in the Oyster Grounds (O.135: 11.1 ± 11.4 mmol m^{-3}), and the Fladen Grounds were lower (F.695: 9.0 ± 2.9 mmol m^{-3}). Nitrate profiles did not display consistent features in the first 5 stations starting from the coast, and concentrations remained low all over the sediment (range of 1.6 ± 1.4 to 3.4 ± 6.2 mmol m^{-3}). From C.380 northwards, nitrate concentrations clearly decreased just below the sediment water interface. These were also the locations where the oxygen penetration depths were markedly higher and ranged from 6.8 ± 2.0 mm to 7.9 ± 0.4 mm, as opposed to lowest values on the Oyster Grounds (2.4 ± 0.9 mm to 5.9 ± 2.4 mm), and intermediate values in the central North Sea (3.2 ± 0.2 mm to 4.4 ± 0.4 mm).
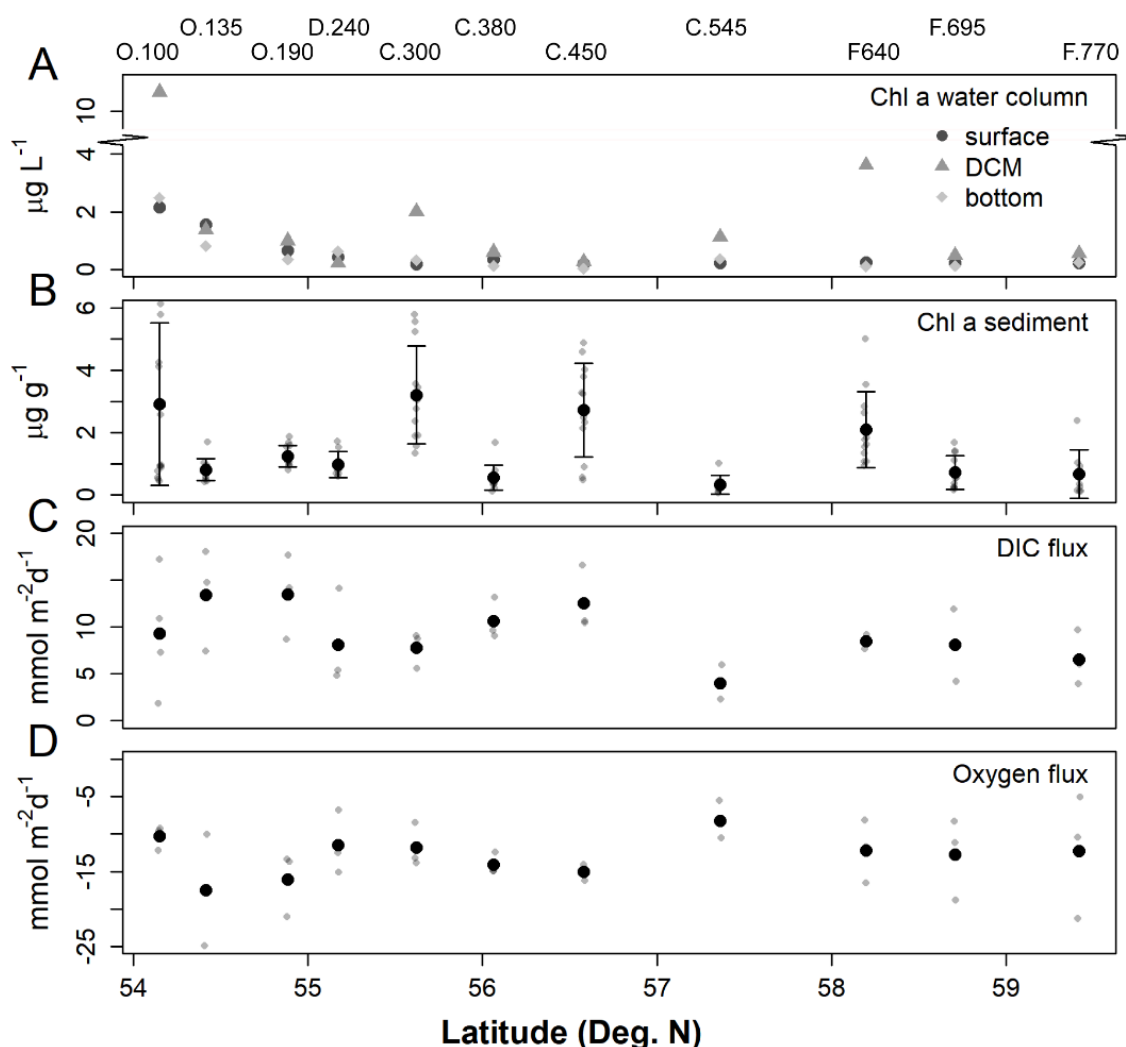
Fig. 3-2: (A) Chlorophyll a concentrations in the water column at the surface, the bottom, and the deep chlorophyll maximum (DCM, µg Chl a L^{-1}), (B) in the upper 2 cm of the sediment (µg Chl a g^{-1}), (C) the DIC flux (mmol m^{-2} d^{-1}), and (D) oxygen fluxes (mmol m^{-2} d^{-1}) measured along the transect. Black points in B, C, and D represent the means, gray points the measured values, error bars (in B) the standard deviation.

T. 3-4: Sediment parameters (mean ± sd) for each sampling station.

Parameter	MGS	Fines	vFines	Silt	Permeability	Porosity	Chl a	C_{org}	N_{tot}	C/N
Unit	(µm)	(%)	(%)	(%)	(m^2)	(-)	(µg g^{-1})	(%)	(%)	(mol mol^{-1})
O.100	82 ± 9	17 ± 1	51 ± 12	32 ± 11	$3.14 \cdot 10^{-14} \pm 2.58 \cdot 10^{-14}$	0.57 ± 0.08	3.62 ± 0.93	0.28 ± 0.09	0.03 ± 0.01	10.20 ± 0.24
O.135	103 ± 3	29 ± 2	55 ± 1	16 ± 0	$5.72 \cdot 10^{-14} \pm 3.28 \cdot 10^{-14}$	0.46 ± 0.01	0.84 ± 0.27	0.17 ± 0.01	0.02 ± 0.00	8.91 ± 0.25
O.190	125 ± 5	47 ± 3	36 ± 1	15 ± 5	$6.18 \cdot 10^{-14} \pm 0.33 \cdot 10^{-14}$	0.45 ± 0.01	1.28 ± 0.25	0.20 ± 0.07	0.03 ± 0.01	8.57 ± 0.54
D.240	217 ± 2	63 ± 2	4 ± 0	0 ± 0	$7.39 \cdot 10^{-12} \pm 0.42 \cdot 10^{-12}$	0.39 ± 0.01	0.99 ± 0.01	0.06 ± 0.01	0.01 ± 0.00	6.66 ± 1.41
C.300	113 ± 1	39 ± 0	47 ± 1	14 ± 1	$7.24 \cdot 10^{-13} \pm 6.02 \cdot 10^{-13}$	0.48 ± 0.00	3.35 ± 1.16	0.27 ± 0.01	0.03 ± 0.00	9.37 ± 0.65
C.380	212 ± 2	48 ± 2	6 ± 1	9 ± 2	$1.01 \cdot 10^{-12} \pm 0.08 \cdot 10^{-12}$	0.43 ± 0.02	0.59 ± 0.28	0.22 ± 0.02	0.03 ± 0.00	9.13 ± 0.17
C.450	70 ± 8	19 ± 4	35 ± 1	45 ± 5	$1.71 \cdot 10^{-14} \pm 0.34 \cdot 10^{-14}$	0.57 ± 0.03	2.85 ± 1.56	0.67 ± 0.02	0.09 ± 0.00	9.03 ± 0.07
C.545	192 ± 1	59 ± 1	8 ± 0	9 ± 1	$4.86 \cdot 10^{-12} \pm 1.67 \cdot 10^{-12}$	0.46 ± 0.01	0.35 ± 0.01	0.23 ± 0.02	0.03 ± 0.00	8.51 ± 0.24
F.640	25 ± 1	1 ± 1	11 ± 1	88 ± 2	$5.11 \cdot 10^{-15} \pm 5.37 \cdot 10^{-15}$	0.71 ± 0.02	2.26 ± 0.53	1.12 ± 0.03	0.14 ± 0.01	9.04 ± 0.11
F.695	57 ± 52	24 ± 1	16 ± 1	40 ± 4	$1.00 \cdot 10^{-15} \pm 0$	0.49 ± 0.08	0.78 ± 0.24	0.45 ± 0.06	0.05 ± 0.01	10.13 ± 1.21
F.770	55 ± 1	10 ± 0	34 ± 1	56 ± 1	$1.59 \cdot 10^{-14} \pm 0.40 \cdot 10^{-14}$	0.61 ± 0.05	0.73 ± 0.53	0.65 ± 0.02	0.08 ± 0.00	9.35 ± 0.09

3.3.3. Sediment fluxes

The measured oxygen influxes varied from -8.24 ± 2.52 mmol m^{-2} d^{-1} at C.545, to -16.03 ± 4.35 and -17.52 ± 7.45 mmol m^{-2} d^{-1} at O.135 and O.190 (T. 3-5). Note that negative fluxes represent an uptake in the sediment, positive fluxes exit the sediment. The DIC effluxes were also lowest for C.545 (3.98 ± 1.85 mmol m^{-2} d^{-1}), and highest at O.190 (13.52 ± 4.54 mmol m^{-2} d^{-1}). Oxygen and DIC fluxes were significantly correlated (r = -0.47, p = 0.005), and the DIC release significantly decreased with latitude (r = -0.35, p = 0.045), which was not the case for the oxygen fluxes (r = -0.13, p = 0.46) (Fig. 3-2).

The measured nutrient fluxes displayed a high heterogeneity within sampling replicates, with replicate cores of the same stations sometimes resulting in in- and effluxes for the same solute (T. 3-5). In general, more than 40% of regressions of nutrient concentrations over time were not significant, so that nutrient fluxes were assumed 0 mmol m^{-2} d^{-1}. Highest ammonium release was measured on the Dogger Bank (0.85 ± 1.29 mmol m^{-2} d^{-1}), and the bordering stations (O.190, C.300), whereas NH_4^+ uptake by the sediment was measured at O.135, and in the northern third of the transect (sts. C.545, F.640, F.770). Besides O.100, where nitrate uptake was measured (-0.21 ± 0.55 mmol m^{-2} d^{-1}), NO_3^- efflux varied between 0 mmol m^{-2} d^{-1} at C.300 to 0.56 ± 0.96 mmol m^{-2} d^{-1} at F.640. Phosphate exchange was significantly correlated with the station depth (r = 0.67, p = 0.025); in the southern half of the transect, PO_4^{3-} uptake occurred in O.100, and the Dogger Bank, whereas in the northern part exclusively PO_4^{3-} release occurred (with highest efflux measured at Devils Hole, 0.08 ± 0.09 mmol m^{-2} d^{-1}).

T. 3-5: Measured solute fluxes of ammonium (NH_4^+), nitrate (NO_3^-), phosphate (PO_4^{3-}), oxygen (O_2), and dissolved inorganic carbon (DIC) in mmol m^{-2} d^{-1}, with negative values indicating a flux into the sediment, positive values a flux out of the sediment.

Station	NH_4^+	NO_3^-	PO_4^{3-}	DIC	O_2
O.100	0.04 ± 0.77	-0.21 ± 0.55	-0.04 ± 0.05	9.3 ± 6.46	-10.27 ± 1.32
O.135	-0.22 ± 0.38	0.35 ± 0.31	0.09 ± 0.08	13.43 ± 5.45	-17.52 ± 7.45
O.190	0.73 ± 0.64	0.26 ± 0.03	0.00 ± 0.00	13.52 ± 4.54	-16.03 ± 4.35
D.240	0.85 ± 1.29	0.15 ± 0.26	-0.01 ± 0.12	8.11 ± 5.2	-11.45 ± 4.25
C.300	0.84 ± 0.24	0.00 ± 0.00	0.00 ± 0.00	7.82 ± 1.93	-11.82 ± 2.94
C.380	0.71 ± 0.44	0.43 ± 0.74	0.00 ± 0.00	10.64 ± 2.21	-14.11 ± 1.43
C.450	0.68 ± 0.38	0.43 ± 0.37	0.08 ± 0.09	12.56 ± 3.52	-15.02 ± 1.08
C.545	-0.10 ± 0.16	0.33 ± 0.40	0.01 ± 0.02	3.98 ± 1.85	-8.24 ± 2.52
F.640	0.00 ± 0.00	0.56 ± 0.96	0.04 ± 0.04	8.48 ± 0.74	-12.15 ± 4.22
F.695	0.45 ± 0.43	0.24 ± 0.41	0.03 ± 0.03	8.12 ± 3.85	-12.77 ± 5.41
F.770	0.00 ± 0.00	0.25 ± 0.43	0.04 ± 0.07	6.54 ± 2.92	-12.27 ± 8.23

3.3.4. Modelling results

3.3.4.1. Model parametrization

The combination of the heuristic (manual) profile fitting step and the optimization algorithm produced parameter sets which adequately describe the measured porewater solute profiles (Fig. 3-3). Ammonium and oxygen profiles were shaped initially by a combination of the bioturbation rate *Db*, and the decay rate of the slow degrading organic matter *rSlow*. Decreasing the bioturbation rate reduced the build-up of NH_4^+ (and PO_4^{3-}) with depth, increased the oxygen penetration depth, and changed the shape of the NO_3^- profile (deepening the NO_3^- peak). While the degradation rate of the slow degrading organic matter also impacted the deep NH_4^+ concentrations, it had the largest effect on the *shape* of the NH_4^+ profile, with lower degradation rates causing a more gradual build-up with sediment depth. Derived bioturbation rates ranged from 0.001 $cm^2 \, d^{-1}$ at O.135 to 0.019 $cm^2 \, d^{-1}$ at C.545, and degradation rates of slow degrading carbon ranged from $1 \cdot 10^{-4} \, d^{-1}$ at D.240 to $5.3 \cdot 10^{-4} \, d^{-1}$ at C.545. The nitrification rate was the parameter used to reconcile the nitrate and ammonium profiles. Increasing the nitrification rate slightly decreased the build-up of NH_4^+ and increased concentrations of NO_3^-, typically producing a nitrate concentration peak within the oxic zone. Parameters concerning the oxidation of ODU's (*rODUox*, *ksO2oduox*), and oxygen inhibition parameters for denitrification and anoxic mineralization (*kinO2denit*, *kinO2anox*) were adjusted where necessary to better fit the nitrate profiles. In some cases (Fig. 3-3: O.100, C.300), the model was unable to fit a NO_3^- profile without a subsurface peak between 0 and 1 cm, without simultaneously compromising the NH_4^+ concentration.

After fitting the O_2, NH_4^+, and NO_3^- profiles, phosphate concentrations were generally already in the correct order of magnitude, and the parameters describing the FeP and CaP dynamics were mostly needed to further define the shape of the profiles. Phosphate profiles with a visible subsurface peak, such as D.240, C.300, C.380, and C.545, could only be generated by the formation of CaP (*CaPprod*), thus causing a decrease of PO_4^{3-} with depth. The FeP formation rate (*FePads*) proved a necessary parameter to regulate the phosphate concentrations in the oxic region. This was often coupled to FeP desorption (*FePdes*) in deeper layers, as this shuttle of P was needed to supply free phosphate to be used in CaP production in deeper layers (T. 3-6).

Modelled fluxes for DIC and O_2 were positively correlated with their measured counterparts (*r* of 0.97, and 0.90 respectively, $p < 0.001$). For NO_3^-, NH_4^+, and PO_4^{3-} no significant correlation between measured and modelled fluxes could be achieved (NO_3^-: $r = -0.44$, $p = 0.18$; NH_4^+: $r = 0.25$, $p = 0.46$; PO_4^{3-}: $r = 0.4$, $p = 0.22$).
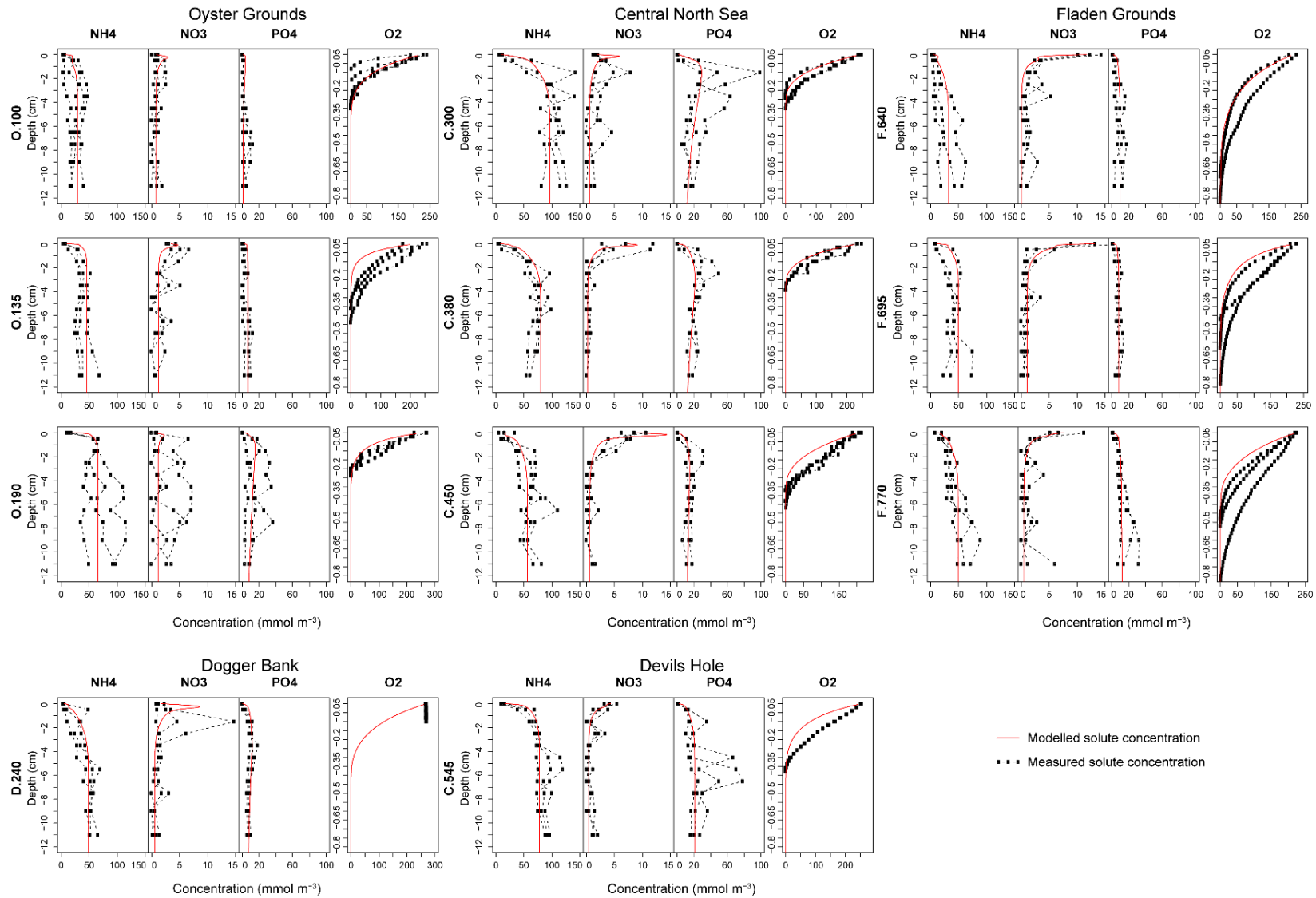
Fig. 3-3: Measured porewater solute profiles (dotted lines) and model fits (red lines) for NH_4^+, NO_3^-, PO_4^{3-} and O_2, with concentrations in mmol m^{-3}.

3.3.4.2. Model output

The total carbon mineralization rates showed a decreasing trend northward ($r = -0.55$, $p = 0.079$; T. 3-6). Most of the carbon mineralization was due to oxic processes (57 - 90 %) (Fig. 3-4). The lowest contribution of oxic mineralization to total carbon mineralization was found in the central North Sea stations, where its contribution ranged between 57 and 72 % (C.300, C.380, C.450, C.545). Here, the contribution of anoxic mineralization was maximal, and reached 30-39 %. The relative importance of oxic mineralization (and inversely, the anoxic mineralization, though not significantly) was negatively correlated to both the bioturbation rates (Db, oxic: $r. = -0.79$, $p = 0.004$; anoxic: $r = 0.58$, $p = 0.07$), and the nitrification rates ($rnit$, oxic: $r = -0.64$, $p = 0.03$; anoxic: $r. = 0.43$, $p = 0.17$).

Nitrification (range: 0.30 - 1.25 mmol O_2 m^{-2} d^{-1}) contributed on average 10 % ($\pm$ 7) to the oxygen consumption budget, with a clear outlier at C.545 (25 %, T. 3-6). No clear latitudinal patterns in nitrification were observed.
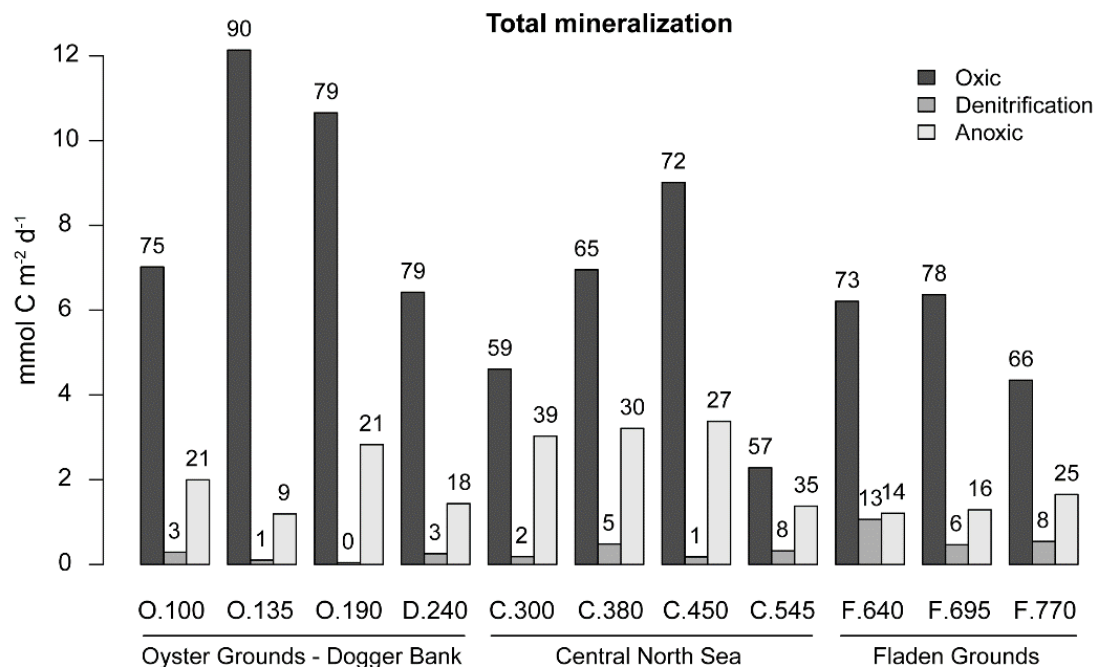
Fig. 3-4: Model-derived C mineralization rates for oxic mineralization, denitrification, and anoxic mineralization in mmol m^{-2} d^{-1} (bars), and what they represent as a percentage of the total mineralization at each site (numbers above the bars).

Denitrification had a relatively smaller contribution to total mineralization in most southern stations up to Devils hole (C.450, 0 - 5%), but was responsible for up to 6-13 % of the total carbon mineralization in the most Northern stations (C.545 and Fladen Grounds), leading to a significant latitudinal increase ($r = 0.69$, $p = 0.018$). As a result of increased denitrification rates, sediments in this zone removed the highest amount of nitrogen from the sediment: denitrification removed 30 - 66 % of all organic N mineralized in the Fladen Grounds, vs. 2 - 16 % in the Oyster Grounds in the form of dinitrogen gas (T. 3-6). In contrast, phosphate removal rates were highest at O.100 and O.135 (resp. 25 and 9 % of all produced P). In these stations, high P removal rates were found in the oxic zone (resp. 0.16 and 0.12 μmol P m^{-2} d^{-1}), also characteristic for O.190 and C.300 (resp. 0.12 and 0.09 μmol P m^{-2} d^{-1}). For the remainder of the stations, P removal was between 0 and 6 %.

T. 3-6: Model derived mineralization rates (mmol C m^{-2} d^{-1}), nitrification (mmol O$_2$ m^{-2} d^{-1}), relative contributions of each mineralization process to the total mineralization, net P removal and release in the oxic and anoxic sediment layers (μmol m^{-2} d^{-1}), the proportion of incoming nitrogen removed from the sediment, and the stock of carbon in the top 0.1 m of sediment (moles m^{-2}).

	Mineralization Rates (mmol m^{-2} d^{-1})					Relative proportions (%)		
	Oxic	Denitrification	Anoxic	Total	Nitrification	Oxic	Denitrification	Anoxic
O.100	7.02	0.29	2	9.3	0.91	75.4	3.1	21.5
O.135	12.14	0.1	1.19	13.43	0.53	90.4	0.7	8.9
O.190	10.66	0.04	2.83	13.52	0.3	78.8	0.3	20.9
D.240	6.42	0.25	1.44	8.11	0.84	79.2	3.1	17.7
C.300	4.61	0.18	3.03	7.82	0.96	58.9	2.4	38.7
C.380	6.95	0.48	3.21	10.64	1.25	65.3	4.5	30.2
C.450	9.01	0.18	3.38	12.56	0.56	71.7	1.4	26.9
C.545	2.28	0.32	1.37	3.98	1.17	57.4	8.1	34.5
F.640	6.21	1.06	1.21	8.48	1.12	73.2	12.5	14.3
F.695	6.36	0.46	1.29	8.12	0.31	78.4	5.7	15.9
F.770	4.35	0.54	1.65	6.54	1.12	66.4	8.3	25.2

	Net. free P scavenging (-) or release (+) (μmol P m^{-2} d^{-1})		Removal proportions (% of produced)		Stock in top 0.1 m of sediment (moles m^{-2})	
	Oxic sed.	Anoxic sed.	Nitrogen	Phosphorus	POC	DIC
O.100	-0.16	0.04	16	25	25.41	0.3
O.135	-0.08	-0.04	4	9	4.31	0.28
O.190	-0.12	0.09	2	1	8.38	0.29
D.240	-0.01	-0.01	17	1	2.47	0.31
C.300	-0.09	0.06	12	6	14.70	0.35
C.380	-0.06	0.05	24	0	12.02	0.35
C.450	-0.05	0.07	7	0	67.95	0.31
C.545	-0.04	0.03	43	1	18.95	0.31
F.640	-0.02	-0.01	66	4	143.51	0.29
F.695	-0.01	0.00	30	2	33.99	0.28
F.770	-0.02	0.01	44	0	73.67	0.29

Stocks of particulate organic carbon (POC) in the upper 10 cm ranged from 2.47 moles m^{-2} at C.300 to 143.51 moles m^{-2} at the Fladen Grounds (T. 3-6). POC values were significantly correlated to water depth ($r = 0.71$, $p < 0.015$) as well as the silt content of the sediment ($r = 0.96$, $p < 0.001$).
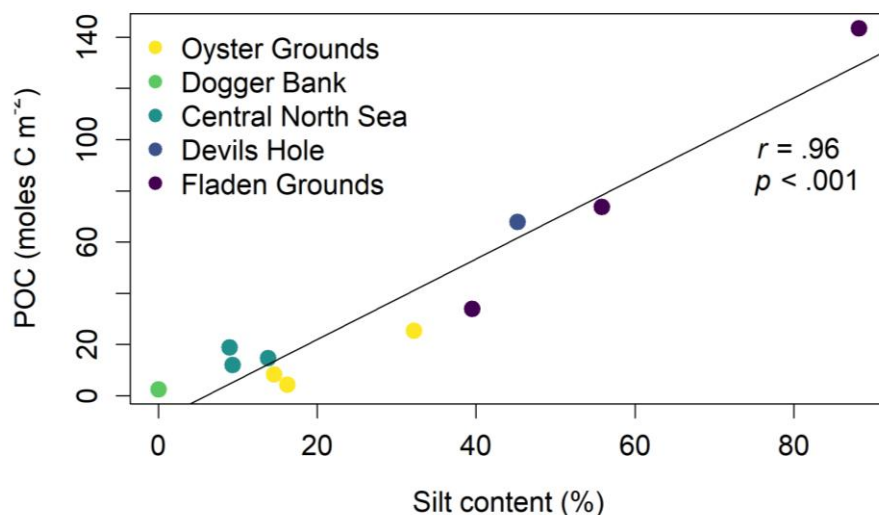
Fig. 3-5: Particulate organic carbon (POC, moles m⁻²) in the top 0.1 m of the sediment, as a function of the silt content per station.

3.4. Discussion

In this study, we set out to characterize the response of organic matter mineralization processes to spring bloom deposition in several distinct regions of the North Sea. The chl *a* values measured in the water column along the transect indicate that the sampling indeed took place after the spring bloom (Fig. 3-2). The water column was highly stratified, with a prominent deep chlorophyll maximum (DCM) present for most of the stations (observed from CTD casts). Surface and bottom water chl *a* values (resp. 1.45 ± 0.75 and $1.21 \pm 1.13 \, \mu g \, L^{-1}$) for the Oyster Grounds correspond to those found in this region by Boon et al. (1998), whereas the values found in the Fladen Grounds ($0.22 \pm 0.01 \, \mu g \, L^{-1}$) are similar to the post-bloom values reported in Eiane and Ohman (2004) in the same region. Naturally, the spring bloom is a heterogeneous event throughout the sampled region (Desmit et al., 2019; van Leeuwen et al., 2015); and there were 12 days between the first, and last station sampled (T. 3-1). For these reasons, it is likely that an unknown amount of variability seen in the data will reflect this difference in timing.

Despite this temporal variation and the heterogeneity of sediments (T. 3-4) sampled over a considerable distance (670 km), total mineralization rates differed with a factor 3.4 at most ($3.98 - 13.52 \, mmol \, C \, m^{-2} \, d^{-1}$), with measured DIC fluxes ranging between 2 and 18 $mmol \, m^{-2} \, d^{-1}$ (T. 3-5). Previously reported values of DIC fluxes in the southern North Sea (the area up to the Fladen Grounds, $2 - 29 \, mmol \, m^{-2} \, d^{-1}$), and northern North Sea (Fladen Grounds, $0 - 6 \, mmol \, m^{-2} \, d^{-1}$), showed a slightly wider range (values measured in September, Brenner et al., 2016). Our measured oxygen consumption rates ($5 - 25 \, mmol \, O_2 \, m^{-2} \, d^{-1}$) also compared well to previously measured values in spring/early summer available for the Oyster Grounds and Dogger Bank ($4 - 14 \, mmol \, O_2 \, m^{-2} \, d^{-1}$, Osinga et al., (1996), Raaphorst et al., (1990), Wilde et al., (1984)), the German Bight ($15.5 – 25.1$, Oehler et al. (2015), the Central North Sea area ($7 - 18 \, mmol \, O_2 \, m^{-2} \, d^{-1}$, Upton et al. (1993)), and the Fladen Grounds ($1 - 7 \, mmol \, O_2 \, m^{-2} \, d^{-1}$, de Wilde et al (1986)).

The measurements and modelling results suggest that the response to carbon deposition was broadly similar for all studied sites: a mostly oxic mineralization of organic matter, resulting in a low sedimentary nutrient build-up. However, there were differences in the biogeochemical signatures between regions with different sediment characteristics. The sediments in the Oyster Ground stations displayed coarser particle size and greater permeability towards the Dogger Bank (T. 3-4). Mineralization in this zone was predominantly coupled to oxygen consumption (75 - 90 %, Fig. 3-4), with a small contribution of denitrification (0 - 3 %) to total mineralization. The sediments in the Central North Sea were more permeable and relatively coarse grained, except for Devils Hole sediments which were characterized by high silt contents and a low permeability. Anoxic mineralization was more important in this central region (27 - 39 %), while denitrification contributed more to total mineralization (1 - 8 %). Lastly, the Fladen Grounds had the finest sediments, with an intermediate importance of oxic mineralization (66 - 78 %) and the highest proportion of mineralization as denitrification (6 - 13 %).

3.4.1. Rapid, oxic mineralization

While a surficial, mostly oxic mineralization of organic matter has been observed for several regions in the southeast of the North Sea (Upton et al., 1993; Lohse et al., 1995; Raaphorst and Malschaert, 1996), our results indicate that this occurs throughout large parts of the North Sea.

The high contribution of oxic mineralization can be deduced from the shape of the solute profiles close to the sediment water interface (Fig. 3-3). In nearly all locations, the gradients in nutrient concentrations were established in the upper 4 - 6 cm, exhibiting a constant concentration below that depth. This shape was observed even where solute concentrations were higher, such as the central North Sea stations northwest of the Dogger Bank (Fig. 3-3). Free nutrients are produced where organic matter mineralization takes place. When most of the organic matter mineralization occurs in oxic conditions (i.e. near the sediment-water interface), the bulk of the free nutrients will be produced near the sediment water interface as well. As a result, solute profiles rapidly reach constant concentrations, as mineralization in deeper layers will not contribute much to the pool of nutrients. In our study, such profiles were observed in the Oyster grounds and Central North Sea. Only on the Dogger Bank, and in two stations in the Fladen Grounds, F.640 and F.770, solute profiles exhibited a more gradual build-up that seemingly continued beyond 12 cm depth, suggesting that organic matter degradation was shifted away from the sediment surface. The degree to which degradation occurs near to the surface was partly caused by the bioturbation rates in the model, which were lowest on the Oyster Grounds ($0.001 \text{ cm}^2 \text{ d}^{-1}$), and highest in the Central North Sea ($0.019 \text{ cm}^2 \text{ d}^{-1}$). Bioturbation mixes fresh organic matter deeper into the sediment, which decreases the substrate for mineralization near the surface, while increasing the organic matter content in deeper (sub- and anoxic) sediment layers.

The stock of particulate organic carbon in the upper 10 cm correlated strongly with the silt content in the sediment (Fig. 3-5). Whereas this relation was not unexpected (Wilson et al., 2018; Serpetti et al., 2012), it confirmed the Fladen Grounds and the Oyster Grounds as areas of increased deposition (Van et al., 1998), while most of the North Sea is bereft of any considerable carbon burial (De Haas et al., 1997). Higher values of the observed POC stock in the Fladen Grounds of $34 - 144 \text{ moles m}^{-2}$, and in Devils Hole: 68 moles m^{-2} actually far exceed average regional values for surrounding sediments of the

Central (37 mol m^{-2}), and Northern North Sea (43 mol m^{-2}) respectively (Legge et al., 2020), and more so resemble POC stocks calculated for the Norwegian Trench (54 - 120 mol m^{-2}).

3.4.2. Large-scale patterns

Several trends were found along the transect. Total mineralization rates, as well as the contribution of oxic mineralization decreased from south to north, whereas the importance of denitrification increased (Fig. 3-4). The decreasing trend in total mineralization has previously been noted in the North Sea, and was attributed to lower temperatures in deeper waters, changes in sediment granulometry, and a weakened coupling to pelagic production (Brenner et al., 2016). While we found no clear latitudinal pattern in sedimentary nor water column chl a concentrations, our data do show examples of correspondence between DCM and top sediment chl a concentrations in multiple locations (O.100, C.300, F.640; Fig. 3-2), signaling a direct input of fresh material to sediments in most regions.

3.4.2.1. Increasing denitrification northward

The increasing proportion of organic matter mineralized in denitrification, appeared to be driven predominantly by increasing bottom water nitrate concentrations towards the north (T. 3-1). Overall, modelled denitrification rates (0.03 - 0.85 mmol N m^{-2} d^{-1}) compared well to measured denitrification rates in the North Sea, ranging from 0 to 0.50 mmol N m^{-2} d^{-1} in the Oyster Grounds and the Dogger Bank (Lohse et al., 1995; Neubacher et al., 2011). Rosales Villa et al. (2019) measured denitrification rates of 0.19 mmol N m^{-2} d^{-1} near the Fladen Grounds (in August), low compared to our modelled rates for this region, but in situ NO_3^- bottom water concentrations were also 30 - 60% lower in the cited study.

On the Oyster Grounds, all NO_3^- produced from nitrification was subsequently denitrified (Fig. 3-6 A). In the Dogger Bank and central North Sea sediments, nitrification rates were slightly higher (with the exception of Devils Hole), and exceeded the NO_3^- demand of denitrification (Fig. 3-6 A). The significant negative correlation between the nitrification rates and the proportion of oxic mineralization indicates that nitrification in the Dogger Bank and the central North Sea sediments competes for oxygen with organic matter mineralization processes, with this decrease in available oxygen resulting in a higher proportion of anoxic mineralization of organic matter.

In contrast, higher denitrification rates on the Fladen Grounds were only sustained for ~25 % by nitrate produced from nitrification, with most of the NO_3^- provided by the overlying water (Fig. 3-6 A). This intake of nitrate from the bottom water is seen in the NO_3^- profiles in the Fladen Grounds, which have highest values near the sediment water interface, and a steep decline below where it is consumed (Fig. 3-3). Elevated bottom water NO_3^- concentrations in the Fladen Grounds, up to ten times those on the Oyster Grounds, are most likely explained explained by the inflow of nutrient rich Atlantic water (Holt et al., 2012; Vermaat et al., 2008). These bottom water concentrations explain these profiles, and the NO_3^- uptake in the sediment (T. 3-1). A result of this increased denitrification towards the north, was that in the Oyster Grounds only 2 - 26 % of all mineralized N was removed from the sediment, whereas in the Fladen Grounds this increased to 30 - 66 % (Fig. 3-6 B). This shows that the deep regions of the North Sea are potentially considerable sinks of nitrogen, driven by bottom water nitrate concentrations.
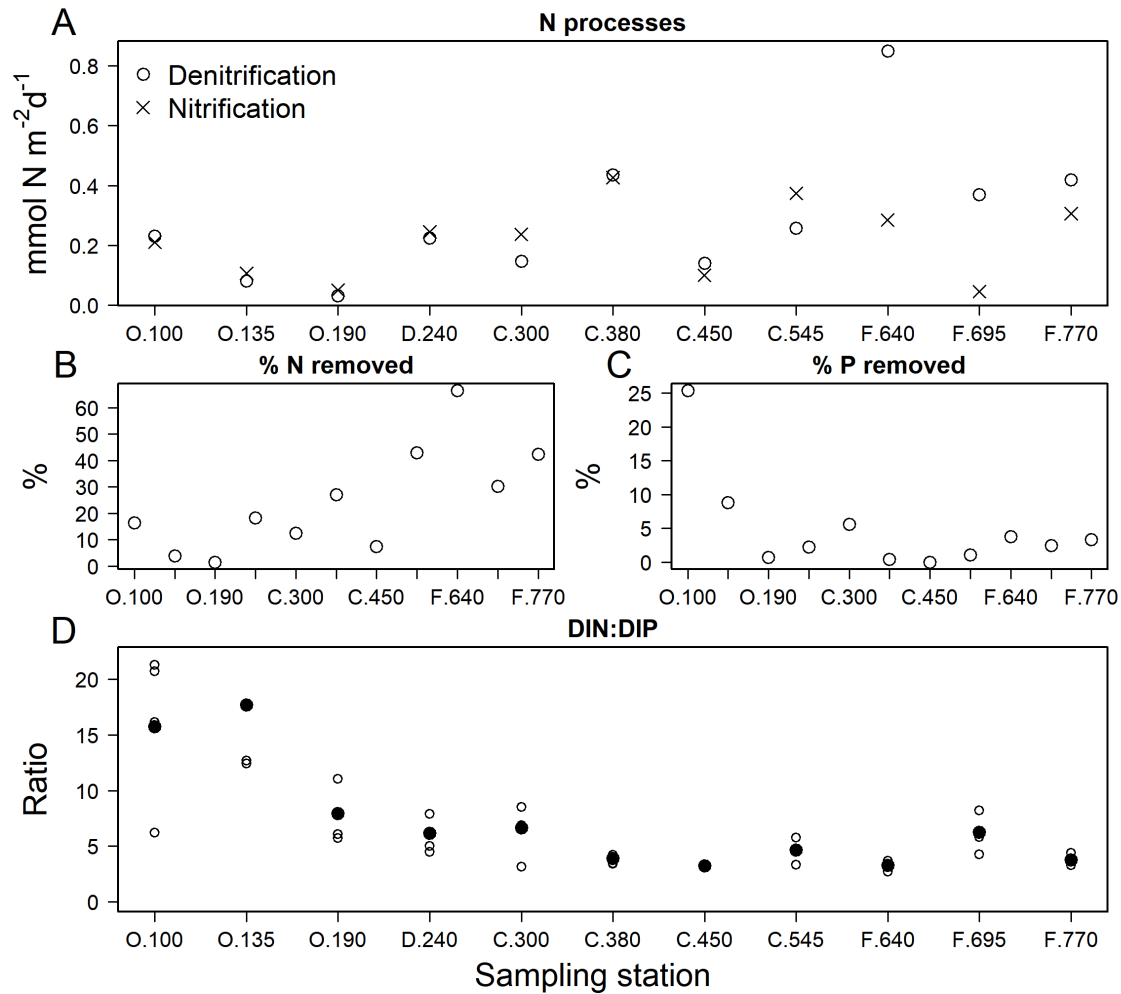
Fig. 3-6: (A) Nitrification and denitrification (mmol N m^{-2} d^{-1}) for each station; (B) net % of mineralized nitrogen removed from the sediment; (C) net % of mineralized phosphorus buried or removed from the sediment; (D) The DIN:DIP ratio in the sediment (from 2 cm downwards, black dots = average, empty dots = replicate values).

It should be noted that the absence of additional relations between denitrification rates and other determining factors (e.g. carbon flux, C/N ratio, OPD) could point to the fact that we could not distinguish between so-called canonical denitrification (as used in the current model; Brandes and Devol, 2002), and anammox (anaerobic ammonium oxidation). Both processes consume NH$_4$+, and produce N$_2$, but different drivers influence the occurrence of annamox and canonical denitrification. Anammox can be of considerable importance in hemipelagic sediments, and may account for up to 25% of N$_2$ production on continental shelf sediments (Dale et al., 2011). The relative importance of anammox over denitrification has been linked to increasing depth, changes to organic matter quantity and quality, as well as nitrite availability and faunal ventilation activity (Dalsgaard et al., 2005; Dale et al., 2011). To separate both with certainty, high resolution nitrite profiles and fluxes, as well as N$_2$ fluxes are needed. That being said, a previous study on nitrogen cycling that included samples in the Fladen Grounds (in August) reported only denitrification as a cause of N$_2$ production, and not anammox (Rosales Villa et al., 2019).

3.4.2.2. Decreasing DIN:DIP ratios northward.

Differences in N cycling along the transect caused changes in the sedimentary concentration of dissolved inorganic nitrogen (NOx + NHx, DIN), relative to dissolved inorganic phosphorus (PO_4^{3-}, DIP), but differences in P-cycling between the different stations altered this ratio just as well (Fig. 3-6 C). The DIN:DIP ratio gives an indication of the efficiency with which N compared to P is retained (or conversely, removed) in the sediment as mineralization proceeds. Higher and lower DIN:DIP ratios in deep sediments indicate more efficient removal of P or N respectively. For the deeper layers (2-12 cm) the DIN:DIP ratio was highest in O.100 and O.135 (16 ± 11 and 18 ± 16), but for the other stations values were much lower, ranging between 3 ± 1 (C.450) to 8 ± 4 (O.190), often indicating a depletion of DIN relative to DIP in the sediments (Fig. 3-6 D). Whereas denitrification decreases DIN concentrations in the sediment relative to DIP, the processes that affect DIP are more complex.

The P-cycle in marine sediments is strongly driven by the deposition of organic matter, and the redox conditions in the sediment. In oxic conditions, iron is present in solid form as oxides, and this binds phosphate to form FeP complexes (Slomp et al., 1996a, 1996b). As the FeP is mixed below the oxic zone, the Fe-oxides will reductively dissolve through dissimilatory Fe-reduction, or sulphide induced dissolution (an end product of anoxic sulphate reduction). This resulting PO_4^{3-} release from FeP dissolution increases phosphate concentrations in deeper sediment layers (Mortimer, 1942; Ingall and Jahnke, 1994; Colman and Holland, 2000; Slomp, 2012). The sequestration of P in the oxic zone, and release of P in the anoxic zone has been called the P-shuttle mechanism, and causes a preferential build-up of phosphate over ammonium at depth into the sediment. In addition, in deeper sediment layers, calcium phosphate minerals can be formed (authigenic CaP), with or without FeP as an intermediate (Slomp, 2011). This causes removal of dissolved P and burial of solid-phase P, which constitutes the main P-sink in the sediment.

The removal of dissolved P to the solid phase is evident in PO_4^{3-} profiles as a gradual decrease of PO_4^{3-} with increasing sediment depth in the anoxic zone, causing inorganic phosphorus to be depleted compared to ammonium at depth. It should be noted that, as we did not measure neither FeP nor CaP, our model could not distinguish between P shuttling and removal by either Fe- or Ca-related processes. However, the net P removal to the solid phase could be deduced from the decrease of phosphate with sediment depth.

The highest removal of P in the oxic zone occurred in O.100 and O.135, and this was not (O.135), or only partially (O.100) linked to release in the anoxic zone (T. 3-6). On the Oyster Grounds and Dogger Bank sediments in general, surficial (0 - 2 cm) and deep PO_4^{3-} concentrations were lowest relative to DIN (DIN:DIP surface: 24 ± 23; below 2 cm: 16 and 18, Fig. 3-6 D).

In the central North Sea sediments, the model also indicated significant removal of phosphate in the oxic zone, leading to surface N:P values of 16 ± 11. However, in the Central North Sea – Fladen Ground stations deep DIN:DIP ratios varied from 3 – 9, as in these stations more solid P was released back to free PO_4^{3-} in the anoxic zone (T. 3-6). This shuttle caused build-up of PO_4^{3-} deeper in the sediment which, in combination with slightly higher denitrification rates, led to low DIN:DIP ratios (3 - 6 average). In

the Central North Sea and the Fladen Ground sediments, modeled PO_4^{3-} processes showed less formation of solid P. The amount of buried P was thus much higher in the Oyster Grounds (specifically O.100, and O.135), with more constant values for the rest of the transect (Fig. 3-6 C).

Because of the combination of increasing nitrogen removal and decreasing DIP removal, the DIN:DIP ratio in the deep porewater was highest near the coast, and decreased further offshore (Fig. 3-6 D). Interestingly, this pattern is consistent with the decreasing DIN:DIP ratio in the water column with distance from the coast that has been observed since the 1990's (Burson et al., 2016). De-eutrophication efforts (OSPAR, 1988), have decreased P inputs to coastal waters of the North Sea by 50 - 70 %, but reduced the N load by only 20 - 30 % (Lenhart et al., 2010; Passy et al., 2013). As a result of this, DIN:DIP ratios in the water column have been observed to be elevated above Redfield (N:P of 16:1, Redfield (1960)) from the coast, up to the eastern slope of the Dogger Bank in April (Burson et al., 2016). In summary, the pattern of decreasing DIN:DIP ratios we observed is explained on one hand by increased P burial, and a link to similar DIN:DIP dynamics in the water column closer to shore, and on the other hand by increasing N removal by denitrification towards the north.

3.5. Conclusions

The combination of field measurements and diagenetic modelling showed rapid mineralization of fresh organic matter in the sediments of a region of the North Sea extending from 100 km from the Dutch coast up to the Fladen Grounds in the northern part of the North Sea. This resulted in an overall low nutrient build-up, despite significant differences in sediment characteristics and environmental conditions. The similarity of the mineralization response characterizes the study area as a zone of fast nutrient recycling, where fresh organic material is recycled to nutrients that are available to the water column within weeks, or a few months after deposition. Total mineralization decreased with increasing latitude, revealing subtle differences in mineralization processes, such as increased removal of nitrogen and decreased removal of P towards the north. 1-D diagenetic modelling, combined with measured solute fluxes, and porewater nutrient profiles proved a robust tool in deriving mineralization rates. The results of this research expedition contribute valuable knowledge about the biogeochemical functioning of several understudied regions of the North Sea.

Acknowledgements

Chapter 4. BIOLOGICAL AND BIOGEOCHEMICAL METHODS FOR ESTIMATING BIO-IRRIGATION: A CASE STUDY IN THE OOSTERSCHELDE ESTUARY.

Emil De Borger, Justin Tiano, Ulrike Braeckman, Tom Ysebaert, Karline Soetaert

Abstract

Bio-irrigation, the exchange of solutes between overlying water and sediment by benthic organisms, plays an important role in sediment biogeochemistry. Bio-irrigation is either quantified based on tracer data or, a community (bio-) irrigation potential (IP_c) can be derived based on biological traits. Both these techniques were applied in a seasonal study of bio-irrigation in subtidal and intertidal habitats in a temperate estuary. The combination of a tracer time series with high temporal resolution and a mechanistic model allowed to simultaneously estimate the pumping rate, and the sediment attenuation, a parameter that determines irrigation depth. We show that although the total pumping rate is similar in both intertidal and subtidal areas, there is deeper bio-irrigation in intertidal areas. This is explained by higher densities of bio-irrigators such as *Corophium sp.*, *Heteromastus filiformis* and *Arenicola marina* in the intertidal, as opposed to the subtidal. The IP_c correlated more strongly with the attenuation coefficient than the pumping rate, which highlights that the IP_c index reflects more the bio-irrigation depth rather than the rate.

4.1. Introduction

Bio-irrigation is the process in which benthic organisms actively or passively exchange sediment porewater solutes with the overlying water column as a result of burrowing, pumping (ventilation) and feeding activities (Kristensen et al., 2012). This exchange plays an important role in marine and lacustrine sediment biogeochemistry, as oxygen rich water is brought into an otherwise sub- or anoxic sediment matrix. This allows for aerobic degradation processes to take place, as well as the reoxidation of reduced substances (Aller and Aller, 1998; Kristensen, 2001), and enables sediment dwelling organisms to forage and live in the otherwise anoxic deeper sediment layers (Olaffson, 2003; Braeckman et al., 2011). By extending the sediment- water interface in the vertical dimension, burrowing organisms increase the exchange surface, especially when burrow water is refreshed by ventilation activities. This enhances nutrient exchange (Quintana et al., 2007), and increases degradation rates (Na et al., 2008).

Sedimentary bio-irrigation is the result of the combined actions of a multitude of organisms sharing the same habitat. Some organisms such as the smaller meiofauna, located close to the sediment water interface, exchange only small amounts of solutes, but due to their high densities their activities affect the sediment porosity and as such exert a significant effect on sediment-water exchanges in the top layers of the sediment (Aller and Aller, 1992; Rysgaard et al., 2000). On the opposite end of the spectrum are larger infaunal species such as the burrowing shrimp *Upogebia pugettensis* (Dana, 1852) which constructs burrows that extend up to 1 m into the sediment and that actively ventilates these burrows using its pleiopods (D'Andrea and DeWitt, 2009). These deep burrows substantially extend the oxic sediment-water interface into the sediment, influencing the associated microbial respiration through various pathways (Nielsen et al., 2004). The effect of bio-irrigation also depends on the sediment matrix. In muddy sediments, where permeability is low, bio-irrigation impacts are localized close to the burrow wall, as the transport of solutes radiating from the burrows is governed by diffusion (Aller, 1980). In sandy, more permeable sediments the pressure gradients caused by ventilation activities induce water flows through the surrounding sediments, thus affecting the sediment matrix further away from the burrow walls (Meysman et al., 2005a; Timmermann et al., 2007). Therefore, the effects of bio-irrigation depend on a combination of the species community, species' individual behavior including ventilation activity, the depths at which they occur, and the sediment matrix they inhabit.

Bio-irrigation can be quantified with biogeochemical methods, or a qualitative estimate can be calculated by an index of bio-irrigation based on biological information. The biogeochemical methods estimate the exchange rates of a tracer substance (usually inert) between the overlying water and the sediment, by fitting a linear model (De Smet et al., 2016; Mestdagh et al., 2018; Wrede et al., 2018), or a quasi-mechanistic model (Berelson et al., 1998; Andersson et al., 2006) through measured concentration time series. A linear decrease returns the rate of disappearance of the tracer from the water column over a given time period, but it gives little information on the bio-irrigation process itself, e.g. what is the actual pumping rate, and where in the sediment are solutes exchanged. While sometimes the depth distribution of the tracer in the sediment is characterized post-experiment to obtain this information (Martin and Banta, 1992; Berg et al., 2001; Hedman et al., 2011), this step is often overlooked. By increasing the temporal resolution of the tracer concentration measurements, an exponential decrease can be fitted through the data, from which a bio-irrigation rate can be derived which is independent of the length of the experiment (Meysman et al., 2006a; Na et al., 2008). For these applications fluorescent tracers are used, as they can be monitored *in-situ*, and the measurement is instantaneous. So far, this method has been applied in controlled settings, but not yet in field applications.

The index approach starts with the quantification of the abundance and biomass of organisms inhabiting the sediment, and an assessment of how these organisms bio-irrigate. The latter is done based on a set of life history traits which are assumed to contribute to bio-irrigation: the type of burrow they inhabit, their feeding type and their burrowing depth. Species are assigned one trait score for each trait, independent of the biological context in which they occur (but see Renz et al. (2018)). The species biomass and abundance, combined with their trait scores are then used to derive an index that represents the community (bio-) irrigation potential (BIP_c and IP_c in Renz et al., 2018 and Wrede et al., 2018

respectively), a similar practice to what is done for bioturbation with the community bioturbation potential (BP$_C$; Queirós et al., 2013). The inherent assumptions of this approach are that bio-irrigation activity increases linearly with the number of organisms, and scales with their mean weight through a metabolic scaling factor. The advantage of biologically-based indices is that large datasets of benthic communities are currently available (e.g. Craeymeersch et al., 1986; Degraer et al., 2006; Northeast Fisheries Science Center, 2018), so that these data have great potential to derive information on the temporal and spatial variability of bio-irrigation. However, in contrast to the related bioturbation potential (Solan, 2004a), the classification of sediments according to their bio-irrigation potential is a very recent endeavor, and the underlying mechanistic basis of these indices, i.e. what they actually describe, should be explored further. As a first step in this direction, the IP$_c$ index of Wrede et al. (2018) has been calibrated against bromide uptake rates for selected individual species and communities in the German Bight of the North Sea.

The aim of the current study was to compare bio-irrigation rate measurements with an index of bio-irrigation in natural sediments of a temperate estuarine system, the Oosterschelde. Samples were collected across different seasons in three subtidal and three intertidal sites with different benthic communities, and sediments varying from muddy to sandy. Bio-irrigation rates were derived by fitting a novel mechanistic model through a quasi-continuous time series of a fluorescent tracer, while biological information was used to calculate the IP$_c$ index.

4.2. Materials and methods

4.2.1. Sampling

Field samples were collected in the Oosterschelde (SW Netherlands) from August 2016 to December 2017 (Fig. 4-1). Six sites (3 subtidal, 3 intertidal) were selected based on results from previous sampling efforts, to reflect the variability in inundation time and sediment composition present in this area (Fig. 4-1). The intertidal sites Zandkreek (N 51.55354°, E 3.87278°), Dortsman (N 51.56804°, E 4.01425°) and Olzendenpolder (N 51.46694°, E 4.072694°) were sampled by pressing two cylindrical PVC cores (14.5 cm Ø, 30 cm height) in the sediment at low tide up to a depth of 20 cm at most, and extracting them from the sediment. The subtidal sites Hammen (N 51.65607°, E 3.858717°), Viane (N 51.60675°, E 3.98501°), and Lodijksegat (N 51.48463°, E 4.166001°) were sampled in the same way, but sediment was retrieved from duplicate deployments of a NIOZ box-corer aboard the Research Vessel Delta. In total 70 individual cores in the intertidal, and 47 in the subtidal were retrieved. Sediment permeability has a strong influence on bio-irrigation rates (Aller, 1983; Meysman et al., 2006). Sediment permeability was not directly measured, but additional samples for sediment characteristics relating to this property (grain size distribution and porosity) were taken from the top 2 cm of sediment at each site, using a cut-off syringe. From the same samples a subsample was collected for determining the chlorophyll *a* content, and C/N ratios in the sediment, as measures of food availability and quality respectively.

After transportation to the laboratory, the cores were placed into seawater tanks in a climate room set to the average water temperature of the month in which the samples were taken (T. 4-1: seasonal

averages). By adding 0.45 μm filtered Oosterschelde water, the overlying water height was brought to at least 10 cm, and air stones and a stirring lid (central Teflon coated magnet stirrer) with sampling ports were used to keep the water oxygenated. The sediment cores were left to acclimatize for 24 to 48 hours before starting the irrigation experiment. For the irrigation measurements, a stock solution of 1 mg L^{-1} uranine (sodium fluoresceine - $C_{20}H_{10}NaO_5^-$) was prepared by dissolving 1 mg of uranine salts into 1 L of 0.45 μm filtered Oosterschelde water. Short experiments were performed to assess possible interactions between the tracer, and the incubation cores and stirring devices (Appendix D). To start the experiment 30 to 40 mL of the stock solution was added to the overlying water to achieve a starting concentration of uranine of about 10 μg L^{-1}. The concentration of the fluorescent tracer was subsequently measured every 30 seconds for a period of at least 12 hours with a fluorometer (Turner designs cyclops 6) placed in the water column through a sampling port in the stirring lid of the core, ± 6 cm below the water surface. After the measurement, the sediment was sieved over a 1 mm sieve and the macrofauna was collected and stored in 4% buffered formalin for species identification and abundance and biomass determination.

Sediment grain size was determined by laser diffraction on freeze dried and sieved (< 1 mm) sediment samples in a Malvern Mastersizer 2000 (McCave et al., 1986). Water content was determined as the volume of water removed by freeze drying wet sediment samples. Sediment porosity was determined from water content and solid phase density measurements, accounting for the salt content of the pore water. Chl *a* was extracted from the freeze dried sediment sample using acetone, and quantified through UV spectrophotometry (Ritchie, 2006). The C/N ratio was calculated from total C and N concentrations, determined using an Interscience Flash 2000 organic element analyser.

Fig. 4-1: Subtidal (white dots) and intertidal (black dots) sampling stations in the Oosterschelde estuary.

T. 4-1: Sampling frequency of the different research sites, and average seasonal temperature of the water in the incubation cores during the measurements

Season	Spring	Summer	Autumn	Winter
Months	Apr – Jun	Jul – Sep	Oct – Dec	Jan – Mar
Avg. Temperature (°C)	12.8	17.9	11.9	7.3
Dortsman	4	5	9	5
Zandkreek	4	6	9	6
Olzendenpoder	4	4	8	6
Lodijksegat	4	4	8	2
Hammen	4	4	8	2
Viane	3	0	6	2

4.2.2. Model

The exchange of a tracer (T) between the sediment and the overlying water is described in a (vertical) one-dimensional mechanistic model, that includes molecular diffusion, adsorption to sediment particles, and bio-irrigation. The bio-irrigation is implemented as a non-local exchange in which a pumping rate (r) exponentially decays with distance from the sediment surface (z). This exponential decay mimics the depth dependent distribution of faunal biomass often found in sediments (Morys et al., 2017) and the associated decreasing amount of burrow cross-sections with depth (Martin and Banta, 1992; Furukawa et al., 2001).

The mass balance for a dissolved tracer (T, Eq. 1) and the adsorbed tracer (A, Eq. 2) in an incubated sediment with height h_s, at a given depth (z, cm) and time (t, hours) in the sediment is:

$$\frac{\partial T_z}{\partial t} = \frac{1}{\varphi_z} \cdot \frac{\partial}{\partial z}\left[D_s \varphi_z \frac{\partial T_z}{\partial z}\right] + r\frac{e^{-az}}{\int_0^{h_S} e^{-az}\,dz} \cdot (T_{OW} - T_z) - k \cdot (Eq_A \cdot T_z - A_z) \cdot \rho \cdot \frac{(1-\varphi_z)}{\varphi_z} \qquad \text{(Eq. 1)}$$

$$\frac{\partial A_z}{\partial t} = k \cdot (Eq_A \cdot T_z - A_z) \qquad \text{(Eq. 2)}$$

In this equation φ_z is sediment porosity (-), and ρ is sediment density (g cm^{-3}).

In the equation for T (Eq. 1), the first term represents transport due to molecular diffusion, where D_s is the sediment diffusion coefficient (cm^2 h^{-1}). The second term represents the exchange of tracer between the water column (T_{OW}) and any sediment depth z due to irrigation, where the exchange rate decreases exponentially as modulated by the attenuation coefficient a (cm^{-1}). The exponential term is scaled with the integrated value, so that the exchange rate r reflects the total rate of bio-irrigation, expressed in (cm h^{-1}).

The loss term for the tracer by adsorption (third term) depends on the deviation from the local equilibrium of the tracer with the actual adsorbed fraction on the sediment and with parameters k (h^{-1}), the rate of adsorption, and Eq_A, the adsorption equilibrium (ml g^{-1}).

The dissolved tracer concentration in the water column (T_{OW}) (Eq. 3) decreases by the diffusive flux into the sediment and the integrated irrigation flux, corrected for the thickness of the overlying water (h_{OW}, cm):

$$\frac{\partial T_{OW}}{\partial t} = \frac{1}{h_{OW}} \left(-D_s \varphi_0 \frac{\partial T_z}{\partial z} \Big|_{z=0} - \int_0^{h_S} r \cdot \frac{e^{-az}}{\int_0^{h_S} e^{-az} \, dz} (T_{OW} - T_z) dz \right) \qquad \text{(Eq. 3)}$$

The concentration of *A* in the overlaying water equals 0.

The model was implemented in FORTRAN and integrated using the ode.1D solver from the R package deSolve (Soetaert et al., 2010; R Core Team, 2013). The sediment was subdivided into 50 layers; thickness of the first layer set equal to 0.5 mm and then exponentially increasing until the total sediment modelled was equal to the sediment height in each laboratory experiment.

4.2.3. Model fitting

Most of the input parameters of the model were constrained by physical measurements. Sediment porosity ϕ and specific density ρ (g cm^{-3}) were derived from sediment samples taken alongside the cores in the field. The adsorption equilibrium Eq_A (in ml g^{-1}) was determined from batch adsorption experiments (See Appendix D). The modelled sediment height (h_S) and water column height (h_{OW}) were set equal to the experimental conditions. This left two parameters governing the bio-irrigation rate to be estimated by model fitting: r, the integrated pumping rate and a, the attenuation coefficient. Fitting of the model to the experimental data was done with the R package FME (Soetaert and Petzoldt, 2010). First an identifiability analysis was performed to investigate the certainty with which these parameters could be derived from model fitting given the experimental data. This entails a local sensitivity analysis to quantify the relative effects of said parameters on model output, and a collinearity analysis to test whether parameters were critically correlated, and thus not separately identifiable, or the opposite. Then both parameters were estimated by fitting the model to each individual tracer time series through minimization of the model cost (the weighted sum of squares) using the pseudo-random search algorithm (Price, 1977) followed by the Levenberg-Marquardt algorithm. Lastly, a sensitivity analysis was performed to calculate confidence bands around the model output, based on the parameter covariance matrix derived from the fitting procedure (Soetaert and Petzoldt, 2010).

4.2.4. Calculation of IP$_c$ and BP$_c$

The retrieved benthic macrofauna were identified down to lowest possible taxonomic level, counted and their ash-free dry weight (gAFDW m^{-2}) was converted from blotted wet weight according to Sistermans et al. (2006). Based on the species abundance and biomass, the irrigation potential of the benthic community in a sediment core (IP$_c$, Eq. 4) was calculated as described in Wrede et al. (2018):

$$IP_c = \sum_{i=1}^{n} \left(\frac{B_i}{A_i} \right)^{0.75} \cdot A_i \cdot BT_i \cdot FT_i \cdot ID_i \qquad \text{(Eq. 4)}$$

in which B_i represents the biomass (gAFDW m^{-2}), A_i the abundance (ind. m^{-2}) of species i in the core, and BT_i, FT_i and ID_i are descriptive numerical scores for the species burrowing type, feeding type and injection pocket depth respectively. The values for FT_i, BT_i and ID_i were the same as applied by Wrede et al. (2018). If not available, values were assigned based on the closest taxonomic relative, with possible adjustments to correct for size differences and feeding type as taxonomic relation is not always a measure for similarity in traits.

The community bioturbation potential (BP$_c$, Eq. 5) was calculated as described in Solan et al. (2004):

$$BP_c = \sum_{i=1}^{n} \left(\frac{B_i}{A_i}\right)^{0.5} \cdot A_i \cdot M_i \cdot R_i \qquad \text{(Eq. 5)}$$

with M_i the mobility score and R_i the reworking score for species i from Queirós et al. (2013). Note that the biomass B in this case is the blotted wet weight of the organisms.

4.2.5. Data analysis

Differences in model derived pumping rates r and attenuation coefficient a between subtidal and intertidal were tested using a two-sided T-test (using a significance level of 0.05). For further multivariate analysis, species densities, biomass, and estimated irrigation parameters were averaged per station, and per season (Fig. 4-2) since not all six stations were sampled on the same date. The patterns in abiotic conditions, species composition and bio-irrigation rates were analysed using ordination techniques for multivariate datasets as described in Thioulouse et al.(2018), and implemented in the ade4 R package (Dray and Dufour, 2007). In this procedure, a coinertia analysis and permutation first tests the null hypothesis that there is no significant relationship between environmental variables and species densities, and then the correlation of the bio-irrigation rates to the environment-species data is assessed. In a first step, the species data matrix was processed by centered Principle Component Analysis (PCA). For this the species relative densities were used to emphasize the specific functional role of some species within the communities (Beauchard et al., 2017) and to reduce the effects of heavy outliers. Secondly the environmental variable matrix was processed by Multiple Correspondence Analysis (MCA; Tenenhaus and Young (1985). This technique can account for non-linear relationships between variables, but requires all variables to be categorical. Sediments were categorized based on grain size into the Udden-Wentworth scale (Wentworth, 1922) of silt (< 63 μm), very fine sand (> 63 μm, < 125 μm) and fine sand (> 125 μm, < 250 μm); the Chl a content was categorized to distinguish sites with low (< 8 μg g^{-1}), intermediate (8-16 μg g^{-1}) and high (> 16 μg g^{-1}) chlorophyll content. Two abiotic variables were already categorical: habitat type (intertidal versus subtidal) and season. Sediment porosity and C/N ratio were not used in the analysis given the small range within these data (T. 4-2). In a third step, the two ordinations were combined in a Co-Inertia Analysis (CoIA; Dray et al. (2003)), to explore the co-structure between the species and the environmental variables. The significance of the overall relationship (the co-structure of species and environment) between the two matrices was tested by a Monte-Carlo procedure based on 999 random permutations of the row matrices (Heo and Gabriel, 1998). Finally, the correlations between the response variables relating to irrigation (estimated irrigation parameters, calculated IP$_c$, BP$_c$) and the two axes of the co-inertia analysis were assessed using the Pearson correlation coefficient assuming a significance level of 0.05. Results are expressed as mean ± sd.

4.3. Results

4.3.1. Environmental variables

Sediment descriptors are summarized in T. 4-2. Chlorophyll a concentrations in the upper 2 cm of the sediment varied from 3.76 ± 2.43 μg g^{-1} in Hammen to 20.60 ± 4.19 μg g^{-1} in Zandkreek and were higher in the intertidal (13.34 ± 6.53 μg g^{-1}) than in the subtidal (5.88 ± 4.20 μg g^{-1}). In the intertidal, the median

grain size (d50) and silt content ranged from 59 μm with 52% silt to 140 μm with 0% silt. In the subtidal the range in grain size was broader, from 53 μm with 63% silt to 201 μm with 24% silt. The C/N ratio (mol mol^{-1}) was similar for all sites (9.3 ± 1.0 – 12.3 ± 1.4) with the exception of Dortsman, where values were lower (6.5 ± 1.2). Dortsman was also the site where the organic carbon content was lowest (0.07 ± 0.02 %). The organic carbon content increased with silt content, to highest values in the most silty station Viane (1.16 ± 0.36 %).

T. 4-2: Sediment characteristics averaged over the study period (n= 8 per sampling site) represented with standard deviation for the intertidal sites Dortsman, Olzendenpolder and Zandkreek, and the subtidal sites Lodijksegat, Hammen and Viane.

	Dortsman	Olzendenpolder	Zandkreek	Lodijksegat	Hammen	Viane
% Silt	0 ± 0	14 ± 16	51 ± 7	25 ± 5	24 ± 5	63 ± 19
CN ratio (mol mol^{-1})	6.5 ± 1.2	11.3 ± 2.4	9.3 ± 1.0	12.4 ± 1.4	9.8 ± 0.9	9.9 ± 1.0
% C$_{org}$	0.07 ± 0.02	0.30 ± 0.27	0.79 ± 0.33	0.58 ± 0.12	0.35 ± 0.07	1.16 ± 0.36
d50 (μm)	140 ± 2	112 ± 24	59 ± 14	116 ± 7	201 ± 38	53 ± 60
Porosity (-)	0.43 ± 0.07	0.53 ± 0.07	0.45 ± 0.09	0.52 ± 0.03	0.45 ± 0.03	0.73 ± 0.06
***Chl* a (μg g^{-1})**	8.65 ± 3.53	9.97 ± 2.80	20.60 ± 4.19	5.33 ± 3.92	3.76 ± 2.43	10.26 ± 3.92

4.3.2. Macrofauna

In total, 60 species were identified in the 6 different stations (T. 4-3). Species abundances in the intertidal were generally one, sometimes two orders of magnitude higher than in the subtidal (see T. 4-3: a, b for seasonal species density and biomass data). In the intertidal, maximum abundances were observed in Dortsman in autumn and spring, with peak values of 15202 ± 4863 and 16054 ± 13939 ind. m^{-2} respectively, mainly due to high abundances of the amphipods *Corophium sp.* and *Bathyporeia* sp. (respective peak values of 9957 ± 4465 and 3934 ± 3087 ind. m^{-2}). Subtidal densities varied less and were highest in Lodijksegat in autumn and summer (peak values of 661 ± 502 and 790 ± 678 ind. m^{-2} respectively). Faunal biomass was larger in the subtidal (22.31 ± 26.42 gAFDW m^{-2}) as opposed to the intertidal (10.51 ± 8.59 gAFDW m^{-2}), with peak summer values at the subtidal Lodijksegat station (39.90 ± 34.87 gAFDW m^{-2}) coinciding with high abundances (972 ± 172 ind. m^{-2}) of the common slipper limpet *Crepidula fornicata* (Linnaeus, 1758).

T. 4-3: Species densities per station and per season (ind m^{-2}), excluding species that were only encountered once.

	Species	Autumn	Spring	Summer	Winter	Annual
	Arenicola marina	113 ± 74	440 ± 395	91 ± 35	0	194 ± 244
	Bathyporeia sp.	1789 ± 1381	3934 ± 3087	1443 ± 1452	577 ± 350	1735 ± 1833
	Capitella capitata	289 ± 416	223 ± 153	304 ± 0	73 ± 27	192 ± 240
Dortsman **Intertidal**	*Cerastoderma edule*	61 ± 0	61 ± 0	61 ± 0	81 ± 35	69 ± 23
	Corophium sp.	9957 ± 4465	7120 ± 9205	5848 ± 2792	2977 ± 1850	6781 ± 5289
	Eteone longa	61 ± 0	0	122 ± 0	61 ± 0	85 ± 33
	Hediste diversicolor	91 ± 61	547 ± 687	304 ± 182	61 ± 0	243 ± 311

	Limecola balthica	122 ± 0	0	152 ± 43	61 ± 0	109 ± 51
	Nematoda	0	273 ± 129	61 ± 0	0	203 ± 153
	Oligochaeta	219 ± 164	851 ± 0	1175 ± 1719	122 ± 50	458 ± 839
	Peringia ulvae	1409 ± 1538	365 ± 0	658 ± 729	840 ± 381	911 ± 933
	Pygospio elegans	425 ± 0	0	0	61 ± 0	134 ± 163
	Scoloplos armiger	1782 ± 1197	1470 ± 1195	1288 ± 691	1580 ± 970	1572 ± 1013
	Scrobicularia plana	1175 ± 460	608 ± 662	759 ± 301	61 ± 0	753 ± 570
	Tellinoidea	61 ± 0	61 ± 0	0	61 ± 0	61 ± 0
	Abra alba	76 ± 30	152 ± 43	91 ± 43	61 ± 0	95 ± 44
	Arenicola marina	61 ± 0	152 ± 43	0	0	122 ± 61
Zandkreek	*Hediste diversicolor*	1013 ± 737	1409 ± 780	1033 ± 392	1326 ± 520	1156 ± 609
Intertidal	*Heteromastus filiformis*	0	182 ± 0	0	76 ± 30	97 ± 54
	Oligochaeta	324 ± 175	0	0	375 ± 383	358 ± 316
	Tharyx sp.	61 ± 0	0	0	91 ± 43	81 ± 35
	Arenicola marina	142 ± 93	122 ± 105	122 ± 105	122 ± 0	128 ± 83
	Capitella capitata	61 ± 0	101 ± 35	61 ± 0	0	85 ± 33
	Cerastoderma edule	61 ± 0	61 ± 0	61 ± 0	0	61 ± 0
	Crangon crangon	0	61 ± 0	122 ± 0	0	76 ± 30
	Hediste diversicolor	61 ± 0	61 ± 0	0	182 ± 0	122 ± 70
Olzendenpolder	*Heteromastus filiformis*	0	122 ± 0	0	61 ± 0	101 ± 35
Intertidal	*Notomastus sp.*	81 ± 35	61 ± 0	61 ± 0	152 ± 78	108 ± 66
	Oligochaeta	0	122 ± 0	152 ± 43	213 ± 215	170 ± 117
	Peringia ulvae	61 ± 0	0	12454 ± 10795	304 ± 86	6339 ± 9566
	Polydora ciliata	122 ± 0	0	0	61 ± 0	101 ± 35
	Scoloplos armiger	344 ± 220	410 ± 135	182 ± 105	279 ± 213	314 ± 188
	Tharyx sp.	243 ± 61	0	0	61 ± 0	152 ± 107
	Actiniaria	144 ± 72	97 ± 54	134 ± 51	61 ± 0	125 ± 62
	Ensis sp.	61 ± 0	0	61 ± 0	0	61 ± 0
	Hemigrapsus sp.	61 ± 0	0	122 ± 0	0	81 ± 35
	Mytilus edulis	61 ± 0	3311 ± 215	2886 ± 2105	0 ± 0	2491 ± 1735
Hammen	*Nephtys hombergii*	85 ± 33	61 ± 0	61 ± 0	61 ± 0	71 ± 24
Subtidal	*Notomastus sp.*	111 ± 81	203 ± 93	152 ± 43	61 ± 0	137 ± 82
	Ophiura ophiura	122 ± 0	0	243 ± 161	0	213 ± 145
	Scoloplos armiger	0	61 ± 0	0	91 ± 43	81 ± 35
	Terebellidae	61 ± 0	61 ± 0	61 ± 0	0 ± 0	61 ± 0
	Crepidula fornicata	319 ± 152	122 ± 0	972 ± 172	0	477 ± 369
	Hemigrapsus sp.	61 ± 0	0	61 ± 0	0	61 ± 0
Lodijksegat	*Lanice conchilega*	375 ± 225	304 ± 0	91 ± 43	273 ± 301	298 ± 216
Subtidal	*Malmgrenia darbouxi*	91 ± 43	0	0	182 ± 0	122 ± 61
	Nephtys hombergii	111 ± 60	158 ± 92	0	0	133 ± 76

	Notomastus sp.	81 ± 35	91 ± 43	61 ± 0	61 ± 0	78 ± 30
	Pholoe baltica	61 ± 0	0	122 ± 0	61 ± 0	76 ± 30
	Scoloplos armiger	122 ± 0	61 ± 0	122 ± 0	122 ± 0	106 ± 30
	Terebellidae	31 ± 42	0	0	61 ± 0	41 ± 34
Viane	*Nephtys hombergii*	162 ± 93	101 ± 70	0	122 ± 0	129 ± 68
Subtidal	*Ophiura ophiura*	167 ± 58	0	0	91 ± 43	142 ± 63

4.3.3. Bio-irrigation rates

A typical time series of uranine concentrations shows the tracer to exponentially decrease towards a steady value (Fig. 4-3 a). The pumping rate and irrigation attenuation (parameters r and a) have an opposite effect on tracer concentrations in the overlying water, but a collinearity analysis (Soetaert and Petzoldt, 2010) showed that these two parameters could be fitted simultaneously. The attenuation coefficient a affects the depth of the sediment which is irrigated, with larger values of a resulting in more shallow bio-irrigation. Higher pumping rates, r, entail a faster removal of the tracer from the water. Compared to the parameters r and a, the rate of adsorption, k had a 1000-fold weaker effect on the outcome. Its value was set to 1 (h^{-1}) implying that it takes about 1 hour for the sediment adsorbed tracer fraction to be in equilibrium with the porewater tracer fraction.

In 11 out of 117 cases the fitting procedure yielded fits for which both the attenuation coefficient a and the pumping rate r were not significantly different from 0 and for which bio-irrigation was thus assumed to be absent. These were predominantly observed in November and December (7 out of 11 non-significant fits) and in these cases the tracer concentration did not notably change but rather fluctuated around a constant value.

The fitted irrigation rates and attenuation coefficients did not show clear seasonal trends in the intertidal stations (Fig. 4-2, T. 4-4). In the subtidal stations, irrigation rates were lowest in autumn, and highest in winter (Fig. 4-2 c). There was no significant difference in irrigation rates between the subtidal (0.547 ± 1.002 mL cm^{-2} h^{-1}) and intertidal (0.850 ± 1.157 mL cm^{-2} h^{-1}) (Welch two-sample T-test: p = 0.708). Seasonally averaged irrigation rates were highest at Lodijksegat in winter (1.693 ± 1.375 mL cm^{-2} h^{-1}), whereas in autumn at that same station they were lowest (0.091 ± 0.078 mL cm^{-2} h^{-1}). The model derived attenuation coefficients were significantly higher in the subtidal (2.387 ± 3.552 cm^{-1}) than in the intertidal (0.929 ± 1.793 cm^{-1}) (Welch two-sample T-test: p = 0.041).
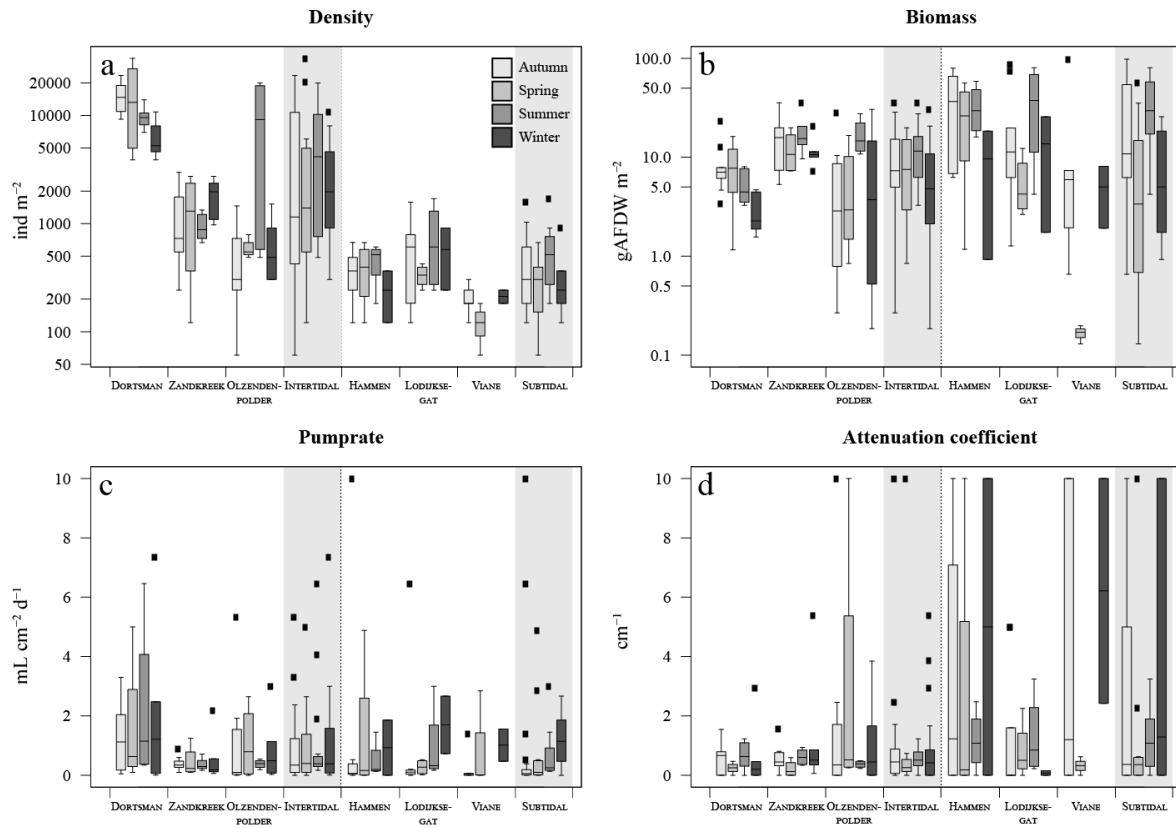
Fig. 4-2: (a) organism densities (ind m^{-2}); (b) organism biomass as ash-free dry weight (gAFDW m^{-2}); (c) model derived pumping rate (mL cm^{-2} d^{-1}); (d) model derived attenuation coefficient (cm^{-1}). Data arranged per station (white areas) and per habitat type, intertidal and subtidal (grey shaded areas). Black squares = outliers.
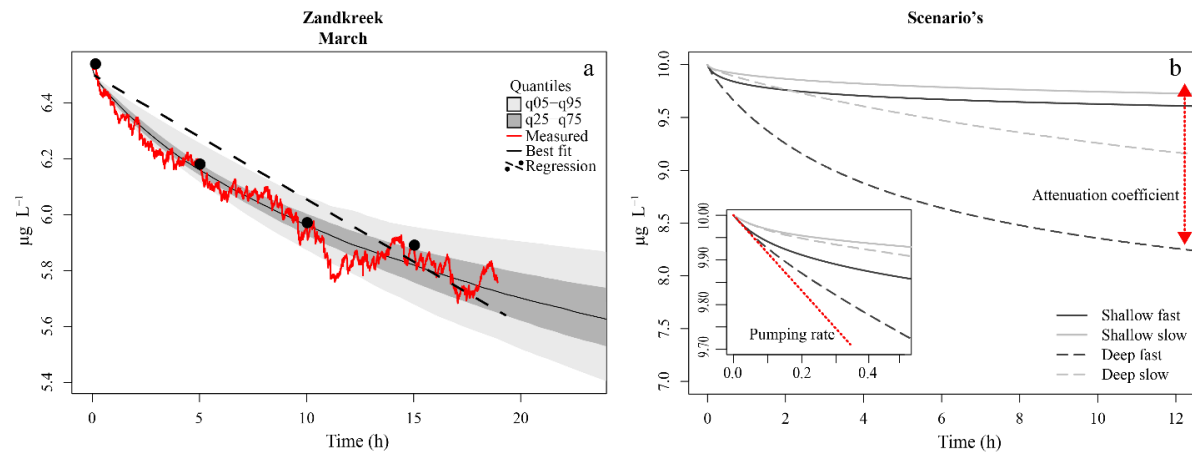
Fig. 4-3: (a) Model fit to data (red line) from a core at Zandkreek in March 2017. The best fit tracer profile (full black line) is shown, along with the range of model outputs as quantiles (light and dark grey). An example of a linear fit (dashed line) through (fictitious) samples taken every 5 hours (dots) is also shown. (b) Example model output for different combinations of pumping rate (slow = 0.15 mL cm^{-2} h^{-1} , fast = 0.8 mL cm^{-2} h^{-1}), and attenuation coefficients (shallow = 5 cm^{-1}- deep = 0.5 cm^{-1}). The inset shows a close-up of the first half hour of the simulation. Red line illustrates the effect of the pumping rate, which has the strongest initial effect; red arrow illustrates the effect of the attenuation coefficient, which determines the depth of the irrigation.

T. 4-4: Seasonally averaged values for Chl a in the upper 2 cm of the sediment (µg Chl a g⁻¹), species density (ind m⁻²), biomass (gAFDW m⁻²), pumping rate (mL cm⁻² h⁻¹), and the attenuation coefficient (cm⁻¹)[3] for the intertidal and the subtidal.

	Season	Chl *a*	Individual density	Biomass	Pump rate	Attenuation
Intertidal	Autumn	12.49 ± 6.92	5828 ± 7509	11.16 ± 9.31	0.88 ± 1.24	0.97 ± 1.91
	Spring	12.30 ± 3.89	6005 ± 10421	8.72 ± 6.48	1.03 ± 1.48	1.09 ± 2.81
	Summer	14.69 ± 6.58	6193 ± 6763	13.65 ± 8.91	0.72 ± 1.02	0.59 ± 0.34
	Winter	14.17 ± 7.52	2645 ± 2702	8.02 ± 8.10	0.79 ± 0.96	1.05 ± 1.56
Subtidal	Autumn	5.90 ± 4.37	439 ± 365	25.67 ± 30.42	0.16 ± 0.31	2.96 ± 3.91
	Spring	7.00 ± 3.00	298 ± 181	12.15 ± 18.08	0.83 ± 1.58	1.33 ± 2.95
	Summer	4.20 ± 2.27	623 ± 494	36.67 ± 26.29	0.73 ± 1.02	1.23 ± 1.14
	Winter	6.02 ± 7.08	344 ± 289	9.45 ± 10.32	1.22 ± 0.99	3.76 ± 4.92

4.3.4. Co-inertia analysis

The first and second axes of the co-inertia analysis (CoiA) explained 57% and 19% of the variance in the dataset respectively (histogram inset Fig. 4-4 a). The Monte-Carlo permutation test resulted in a significant RV coefficient (the multivariate generalization of the squared Pearson correlation coefficient) of 0.62 ($p < 0.001$), showing that the species data and the environmental data are significantly correlated. Both the first and second axes of the MCA performed on the environmental parameters and of the PCA performed on the species community were correlated, indicated by high Pearson correlation coefficients (Fig. 4-4). In the MCA of the environmental variables, the first axis reflected mainly a grain size gradient from very fine sandy to silty (Fig. 4-4 b), with subtidal sites Lodijksegat (L) and Hammen (H) on the very fine sandy end, and the intertidal site Zandkreek (Z) in the high silt end (Fig. 4-4 a). The Chl *a* content and the immersion type (intertidal *vs* subtidal) were the main factors associated with axis 2. This axis separated the subtidal station Viane (V) from the intertidal stations Dortsman (D) and Olzendenpolder (O) (Fig. 4-4 a). Of the different seasons, only summer correlated to the second axis. The PCA of the relative species abundances showed that in more fine sandy subtidal stations species such as the reef forming *Mytilus edulis* (Linnaeus, 1758), and *Lanice conchilega* (Pallas 1766) were found (Fig. 4-4 c). The species *Corophium sp.* and *Peringia ulvae* (Pennant, 1777) dominated in the intertidal, while *Ophiura ophiura* (Linnaeus, 1758) and *Nephtys hombergii* (Lamarck, 1818) were mainly found in the subtidal.

---

[3] The use of mean ± sd is invalid for the pump rate and attenuation, as these data are non-normal. A table reporting the median, Q1, and Q3 may be found in Appendix B. This has only been noticed after publication of this article.

T. 4-5: Pearson correlations of the response variables against the ordination axes of the coinertia analysis, with p-values reported under the values in italics.

| | Irrigation r | Attenuation a | BP_c | IP_c |
	mL cm^{-2} h^{-1}	cm^{-1}	gWW$^{0.5}$ m^{-2}	gAFDW$^{0.75}$ m^{-2}
Axis 1	-0.345	-0.288	0.540	0.780
	0.107	*0.182*	*0.008*	*< 0.001*
Axis 2	0.263	-0.565	0.646	0.395
	0.226	*0.005*	*< 0.001*	*0.062*

Fig. 4-4: Summary of the coinertia analysis (CoIA). (a) Co-structure between abiotic samples (circles) and species samples (arrow tips); grey circles "D", "O","Z" for intertidal sites Dortsman, Olzendenpolder and Zandkreek respectively; white circles "H", "L", "V" for subtidal sites Hammen, Lodijksegat and Viane respectively. Arrow length corresponds to the dissimilarity between the abiotic data and the species data (the larger the arrow, the larger the dissimilarity). Pearson's correlation between the circle and arrow tip coordinates on the first axis: r = 0.95, p < 0.001; on the second axis, r = 0.92, p < 0.001. Sites are more similar in terms of environmental conditions (circles), or species (arrow tips), when they group closer together. Inset: eigenvalue diagram of the co-structure; first axis explains 57%, second axis explains 19% of the variation in the dataset. (b) MBA based on environmental variables. (c) Species projections (dark arrows) and projected response variables (bio-irrigation parameters and bioturbation and bio-irrigation index) onto the co-inertia axes (grey arrows). The directions of arrows in figures b and c corresponds to the directions in which stations are grouped in terms of abiotic data (circles) and species composition (arrow tips) in figure a.

The correlation tests resulted in significant correlations between the first and the second axes of the co-inertia analysis (CoIA) with the BP_c (axis 1: $r = 0.54$, $p = 0.008$; axis 2: $r = 0.65$, $p = < 0.001$), and between the first CoIA axis and the IP_c (axis 1: $r = 0.78$, $p = < 0.001$; Fig. 4-4 c; see T. 4-5 for full correlation statistics). Values for these indices are highest in the intertidal samples (Dortsman) and lowest in the

subtidal, high Chl *a* samples (Viane), where also respectively the highest and lowest species densities were recorded. The attenuation coefficient *a*, was significantly and negatively correlated with the second axis (r = -0.57, *p* = 0.005). The attenuation coefficient increased in the opposite direction of the BP_c and IP_c indices (Fig. 4-4 c). No significant correlations were found for the model derived pumping rate *r* (axis 1: *r* = -0.35, *p* = 0.107; axis 2: *r* = 0.263, *p* = < 0.226). The pumping rate increased towards the intermediate – low Chl *a* samples, almost perpendicular to both the IP_c/BP_c arrows and the attenuation coefficient (Fig. 4-4 c).

4.4.   Discussion

4.4.1.   Advantages of mechanistic modelling

Bio-irrigation is a complex process with profound effects on sediment biogeochemistry (Aller and Aller, 1998; Kristensen, 2001). For a better understanding of how bio-irrigation affects the sediment matrix, and to construct indices of irrigation based on species composition and life history traits, it is crucial to understand the mechanistic bases of the process. This is the first study in which continuous measurements of a tracer substance, and a mechanistic model have been combined to study the bio-irrigation behaviour of species assemblages across a range of estuarine habitats. In bio-irrigation experiments, the tracer concentration in the overlying water decreases as it is diluted through mixing with porewater from the sediment. Initially, the sediment porewater is devoid of tracer, so that the dilution of the overlying water concentration is maximal. As the sediment itself becomes charged with tracer, the effect of sediment-water exchange on the bottom water concentration will decrease until the tracer concentration in the bio-irrigated part of the sediment and bottom water concentration are equal, and a quasi-steady state is achieved in which only molecular diffusion further slowly redistributes the tracer in the sediment. This verbal description of a bio-irrigation experiment shows that there are two important aspects to the data: the rate of bio-irrigation determines the initial decrease of tracer and how quickly the steady state will be reached, while the sediment volume over which bio-irrigation occurs determines the difference between initial and ultimate water column tracer concentrations at steady state.

The 1-D mechanistic model applied to our data comprises both these aspects, which are encompassed in two parameters: the integrated rate of bio-irrigation (*r*), and the attenuation coefficient (*a*) that determines the irrigation depth. In model simulations, the differences between fast and slow pumping rates mainly manifest themselves in the first part of the time series, while differences in irrigation depths are mainly discernable after several hours (Fig. 4-3 b). This adds nuance to the interpretation of bio-irrigation rates, as similar irrigation rates may have divergent effects on sediment biogeochemistry when the depth over which solutes are exchanged differs. We have shown here that this nuance is at play in the Oosterschelde, where model derived pumping rates are very similar in subtidal and intertidal sediments, but the attenuation coefficient was higher for subtidal sites than for intertidal sites, implying a more shallow bio-irrigation pattern in the former. It should be noted that, as the incubation chambers contained at most 20 cm of sediment, the effects of individuals living deeper (e.g. larger *A. marina*, or

N. latericeus) were not included in the incubations, and thus these were not accounted for in our estimates of bio-irrigation. This means that the bio-irrigation patterns described are only applicable to the upper 20 cm of the sediment.

Our tracer time series were measured at sufficiently high resolution (0.033 Hz), and for a sufficiently long time so that both the initial decrease, and the concentration to which the tracer converges were recorded. Indeed, identifiability analysis, a procedure to discover which model parameters can be estimated from data (Soetaert and Petzoldt, 2010) showed that the information in our data was sufficient to estimate these two parameters (*r* and *a*) with high confidence. This represents a significant improvement over discrete tracer measurements, from which deriving information of the depth distribution of irrigation is problematic (Andersson et al., 2006). Other data and/or models may not be able to derive these two quantities. Often bio-irrigation is estimated from linear fits through scarce (≤ 5 measurements) tracer concentration measurements (De Smet et al., 2016; Mestdagh et al., 2018; Wrede et al., 2018). This procedure is mainly applied when bromide is used as a tracer, as concentrations of this substance need to be measured in an elemental analyser, a procedure which, for practical reasons, does not allow quasi-continuous measurements from the same sample. This has a major drawback, as the linearization of the exponential decrease will clearly underestimate the pumping rates, and it will be influenced by the (unknown) tracer depth (Fig. 4-3). Indeed, these linear fit methods are sensitive to the chosen duration of the experiment, and results based on a time series of 6 hours will not give the same results as those based on a 12 hour measurement.

4.4.2. Spatio-temporal variability in bio-irrigation

Our data show that although total pumping rates are similar in the subtidal and intertidal sediments of the Oosterschelde, irrigation is shallower in the subtidal, as indicated by the higher attenuation coefficient (Fig. 4-2 c, d). The species community in the subtidal that is responsible for pumping is less dense, but (on average) the biomass is higher than in the intertidal (Fig. 4-2). In Viane, the site where bio-irrigation is lowest, only two species occur, *Ophiura ophiura* (Linneaus 1758), and *Nephtys hombergii*, and neither are typically associated with bio-irrigation, although *O. ophiura* can significantly disturb the sediment surface, inducing shallow irrigation (Fig. 4-4 c). The other two subtidal stations harbor two polychaete species that have been found to be prominent bio-irrigators: *Lanice conchilega* (Lodijksegat) and *Notomastus latericeus* (Sars 1851) (both Lodijksegat and Hammen). The sand mason worm *L. conchilega* lives in tubes constructed from shell fragments and sand particles which extend down to 10-15 cm (in the study area) and significantly affects the surrounding biogeochemistry (Forster and Graf, 1995; Braeckman et al., 2010). Highest densities of this species were observed in autumn at Lodijksegat, but interestingly this coincided with lowest bio-irrigation values for this station (T. 4-3: densities = 375 ± 22 ind m^{-2}; Fig. 4-2 c: bio-irrigation = 0.091 ± 0.176 mL cm^{-2} h^{-1}). High densities of *C. fornicata*, an epibenthic gastropod, in the same samples may possibly compete with the infauna, suppressing the bio-irrigation behavior through constant agitation of the feeding apparatus, similar to what happens in non-lethal predator-prey interactions (Maire et al., 2010; De Smet et al., 2016). *C. fornicata* is also known to cause significant biodeposition of fine particles on the sediment surface (Ehrhold et al., 1998; Ragueneau et al., 2005). This could decrease the permeability of the surface layers

and as such decrease the extent of possible bio-irrigation. Burrows of *N. latericeus* extend down to 40 cm, and they have no lining, which –in theory- would facilitate irrigation. However, the burrows are considered semi-permanent, which in turn limits the depth up to which bio-irrigation plays a role (Kikuchi, 1987; Holtmann et al., 1996). The presence of these polychaetes is thus not per se translated in high irrigation rates, though there does appear to be a link to the depth over which bio-irrigation occurs, with this being deepest in Lodijksegat (lowest *a*) where the species are present, and shallowest in Viane (highest *a*) that lacks these species.

In the intertidal stations the main species described as bio-irrigators are the mud shrimp *Corophium* sp., the lugworm *Arenicola marina* (Linnaeus, 1758)*,* and the capitellid polychaete *Heteromastus filiformis* (Claparède, 1864). *Corophium sp.* is an active bio-irrigator that lives in lined U-shaped burrows 5 to 10 cm in depth (McCurdy et al., 2000; De Backer et al., 2010). *A. marina* is often noted as the main bio-irrigator and bioturbator in marine intertidal areas (Huettel, 1990; Volkenborn et al., 2007). This species constructs U shaped burrows of 20 to 40 cm deep, and typically injects water to this depth in irrigation bouts of 15 minutes (Timmermann et al., 2007). *H. filiformis* creates mucus-lined permanent burrows in sediments up to 30 cm deep (Aller and Yingst, 1985). These species are present in all intertidal sites presented here. High densities of *Corophium sp.* are found there where high irrigation rates are measured (T. 4-3 and Fig. 4-2: Dortsman, 6781 ± 5289 ind. m^{-2}, bio-irrigation rates between 0.942 and 1.149 mL $cm^{-2} h^{-1}$).

The higher abundance of previously mentioned bio-irrigators in the intertidal, as opposed to the subtidal, explains the lower attenuation coefficient values in the intertidal. Intertidal areas also experience stronger variations in physical stressors such as waves, temperature, light, salinity and precipitation than subtidal areas (Herman et al., 2001), and to biological stressors such as predation by birds (Fleischer, 1983; Granadeiro et al., 2006; Ponsero et al., 2016). Burrowing deeper, or simply residing in deeper sediment layers for a longer time, are valid strategies for species in the intertidal to combat these pressures (Koo et al., 2007; MacDonald et al., 2014).

4.4.3. The Bio-irrigation Potential

The Community Irrigation potential (Eq. 4, Wrede et al., 2018) subsumes both the depth of bio-irrigation and the rate. The former is represented by the injection depth (*ID*), while the latter relates to the burrowing (*BT*) and feeding type (*FT*) of the species traits scaled with their size and abundance. Interestingly, in the Oosterschelde data, only one of the irrigation parameters correlates to the IP_c: the attenuation coefficient (Fig. 4-4 c). This is most likely a consequence of the fact that the IP_c index was calibrated using the Br^- linear regression method (Wrede et al., 2018), which may mainly quantify the irrigation depth. Nevertheless, the lack of a relation between the pumping rate and the IP_c is surprising, since this index does include traits that are expected to affect the pumping rate, and it is scaled for metabolic activity. This suggests that bio-irrigation is a process which not only depends on the species characteristics but also includes context dependent trait modalities that need to be considered.

Functional roles of species may differ depending on the context in which they are evaluated, and the *a priori* assignment of a species to a functional effect group may therefore be too simplistic (Hale et al.,

2014; Murray et al., 2014). Christensen et al. (2000) for instance reported irrigation rates of sediments in Kertinge Nor, Denmark with high abundances of *Hediste diversicolor* (O.F. Müller, 1776) (600 ind. m^{-2} at 15 °C) that varied with a factor 4 whether the organism was suspension feeding (2704 ± 185 L m^{-2} d^{-1}) or deposit-feeding (754 ± 80 L m^{-2} d^{-1}). In our study, the intertidal station Zandkreek also had very high abundances of *H. diversicolor* (peak at 2550 ind. m^{-2} in April) but much lower irrigation rates (128.6 ± 160.6 L m^{-2} d^{-1}). Possibly, the higher Chl *a* concentrations in Zandkreek (20.2 μg gDW^{-1}) compared to the sediment in Christensen et al. (2000) (±7 μg gDW^{-1}, converted from μg gWW^{-1}) caused the species to shift even more to deposit feeding. Similarly, previously reported irrigation rates of *Lanice conchilega* in late summer were quantified to range between 26.45 and 33.55 L m^{-2} d^{-1} (3243 ± 1094 ind. m^{-2}), in an intertidal area in Boulogne-Sur-Mer, France (De Smet et al., 2016), whereas we measured rates that were more than an order of magnitude higher in the same season (229.3 ± 327.8 L m^{-2} d^{-1}; Fig. 4-2 c), although densities were an order of magnitude lower (298 ± 216 ind. m^{-2}). *Lanice conchilega* is also known to switch from suspension-feeding to deposit-feeding when densities are lower (Buhr, 1976; Buhr and Winter, 1977). This suggests that bio-irrigation activity is higher when the *L. conchilega* is deposit feeding, although there could be of course additional context-dependent factors at play.

The species community in which an organism occurs can also affect the bio-irrigation behavior. Species regularly compete for the same source of food (e.g. filter feeders), with species changing their feeding mode to escape competitive pressure (Miron et al., 1992). Species also compete in the form of predator-prey interactions, which have also been shown to alter behavior. For example, the presence of *Crangon crangon* has been shown to reduce the food uptake of *L. conchilega* (De Smet et al., 2016), and alter the sediment reworking mode of *L. balthica* (Maire et al., 2010), in both cases because *C. crangon* preys on the feeding apparatus of these species protruding from the sediment. If bio-irrigation is to provide oxygen or to reduce the build-up of metabolites, then, given sufficient densities of other bio-irrigating organisms, oxygen halo's may overlap (Dornhoffer et al., 2012), reducing the need for individuals to pump. In Zandkreek for instance, *Arenicola marina* (Linnaeus, 1758) was present in many samples, except during summer and autumn (Fig. 4-2 b), while *Hediste diversicolor* was present in constant densities throughout the year. Although *A. marina* is a very vigorous bio-irrigator, its presence did not lead to a doubled pumping rate, suggesting an adaptation of the ventilation behaviour to the activity of *H. diversicolor*, or vice versa. This implies that simply summing of individual species irrigation scores to obtain a bio-irrigation rate may be too simplistic.

With these considerations in mind it appears that a comprehensive understanding of the ecology of species within the appropriate spatial scale and environmental context is a prerequisite for the application of an index to predict bio-irrigation rates (and by extension other functional traits). The current index (Eq. 4) contains burrow type, feeding mode, burrow depth, and an exponent to scale the metabolic rate, but from our analysis it appears that introducing more context-dependency could improve results. In Renz et al. (2018) for example, a distinction was made between an organism's activity based on the sediment type in which it occurred (cohesive or permeable sediment) in the calculation of their index, the Community Bioirrigation Potential (BIP$_c$), although no comparison with measured irrigation rates has taken place. Furthermore, Wrede et al. (2018) suggested to include a temperature

correction factor (Q_{10}) in the calculations to account for the expected metabolic response of macrofauna to increasing water temperatures (Brey, 2010). This temperature effect on benthic activity has indeed been noticed in similar works (Magni and Montani, 2006; Rao et al., 2014), but in our study and others the highest temperatures were not clearly associated with highest functional process rates (Schlüter et al., 2000: Braeckman et al., 2010; Queirios et al., 2015). The reasons for this ranged from a non-coincidence of the annual food pulse and the temperature peak, or the presence of confounding factors in the analysis such as faunal abundances and behavior (Forster et al., 2003b).

Based on the above, we stress the importance of measuring bio-irrigation rates in field settings, as it is through repeated measurements that the complex interactions of species communities and their environment will be best understood.

4.5. Conclusions

By fitting fluorescent tracer measurements using a mechanistic model we were able to infer more detailed information on the bio-irrigation process in species communities than an exchange rate alone, thereby improving on linear regression techniques. Benthic organisms differ strongly in the magnitude and mode in which they express functional traits. With this study we aimed to determine whether bio-irrigation can be predicted by an index of bio-irrigation, calculated based on functional traits. This index was correlated to the attenuation coefficient, but not the bio-irrigation rate. Our findings also highlight the importance of the context in which indices for functional processes should be evaluated, because of the confounding roles of environmental conditions and behaviour. Different species assemblages can have the same bio-irrigation rates, but differ in sediment depth over which they exchange solutes. This is important to consider when implementing bio-irrigation in models of sediment biogeochemistry.

Acknowledgements

Chapter 5. IMPACT OF BOTTOM TRAWLING ON SEDIMENT BIOGEOCHEMISTRY: A MODELLING APPROACH

Emil De Borger, Justin Tiano, Ulrike Braeckman, Adriaan D. Rijnsdorp, Karline Soetaert.

Abstract

Bottom trawling in shelf seas can occur more than 10 times per year for a given location. This affects the benthic metabolism, through a mortality of the macrofauna, resuspension of organic matter from the sediment, and alterations of the physical sediment structure. However, the trawling impacts on organic carbon mineralization and associated processes are not well known. Using a modelling approach, the effects of increasing trawling frequencies on early diagenesis were studied in five different sedimentary environments, simulating the effects of a deep penetrating gear (e.g. a tickler chain beam trawl) versus a shallower, more variable penetrating gear (e.g. an electric pulse trawl). Trawling events strongly increased oxygen and nitrate concentrations in surface sediment layers, and led to significantly lower amounts of ammonium (43 – 99 % reduction) and organic carbon in the top 10 cm of the sediment (62 – 96 % reduction). As a result, total mineralization rates in the sediment were decreased by up to 28 %. The effect on different mineralization processes differed both between sediment types, and between trawling frequencies. The shallow penetrating gear had a slightly smaller effect on benthic denitrification than the deeper penetrating gear, but there were no statistically different results between gear types for all other parameters. Denitrification was reduced by 69 % in a fine sandy sediment, whereas nitrogen removal nearly doubled in a highly eutrophic mud. This suggests that even relatively low penetration depths from bottom fishing gears generate significant biogeochemical alterations. Physical organic carbon removal through trawl-induced resuspension of sediments, exacerbated by a removal of bioturbating macrofauna, was identified as the main cause of the changes in the mineralization process.

5.1. Introduction

Bottom trawl fisheries provide for 23% of global fish landings (Cashion et al., 2018), with the vast majority of this type of fishing taking place in productive coastal shelf seas (Amoroso et al., 2018). In bottom trawl fisheries, nets are dragged along the bottom with the help of weighted devices such as otter boards, shoes, or beams, while chains, groundropes, and/or electrical stimuli are used to coerce fish into the net. Bottom trawl gears penetrate the seafloor, up to 35 cm deep for otter trawl boards, and 10 cm

deep for tickler chain rigged beam trawls, depending on the gear specifics and the sediment type (Paschen et al., 2000; Lucchetti and Sala, 2012; Depestele et al., 2016). Hence, during a trawling event, sediment is mixed down to a certain depth, and hydraulic drag introduced by the moving gear can cause the erosion of an additional sediment layer (Depestele et al., 2016, 2019; O'Neill and Summerbell, 2011; O'Neill and Ivanović, 2016). Sediment disturbances by bottom trawling occur on very large scales: 63% of all North Sea sediments are trawled between 1 and more than 10 times per year (Eigaard et al., 2017). Scientific literature is rich in studies showing the physical and ecological alterations to the benthic environment caused by bottom trawling. Acute impacts of bottom trawling include the homogenization of surface sediment (Depestele et al., 2019; Ferguson et al., 2020) and the removal of significant proportions of benthic fauna (Bergman and Hup, 1992; Bergman and Van Santbrink, 2000, Tiano et al., 2020). Consistent fishing pressure favors organisms with shorter life spans and/or increasing resistance to trawling, while communities become depleted of species with key functional roles (Kaiser et al., 2006; Hiddink et al., 2017; Sciberras et al., 2018). Both fining (Trimmer et al., 2005) and coarsening (Palanques et al., 2014; Mengual et al., 2016) of the sediment has been attributed to trawling, as well as chronic organic matter depletion (Pusceddu et al., 2014; Paradis et al., 2019). The effects of bottom trawling on biogeochemical dynamics, however, remain relatively understudied. Trawling has been linked with enhanced carbon mineralization rates due to organic matter priming (van de Velde et al., 2018) and/or trawl-induced increases in organic material (Polymenakou et al., 2005; Pusceddu et al., 2005; Palanques et al., 2014; Sciberras et al., 2016). These results seemingly contrast with findings of organic matter depletion (Mayer et al., 1991; Brylinsky et al., 1994; Watling et al., 2001) and reduced mineralization rates after acute trawling (Tiano et al., 2019), highlighting the lack of knowledge on this topic and the need for further investigation.

Geochemical alterations impact the capacity of the sediment to recycle organic matter back to bioavailable nutrients (i.e. the sediment biogeochemistry). These are important processes in shallow coastal seas where primary production, and the food-chain it supports, are strongly dependent on nutrients regenerated in the sediment (Soetaert and Middelburg, 2009; Provoost et al., 2013). Observed biogeochemical changes caused by sediment resuspension can lead to the instantaneous release of nutrients from the sediment into the water column, temporarily enhanced oxygen consumption (Tiano et al., 2019) and increased nutrient concentrations in the bottom water (Riemann and Hoffmann, 1991; Almroth et al., 2009; Couceiro et al., 2013). Furthermore, trawling has been linked to an increase of the sediment oxygenated layer depth (Allen and Clarke, 2007; Tiano et al., 2019) and a reduction of the denitrification capacity of cohesive sediments (Ferguson et al., 2020). It has been argued, based on *in situ* measurements, that the sediment biogeochemistry in consistently disturbed sediments remains in a transient state, i.e. the sediments are permanently recovering from a disturbance event (Van De Velde et al., 2018). These effects can potentially be mitigated with alternative fishing gears or modified gear configurations, however, the effectiveness of which needs to be assessed.

To reduce fishing impacts, alternative bottom trawl gears such as pulse fishing gears are being investigated (Van Marlen et al., 2014; McConnaughey et al., 2020). With pulse gears, the heavy tickler chains are replaced by electrodes, which emit electrical pulses that induce a cramping response in flatfish

(Soetaert et al., 2015b). This causes fish to become temporarily immobilized, allowing their capture in a net which drags behind the electrodes. Pulse gears exhibit lower penetration depths (~50%) than conventional beam trawls (Depestele et al., 2019), and also erode less material into suspension through hydrodynamic drag due to a reduced towing speed (Rijnsdorp et al., 2020a). The lower penetration depth of the pulse gear compared to standard tickler chain methods, has been shown to decrease the effects of bottom trawling on the sediment redox layer (Depestele et al., 2019) and on chlorophyll *a* reduction (Tiano et al., 2019), but it is yet unclear how specific mineralization processes might be affected on longer temporal scales.

The aim of this study was to explore the possible impacts of bottom trawling on the sediment carbon and nitrogen cycling for two gears with different penetration depth distributions, and with increasing trawling frequency. We use a dynamic diagenetic model, to which trawling disturbances were added. We parametrized the model for five locations in the North Sea, with sediments ranging from coarse sands to fine mud. Our hypotheses were (1) that the effects of bottom trawling would differ depending on the sedimentary environment, and (2) that fishing gear with reduced sediment penetration would incur less changes in biogeochemical cycling.

5.2. Materials and methods

5.2.1. Model setup

5.2.1.1. Model description.

To model the effects of bottom trawling on sediment biogeochemistry, disturbance events were added to a dynamic implementation of the early diagenesis model OMEXDIA (Soetaert et al., 1996a, 1996b). This model describes the concentrations of organic matter, oxygen, nitrate, ammonium, dissolved inorganic carbon (DIC) and oxygen demand units (ODU's, reduced reaction products of anoxic mineralization). These are calculated on a 1D grid, with 100 layers increasing in thickness, starting from 0.01 cm at the sediment water interface (SWI) and extending up to a sediment depth of 100 cm. The incoming flux of organic matter (detritus) consists of a labile, fast decaying fraction (FDET) and a refractory, slow decaying fraction (SDET), and is mineralized in either oxic mineralization, denitrification, or anoxic mineralization (T. 5-1). With oxic mineralization and denitrification, the consumption of oxygen and nitrate as terminal acceptors is explicitly modelled (T. 5-1; Eqs. 1.1, 1.2). Anoxic mineralization processes with alternative oxidants such as manganese oxides, iron oxides, sulphate, and organic matter are collected into one process that produces oxygen demand units (ODU's) as reaction products (T. 5-1; Eq. 1.3). ODU reoxidation, and nitrification, the biological oxidation of ammonia to nitrate, are two additional processes that consume oxygen (T. 5-1; Eqs. 1.4, 1.5). Mineralization rates are dependent on carbon availability (first order kinetics), and oxidant availability (Michaelis-Menten type kinetics), and inhibited by concentrations of inhibiting solutes (e.g., oxygen inhibits denitrification and anoxic mineralization). FDET, SDET, O_2, NO_3^-, NH_4^+, ODU's, and DIC are the 7 state variables of which the concentrations are modelled in every layer.

Exchange of state variables between the different layers is caused by advection (sediment accretion, v) or molecular diffusion (for solutes), and bioturbation (for solids). The solute flux J_D due to molecular diffusion and advection is described by Fick's first law (Fick, 1855),

$$J_D = \varphi D_i \frac{\partial C}{\partial z} + \varphi v C \qquad \text{(Eq. 1)}$$

where the effective diffusion coefficient is estimated as $D_i = D_0/\theta^2$, with D_0 the molecular diffusivity of the solute, $\theta^2 = 1 - 2\ln(\varphi)$ the factor correcting for sediment tortuosity (Boudreau, 1996), φ the sediment porosity, which was kept constant with depth z, and C the concentration of the state variable. Molecular diffusion coefficients were calculated using R-package marelac (Soetaert and Petzoldt, 2018). Bioturbation is depth-dependent, and assumes a constant biodiffusivity value Db_0 in a layer with thickness L_{mix}. Below this depth, bioturbation decreases rapidly to zero, determined by the attenuation coefficient for bioturbation (Db_{coeff}).

$$Db_z = Db_0 e^{-(z - L_{mix})/Db_{coeff}} \qquad \text{(Eq. 2)}$$

T. 5-1: Diagenetic reactions used in OMEXDIA. x denotes the molar C:P ratio, y the molar N:P ratio in organic matter per mole of phosphorus (for Redfield Stoichiometry, x = 106, y = 16).

Process	Reaction	
Oxic mineralization	$(CH_2O)x\,(NH_3)y\,(H_3PO_4) + xO_2 \rightarrow xCO_2 + yNH_3 + H_3PO_4 + xH_2O$	(1)
Denitrification	$(CH_2O)x\,(NH_3)y\,(H_3PO_4) + 0.8 \cdot HNO_3 \rightarrow xCO_2 + yNH_3 + 0.4 \cdot N_2 + H_3PO_4 + 1.4 \cdot H_2O$	(2)
Anoxic mineralization	$(CH_2O)x\,(NH_3)y\,(H_3PO_4) + \text{an oxidant} \rightarrow xCO_2 + yNH_3 + H_3PO_4 + xODU + xH_2O$	(3)
Nitrification	$NH_3 + 2O_2 \rightarrow HNO_3 + H_2O$	(4)
ODU oxidation	$ODU + O_2 \rightarrow \text{an oxidant}$	(5)

5.2.1.2.   Model parametrization

The model was parametrized for 5 different sedimentary settings in the Southern North Sea (Fig. 5-1, T. 5-2): a coarse sandy sediment (hereafter denoted as "Coarse") with a median grain size of 433 μm located on a sandbank in the Belgian part of the North Sea (BPNS). Two sediments with intermediate grainsizes (216 – 220 μm): one with a low nutrient load situated on the Dogger Bank ("FineL"), the other nearshore (BPNS) with a comparatively high nutrient load ("FineH"). Finally two muddy sediments with a high silt content (74 – 88 %): one with a low nutrient load situated offshore, on the Fladen Grounds ("MudL"), and one with a comparatively high nutrient load, situated nearshore in the BPNS ("MudH").

Biogeochemical data from these stations were collected from boxcore samples (30 cm ID, 25-30 cm sediment height) in two separate sampling campaigns on the North Sea, one in September 2017 (Coarse, FineH, MudH; Chapter 2), the other in May-June 2018 (FineL, MudL; Chapter 3). From these boxcore samples, sediment characteristics and the distribution of nutrients in the sediment were subsampled, and nutrient exchange rates across the sediment-water interface were determined in incubation experiments (see Appendix C for an extensive description of the methodology used to derive this information).

Model parameters included both measured concentrations in the bottom water, as well as process rate parameters that were derived following a 2-step steady state fitting procedure (T. 3-3). Using the measured DIC flux as the upper boundary organic carbon input flux, the O_2 flux and porewater profiles of O_2, NO_3^-, and NH_4^+ were first fitted manually by tweaking a limited set of model parameters. The degradation rate of refractory material (*rSlow*), and the biodiffusivity constant (*Db*) were constrained by fitting NH_4^+ and O_2 profiles. Mechanistically, decreasing the bioturbation rate *Db* reduces the build-up of NH_4^+ with depth, increases the oxygen penetration depth, and changes the shape of the NO_3^- profile (deepening the NO_3^- peak). Whereas the degradation rate of the refractory organic matter also impacts deep NH_4^+ concentrations, it has a larger effect on the *shape* of the NH_4^+ profile, with lower degradation rates causing a more gradual build-up with sediment depth. Subsequently, parameters affecting the NO_3^- and NH_4^+ profiles were tuned (the nitrification rate *rnit*, and denitrification constants *ksNO3denit* and *kinO2denit*). Higher nitrification rates increase the build-up of NH_4^+, and increase concentrations of NO_3^-, typically producing a nitrate concentration peak within the oxic zone. The shape of the oxygen profiles further constrained the oxidation rate of oxygen demanding units (ODU's), and inhibition constants for anoxic mineralization (*kinO2anox*, *kinNO3anox*). Then followed an automated constrained parameter fitting step using an optimization algorithm. In this second step, the fitted parameters were allowed to vary in a range ± 10 % around the manually fitted parameter values. Also the DIC fluxes were refitted within a narrow range (0.98 -1.02 of measured value), to allow freedom to the fitting algorithm. A random-based minimization algorithm (Price, 1977) implemented in the R package FME (Soetaert and Petzoldt, 2010) was used. This algorithm pseudo-randomly sampled the parameter space, until the parameter set was found which returned the minimal model cost, the latter defined as the sum of variable costs (modeled - measured values), scaled using the mean - standard deviation relation determined for each nutrient (Figure C 1, Appendix C).

Using the steady-state condition as initial condition, several time variable boundary conditions were imposed for the dynamic model simulations. A sinusoidally varying carbon deposition flux with the model derived carbon flux (*Cflux*, T. 5-3) as the annual average, and imposing an amplitude of 1 was used as the upper boundary organic carbon flux (Fig. 5-2 A). This resulted in differing organic carbon fluxes for each location. Additional time variable boundary conditions (daily bottom water concentrations of O_2, NH_4^+, NO_3^- and PO_4^{3-}, as well as bottom water temperature) were extracted from the Copernicus Marine Environmental Monitoring Service implementation of the ERSEM model (European Regional Seas Ecosystem Model, Butenschön et al., 2016; Copernicus Marine Service Information, 2020) for each location.
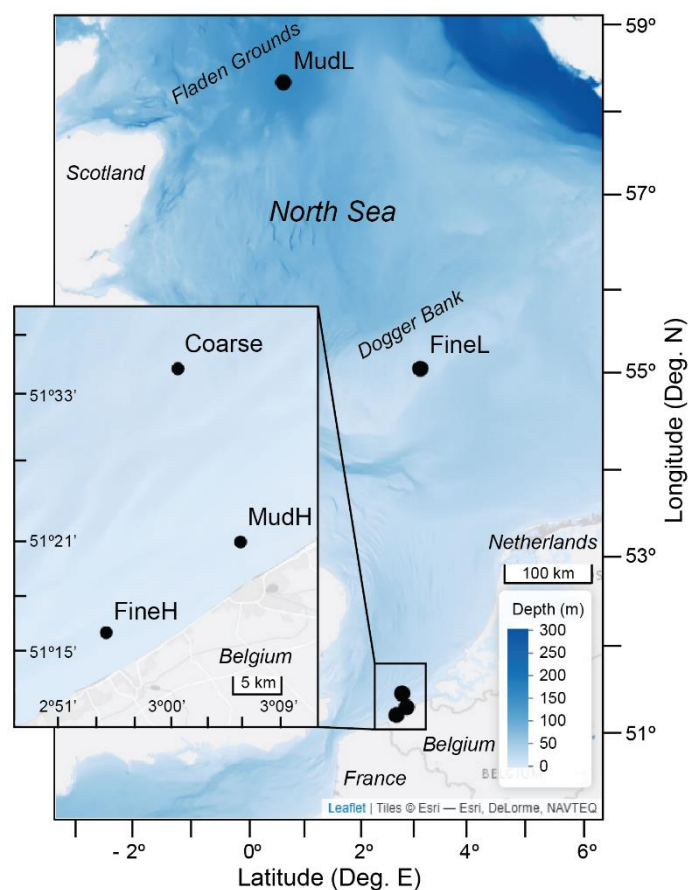
Fig. 5-1: Sampling locations in the North Sea. Offshore stations MudL and FineL sampled by De Borger et al. (2020), and nearshore stations (inset) in the Belgian part of the North Sea by Toussaint et al. (2020). L = low nutrient content relative to H high nutrient content. Basemap: © Esri, depth raster by GEBCO Compilation Group (2020).

T. 5-2: Characteristics of the selected sites. Low and High nutrient classification is based on relative differences in nutrient build-up for the same sediment type (see Fig. C 1 in Appendix C).

Sediment	Nutrients	Name	Lat (Deg. N)	Lon (Deg. E)	Depth (m)	MGS (µm)	SD.1 (µm)	SD.9 (µm)	Sand (%)	Mud (%)	Source *
Coarse sand	Low	Coarse	51.4348	2.80982	22	433 ± 43	286 ± 31	660 ± 67	99 ± 1	0 ± 0	a
Fine sand	Low	FineL	55.1737	3.16126	26	216 ± 2	143 ± 0	328 ± 7	99 ± 7	0 ± 0	b
	High	FineH	51.1853	2.7013	9	220 ± 8	91 ± 61	394 ± 67	81 ± 5	9 ± 5	a
Mud	Low	MudL	58.2009	0.52587	148	24 ± 1	4 ± 0	67 ± 3	10 ± 7	88 ± 1	b
	High	MudH	51.2714	2.90503	11	19 ± 1	3 ± 0	208 ± 28	25 ± 4	74 ± 5	a

*Sources: (a) Toussaint et al. (in review), (b) De Borger et al. (in press).

T. 5-3: Parameters used for modelling the different sediment types.

Parameter	Description	Unit	Coarse	FineL	FineH	MudL	MudH
a.	**Fitted parameters**						
wSed	Advection rate	cm d⁻¹	$3.00 \cdot 10^{-4}$	$3.00 \cdot 10^{-7}$	$3.00 \cdot 10^{-4}$	$3.00 \cdot 10^{-7}$	$3.00 \cdot 10^{-4}$
pFast	Fast degrading fraction organic matter	-	0.94	0.95	0.93	0.95	0.90

pSlow	Slow degrading fraction organic matter	-	0.06	0.05	0.07	0.05	0.10
rFast	Decay rate FDET	d^{-1}	0.07	0.05	0.05	0.05	0.06
rSlow	Decay rate SDET	d^{-1}	$3.82\ 10^{-4}$	$1.00\ 10^{-4}$	$1.86\ 10^{-4}$	$1.08\ 10^{-4}$	$3.65\ 10^{-5}$
Db	Biodiffusivity coefficient	$cm^2\ d^{-1}$	$0.10\ 10^{-6}$	$1.03\ 10^{-3}$	$2.18\ 10^{-6}$	$1.11\ 10^{-3}$	$1.73\ 10^{-3}$
biotdepth	Mixed layer depth	cm	0.50	2.00	2.00	2.00	0.50
rnit	Max. nitrification rate	d^{-1}	1.76	24.84	1.92	11.62	3.62
rODUox	Max. ODU oxidation rate	d^{-1}	0.70	3.82	2.26	5.92	3.58
ksO2oduox	Half saturation, O_2 in ODU oxidation	$mmol\ O_2\ m^{-3}$	1.11	2.74	0.69	4.61	3.50
ksNO3denit	Half saturation, NO_3^- in denitrification	$mmol\ NO_3\ m^{-3}$	72.73	48.02	68.70	14.47	8.80
kinO2denit	Half saturation, O_2 inhibition of denitrification	$mmol\ O_2\ m^{-3}$	82.63	57.69	33.56	86.55	77.00
kinNO3anox	Half saturation, NO_3^- inhibition anoxic mineralization	$mmol\ NO_3\ m^{-3}$	6.44	1.26	6.30	2.33	8.67
kinO2anox	Half saturation, O_2 inhibition anoxic mineralization	$mmol\ O_2\ m^{-3}$	91.00	57.69	95.08	42.19	75.84
rCaPprod	Rate of CaP production	d^{-1}	0.08	$1.85\ 10^{-3}$	$2.19\ 10^{-3}$	0.00	$9.82\ 10^{-7}$
rCaPdiss	Rate of CaP dissolution	d^{-1}	$6.60\ 10^{-5}$	$9.01\ 10^{-9}$	0.00	0.00	$4.47\ 10^{-6}$
rFePadsorp	Rate of FeP adsorption	d^{-1}	0.094	0.16	4.06	0.10	0.36
rFePdesorp	Rate of FeP desorption	d^{-1}	0.00	$9.26\ 10^{-5}$	0.02	0.00	0.11
b. Measured parameters							
Cflux	Carbon deposition flux	$nmolC\ cm^{-2}\ d^{-1}$	1354.7	810.9	2994.0	848.0	9025.5
Φ	Porosity	-	0.35	0.59	0.42	0.71	0.73

5.2.1.3.   Disturbance modelling

Trawling disturbances were modelled as events causing the instantaneous removal of the surface layer due to hydraulic erosion (Depestele et al., 2016), followed by the mixing of a layer below that due to the actual gear penetration (Fig. 5-3). The hydraulic erosion was implemented as a reset of the sediment water interface (SWI) to the depth of the eroded layer. The mixing was implemented as a homogenization of solids (FDET, SDET) over the mixing depth (Fig. 5-3A), whereas solutes in the mixing depth (O_2, NO_3^-, NH_4^+, DIC) were set equal to the bottom water concentration of the respective solute to represent a complete flushing of the mixed layer with bottom water (Fig. 5-3 B).

Modelled trawling events also caused an immediate reduction in bioturbation rates, due to the mortality of benthic fauna after a trawl pass (Fig. 5-2C). Benthic mortality is mostly dependent on the total penetration depth of the gear (Fig. 5-2 B; Hiddink et al., 2017), but also varies with habitat (Pitcher et al., 2017). The instantaneous reduction in bioturbation was included as a proportional depletion (*d*), dependent on the sediment type (lowest in coarse sand, highest in mud) and the penetration depth (Fig. 5-2 C). It was calculated based on the total gear penetration depth (*TPD*, i.e. the sum of the eroded layer

depth and the penetration depth, in cm), and the mud content (% *mud*, particles < 63 µm) of the sediment, as described in (*Eq.* 3 derived from Sciberras et al. (2018).

$$d = (TPD \cdot 3 + mud \cdot 0.3) / 100 \qquad \text{(Eq. 3)}$$

The subsequent recovery of the bioturbation was modelled based on the logistic growth equation (Eq. 4), with the recovery rate (*r*) the inverse of the longevity of the species community, kept constant at 0.04 y^{-1} (Rijnsdorp et al., 2016; Hiddink et al., 2019).

$$\frac{dN}{dt} = r \cdot N \left(1 - \frac{N}{K}\right) \qquad \text{(Eq. 4)}$$

Here *N* is the bioturbation rate (cm^{-2} d^{-1}), with *K* the full bioturbation rate for a species community at carrying capacity. The maximum reduction of the bioturbation was set to 90 %, to account for quasi immediate recolonization of trawled sediment by scavengers (Sciberras et al., 2018), and deeper living species that can survive intense trawling activity (Rijnsdorp et al., 2018). Electrical pulses were assumed to not affect benthos mortality in addition to the physical effects, since current available research shows very limited to no increased mortality by electrical pulses when compared to control situations (ICES, 2020; van Marlen et al., 2009; Murray et al., 2016; Soetaert et al., 2015a, 2016).
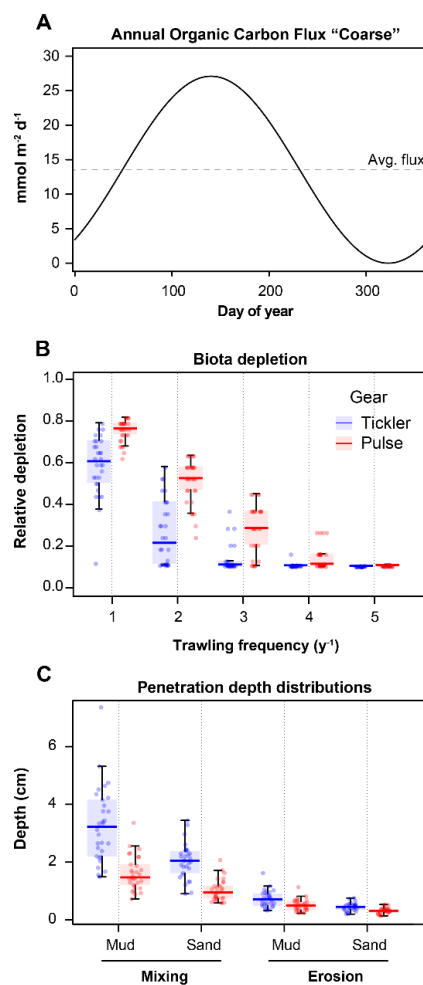
Fig. 5-2: (A) Example of sinusoidal varying organic carbon deposition flux, based on average DIC efflux measured by Toussaint et al. (2020) for the Coarse sediment. (B) Simulated depletion of bioturbation, relative to the maximum (y-axis), with increasing trawling frequency (y^{-1}, x-axis) in fine sands. Doy = day of year. (C) Imposed mixing and erosion depths (cm), for fine sandy and muddy sediments, for the two gear types (tickler chain and pulse gear).
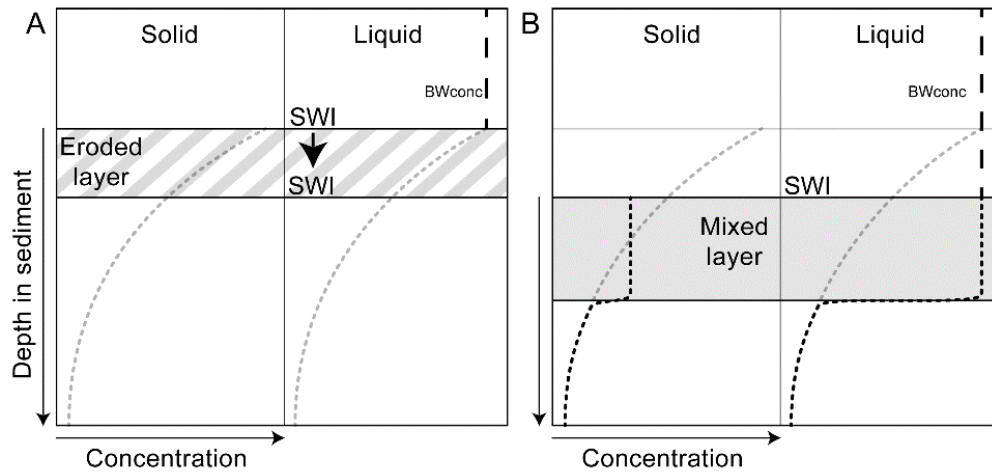
Fig. 5-3: Implementation of a trawling event, on sediment concentrations of solids and liquids. Dotted grey lines: initial concentration profile, black line: profile after the event. (A) Hydraulic erosion removes a layer of sediment, moving the sediment-water interface (SWI) downward; the effect is implemented similarly for solids and liquids. (B) Subsequent mixing of the sediment homogenises the solid concentration over the mixed layer depth whereas liquids are set to the overlying bottom water concentration (BWconc). Depths of both impacts are defined in the text.

5.2.2. Simulations

The model description was implemented in R (R Core Team, 2020), the concentration changes of simulated species due to transport were calculated using the R-package ReacTran (Soetaert and Meysman, 2012), and the resulting system of differential equations was solved using the deSolve package (Soetaert et al., 2010). Dynamic model simulations were initialized with a steady state solution calculated with annually averaged boundary conditions as input parameters, using the R-package rootSolve (Soetaert, 2009). This is necessary to build up an organic carbon, ammonium, ODU and DIC stock in the sediment (Soetaert et al., 1996b). Dynamic simulations were run for 15 years, with daily output, to generate sufficient independence from starting conditions. Reported modelling results stem from the last simulated year.

The frequency of the trawling events imposed ranged from 0 (the baseline) to 5 y^{-1}, based on realistic values of bottom trawling intensities in the North Sea (Rijnsdorp et al., 1998; Eigaard et al., 2017). Events were distributed randomly throughout the year, given the absence of a clear seasonal pattern in trawling intensities (Rijnsdorp et al., 2020a). For each trawling frequency and site, 30 model simulations were performed, each with a different pair of penetration and erosion depths, generated from a log-normal distribution of penetration depths. For the tickler chain trawl, a log normal distribution of penetration depths was generated given the average values (95% confidence limits) for sand and mud summarized by Pitcher et al. (pers. comm): 3.2 (1.5, 6.7) cm and 1.9 (1.0, 3.7) cm for mud and sand respectively; the erosion depth was set to 22% of the penetration depth. The penetration depths for the pulse gear were set to 50 % of the tickler gear: 1.6 cm (0.75, 3.38) and 0.95 (0.49, 1.83) cm for mud and sand. The erosion depth for the pulse gear was set to 70 % of the tickler gear (Fig. 5-3 B; Depestele et al., 2016, 2019; Rijnsdorp et al., 2020b).

5.2.3. Statistical analysis

Linear models were constructed with selected model output variables to analyse the effects of the different gear types, trawling frequency, and the sedimentary context, on the rates of the different mineralization processes and on the total mineralization (the sum of the separate mineralization processes). A normal distribution was adopted for the process responses. To deal with heterogeneity of variances of the residuals (for all models) in the linear models, a generalized least squares (GLS) structure was added (Pinheiro and Bates, 2000; Zuur et al., 2009; West et al., 2014), which allowed for unequal variances among treatment combinations to be included as a variance structure (Pinheiro and Bates, 2000; West et al., 2014). This variance structure was of the form sediment*frequency, using the "varIdent" function of the R package "nlme" (Pinheiro et al., 2019). To find the most suitable variance structure, models with different variance structures were compared using AIC scores (Akaike, 1974), and plots of fitted values and individual model terms versus the residuals (Zuur et al., 2009). For all models, a variance structure was selected that allowed for variances conditional on the station, and trawling frequency. Subsequently the fixed model component was optimized by manual stepwise selection, using the likelihood ratio test, and associated *p*-values as validation for removing excess terms (Zuur et al., 2009). During this step, the philosophy was adopted to not include significant interaction terms containing a certain variable, when said variable was not significant by itself. The minimal adequate model was represented using restricted maximum likelihood estimation (REML, West et al., 2014). GLS models were implemented using the R package "nlme" (Pinheiro et al., 2019).

5.3.   Results

5.3.1.   Baseline model simulations

Baseline model simulations (undisturbed) show the differences in organic matter cycling between the chosen locations. In the coarse sand station (Coarse), the average total mineralization rate was 13.6 mmol C m^{-2} d^{-1}, with 89 % of this due to oxic mineralization, 6 % due to anoxic mineralization, and 5 % was denitrified (Table C 2, Appendix C). The two muddy stations had either very high or very low total mineralization rates (MudH: 82 mmol C m^{-2} d^{-1}, MudL: 8.5 mmol C m^{-2} d^{-1}), and similar for the two fine sandy stations (FineH: 30 mmol C m^{-2} d^{-1}, FineL: 8.1 mmol C m^{-2} d^{-1}), related to differences in organic matter deposition between nearshore – offshore locations. Oxic mineralization dominated in FineL (oxic: 81 %, anoxic: 12 %, denit.: 6 %), FineH (oxic: 78 %, anoxic: 22 %, denit.: 0 %) and MudL (oxic: 72 %, anoxic: 18 %, denit.: 10 %), whereas the mineralization in the nearshore muddy station (MudH) was dominated by anoxic processes (oxic: 27 %, anoxic: 68 %, denit.: 5 %).

5.3.2.   Impact on biota

Trawling-induced depletion of fauna substantially decreased average annual bioturbation rates. Bioturbation decreased with increasing penetration depth (Fig. 5-2 B, C), resulting in strongest decreases in muddy sediment (MudL, MudH), and larger decreases in the deep penetrating gear versus the shallow penetrating gear (T. 5-4). In the Coarse sediment, the annually averaged bioturbation decreased gradually, from 81 % of its original value at 1 trawl y^{-1} to 19 % at 5 trawls y^{-1} in the tickler gear, and 49 %

at 5 trawls y^{-1} for the pulse gear. For the fine (FineL, FineH) and muddy (MudL, MudH) sediments the maximum depletion was reached after 4 (5 for the shallow gear) and 2 trawling events respectively.

T. 5-4: Percentage of bioturbation (average ± sd) remaining after sustained trawling activity at a given trawling frequency (y^{-1}), for the different sediment types. T: deeply penetrating tickler gear, P: shallow penetrating pulse gear.

Frequency	Coarse		Fine		Mud	
	T	P	T	P	T	P
1	81 ± 7	90 ± 3	60 ± 16	76 ± 7	27 ± 17	42 ± 12
2	61 ± 13	80 ± 14	26 ± 16	51 ± 1	11 ± 1	11 ± 1
3	42 ± 17	69 ± 21	14 ± 7	28 ± 12	11 ± 0	11 ± 0
4	27 ± 18	59 ± 25	11 ± 1	15 ± 6	11 ± 0	11 ± 0
5	19 ± 15	49 ± 26	11 ± 1	11 ± 1	11 ± 0	11 ± 0

5.3.3. Nutrient and organic carbon distribution

With higher trawling frequencies, concentrations of oxygen and nitrate in the sediment generally increased, whereas ammonium and organic carbon contents were always reduced (Fig. 5-4, Fig. 5-5). The magnitude of concentration changes was similar for both gear types (Table C 1, Appendix C, mean percentage change relative to baseline concentrations reported). Increases in oxygen (Fig. 5-4: A-E) and nitrate (Fig. 5-4: F-J) concentrations were largest in the oligotrophic stations FineL and MudL, where concentrations of oxygen in the upper 5 cm increased 15 – 16 fold (resp. 1604 and 1516 %), while nitrate concentrations increased 9 - 19 fold (resp. 909 and 1911 %) at highest trawling intensities (See Figure C 2, Appendix C for the range of nutrient concentrations throughout the year). In contrast, O_2 and NO_3^- concentrations initially decreased at MudH by 25 and -50 % maximally for 1 – 2 trawls y^{-1}, before increasing by 52 to 81 % (O_2), and 123 to 188 % (NO_3^-) at 5 trawls y^{-1}. Ammonium (NH_4^+) concentrations decreased strongly in all sediments, with a decrease of up to 69 % in Coarse, 68 % in MudH, and > 90 % in FineL, FineH, MudL (Fig. 5-4: K-O, Table B 1).

Increasing the trawling frequency reduced the total amount of reactive organic carbon (labile + semi-labile, OC) in the sediment, and reduced the penetration depth of the OC (Fig. 5-5). Trawling frequencies of 3-5 y^{-1} led to near-total depletion of reactive OC in all sediments in the upper 10 cm (> 95 % removed for Coarse and FineH, > 90 % for FineL, MudL and MudH, Fig. 5-5The mean OC profiles for both gears at a given frequency were often visually different (dotted vs. full lines on), but the average concentrations over 10 cm did not differ significantly. A redistribution of organic carbon was visible in the upper cm of the sediment, where organic carbon concentrations were higher in the impacted than in the baseline simulation (example in the cutout of the top 5 mm shown for MudH, Fig. 5-5). In FineL, MudL and MudH the ratio of labile organic carbon (FDET) to semi-labile organic carbon (SDET) increased between 25 and 34 % (Figure C 3, Appendix C). This effect was only noticeable in the upper 0.2 – 0.5 cm, below this depth values of this ratio in all trawling frequencies converged to 0, due to the depletion of labile organic carbon.
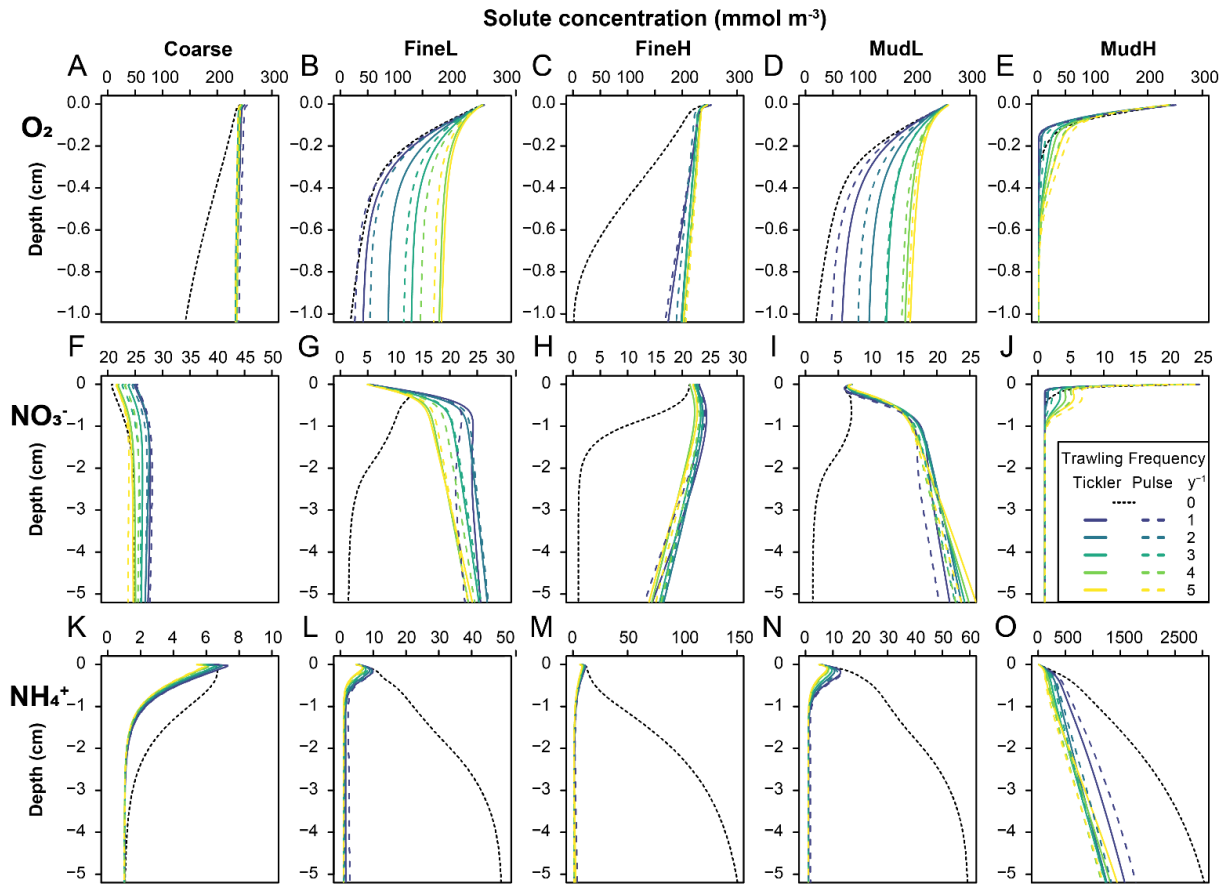
Fig. 5-4: Annually averaged modelled concentrations (mmol m^{-3}) of oxygen (A - E), nitrate (F - J), and ammonium (K – O; rows) in the different types of sediment used as the basis for the disturbance simulations (columns). Black dotted line is the 0 trawl default, full and dotted coloured lines are tickler and pulse gear respectively, with increasing trawling frequencies as different colours.
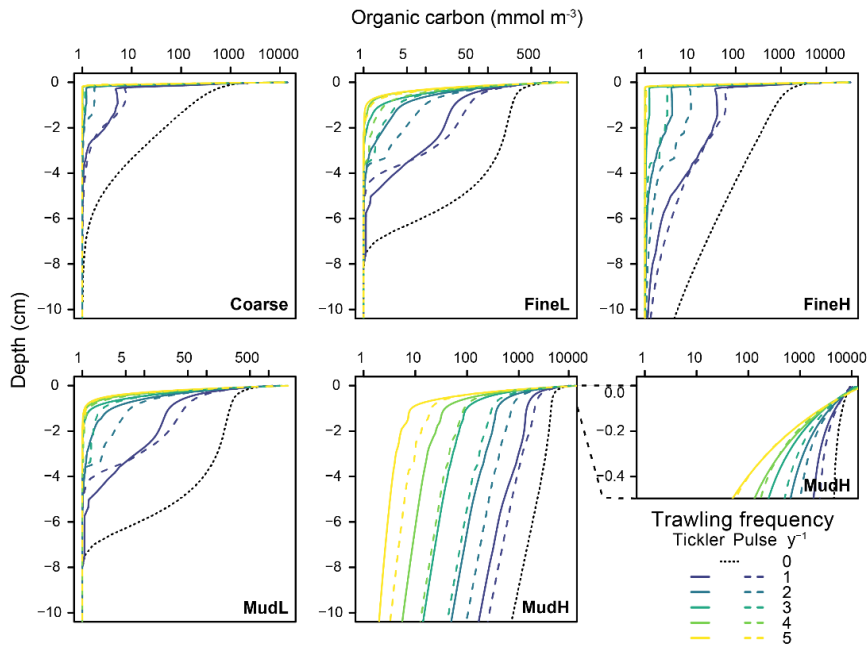
Fig. 5-5: Total organic carbon concentrations in the upper 10 cm of the sediment (mmol m^{-3}) for the different stations (X-axis on log-scale). Profiles represent the average profile per trawling intensity (n = 30), for the deep penetrating gear (full), and shallow penetrating gear (dotted line). For station MudH a cut-out of the first 0.5 cm is inflated to show the displacement of OC to the surface.

5.3.4. Total mineralization rates

The trawling frequency had a significant negative impact on all studied mineralization process rates (oxic, anoxic, denitrification), and on the total organic carbon mineralization, as confirmed by the negative coefficients in the GLS models ("Freq",

T. 5-5). Changes in process rates also differed between the studied sediments, as seen by the inclusion of an interaction term between the sediment type and the trawling frequency (Freq:Sed). The sediment biogeochemical response to increasing trawling frequency was often nonlinear warranting the inclusion of a squared frequency term ($Freq^2$). The gear type was only included as a significant explanatory variable in the model for denitrification, where the deeper penetrating gear (tickler) decreased denitrification rates more than the shallow penetrating gear (

T. 5-5).

The total mineralization rate was impacted negatively in all cases, and decreases ranged from 5 % for 1 trawl y^{-1} for MudL to -28.9 % for 5 trawls y^{-1}, for FineL (Fig. 5-6: A-E, values in Table C 2, Appendix C). The change in oxic mineralization rates (base: 12.0, 23.3, 6.5, 6.1, 23.1 mmol m^{-2} d^{-1} for Coarse, FineL, FineH; MudL, and MudH resp.) showed different patterns depending on the station (Fig. 5-6: F-J). For Coarse and FineH there was a consistent decrease in oxic mineralization rates with increasing trawling frequency, with maximum decreases at 5 trawls y^{-1} of 21 % and 23 % for the tickler gear, and 21 % and 25 % for the pulse gear. In contrast, for FineL and MudL oxic mineralization increased at a frequency of 1 trawl y^{-1} (8 % and 11 %), followed by a decrease at higher trawling frequencies with maximal decreases of 15 % and 10 % at 5 trawls y^{-1} for the tickler gear; the values for the pulse gear were similar (Fig. 5-6: F-J). For MudH oxic mineralization increased by a maximum of 56 % at 5 trawls y^{-1} for both gears.

T. 5-5: Generalized least squares (GLS) models for the total mineralization, oxic mineralization; anoxic mineralization, and denitrification as a function of increasing trawling frequency (Freq and $Freq^2$), the fishing gear type (Gear), and the sediment context (Sed) and interactions between model terms Freq:Stat, $Freq^2$:Sed.

Response variable y	Model
Total mineralization	y = Intercept + a · Freq + b · $Freq^2$ + c · Sed + d · Freq:Sed + e · $Freq^2$:Sed y = 29.96 − 1.93 Freq + 0.07 $Freq^2$ + 55.05 S1* − 21.85 S2* − 16.40 S3* − 21.48 S4* + 2.62 Freq:S1 + 1.49 Freq:S2 + 1.31 Freq:S3 + 1.50 Freq:S4 − 0.95 $Freq^2$:S1 − 0.07 $Freq^2$:S2 − 0.07 $Freq^2$:S3 − 0.07 $Freq^2$:S4
Oxic mineralization	y = Intercept + a · Freq + b · $Freq^2$ + c · Sed + d · Freq:Sed + e · $Freq^2$:Sed y = 23.29 - 0.12 Freq − 0.20 $Freq^2$ - 0.21 S1 − 16.74 S2 − 11.28 S3 − 17.17 S4 + 7.63 Freq:S1 + 0.58 Freq:S2 − 0.38 Freq:S3 + 0.91 Freq:S4 − 0.90 $Freq^2$:S1 + 0.06 $Freq^2$:S2 + 0.19 $Freq^2$:S3 + 0.01 $Freq^2$:S4
Anoxic mineralization	y = Intercept + a · Freq + b · $Freq^2$ + c · Sed + d · Freq:Sed + e · $Freq^2$:Sed y = 6.57 − 1.23 Freq + 0.14 $Freq^2$ + 51.14 S1 − 5.53 S2 − 5.67 S3 − 5.03 S4 − 8.27 Freq:S1 + 0.80 Freq:S2 + 1.12 Freq:S3 + 0.59 Freq:S4 + 0.55 $Freq^2$:S1 − 0.09 $Freq^2$:S3 − 0.13 $Freq^2$:S3 − 0.07 $Freq^2$:S4
Denitrification	y = Intercept + a · Freq + b · $Freq^2$ + c · Gear + d · Sed + e · Freq:Sed + f · $Freq^2$:Sed y = 0.09 − 0.0034 Freq - 0.00035 $Freq^2$ − 0.00038 TicklerGear + 4.14 S1 + 0.44 S2 + 0.55 S3 + 0.73 S4 + 1.26 Freq:S1 - 0.11 Freq:S2 + 0.06 Freq:S3 − 0.03 Freq:S4 − 0.18 $Freq^2$:S1 + 0.01 $Freq^2$:S2 − 0.02 $Freq^2$:S3 - 0.01 $Freq^2$:S4

*S1 = MudH, **S2 = FineL, ***S3 = Coarse, ****S4 = MudL

Anoxic mineralization rates (base: 0.9, 1.0, 6.6, 1.5, 57.7 mmol m^{-2} d^{-1} for Coarse, FineL, FineH; MudL, and MudH resp.) were also affected similarly by the two gear types and decreased for all stations, though with differing magnitudes (Fig. 5-6: K-L). The lowest decrease was in the Coarse sediment, where the decrease in the anoxic mineralization rate was similar for all trawling frequencies (range of 18 % to 25 %), and the highest decrease was modelled at MudL, where anoxic rates decreased between 73 % and 83 %.

Denitrification rates (base: 0.6, 0.5, 0.1, 0.8, 4.2 mmol m^{-2} d^{-1} for Coarse, FineL, FineH; MudL, and MudH respectively) decreased with increasing trawling frequencies at 4 out of 5 stations, with a maximum reduction of 74 % (tickler) and 68 % (pulse) at FineL (Fig. 5-6: P-T). Trawling frequencies of 1 – 2 y^{-1} did not consistently alter denitrification for the Coarse sediment, and FineH and MudL. For the MudH trawls, denitrification rates increased by 50 and 49 % towards 5 trawls y^{-1} for tickler and pulse gear respectively.

As a result of the changes to denitrification, the removal of reactive N from the sediment changed. The sediments where denitrification decreased most (FineL, MudL), had 35 and 51 % of N produced by mineralization removed by denitrification when undisturbed and this reduced to 11 % and 45 % respectively for 5 trawls y^{-1}. For the Coarse sediment the fraction of N removed increased from 26 % when undisturbed to 30 % for 1 trawl y^{-1}, and then decreased again to 25 %. In MudH more N was removed as well, with a near-doubling as a peak at 5 trawls y^{-1} (48 %, up from 26 % as the base).

All previous results represent average changes throughout the year, but trawling also showed instantaneous effects, as illustrated by the decrease of denitrification rates (to nearly 0 mmol m^{-2} d^{-1}) immediately after a trawl events (Fig. 5-7).

5.3.5. Relative changes

The relative contribution of the mineralization processes to the total mineralization changed markedly between trawling frequencies and stations (Fig. 5-8). In general, the proportion of oxic mineralization increased, at the expense of anoxic mineralization (Fig. 4-8: F-J). The largest changes occurred when switching from 0 to 1 trawling event y^{-1}, and values remained stable from 2 events y^{-1} onwards. The proportion of oxic mineralization increased most at MudH (tickler: 116 %, pulse: 112% for 5 trawls y^{-1}), and smallest changes occurred at Coarse (<1% for both gears). The proportion of anoxic mineralization on the other hand, decreased in all simulations (Fig. 5-8). Largest changes were modelled at FineL and MudL (69 % and 78 % respectively), and smallest for Coarse and FineH (14 and 18 % respectively). The proportion of mineralization performed by denitrification decreased in FineL and MudL (71 % and 10 %, 5 events y^{-1}), doubled at MudH (100 %) and remained practically the same for Coarse and FineH (Fig. 5-8: K-O).
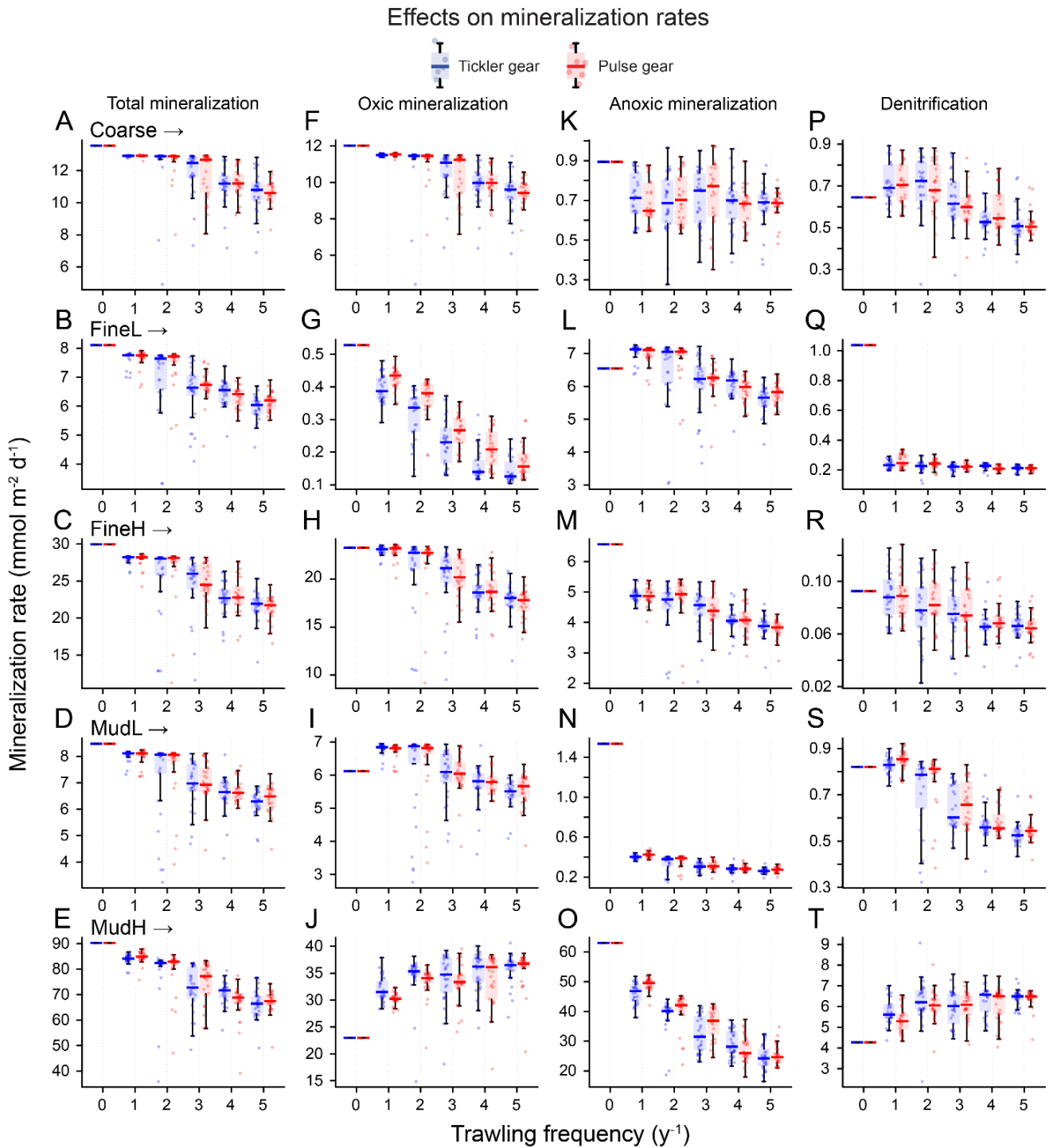
Fig. 5-6: Rates of total mineralization (A - E), and the three main mineralization processes (F - J: oxic; K - O: anoxic; P - T: denitrification) (y-axis, mmol m^{-2} d^{-1}) for each gear type (blue boxes: tickler gear; red boxes: pulse gear), and for increasing trawling frequency (x-axis, y^{-1}).
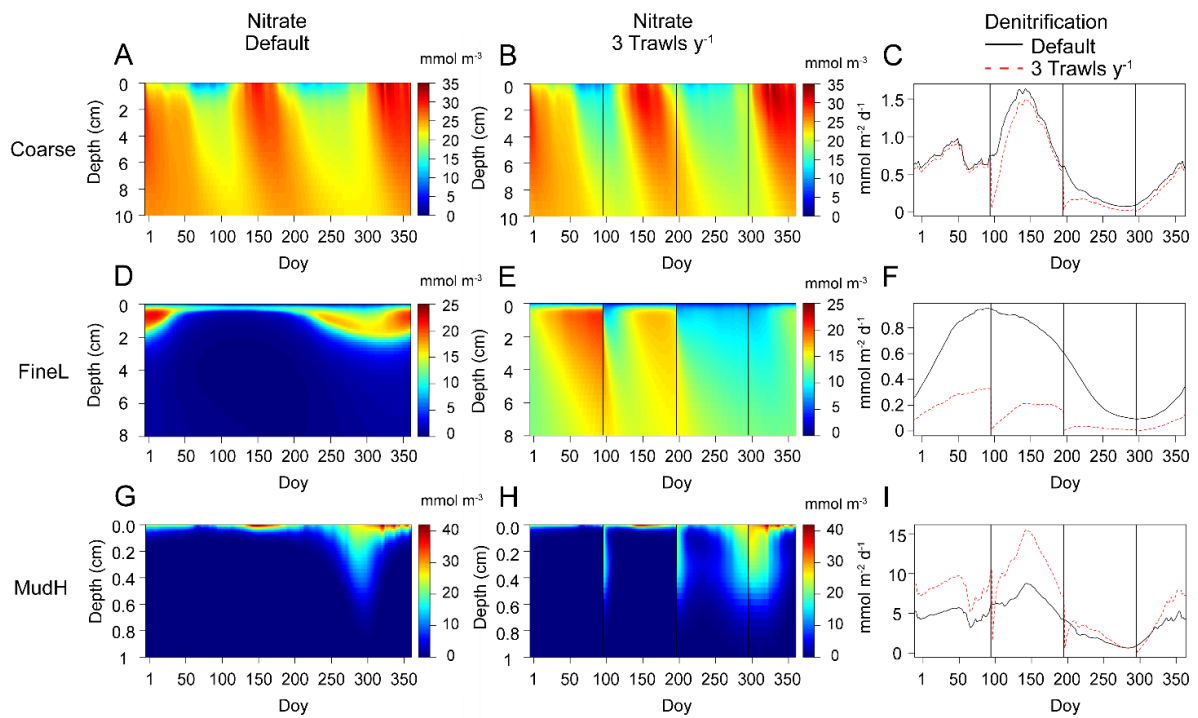
Fig. 5-7: Nitrate concentrations (mmol m^{-3}) in the sediment for a no-trawling simulation (A, D, G), and for 3 trawls y^{-1} (D, E, F), and associated annual denitrification rates (mmol m^{-2} d^{-1}, black lines = default (0 trawls y^{-1}), red dotted lines = trawling simulation). Represented stations are Coarse (A – C), FineL (D - F), and MudH (G - I). Black vertical lines indicate when trawling events take place.
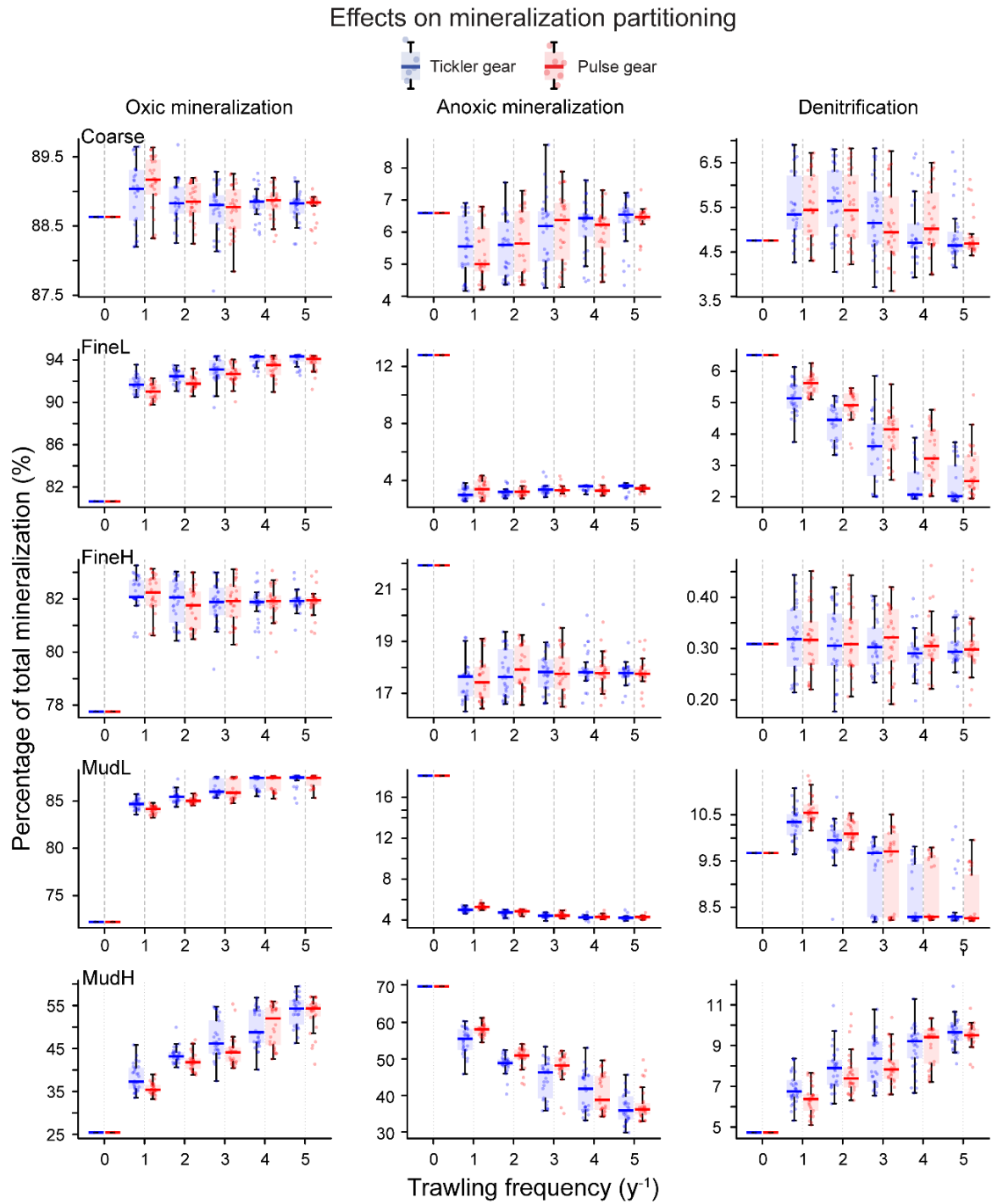
Fig. 5-8: Relative contributions (x-axis, as proportion) of the three main mineralization processes (left column: oxic; middle: anoxic; right: denitrification) to the total mineralization for each gear type (blue boxes: tickler gear; red boxes: pulse gear), and for increasing trawling frequency (y-axis, y⁻¹).

5.4.   Discussion

5.4.1.   Organic carbon depletion

Simulated trawling of the seafloor impacted the sediment biogeochemistry in all environments, and for all trawling frequencies. The amount of total mineralizable carbon in the sediment consistently

decreased with higher trawl frequencies, but the changes in mineralization pathways differed from case to case. The main drivers of the biogeochemical changes were found to be the depletion of organic carbon (OC) in the sediment (i.e. the substrate for mineralization itself), the redistribution of this OC nearer to the SWI (Fig. 5-5), and the increasing oxygenation of the sediment. With each trawl pass, a part of the organic carbon is removed along with the top sediment layer, preventing the OC to be transported to deeper layers through advective or bioturbation processes. In addition, part of the benthos in the sediment is removed, often strongly decreasing the bioturbation rate (especially after multiple trawling events y^{-1}, T. 5-4), which also affects the rate at which organic matter is distributed in the sediment. Thus, with increasing trawling frequency, organic matter is concentrated more near the sediment water interface, and becomes more vulnerable to erosion in subsequent trawling events. The fine sandy station with low organic matter content (FineL), as well as both muddy stations (MudL, mudH), showed smaller decreases in surface organic carbon concentrations compared to the eutrophic fine sandy (FineH) and Coarse sediments (Fig. 5-5, Table B 1), mainly because baseline bioturbation rates in the former were 3 orders of magnitude larger (T. 5-3). As such, bioturbation seems to cause an increased resistance to carbon loss by facilitating transport to deeper layers, making it less vulnerable to surface disturbances.

While the physical OC depletion caused by the penetrating gear is aggravated by the loss of bioturbating fauna in the sediment, this effect is context-dependent as bioturbators show variable levels of resistance to trawling (Hale et al., 2017; Tiano et al., 2020). Our modelled results provide further evidence that surviving fauna help buffer and mitigate the biogeochemical effects of trawling (Duplisea et al., 2001). The comparison with the work of Duplisea et al. (2001) is in fact remarkable, as Duplisea et al. (2001) used a food-web based model to investigate changes to carbon cycling, whereas a diagenetic model was used in this work. Both very different approaches, that both highlight a shift to more oxic mineralization, and the importance of benthic fauna as a stabilizing factor. Tiano et al. (2019) observed decreases in sedimentary chl *a* in the upper 1 cm immediately after trawling, of 41 and 83 % for pulse and tickler gears respectively. Also, OM depletion as a result of long term fishing has been reported, even at water depths beyond 500 m (Martín et al., 2014; Pusceddu et al., 2014; Paradis et al., 2019), where comparisons between trawled and untrawled sites yielded a difference in OC between 20 and 60 % (Paradis et al., 2019), or 60 – 100 % of the daily input flux of organic carbon was removed from sediments by trawling (Pusceddu et al., 2014). In fact, these deep-water sediments are particularly sensitive to trawling disturbances, a concerning feature given the steady expansion of fishing practices into deeper waters in recent decades (Morato et al., 2006; Puig et al., 2012; Watson and Morato, 2013). Deep-water species communities are slow-growing and thus recover slowly, organic matter deposition rates are low, and finer-grained sediments of the deep are easily resuspended following a trawl passage (Norse et al., 2012; Mengual et al., 2016). All three of these factors increase the impacts of trawling events on organic matter cycling in the model presented in this work. There are also studies reporting enhanced OC concentrations in trawled areas, in contrast with our results (Palanques et al., 2014; Pusceddu et al., 2005; Sciberras et al., 2016), possibly due to differing hydrodynamic and morphological conditions of the North Sea compared to other areas.

The decrease in total mineralization rates may partly be offset by re-deposition of organic matter, which was not considered in our model. Not all eroded organic matter stays in the water column, but a part resettles on the sediments. How this redistribution occurs depends on the sediment type and the local hydrodynamics, which determine the distance over which eroded sediment particles are transported (Le Bot et al., 2010; Robinson et al., 2005). It can be expected that for coarser, heavier sediments, a fraction will be redeposited in the trawling track, but that for muddy sediments, lighter and rich in organic matter (Mayer, 1994), eroded material remains in suspension long enough to be transported elsewhere. In the North Sea, suspended material is transported from the Southern Bight northward by counterclockwise residual currents. Ultimately, the partially degraded materials are deposited in the Skagerrak (Dauwe et al., 1998). So given the intensity, and the persistence with which vast areas of the southern North Sea are trawled (e.g. total annual sediment mobilization by the Dutch trawling fleet varied between 8 and 17 10^{14} kg of sediment between 2010 and 2016, Rijnsdorp et al., 2020a), we expect that trawling-induced sediment resuspension plays a significant role in the northward transport, and actively contributes to organic matter depletion in southern areas.

5.4.2.   Changes to mineralization pathways

Trawling activities generally caused strong increases in sedimentary oxygen and nitrate availability, and decreases in the ammonium content (Fig. 5-4). Sediment oxygenation increased both because of a direct injection of oxygen rich bottom water in deeper sediment layers during a trawling event, and because oxygen consumption by mineralization processes decreased as a result of strong decreases in OC and ammonium. As a result of increased oxygen availability, the importance of oxic mineralization generally increased with trawling, whereas anoxic mineralization decreased (Fig. 5-8).

Strongest increases in the proportion of oxic mineralization were modelled for the sediment characterized by a high silt percentage and organic matter load (mudH). These types of sediments also have a low permeability, high mineralization rates and a low oxygen penetration depth (Braeckman et al., 2014), with a lesser importance of oxic relative to anoxic mineralization in undisturbed conditions. Fishing gears penetrate deepest in these muds, and as such provide oxygen to deeper layers, although this is consumed rapidly. Van De Velde et al. (2018) found an increase in mineralization rates of over 200 % after a disturbance event in muddy sediments (from the same origin as MudH). This was attributed to multiple possible factors, such as 'self-priming' by mixing refractory with labile organic matter, burial of phytoplankton in settling sediment, and the introduction of oxygen to redox shuttle mechanisms. Our results show an enhancement of total oxic mineralization at mudH, but no increase in the total mineralization rate, perhaps because the aforementioned processes were not included in the used model.

The higher oxygen concentrations also had a clear inhibiting effect on denitrification rates (Fig. 5-7). Denitrification in coastal shelf sediments accounts for an estimated third of all nitrogen loss in Earth's marine surfaces (Middelburg et al., 1996), making these regions crucial to counteract nitrogen eutrophication (Galloway et al., 2004; Seitzinger et al., 2006). For all stations, trawling events caused an instantaneous dip in denitrification rates, because of the injection of O_2, and removal of the electron acceptor (NO_3^-) from the sediment, similar to the results of van der Molen et al. (2013) (Fig. 5-7, black

vertical lines). However, a discrepancy was noted between the biogeochemical impacts of trawling in cohesive sediments with high organic matter concentrations versus sandier and comparatively low nutrient sediments, consistent with literature findings (Polymenakou et al., 2005; Van De Velde et al., 2018; Tiano et al., 2019). The coarsest sandy sediments (Coarse) were by default deeply oxygenated (Fig. 5-4 A, B), with denitrification maximally inhibited by oxygen concentrations. Larger pore-spaces in these sediments allow for bottom water to penetrate more deeply into the sediment matrix, bringing oxygen and other reactants into deeper sediment layers. As a result, oxygen often fuels rapid mineralization in coarse grained sediments (Ehrenhauss et al., 2004a; Huettel and Rusch, 2000). The increasing trawling frequency in coarse sediments thus had little effect on oxygen penetration, and nitrate concentrations only marginally increased (Fig. 5-4 A, B), resulting in minor changes to mineralization pathways such as denitrification on average, although instantaneous effects could be prominent (Fig. 5-7 C). In oligotrophic finer sediments (FineL, mudL), there was a massive increase in both oxygen and nitrate concentrations as a result of trawling (Fig. 5-4 D, E; Fig. 5-7 D, E). Whereas increasing NO_3^- concentrations would stimulate denitrification on their own, the rise of oxygen concentrations strongly inhibited denitrification, leading to a drop in denitrification rates throughout the year (Fig. 5-7 F). The more eutrophic fine sediment FineH displayed a similar pattern of increased oxygenation mineralization as the other fine sandy sites, but the already low baseline denitrification rates could not decrease further. In the unperturbed simulation of MudH, mineralization was predominantly anoxic (68 %), with denitrification limited by NO_3^- availability. Increasing the oxygenation in this type of sediment caused the denitrification to double, by increasing the nitrate availability (Fig. 5-7, Fig. 5-6 G-I).

Ferguson et al. (2020) found that denitrification rates in Moreton Bay, Australia were reduced between 11 and 50 %, within 3 hours after a trawling event, and this rate decreased after successive trawling events during the studied period. These decreases were attributed to homogenization of the sediment, which removes oxic microniches created by fauna, and thus zones of intense coupled nitrification-denitrification (Ferguson et al., 2020). Though the key role of redox microniches is not directly investigated here, we acquired decreases in denitrification rates in a similar range in all sediments apart from MudH, especially when trawling frequencies increased.

Within the marine environment, shelf sediments are sites characterized by high nutrient concentrations, therefore offering resilience against changes to nutrient loadings. Soetaert and Middelburg (2009) showed that storage of ammonium in sediments significantly delays the response of shallow systems to oligotrophication, as the efflux of nitrogen from the sediment will compensate part of the losses in the water column. The increased reduction of the ammonium concentrations with fishing intensity will affect this buffering capacity of the sediment. The nitrogen buffering capacity of the investigated sediments, representative for a large fraction of North Sea sediments, was affected similarly by both gears. Firstly, the stock of nitrogen (as NH_4^+) in the sediment was directly affected by porewater flushing during trawling (with decreases > 99 % in some cases, Fig. 5-4 F). Secondly, lower availability of reaction substrate (OC, NH_4^+) decreased denitrification rates, reducing N removal to the atmosphere.

5.4.3. Reducing gear penetration depth

In our work the differences with respect to organic matter mineralization dynamics between gear types with differing penetration depths (e.g. 3.2 ± 1.2 cm vs. 1.6 ± 0.6 cm in mud) mostly remained suggestive, rather than statistically conclusive. The fishing gear type was only included as a significant predictor for the denitrification rates, with a small coefficient (-0.00038;). This is because the freshly deposited stocks of organic carbon are present near the sediment surface, and any gear that penetrates the sediment impacts this layer, especially for multiple trawling events per year (Fig. 5-5, T. 5-5). This indicates that only a thin layer of surface sediment needs to be disturbed to generate significant biogeochemical changes (Dounas et al., 2005). Many biogeochemical processes are mediated by the dynamics of oxygen near the sediment-water interface, which itself is influenced by the composition, and permeability of the sediment. Permeable sediments allow for a deeper flow of oxidized bottom water into the sediment matrix, increasing the available oxygen for oxic mineralization processes (Huettel and Gust, 1992). Cohesive sediments on the other hand, mostly lack such advective transport (Huettel and Gust, 1992). Instead the exchange of solutes between sediment and the overlying water is diffusion dominated (molecular and biogenic), resulting in a less deep oxic zone at comparable organic matter loads, and an increased importance of other oxidants (e.g. MnO_2, $FeOOH$, SO_4^{2-}). A shift towards fining (an increased proportion of finer grain size classes) has been described in certain trawled areas, with expected consequences for sediment biogeochemistry, such as an increased rate of sulphate reduction (Trimmer et al., 2005). But the opposite occurs just as well (Depestele et al., 2019; Mengual et al., 2019; Tiano et al., 2019). In these cases resuspended fine-grained material is exported away from the trawling site, leaving a coarsened trawling track, with the results subtly different between gear types (Depestele et al., 2019; Tiano et al., 2019). This means that the effects of fishing gears on grain size sorting should be better characterized for various sediment types, to constrain the uncertainty around predictions of gear impacts on sediment functioning.

This does not imply that the penetration depth is irrelevant. Other studies have reported clear positive effects of reducing the penetrations depths of fishing gears, such as decreased sediment mobilization and homogenization, and reduced organic matter depletion (Depestele et al., 2019; Tiano et al., 2019). Conversely, assuming that the eroded layer and the mixing depth scale with more deeply penetrating gears than those tested here, the depletion effects should become more pronounced. In a single trawling event more of the (reactive carbon rich) top sediment layer would be removed, there would be a higher mortality of organisms, and more of the nutrient build-up would be removed.

Aside from the penetration depth, largest impacts occurred when increasing the trawling frequency from 0 to 1 trawling event per year, and the response of mineralization processes to increased trawling frequency was often non-linear, making them more difficult to predict. This would imply that management strategies aimed at maintaining the ecosystem functions provided by shelf sediments should be focused on spatial controls, bottom impact quotas, and effort control of trawling gears that per definition require contact with the bottom to catch commercially viable target species (McConnaughey et al., 2020). An effective strategy limits the impacted surface area, and allows carbon stocks and faunal communities in the sediment to recover from a disturbance, resulting in the recovery

of vital biogeochemical functions such as denitrification and carbon burial. This includes technical adaptations to improve catch-efficiency. Whereas our study only focused on direct head-to-head comparisons between the two gear types, pulse trawls are associated with lower spatial footprints due to their relatively higher catch efficiencies compared to beam trawls (Poos et al., 2020; Rijnsdorp et al., 2020; ICES, 2020).

Shifting the fishing effort from peripheral areas to core fishing grounds would also reduce the area where the top sediment layer is removed on a regular basis, along with the associated reduction in mineralization of organic matter. This can be achieved through time-restricted bottom trawling, in which fishing grounds are closed off temporarily. Similarly, areas with high denitrification rates, crucial for eutrophication mitigation can be closed to trawling completely, as done in other regions of the world (Ferguson et al., 2020). Site-specific conditions such as rates of biogeochemical recovery and sedimentation rates need to be known to determine the resilience of ecosystems to trawling, and fine-tune management plans (Paradis et al., 2019).

5.5. Conclusion

With the addition of perturbation events to a model of early diagenesis, and a description of faunal mortality and recovery, we simulated the effects of increasing bottom trawling frequencies on sediment biogeochemistry. The results showed that bottom trawl fisheries strongly impacted the sediment biogeochemistry, and the magnitudes of the changes were dependent on the sedimentary context and trawling frequency. Two types of fishing gears were investigated. The exposed top sediment layer rich in organic matter was targeted similarly by both fishing gears, resulting in a similar loss of organic carbon, which was further exacerbated by the loss of bioturbating fauna. A shift towards increasingly oxic mineralization at the cost of anoxic mineralization was observed, driven by an often strongly increased oxygen availability in the sediment. The removal of fixed nitrogen by denitrification was not affected similarly in all sediments. Denitrification increased in nearshore cohesive mud, and decreased elsewhere, with highest decreases in offshore sediments with lower carbon loads. Our modelling results corroborate multiple patterns found in other studies, and can serve to interpret research and search for mitigation strategies. Trawling impacts are hard to mitigate by only reducing the penetration depth of the gear, so additional management strategies are needed to allow for partial, or full recovery of biogeochemical functions that are needed to support the marine food-chain, and for the removal of excess nutrients from the water.

Acknowledgements

Chapter 6. OFFSHORE WINDFARM FOOTPRINT ON SEDIMENT ORGANIC MATTER MINERALIZATION PROCESSES

Emil De Borger, Evgeny Ivanov, Arthur Capet, Ulrike Braeckman, Jan Vanaverbeke, Marilaure Grégoire, Karline Soetaert

Abstract

Offshore windfarms (OWFs) offer part of the solution for the energy transition which is urgently needed to mitigate effects of climate change. Marine life has rapidly exploited the new habitat offered by windfarm structures, resulting in increased opportunities for filter- and suspension feeding organisms. In this study, we investigated the effects of organic matter deposition in the form of faecal pellets expelled by filtering epifauna in OWFs, on mineralization processes in the sediment. Organic matter deposition fluxes produced by a 3D hydrodynamic model of the Southern Bight of the North Sea were used as input in a model of early diagenesis. Two scenarios of OWF development in the Belgian Part of the North Sea and its surrounding waters were calculated. Our results show a strongly increased deposition of reactive organic carbon (OC) within OWFs (28 – 31 %), and corresponding increased total mineralization rates. This leads to a buildup of OC in the upper sediment layers (increase by ~10%) and an increase of anoxic mineralization processes. Similarly, denitrification rates within the OWFs increased, depending on the scenario, by 2 to 3 %. Effects were not limited to the OWF itself: clear changes were noticed in sediments outside of the OWFs, that were mostly opposite to the 'within-OWF' effects. While on average small effects were observed over the full modelling domain, certain changes, such as for example the increased storage of OC in sediments, may be of significant value for national / regional carbon management inventories. Our results add to expectations of large-scale ecosystem effects of windfarms in the marine environments, which need to be researched further given the rapid rate of expansion of OWFs.

6.1. Introduction

Rising concern on global climate change has increased the urgency to lower carbon emissions from individual and industrial energy consumers (United Nations, 2015). The transition from fossil fuel driven energy production towards renewable energy sources from solar, hydrodynamic, and wind sources, is a booming industry in alignment with the goal of achieving "carbon-neutral" anthropogenic development (European Commission, 2020b). Offshore windfarms (OWFs), groupings of wind turbines on submerged sediments, offer part of the solution in the energy transition. Compared to terrestrial windfarms, the advantages of a flat, wind-swept marine area, and the possibility to build larger

structures, overrule increased construction and maintenance costs (Inger et al., 2009; Bergström et al., 2014).

With respect to marine life, the presence of the turbine substructure and the scour protection layer (a layer of rocks around the foundation base that prevents erosion) on the seabed represents the addition of a new type of habitat, that spans the full water column (Krone et al., 2013). Many organisms, mostly filter- and suspension feeders, thrive on this new habitat. For wind turbine substructures in the North Sea, a clear vertical succession of fouling fauna can be observed, from the barnacle *Semibalanus balanoides* in the intertidal zone, to the blue mussel *Mytilus edulis* in the upper subtidal, the amphipod *Jassa herdmani* below that, and the anemone *Metridium senile* in the lower regions of the foundation (De Mesel et al., 2015; Mavraki et al., 2020). The attraction of organisms extends beyond the surface of the turbine foundations. Fish species such as cod (*Gadus morhua*) and pouting (*Trisopterus lusculus*) are known to aggregate near turbine foundations (Reubens et al., 2011; Langhamer, 2012), and benthic communities of macrofauna have been observed to change, alongside a fining of the sediment and an enrichment with organic matter (OM) (Bergström et al., 2012; Coates et al., 2014; Leewis et al., 2018). Deposition of faecal pellets by the fouling fauna, as well as falling biomass are a likely source of this enrichment (Krone et al., 2013; Lefaible et al., 2019).

For sediment biogeochemistry, this increased carbon deposition may have far-reaching effects. In sediments, OM is mineralized to free inorganic nutrients available for water column processes (Soetaert and Middelburg, 2009; Provoost et al., 2013). Sediments in shelf seas represent a considerable sink of carbon, either at the short-term by means of temporary storage through delayed mineralization, or over longer timescales as refractory carbon is buried in deep sediment layers (Legge et al., 2020). Moreover, shelf sea sediments are of vast importance for the removal of excess nitrogen from the ecosystem through denitrification, the mineralization of OM through nitrate reduction, which produces nitrous oxide and dinitrogen gas (Middelburg et al., 1996; Galloway et al., 2004; Seitzinger et al., 2006).

Recently, Slavik et al. (2019) used a model that included the filtration by blue mussels attached to wind turbine foundations to show how this process can decrease primary production up to 8 % in the OWF footprint, but also have effects noticeable 50 km away from these concentrations of filter feeders. Similarly, by upscaling carbon tracer experiments, Mavraki et al. (2020) calculated an uptake of 1.3 % of the primary production standing stock in the Belgian Part of the North Sea (BPNS) by *M. edulis* and *J. herdmani.* This highly localized removal of primary produced carbon will likely cause a significant transfer of reactive organic carbon in the form of faecal pellets and dislodged biomass from the water column to sediments in the vicinity of OWFs.

Observational evidence of mineralization processes in OWF sediments, let alone of changes thereof, is rare (See Chapter 2) due to the difficulties of sampling sediments there. However, consequences of organic enrichment on sediment biogeochemistry are well described for example in fish and mussel aquaculture. Here, increased deposition of organic material (i.e. faeces, fish feed, dead biomass) causes an increase in mineralization activity in the sediment, which increases sedimentary oxygen consumption, and an increase in anoxic mineralization processes. This leads to higher CO_2 release from

sediments, increased exchange of nutrients, and a higher total organic carbon content in the sediment (Bannister et al., 2014; Kalantzi and Karakassis, 2006; Nizzoli et al., 2005; Rampazzo et al., 2013; Valdemarsen et al., 2010).

To describe the effects of increased carbon deposition related to filtration by fouling fauna in OWFs on the benthic mineralization processes, a module describing filtration by blue mussels on turbine substructures was implemented in a hydrodynamic model of the Southern North Sea (Ivanov et al., 2020), comprising the full BPNS and parts of the bordering French and Dutch coastal zones (Fig. 6-1). In biomass, *M. edulis* is by far the dominant species present on turbine foundations (Joschko et al., 2008; Krone et al., 2013). The redistribution of OM deposition fluxes caused by OWFs under different scenarios of placement and turbine types for a new concession area are described in an accompanying paper (Ivanov et al. *in review*). Here, the OM deposition fluxes are used as input for a model of sediment biogeochemistry (OMEXDIA, Soetaert et al., 1996). This was done for two cases, including the current OWFs present in the model domain, and a likely future scenario starting from 2026, when future OWFs will be constructed and fully colonized in planned concession zones in the BPNS, and the Dunkirk OWF in the French coastal zone (Fig. 6-1).

Seeing the analogy with aquaculture developments, we expected to find increased carbon concentrations in the OWF sediments through increased OM input, and increased anoxic mineralization, and nitrogen removal from the sediment through denitrification.
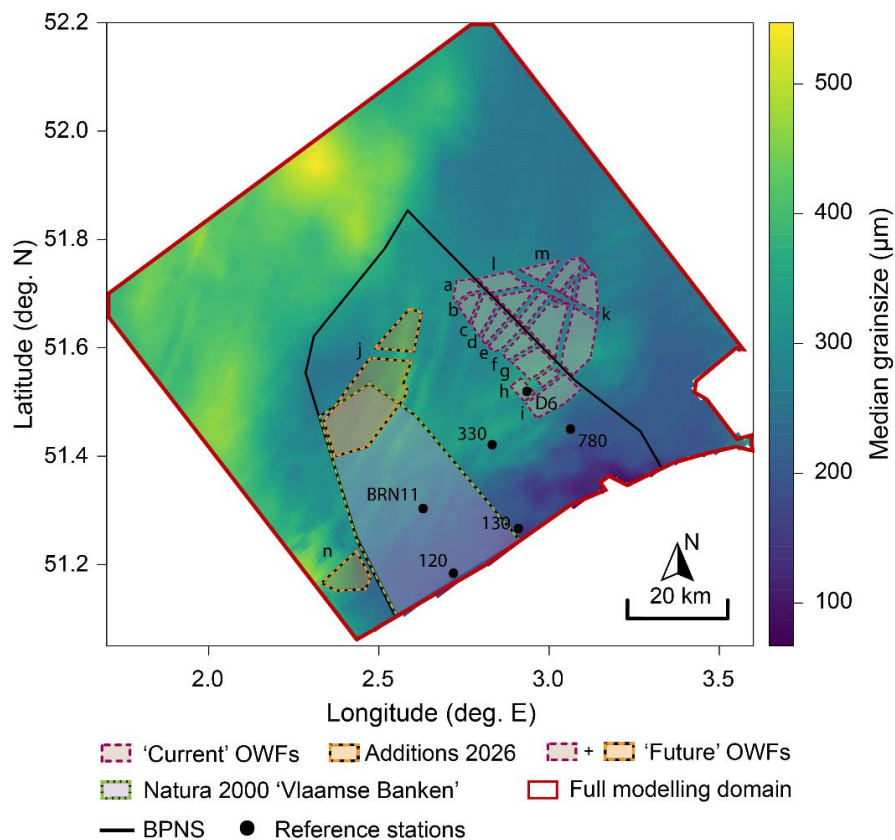
Fig. 6-1: Median grain size (μm) of sediments in the modelled domain, with the Belgian Part of the North Sea (BPNS) delineated in black. Current OWF developments (2021) outlined in purple, and future developments (operational ±2026) in orange, with letters corresponding to concession zone characteristics in T. 6-3. Black dots correspond to stations sampled for sediment biogeochemistry by Toussaint et al. (*in print.*), used as reference material.

6.2.   Materials and Methods

The response of the sediment metabolism to alterations in carbon deposition induced by OWFs was modelled by a dynamic model of early diagenesis (OMEXDIA, Fig. 6-2, Soetaert et al., 1996b). The diagenetic model was forced by the carbon deposition estimated by a three-dimensional hydrodynamical-wave-sediment transport model (COAWST; Warner et al. (2010)), that included a specific module describing the dynamics of mineral and organic carbon particles in the water column and sediment. In particular, this submodule included a representation of the filtration and faeces production processes associated to monopile fouling mussels (Ivanov et al., *in review.*). The coupling was performed in a spatial grid of 91 by 101 cells (50.91204 - 52.21679 deg. N, 1.672024 - 3.748295 deg. E), covering the Belgian Part of the North Sea and surrounding waters (for the full modelling domain, see Fig. 6-1), corresponding to the nested model grid presented in Ivanov et al. (2020).
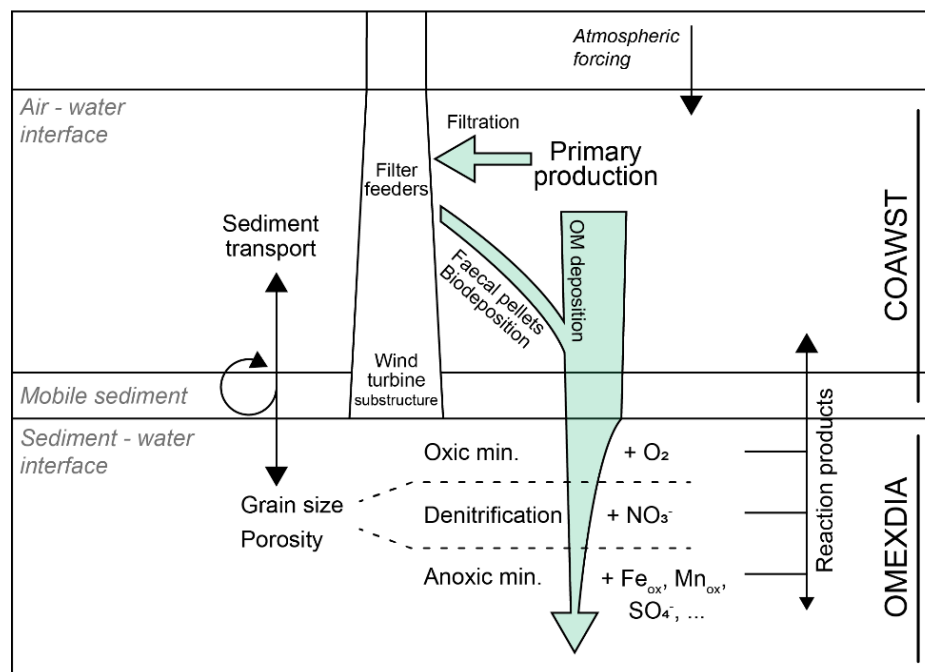
Fig. 6-2: Schema of the coupling of the COAWST hydrodynamic sediment transport model to OMEXDIA.

6.2.1.   Model descriptions

6.2.1.1.   Sediment early diagenesis

Model description

Mineralization processes in the sediment layer were modelled using a dynamic implementation of the early diagenesis model OMEXDIA (Soetaert et al., 1996a, 1996b). In this model, the concentrations of organic detritus (as two fractions: fast decaying detritus FDET, and slow decaying detritus SDET), oxygen (O_2), nitrate (NO_3^-), ammonium (NH_4^+), dissolved inorganic carbon (DIC), and oxygen demand units (ODU's, reduced substances generated in anoxic mineralization) are described on a 1D grid. This vertical grid has 50 layers of increasing thickness, starting from 0.01 cm at the sediment-water interface (SWI), extending down to a sediment depth of 200 cm.

In each sediment layer, the fractions of organic detritus (carbon) are mineralized to DIC and other reaction products in oxic or anoxic mineralization, or in denitrification (resp. reaction 1 – 3 in T. 6-1), with these processes mediated by concentrations of O_2, and NO_3^- in each layer through first order or Monod reaction kinetics (Soetaert et al., 1996a). Oxygen is additionally consumed in nitrification (the oxidation of ammonium), and the reoxidation of reduced substances produced in anoxic mineralization (reaction 4 - 5 in T. 6-1). To investigate changes in OM reactivity, the average reactivity was calculated as follows (Eq. 1):

$$Reactivity_{OM} = \frac{rFast * FDET + rSlow * SDET}{FDET + SDET}, \qquad \text{(Eq. 1)}$$

where *rFast* and *rSlow* are the degradation rates (d^{-1}) of fast and slow decaying detritus.

Transport of modelled substances between layers is caused by advection (sediment accretion), molecular diffusion (for solutes), and bioturbation (for solids). Bioturbation was implemented as a depth-dependent biodiffusion coefficient (*Db,* cm^2 d^{-1}, Eq. 2), starting from the surface biodiffusion coefficient (*Db$_0$,*), remaining constant for a certain mixed depth L_{mix}, and decreasing below that layer to 0 depending on the (constant) attenuation coefficient (*Db$_{coeff}$*). The magnitude of the surface biodiffusion coefficient *Db$_0$,* was modified in each location *i* as dependent on three temporally and/or spatially variable factors: bottom water temperature, sediment median grainsize, and the incoming carbon flux (Eq. 3). The temperature effect assumed a temperature-dependent increase of organismal metabolism using a doubling for every increase in temperature of 10 degrees (Q_{10} of 2, Eq. 3, Davis and Mcintire, 1983; Wrede et al., 2018). Median grain size (*MGS*, retrieved from the COAWST model, Ivanov et al., submitted) was used to scale the surface biodiffusion coefficient (*Db$_0$*), consistent with its relation to the calculated bioturbation potential of the species community (BP$_c$, Solan et al. (2004)). The BP$_c$–MGS relation was based on measurements of Braeckman et al. (2014), and Toussaint et al. (*in print.*). BP$_c$ values peaked between grain sizes of 100 – 175 μm, which represent fine sandy sediments in the BPNS, and were low where sediments consisted mostly of silt and were too anoxic to allow for deep living species (Pearson and Rosenberg, 1978), and in coarse sands starting from 400 μm (see Appendix D). This relation was modelled as a skewed normal distribution (*dsn*, See supplement). Benthic activity was also assumed to be stimulated by high incoming OM concentrations (*Cflux*), relative to maxima in their preferred habitat (*maxFlux$_i$*, Eq. 3, Dauwe et al., 1998; Zhang and Wirtz, 2017). The ratio of fast decaying OM relative to total organic matter deposited (*pFast*) represents the OM quality or palatability, and was used to estimate the mixed layer depth (in cm) analogous to Zhang and Wirtz (2017) (Eq. 4).

$$Db_z = Db_{0,i} e^{-(z - L_{mix})/Db_{coeff}} \qquad \text{(Eq. 2)}$$

$$Db_{0,i} = Db_0 \cdot \frac{Cflux}{maxFlux_i} \cdot \frac{dsn(MGS)}{\max(dsn(MGS))} \cdot \frac{2^{\left(\frac{Temp-10}{10}\right)}}{2^{\left(\frac{maxTemp-10}{10}\right)}} \qquad \text{(Eq. 3)}$$

$$L_{mix} = 5.4 - 114.7 \cdot (-8.7 \cdot \log pFast)^{-1.249} \qquad \text{(Eq. 4)}$$

Parametrization and implementation

Porosity and mean grain size were extracted from the COAWST model for each grid cell. Daily fluxes to the sediment of both carbon classes (FOC, SOC mmol C m^{-2} d^{-1}) from the COAWST model were

mapped 1:1 to upper boundary fluxes of FDET and SDET in OMEXDIA. The ratio FOC/(FOC + SOC) was taken as the measure of the quality (*pFast*) of the total deposited carbon (*Cflux*). Parameter values for rate and inhibition constants were those used by Soetaert et al. (1996a) (T. 6-2). For time-variable upper boundary conditions, daily bottom water concentrations of O_2, NO_3^-, NH_4^+, and DIC were extracted from the IBI MFC biogeochemical analysis and forecast system (Sotillo et al., 2015; E.U. Copernicus Marine Service Information, 2020). An advection rate *w* of 0.1 cm y^{-1}, an average value for a dynamic coastal sea (Boudreau, 1997; Mouret et al., 2009) was used for the entire domain.

The model was implemented in R (R Core Team, 2020), the concentration changes of simulated species due to transport were calculated using the R-package ReacTran (Soetaert and Meysman, 2012), and the resulting system of differential equations was solved using the deSolve package (Soetaert et al., 2010). Molecular diffusion coefficients were calculated using R-package marelac (Soetaert and Petzoldt, 2018). The initial conditions for a dynamic run were obtained by the steady-state solution, using the R-package rootSolve (Soetaert, 2009).

6.2.1.2. Modelling the impact of OWFs fouling mussels on carbon deposition

Inclusion of carbon deposition

The diagenetic model was forced with the annual cycle of the carbon deposition produced by a three-dimensional hydrodynamical model coupled with a module describing carbon and mineral particle dynamics through the water column and sediment (Ivanov et al., *in review*). In short, the sediment module describes the dynamics of three size-classes of mineral particles (i.e. mud, medium sand, coarse sand), and of two classes of (detrital) organic carbon of differing degradability (Fast and Slow organic carbon, resp. FOC and SOC, corresponding to those used in OMEXDIA). The model does not explicitly solve primary producers in the water column, but rather is forced by the daily vertically-integrated primary production product delivered by the Copernicus Marine Environment and Monitoring Service (Copernicus Marine Service Information, 2020). The hydrodynamics of the Southern Bight of the North Sea and Eastern English Channel were solved with a horizontal resolution of 5 km, downscaled to 1-km over the BPNS using a two-way nesting procedure (Ivanov et al., 2020). For assessing the impact of OWFs on carbon and mineral dynamics, ROMS was coupled with the wave model SWAN (Simulating WAves Nearshore) and the sediment model CCSTM (Community Coastal Sediment Transport Model) within the COAWST framework (Warner et al., 2010). Full description, technical details and validation of the simulated hydrodynamics can be found in Ivanov et al (2020) while for the carbon and sediment modelling we refer to Ivanov et al. (*in review*).

Implementation of M. edulis

Filtration of organic matter by the blue mussel *M. edulis* on turbine foundations was implemented in grid cells containing OWFs as a conversion of silt, and two classes of organic matter (FOC, SOC), to faecal silt, faecal fast, and faecal slow degrading matter (Ivanov et al., *in review*). These faecal substances have exactly the same characteristics as the "non-faecal' forms, except for the sinking speed, which is 1000 times higher (18 mm s^{-1}) to account for the increased size and mass of the faecal pellets (Callier et al., 2006). Faecal pellets produced consist of a mixture of silt particles and organic matter in a 64:36 ratio

(Jansen et al., 2012). However, to account for carbon lost in respiration (~20%, Slavik et al. (2019)), we assumed that organic particles are being filtered in higher amounts than what is found in faecal pellets, and ratio of removal from the water column was therefore set to 60:40.

The filtration rate was determined by the *M. edulis* biomass in each grid cell. This was directly dependent on the available substructure surface in the cell. For this, all turbine foundations were assumed to be monopiles (including both C-Power concession zones; T. 6-3). All mussels were assumed to be individuals of an average size (300 mg dry mass, Bayne et al. (1993)), occurring at a density of 6468 ind. m^{-2} of substructure surface over a depth interval of 6 m starting from the water surface (Kerkhof, F., pers. comm.). The *M. edulis* life cycle and seasonal biomass dynamics were not taken into account. Additionally, the filtration was dependent on the carbon concentration in the surrounding water: if the organic matter concentration in the water falls below a threshold of 0.7 mmol m^{-3}, mussels close their shell to save energy and stop filtering (Riisgård et al., 2003; Slavik et al., 2019). The daily carbon flux to the sediment from faecal pellets was added to the daily carbon flux stemming from sinking of primary production, to achieve the net carbon flux to the sediment for each grid cell, for each day of the year (Fig. 6-2).

Several runs of COAWST and OMEXDIA were done to fine-tune model parameters. During these calibration experiments, the SCOC and DIC fluxes produced by OMEXDIA forced by the COAWST carbon deposition were compared with field observations collected at six reference stations (Fig. 6-1, Toussaint et al., subm.). Parameters that were calibrated were organic carbon degradation, sinking rate, and decay rates of the two classes of organic matter. Details of the validation are provided in the supplement (Appendix D), and in Ivanov et al. (*in review*).

T. 6-1: Diagenetic reactions used in OMEXDIA. x denotes the molar C:P ratio, y the molar N:P ratio in organic matter per mole of phosphorus (for Redfield Stoichiometry, x = 106, y = 16).

Process	Reaction	
Oxic mineralization	$(CH_2O)x \, (NH_3)y \, (H_3PO_4) + xO_2 \rightarrow xCO_2 + yNH_3 + H_3PO_4 + xH_2O$	(1)
Denitrification	$(CH_2O)x \, (NH_3)y \, (H_3PO_4) + 0.8 \, x \, HNO_3 \rightarrow xCO_2 + yNH_3 + 0.4 \, x \, N_2 + H_3PO_4 + 1.4 \, x \, H_2O$	(2)
Anoxic mineralization	$(CH_2O)x \, (NH_3)y \, (H_3PO_4) + \text{an oxidant} \rightarrow xCO_2 + yNH_3 + H_3PO_4 + xODU + xH_2O$	(3)
Nitrification	$NH_3 + 2O_2 \rightarrow HNO_3 + H_2O$	(4)
ODU oxidation	$ODU + O_2 \rightarrow \text{an oxidant}$	(5)

T. 6-2: Definition of the parameters, and values.

Parameter	Parameter meaning	Unit	Value
wSed	Solid phase advection rate	cm yr^{-1}	0.1
rFast	Decay rate FDET	d^{-1}	0.05
rSlow	Decay rate SDET	d^{-1}	$0.18 \cdot 10^{-3}$
rnit	Max. nitrification rate	d^{-1}	20
NCrFdet	NC ratio FDET	molN molC^{-1}	0.151
NCrSdet	NC ratio SDET	molN molC^{-1}	0.151

rODUox	Max. ODU oxidation rate	d^{-1}	20
ksO2oduox	Half saturation, O_2 in ODU oxidation	mmol O_2 m^{-3}	1
ksNO3denit	Half saturation, NO_3 in denitrification	mmol NO_3 m^{-3}	30
kinO2denit	Half saturation, O_2 inhibition of denitrification	mmol O_2 m^{-3}	1
kinNO3anox	Half saturation, NO_3 inhibition anoxic mineralization	mmol NO_3 m^{-3}	1
kinO2anox	Half saturation, O_2 inhibition anoxic mineralization	mmol O_2 m^{-3}	1

6.2.2. Study area - scenarios

Three simulations were performed, corresponding to different states of OWF development in and around the BPNS (Fig. 6-1). Simulation 'baseline' represents the situation in the modelling domain pre-2008, in which no OWF development was present. Simulation 'current' is the current situation, in which all turbines in the eastern concession zone in the Belgian Part of the North Sea (BPNS) are constructed, as well as the Borsele OWFs in the Dutch coastal zone bordering the BPNS (T. 6-3). The number of turbines in the concession zones were used to estimate their density (turbines (grid cell)$^{-1}$) in the model (T. 6-3). Simulation 'future' is a likely scenario after 2026 (Fig. 6-1), in which the western concession zone in the BPNS (2100 MW) is developed with a turbine density of 2 km^{-2}, with as little as possible intrusion in the Natura 2000 area 'Vlaamse Banken' (Fig. 6-1). Intrusion into Natura 2000 areas may not be allowed, and requires compensation measures (EC, 2001). In this scenario, the planned OWF in the French coastal zone (598 MW, 2 turbines km^{-2}) bordering the BPNS is also included. Planned capacity and number of turbines for the future scenario were retrieved from 4C offshore (2020), and distributed with a density of 2 turbines km^{-2}. Modelling results were interpreted over the OWF area (grid cells containing OWFs - an area totaling 442.5 and 636.6 km^2 in the 'current' and 'future' scenario), over the full modelling domain (9140.4 km^2), and for the BPNS (3366 km^2). Effects on sediments outside of the OWFs were also quantified, by considering only grid cells without OWFs in either the BPNS, or the full modelling domain ('Beyond OWF'). Effects in these different interpretations were quantified as changes in a given scenario, relative to corresponding cells in the 'baseline' scenario.

The duration of the dynamic simulations was set to 20 years to evaluate the effects of OWF placement near the end of their expected lifetime of 20 – 25 years. Output of the last year of the model simulations, averaged to a daily rate, is presented in the results and discussion sections.

T. 6-3: Properties of current, and future OWF zones implemented in the modelling scenarios. Turbine foundation types correspond to monopile (M), gravity based foundation (G), jacket foundation (J).

country	Map	Operator	Operational year	Type	Diameter m	No. of pylons	Pylons / grid cell
BE	a	Mermaid	2020	M	8	28	1.44
	b	Northwester2	2020	M	8	23	2.33
	c	Belwind	2010	M	5	56	1-5
	d	Nobelwind	2017	M	5	50	1-5
	e	SeaStar	2020	M	8	30	1.88
	f	NorthWind	2014	M	5.2	72	1-5
	g	Rentel	2018	M	8	42	1-5
	h	C-Power (Phase I)	2009	G	6.5	6	1-5
	h	C-Power (Phase II & III)	2013	J	6.5	48	1-5
	i	Norther	2019	M	7.4	44	1-5
	j	Concession zone	~2026	M	8	210	2
ND	k	Borssele I,II	2020-2021	M	8	94	0.99
	l	Borssele III,IV	2021	M	8	77	0.75
	m	Borssele V	2021	M	8	2	1
FR	n	Dunkirk	2026	M	8	46	2

6.3.   Results

6.3.1.   The baseline scenario.

The baseline simulation (no OWFs present) showed a gradient of decreasing organic matter processing away from the shore, with daily averaged total mineralization rates in excess of 40 mmol C m^{-2} d^{-1} nearest to shore, and lowest rates (5 – 10 mmol C m^{-2} d^{-1}) in the northwestern part of the model domain (Fig. 6-3 A). The bulk of the organic matter mineralization occurred through anoxic mineralization, which followed the same patterns as total mineralization (Fig. 6-3 B). Rates of oxic mineralization related inversely to the grain size (compare Fig. 6-3 C with Fig. 6-1), with higher total oxic mineralization rates in coarser sediments on the sandbanks in the center of the BPNS and in the northwest of the model domain, and lowest rates in finest sediments nearshore, and in the northeast of the modelling domain (Fig. 6-3 C). Denitrification rates were highest near the outflow of the Scheldt estuary (0.4 – 1.1 mmol C m^{-2} d^{-1}), decreasing to below 0.4 mmol m^{-2} d^{-1} 20 - 30 km away from this source.
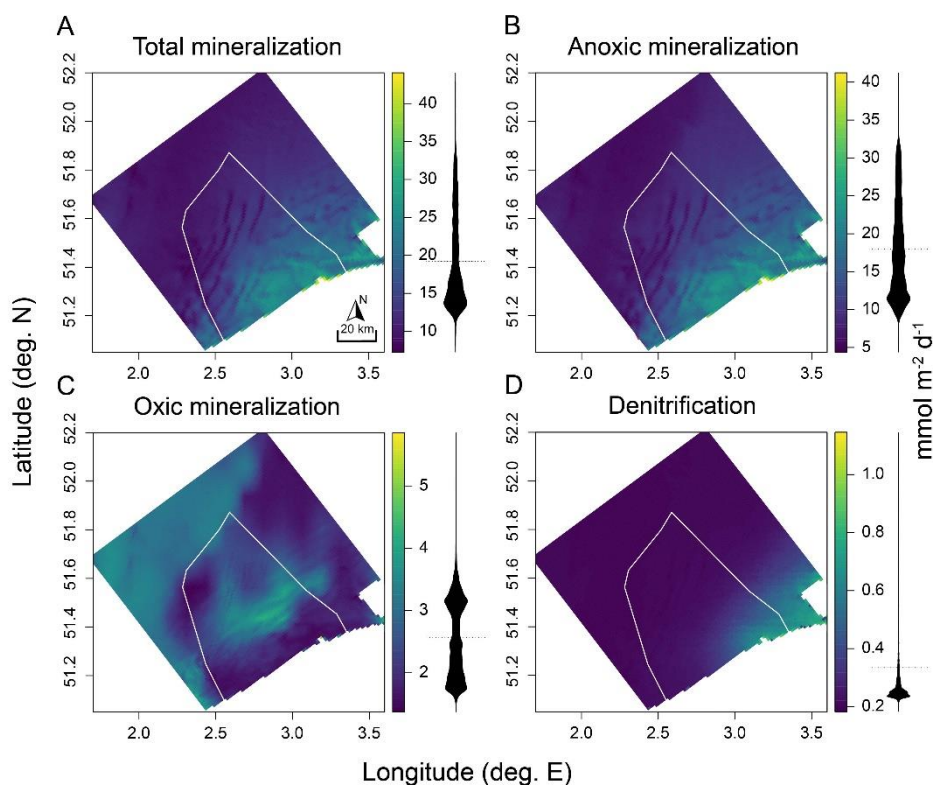
Fig. 6-3: Process rates in mmol C m^{-2} d^{-1} for the baseline scenario (no OWF development) for (A) total mineralization, (B) anoxic mineralization, (C) oxic mineralization, and (D) denitrification. White outline represents the BPNS. Density distributions of the values are represented as black shapes corresponding to the axis from the colour key.

6.3.2. Windfarm effects

Rates of all mineralization processes increased within the OWF areas both in the 'current' and 'future' scenarios, resulting in a higher total mineralization of organic matter within these areas, with maximal increases in individual cells of up to 60 % in the 'current' OWF scenario, and 69 % in the 'future' scenario (Fig. 6-4 A, B). On average, total mineralization rates within OWFs were 26.8 % ('current'), and 29.5 % ('future') higher relative to baseline conditions, in line with the similar increase of the organic carbon flux (T. 6-4). Increases in total mineralization rates were predominantly supported by increased anoxic mineralization, with maximal values exceeding the 'baseline' by 74 % (Fig. 6-4 C, D), followed by oxic mineralization, which increased up to 30 % in the 'current' scenario Fig. 6-4 E), and above 40 % in the 'future' scenario (Fig. 6-4 F). Denitrification increased by 2.3 % ('current') and 2.5 % ('future') on average (Fig. 6-4 G, H), resulting in additional removal of 7 and 10.7 kmol y^{-1} N respectively. Despite these higher denitrification rates, the proportion of denitrified organic matter decreased by 17.8 % in the 'current' scenario, and 19.6 % in the 'future' scenario (T. 6-5).

Less of the incoming organic carbon flux was returned to the water column as DIC, with this conversion decreasing by -3.6 and -4.5 % in the 'current' and 'future' scenario respectively (T. 6-4). Consequently the amount of reactive carbon stored in sediments of OWF's increased. The amount of organic carbon in the upper 10 cm increased up to 25 and 37 % locally (Fig. 6-5), and on average 9.6 and 11 % in the 'current' and 'future' scenario respectively (T. 6-4). The constant deposition of fresh OM additionally increased the reactivity of the organic carbon within OWFs by similar values (Fig. 6-5).

T. 6-4: Averaged values and relative changes between tested scenarios and the baseline of carbon mineralization processes for the current (C) and future (F) scenarios, subdivided in values over locations with OWFs, the BPNS excluding OWFs (far-field BPNS), the domain excluding OWFs (Far-field domain), the BPNS, and the full domain. Values for total mineralization, organic carbon flux, and DIC flux in mmol C m⁻² d⁻¹, the conversion represents the proportion of the incoming organic carbon flux released as DIC, and carbon storage is the total reactive carbon in the top 10 cm of the sediment (mol C m⁻²).

	Total mineralization		Org. C flux		DIC flux		Conversion		Carbon storage	
	mmol C m⁻² d⁻¹		*mmol C m⁻² d⁻¹*		*mmol C m⁻² d⁻¹*		-		*Mol C m⁻²*	
	C	F	C	F	C	F	C	F	C	F
OWF locations										
Baseline	14.7	13.9	17.2	16.4	-14.6	-13.9	1..0	0.9	89.26	88.24
Scenario	18.6	18.0	22.0	21.4	-18.5	-17.9	0.9	0.9	97.9	97.90
% Change	26.9	29.5	28.1	31.0	26.6	29.4	-3.7	-4.6	36.9	43.2
Beyond OWF BPNS										
Baseline	15.7	15.9	17.5	17.7	-15.6	-15.8	1.1	1.1	84.44	84.43
Scenario	15.7	16.0	17.6	17.8	-15.6	-15.9	1.1	1.1	84.39	84.45
% Change	0.3	0.6	0.3	0.4	0.3	0.6	-0.2	-0.6	0.3	2.0
Beyond OWF full domain										
Baseline	13.4	13.5	16.1	16.1	-13.3	-13.3	0.9	0.9	89.86	89.94
Scenario	13.4	13.4	16.0	16.0	-13.3	-13.3	0.9	0.9	89.62	89.69
% Change	-0.1	-0.1	-0.2	-0.3	-0.1	-0.1	-0.1	-0.4	-0.4	0.8
BPNS										
Baseline	15.6	15.6	17.5	17.5	-15.5	-15.5	1.1	1.1	84.66	84.66
Scenario	16.0	16.1	17.9	18.1	-15.8	-16.0	1.0	1.0	85.35	85.82
% Change	2.3	3.4	2.5	3.6	2.2	3.5	-0.4	-1.0	3.3	6.5
Full domain										
Baseline	13.5	13.5	16.1	16.1	-13.4	-13.4	0.9	0.9	89.83	89.83
Scenario	13.7	13.7	16.3	16.4	-13.5	-13.6	0.9	0.9	90.02	90.22
% Change	1.4	1.9	1.3	1.7	1.3	1.9	-0.3	-0.7	1.6	3.6

6.3.3. Beyond OWF

OWFs also affected biogeochemistry in sediments beyond their area ('Beyond OWF full domain', T. 6-4 and T. 6-5), with effects mostly in the opposite direction as observed for the within-OWF changes (Fig. 6-4). Outside of the OWF area, the incoming organic carbon flux decreased for both 'current' and 'future' scenarios (0.2 and 0.3 % vs. baseline). Likewise, the total mineralization rates were lower (0.1 and 0.1 % vs. baseline), with associated decreases in individual mineralization processes (Fig. 6-4 A, E, G, D). In the 'future' scenario, oxic mineralization increased also across most of the modelling domain outside of the OWFs, while denitrification increased only for sediments closest to shore (Fig. 6-4 F, H).

T. 6-5: Averaged values and relative changes between tested scenarios and the baseline of carbon mineralization processes for the current (C) and future (F) scenarios, subdivided in values over locations with OWFs, the BPNS excluding OWFs (far-field BPNS), the domain excluding OWFs (Far-field domain), the BPNS, and the full domain. Values for total denitrification are in mmol m^{-2} d^{-1}, part N removed is the proportion of incoming N removed from the sediment, and part denitrified is the proportion of total mineralization occurring through denitrification.

	Total denitrification		Part N removed		Part Denitrified		N removed	
	mmol C m^{-2} d^{-1}		-		-		kmol N y^{-1}	
	C	F	C	F	C	F	C	F
OWF locations								
Baseline	0.23	0.23	0.13	0.14	0.02	0.03	301.65	421.54
Scenario	0.24	0.23	0.11	0.11	0.02	0.02	308.64	432.28
% Change	2.30	2.54	-17.82	-19.57	-17.82	-19.57	2.32	2.55
Beyond OWF BPNS								
Baseline	0.27	0.27	0.15	0.15	0.03	0.03	2311.04	2179.21
Scenario	0.27	0.27	0.15	0.15	0.03	0.03	2311.24	2182.05
% Change	-0.01	0.11	-0.21	-1.07	-0.21	-1.07	0.01	0.13
Beyond OWF domain								
Baseline	0.26	0.26	0.16	0.16	0.03	0.03	6578.05	6453.69
Scenario	0.26	0.26	0.16	0.15	0.03	0.03	6574.22	6456.78
% Change	-0.08	0.03	0.14	-0.24	0.14	-0.24	-0.06	0.05
BPNS								
Baseline	0.27	0.27	0.15	0.15	0.03	0.03	2638.92	2638.92
Scenario	0.27	0.27	0.15	0.15	0.03	0.03	2643.33	2648.76
% Change	0.15	0.35	-1.38	-3.04	-1.38	-3.04	0.17	0.37
Full domain								
Baseline	0.26	0.26	0.15	0.15	0.03	0.03	6879.7	6879.7
Scenario	0.26	0.26	0.15	0.15	0.03	0.03	6882.9	6892.77
% Change	0.03	0.17	-0.60	-1.35	-0.60	-1.35	0.05	0.19

Overall, this decreased the contribution of denitrification to total mineralization (part denitrified) in the future 'scenario' by 0.2 %, with proportionally less N removed as a result, whereas in the 'current' scenario this proportion increased by 0.1 %. The average storage of reactive carbon outside of the OWFs decreased by 0.4 % in the 'current' scenario (T. 6-4), and decreased more northeast of the OWFs (Fig. 6-5 A, C). For the 'future' scenario (Fig. 6-5 B, D), carbon storage increased by 0.8 % (T. 6-4).

Considering only the BPNS, patterns are reversed ('Beyond OWF BPNS', T. 6-4, T. 6-5). Organic matter deposition fluxes increased slightly outside of the OWF area in both scenarios, by 0.3 and 0.4 %, resulting in increased mineralization rates of 0.3 and 0.6 % ('current' and 'future'). The conversion efficiency of incoming organic matter to DIC on the other hand, decreased by 0.2 and 0.6 %, relative to the baseline

scenario (T. 6-4). This was associated to an increase in the amount of carbon stored in the sediments of the BPNS outside of OWF grid cells, of 0.3 % in the 'current' scenario, and 2 % in the 'future' scenario.
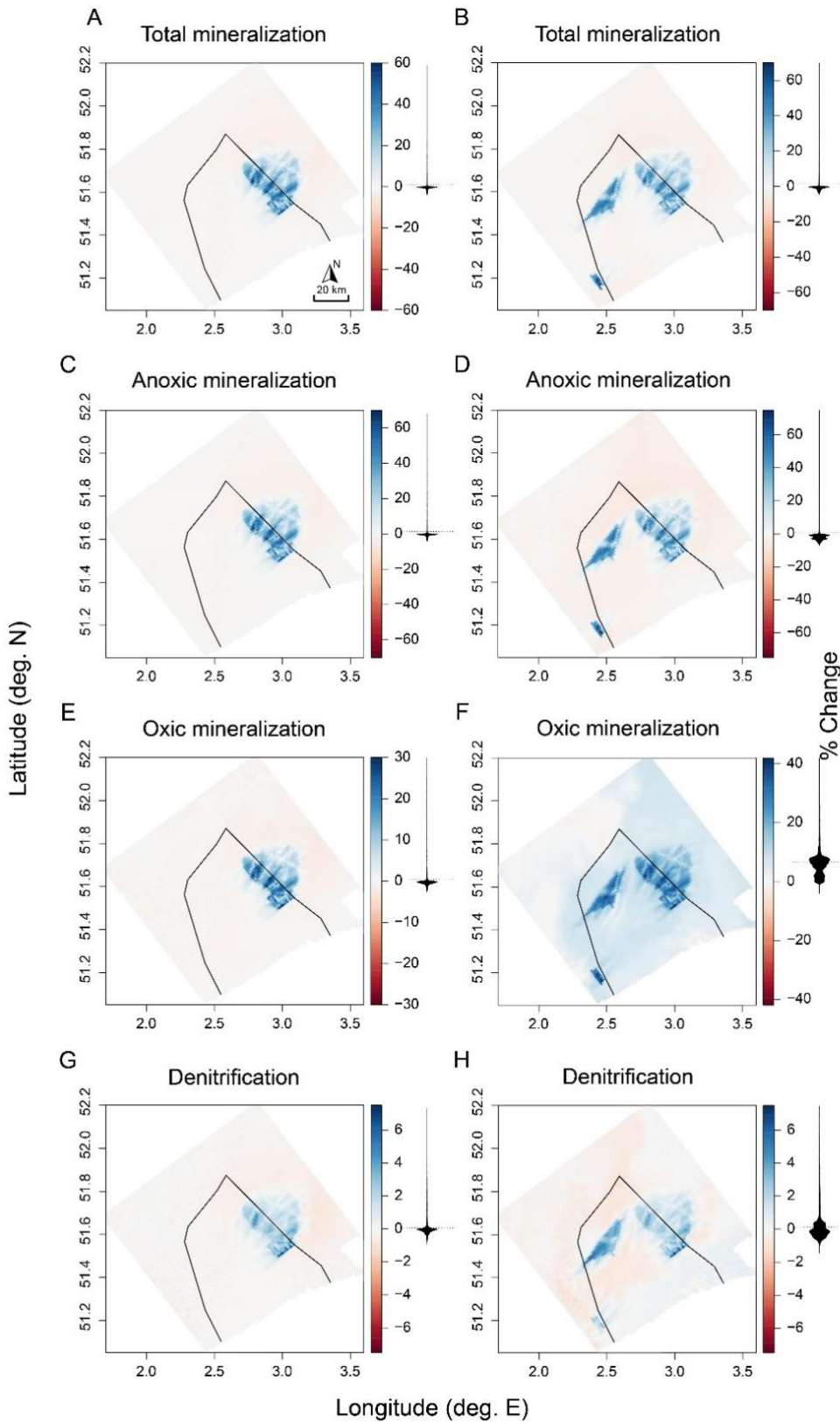
Fig. 6-4: Changes (in %) in rates of total mineralization (A, B), anoxic mineralization (C, D), oxic mineralization (E, F), and denitrification (G, H) relative to the baseline scenarios (in %) for the 'current' scenario (left column), and the 'future' scenario (right column), with the BPNS outlined in black. Density distributions of the values are represented as black shapes.

6.3.4. Total effects

The effect of the presence of OWFs in the entire modelling domain was an average increase in the total benthic mineralization of 1.4 % in the 'current' scenario, increasing to 1.9 % in the 'future' scenario, and an increased reactive carbon content of the sediment by 0.2, and 0.5 % (resp. 'current' and 'future', T. 6-4). Total denitrification also increased over the full domain by 0.03 and 0.2 %, whereas the proportion of denitrified organic material decreased by 0.6 and 1.4 % (T. 6-5). Total annual N removal increased by 0.1 and 0.2 %. Within the BPNS only, the direction of changes to individual processes was similar to patterns seen in the full domain, though percentage-wise, values were higher ('BPNS', T. 6-4 and T. 6-5).
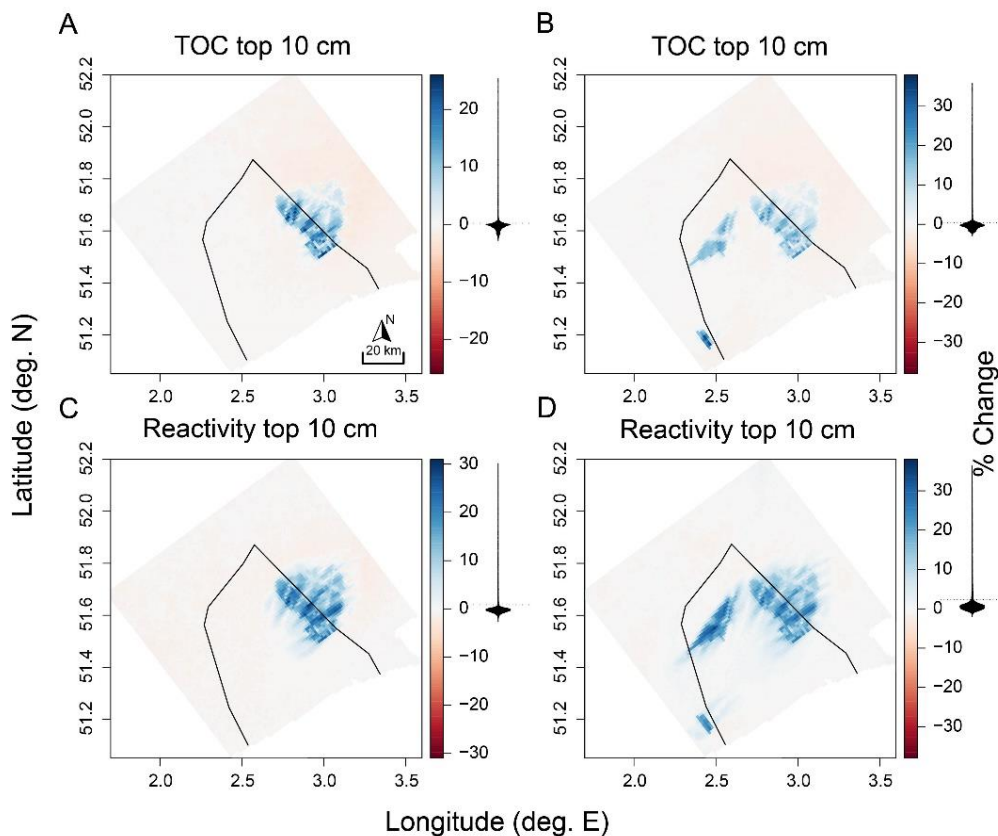
Fig. 6-5: Changes (%) to (A, B) Total organic carbon (FDET + SDET) in the top 10 cm of the sediment and (C, D) reactivity of this organic material, for the 'current' scenario (left column) and 'future' scenario (right column). Belgian BPNS outlined in black. Density distributions of the values are represented as black shapes corresponding to the axis from the colour key.

6.4. Discussion

6.4.1. Strong local effects and far field consequences

Offshore windfarms impacted the full modelling domain, with strongest effects on sediment biogeochemistry within the OWF itself, and weaker but clear effects on surrounding sediments. Deposition of highly reactive organic matter (OM) increased as a result of faecal pellet production by *Mytilus edulis*. Total benthic mineralization within the OWFs thus increased by 26.8 – 29.5 % in two scenarios that either considered the 'current' situation, where OWFs comprised 443 km², or a 'future' situation where the domain of OWFs was increased to 636 km². At the same time, OM deposition and

mineralization decreased in regions surrounding the OWFs. Rates of oxic mineralization, denitrification, and anoxic mineralization as well as the carbon storage all decreased in sediments surrounding the OWFs (Fig. 6-4, Fig. 6-5), with effects extending to the boundaries of the modelling domain. In all likelihood, impacts extend beyond the artificial modelling domain that was chosen to represent the BPNS, until net changes are evened out. Indeed, in this model run, the OWFs merely redistribute the same amount of produced OM, as there was no feed-back provided to the water column and subsequently the level of primary production.

For both scenario's, the halo's of altered benthic processing were mostly situated to the northeast of the OWFs (e.g. see Fig. 6-4 A), in line with the main direction of the residual current present in the region (Appendix C: current rosette). Since OWFs act as filters of organic matter that locally shunt organic matter from the water column to the sediment, water transported further NE becomes relatively depleted of OM compared to the baseline. As a result, OM deposition and subsequent mineralization processes decrease in the wake of the OWFs.

The 'future' placement of additional OWFs in the west of the BPNS and in the French coastal zone towards 2030, changed mineralization patterns considerably compared to the 'current' scenario. With increasing OWF area, the effect halo's of different OWFs begin to overlap, with more pronounced effects throughout the domain (Fig. 6-4). Most striking was the increase of oxic mineralization in the majority of sediments in the modelling domain (Fig. 6-4 F). Within the OWFs, OM is concentrated, resulting in higher organic matter deposition, which is partly mineralized by oxic mineralization, but mostly by anoxic mineralization. This combined effect of OM trapping in multiple OWFs decreased the organic carbon load on the sediments outside of the OWF area to a point where most of it is mineralized in surficial sediment layers, by consuming oxygen.

Denitrification was also affected by the expansion of the OWF area in the model domain, showing on one hand an increase of denitrification in nearshore sediments, and on the other hand a decreasing denitrification further away from the coastline (Fig. 6-4 H). This interesting pattern can be explained by a shift from high to more intermediate organic matter loadings nearshore discussed previously (Fig. 6-5). Denitrification is known to peak at intermediate carbon loadings (Soetaert et al., 2000), and at high nitrate concentrations, conditions that are met nearshore due to high NO_3^- loadings of the Scheldt outflow. While the zones of denitrification shifted spatially, the overall denitrification throughout the entire modelling domain barely increased (0.03 – 0.17 % for 'current' and 'future' scenario, T. 6-5). From this, we derive that the amount of N removed from the aquatic environment is only marginally increased by this scenario, with total increases of 3.2 and 13.1 kmol N on an annual basis, which represents about 0.1 – 0.4 % of the annual N input of the Scheldt estuary (45 kT N y^{-1}; Brion et al., 2006).

Whereas the physical effects of wind turbine foundations on the water column have so far only been noticed within 1 – 5 kilometres away from OWF areas (Floeter et al., 2017; Rivier et al., 2016), the scale over which e.g. water filtration, faeces production, deposition and resuspension interact to alter organic matter dynamics is still relatively unknown. Our results point to a region of influence that is of similar magnitude as the effect on water column primary productivity (NPP). Slavik et al., (2019) described a decrease of NPP of up to 8 % on an annual basis within the OWF and further reductions up to 20 km

away. Conversely, NPP increased up to 50 km away. It is thus increasingly likely that the placement of OWFs has far-reaching effects on benthic-pelagic ecosystem functioning.

These spatial effects raise the issue of transboundary impacts. Biogeochemical alterations of OWFs installed in one country can have an impact on the functioning of the benthic ecosystem in another country. The region on the western boundary of the BPNS, including part of the newly foreseen OWF expansion area, is a Natura 2000 area (Fig. 6-1). Among others, this area contains rare gravel bed habitats, which are highly sensitive to anthropogenic disturbances, but are of great importance for species that require hard substrates for reproduction such as the common whelk, the Atlantic bobtail, and the spotted catshark (resp. *Buccinum undatum, Sepiola atlantica, Scyliorhinus canicula*; Degraer et al. (2009)). For example, increased particle concentrations originating from OWF can clog the filtering apparatus of filter feeders, or limit visibility for visual predators in this valuable Natura 2000 area (Essink, 1999). This region, already directly impacted by the placement of OWFs in the North, and by domain-wide effects caused by the compounding effects of multiple OWFs (Fig. 6-4, Fig. 6-5), additionally may be impacted by the placement of the Dunkirk OWF, whose increased particle production is carried into the BPNS by the residual current.

Whereas the EU is at the forefront of transboundary marine spatial planning (Li and Jay, 2020), the transboundary biogeochemical effects of OWFs are not yet been considered in projects tasked with investigating this complex problem (European MSP platform, 2020). Our results strongly indicate that this will be necessary with future expansions of OWFs.

6.4.2. Increased carbon storage

Twenty years after the installation of OWFs, the deposited organic carbon was returned less efficiently to the water column within the OWF areas, resulting in an increased build-up of organic carbon in the sediment (T. 6-4). The additional deposition primarily translated to an increase in anoxic mineralization rates (by max. 75 % locally), with oxic mineralization increasing less (30 – 40 %,). With higher deposition, concentrations of organic matter in the upper 10 cm of sediment increased by 10 – 11 % within OWFs, while this is 0.2 – 0.5 % when extrapolated over the entire area covered by our model. As such, OWFs installed on the permeable sediments of the Southern North Sea became local sinks for carbon relative to the baseline scenario. As such, the current and future windfarm concession zones in the BPNS increased the total amount of reactive carbon trapped in the upper 10 cm of the sediment by 28715 - 48406 tonnes of carbon respectively, coinciding with 0.014 – 0.025 % of Belgium's greenhouse gas emissions (118.5 million tonnes in CO_2 equivalents in 2018, VMM et al., 2020). In that sense, the carbon potentially stored in OWFs represents a small but significant carbon offset in carbon accounting. Naturally, this storage is of limited duration. Firstly, sediment disturbing activities such as bottom trawling may or may not be prohibited within OWFs (e.g. the UK and France allow trawling outside a 50 m radius around individual turbines, whereas in Belgium, the Netherlands and Germany it is prohibited completely). Bottom trawling will resuspend sediments, lowering the build-up of OM as presented here (De Borger et al., subm). Secondly, the expected lifespan of a wind turbine is 20-25 years (Nghiem and Pineda, 2017) after which, in theory, the concession zone needs to be restored to its original

condition (Kruse et al., 2019). In case of such full decommissioning, the increased OM input will cease while the decommissioning activities itself can trigger the release of accumulated carbon to the water column as they will most likely include sediment disturbing activities. However, when alternative partial decommissioning scenarios would be considered (Fowler et al., 2020), whereby part of the subtidal structure would remain in place, repurposed or translocated, organic matter filtration by fouling fauna and subsequent local carbon storage in sediments should be considered an important decision criterion.

In recent years the call is growing to include the value of ecosystems on and around offshore energy structures in comparative analyses, before it is decided what should happen to these structures at their end-of-life phase (Fowler et al., 2020). This extends the choice of 'full decommissioning', to a variety of scenario's in which structures are repurposed, translocated, or at least partially left in place (Sommer et al., 2019). Once confirmed by field observations, the increased carbon storage capacity noted in our work could be added as a criterion in this decision process.

6.4.3. Growth urges research

The currently installed wind energy capacity in the North Sea is 18.5 GW, and is expected to rise to 70 GW by 2030 in order to achieve 30 % of renewable energy targeted by the EU (Nghiem and Pineda, 2017; Selot et al., 2019). Thus under the impulse of the ongoing "blue acceleration", the rapid development of the ocean economy (Jouffray et al., 2020), new offshore energy provisions are expected to contribute heavilty to the expansion of man-made structures at sea collected under the term "ocean sprawl" (Duarte et al., 2013; Bishop et al., 2017). Concurrently, decommissioning of OWF developments, as well as of oil and gas installations, reaching their end-of-life, is also expected to increase strongly in the coming decades (Kruse et al., 2019; Fowler et al., 2020). This means that despite recently intensified research efforts, a full cycle of OWF development to decommissioning will take place before the ecological effects are fully known. Recently, several knowledge gaps on the ecological effects of decommissioning of offshore structures have been identified (Fowler et al., 2020), but possible effects on benthic ecology extending beyond the OWF areas are still overlooked. Even then, additional factors such as the ongoing expansion of OWF's to deeper waters (Ramirez et al., 2020), where biotic and abiotic factors are different still, will again lead to a novel set of feedbacks to the ecosystem.

The work shown here represents a first investigation of the large-scale effects of biofouling fauna on organic matter mineralization in the sediment. The limited availability of validation material, and some particular assumptions made in the model were the main limitations to this study. By omitting the feedback between the sediment and the water column through a one-way coupling of the COAWST and OMEXDIA models, we assumed that primary production in the water column would not be affected by potential changes in ambient nutrient concentrations, whereas in reality this will definitely be the case (Floeter et al., 2017). Especially in shallow shelf seas, nutrients regenerated in the sediment co-regulate primary production events in the water column (Ruardij and Van Raaphorst, 1995; Soetaert and Middelburg, 2009). A dynamic coupling with a water column biogeochemistry model (Luff and Moll, 2004; Slavik et al., 2019), would inform about potential longer term effects of nutrient depletion or increase on patterns of primary production and carbon storage in sediments. Furthermore, an understanding of the annual variability displayed by carbon cycling processes is needed to understand

the significance of the results. Despite these current shortcomings, modelling studies such as ours generate new hypotheses to validate or falsify in future research on the effects of OWFs on biogeochemistry in the sediment (e.g. do changes in the benthic community around offshore structures affect denitrification rates differently than modelled), and indicate where research should be performed to improve on models (e.g. OM deposition rates and quality). For now, we have provided a simplification of a complex ecological chain of events, that can be used as a basis in future model developments.

6.5. Conclusions

Water-column filtration induced by the presence of large densities of filter feeding fouling fauna on offshore wind turbines caused the displacement and aggregation of fresh organic carbon from the water column to sediments. We show that sediments in OWFs become sites of intense organic carbon mineralization, with a halo of reduced mineralisation outside of the OWF areas. With this, the body of evidence is growing that OWFs have both local and larger scale ecosystem effects. Field measurements of sediment functioning near wind turbines are needed to give weight to our results and guide future model developments. Given the current proliferation of OWFs in North Sea waters and other shelf seas around the globe, more studies towards the positive and negative ecosystem effects of these structures are urgently needed.

Acknowledgements

Chapter 7.   GENERAL DISCUSSION

7.1.   Benthic-pelagic coupling on different spatial scales

With more and more nations developing their "Blue Economy", changes to the marine realm are imminent (European Commission, 2020c). The resources and possibilities of the marine realm are increasingly seen as having a pivotal role in sustaining human needs towards the future by policy makers and scientists alike (Jouffray et al., 2020). In the coming years, the ongoing "Blue acceleration", the near-exponential expansion of offshore wind and other forms of energy production, aquaculture projects, the extraction of mineral resources, and shipping will continue to answer these needs (Jouffray et al., 2020). Whereas a Blue economy (and associated "Blue growth" when speaking of science-based developments) is an ocean economy aimed at the "*improvement of human well-being and social equity, while significantly reducing environmental risks and ecological scarcities*" (UNEP, 2014), it is at times difficult to see how certain economic activities, or the Blue acceleration phenomenon in general can be unified with this aim (Voyer et al., 2018). In many ecosystems such as the North Sea, the structure and functioning of both biological and physical components of the North Sea ecosystem will be affected one way or another (Emeis et al., 2015).

In impact assessment and ecosystem models, the sediment biogeochemistry is often undervalued (Lessin et al., 2018). Yet, it is of major importance in shallow shelf seas. Shallow sediments are the main places in the ocean that counteract eutrophication by nitrogen and phosphorus removal through burial, or formation of biologically unavailable forms (Middelburg et al., 1996; Slomp, 2011). It is also where organic matter of marine or terrestrial origin is sequentially recycled to free nutrients (Heip et al., 1995; Dauwe and Middelburg, 1998), co-regulating primary production processes of the water column (Middelburg and Soetaert, 2004). At the same time, the temporary storage of nutrients offers resilience against changes in the eutrophication state of the aquatic system. This occurs on short timescales (weekly - seasonal) and affects the current carrying capacity of water column primary production (Van Duyl et al., 1993; van Beusekom et al., 1999; Soetaert and Middelburg, 2009). But nutrient storage also affects systems on a much longer time scale: natural sediments constitute the memory of a system, containing nutrients and carbon that have accumulated over decadal to millennial timescales (Legge et al., 2020; Soetaert et al., 2000). In the Northeastern Atlantic Shelf, the top layer (0.1 m) of the sediment contains 520 - 1600 Tmol C[4], and represents a sink of -2.2-6.0 Tmol C y^{-1} coming from the water column (carbon stock: 210 – 230 Tmol), which is up to twice the amount af carbon absorbed from the atmosphere on an annual basis (1.3 – 3.3 Tmol C y^{-1}) (Legge et al., 2020).

And yet, impact assessment studies tend to focus rather on the responses of species, or communities, instead of on the effects of anthropogenic impacts on processes that couple the sediment and the water column (Griffiths et al., 2017). In the North Sea, few studies have recorded the baseline biogeochemistry.

---

[4] 1 Tmol C = 12 million tonnes of carbon.

By our estimates based on published literature, in total about 100 m² of the North Sea sediment surface has been sampled to measure nutrient exchange fluxes, or to determine sediment nutrient profiles (See Appendix E). Within this rather limited dataset, there is a strong focus on the southeastern North Sea: a region from the Belgian Part of the North Sea to the German Bight, and westward to the Dogger Bank, with less data available for the west and north of the North Sea. Additionally, few studies report on the seasonal dynamics of mineralization processes in the sampled locations. In contrast, large datasets are available that document the benthic biology, because this has been part of the monitoring endeavors set out by many countries (e.g. Craeymeersch et al., 1986; Degraer et al., 2006; Kröncke et al., 2011). This is by no means a criticism of these sampling efforts, but rather highlights the potential that is there to extrapolate functional implications from species composition maps, once we have more widespread descriptions of their links to organic matter mineralization processes.

If we do not know the current situation, it will be difficult to evaluate or even perceive future changes. It has been shown that human activities can significantly alter marine primary production (Nohe, 2019), the first link in the food chain. This affects food provision (fisheries), but also other ecosystem services: e.g. carbon sequestration and climate regulation, eutrophication management and oxygen production are all examples of services provided alongside of primary production (Snelgrove et al., 2014).

To contribute to the understanding of anthropogenic impacts on sediment biogeochemistry, we:

1. Set a baseline to assess effects of future anthropogenic impacts on sediment biogeochemistry. This was done in two different spatial contexts. In **Chapter 2** a large range of benthic habitats was sampled to characterize how heterogeneity of sediments affects the biogeochemistry in the Belgian part of the North Sea. In **Chapter 3**, sediments were studied over a large distance, including the understudied Northern North Sea. In both campaigns, the biogeochemistry was measured alongside the biotic and abiotic drivers. Mechanistic or mass balance models were calibrated to the biogeochemistry data, and the modeled process rates were then used to assess the current role of sediments in nutrient cycling.

2. Made a step towards improving mechanistic descriptions of faunal activities, to find a way to synchronize rates of faunal activities with biogeochemical model descriptions (**Chapter 4**).

3. Applied the mechanistic models to scenarios of anthropogenic disturbance, to make inferences of the impacts of bottom trawl fisheries (**Chapter 5**), and current and future OWF development (**Chapter 6**) on sediment biogeochemical functioning.

In the general discussion that follows, first a closer look is taken at the coupling of sediment, fauna, and biogeochemistry at different spatial scales in the North Sea. We explore the implications of the biology-biogeochemistry interaction at the different scales over which the studies in the nearshore and offshore were conducted. We show that the relationship between sediment biogeochemistry and biology can be very different nearshore compared to offshore.

Secondly, the impact of bottom trawling on the North Sea ecosystem is considered from a historical perspective. The seascape this chronic disturbance to the seabed has produced serves as an interesting

viewpoint through which we can interpret the likely effects offshore windfarms will have on their environment.

In the last section, some suggestions for future research directions are presented, based on insights gained during this work.

7.2. Benthic-pelagic coupling in relation to spatial scales

Benthic-pelagic coupling entails those processes which link sediment and water column habitats, through the exchange of mass and energy. These exchange fluxes are shaped by interactions between the physical environment (hydrodynamic regime, sediment characteristics, light availability), and the biological components (primary production, benthic fauna, the food-web), which all express certain gradients over different spatial scales. Understanding the architecture of this web of interactions is imperative for our capacity to predict the occurrence and magnitude of fluxes, and more so, assess the importance of ecosystem functions and their sensitivity to future change (Griffiths et al., 2017). Therefore it is useful to summarize the patterns in sediment characteristics, macrofauna, and mineralization processes in the sediment that were described in either the nearshore habitats (**Chapter 2**), or the offshore habitat (**Chapter 3**).

During the research conducted in the Belgian Part of the North Sea (**Chapter 2**), biogeochemical fluxes and macrofauna were analysed from a diverse set of sediments, with a large range of permeabilities. In contrast, the offshore study (**Chapter 3**) covered a large distance, but contained much less variation in sediment characteristics. While chapter 3 itself reports solely on the biogeochemistry and sediment characteristics, species distributions were also determined. These were not discussed previously, so the species list, and a short description of the patterns in species distribution can be found in Appendix E.

As, both datasets (**Chapter 2 – Chapter 3**) have in common the determination of mineralization process rates (although derived with slightly different methodologies), sediment characteristics, and benthic communities, the animal-sediment interactions can be compared. In the current section, subsets of variables within each dataset (sediment, macrofauna, mineralization rates) are subjected to Principal Component Analysis (PCA). The variables that were used in the analysis were median grain size, % silt, % very fine sands, % fine sands, permeability, % TOC, and chl a concentration for the sediment characteristics, and for the mineralization processes: oxic mineralization, anoxic mineralization, denitrification, total mineralization, nitrification, and oxygen consumption. Sediment and biogeochemical variables were treated in a correlation matrix PCA (which removes variance caused by differing variable units), whereas the species biomass was treated with a centered PCA, using $\log (x + 1)$ transformed biomass (Dray and Dufour (2007), cfr. **Chapter 2**). The overview figure (Fig. 7-1), shows the first axis scores of the individual PCAs combined in one scatterplot for each dataset. This displays the correlation between the dominant variables that contrast samples to one another. The percentage of explained dataset variance by each axis is shown in T. 7-1.
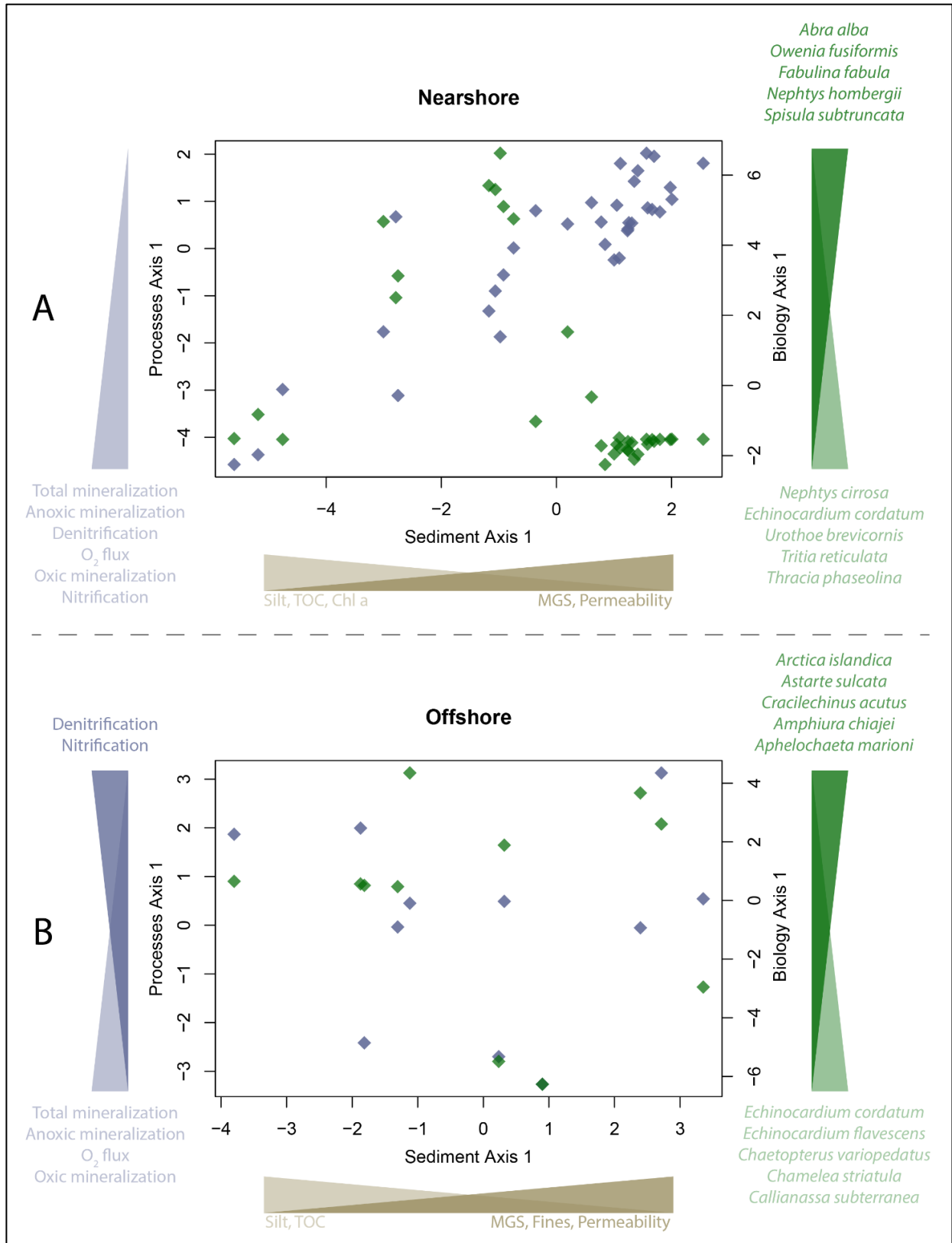
Fig. 7-1: First axis of the PCA of the biogeochemical process rates (left y-axis) and species biomass (right y-axis) plotted over the first PCA axis for sediment variables (x-axis) for (A) the Belgian part of the North Sea (Chapter 2) and (B) the greater North Sea (Chapter 3). Most relevant / highest contributing variables to axis added with their directionality of increase indicated.

Clearly, there is a difference between the nearshore and offshore study areas in the way mineralization processes, sediment, and species composition are coupled. In the nearshore sediments, mineralization processes and species biomass composition closely relate to sediment characteristics (Fig. 7-1 A), whereas this pattern is weaker in the offshore data (Fig. 7-1 B).

Nearshore, the species biomass peaked at intermediary organic matter levels, as expected according to the Pearson and Rosenberg (1978) paradigm. Biomass was lowest in the dynamic coarse-grained, permeable sediments, home to species such as *Nephtys cirrosa*, *Echinocardium cordatum*, *Urothoe brevicornis* (right portion of Fig. 7-1 A). Biomass peaked in finer grained sediments with somewhat higher organic enrichment (st. 780, 130, the middle portion of Fig. 7-1 A), and that was preferred by species such as *Owenia fusiformis*, *Fabulina fabula*, and *Nephtys hombergii*. Biomass then decreased again in the most muddy and organic enriched station (st. 130 in 2016, left portion Fig. 7-1 A), most likely by a combination of frequent disturbance in this area, and the anoxic, reduced environment in this sediment (Van De Velde et al., 2018). It should be noted that, unlike what the axis in Fig. 7-1 suggests, the species composition in this st. 130 is quite different from those in the permeable sediments; it was dominated by *Abra alba*, *Limecola balthica*, and *Ophiura ophiura*, although in low biomasses (Appendix A).

Mineralization processes were also associated clearly to sediment characteristics, but here the relationship was linear, with highest values for most process rates in the finest, organic carbon rich sediments (Fig. 7-1 B), and lowest values in the most permeable sandy sediments (Fig. 7-1 B).

In the offshore transect, there were no such clear links between sediment characteristics, species biomass, and mineralization processes. Values for mineralization rates were quite similar along the entire range, and lowest mineralization rates on the transect coincided with the finest sediments of the Northern North Sea (Fig. 7-1 B), contrary to the trend in the nearshore area. Similarly, macrofaunal biomass was distributed more evenly along the sampled transect, despite the fact that several distinct species communities were discerned, with a main contrast between species found predominantly in the Oyster Ground – Dogger Bank samples (e.g. *Echinocardium cordatum¸ Echinocardium flavescens*, *Chaetopterus variopedatus*) and species occurring most in the Central North Sea – Fladen Ground samples (e.g. *Artica islandica*, *Asterte sulcata*, *Amphiura chiajei*, Fig. 7-1 B).

In part, these discrepancies relate to the difference in range of the sampled sediment gradient between two sampling campaigns: the nearshore samples contained a much wider range of sediment conditions than the offshore samples (T. 2-1, **Chapter 2** - T. 3-4, **Chapter 3**). For example: the nearshore median grain size and TOC content ranged from 14 – 574 μm and 0.03 – 1.67 % respectively, with permeabilities between $2 \cdot 10^{-15}$ and $5.4 \ 10^{-11}$ m^2. Offshore, median grain size and TOC content ranged from 25 - 217 μm, and 0.06 – 1.12 %, whereas permeability ranged from $1 \cdot 10^{-15}$ to $7.4 \cdot 10^{-12}$ m^2, the maximum being one order of magnitude lower.

The different sedimentary conditions nearshore, from coarse sediment shaped by strong hydrodynamic forcing and with a very low nutrient content, to quasi-fully anoxic silt in the nearshore with large buildup of nutrients had a large impact on biomass distribution. These sites are characterized by a high contrast

in food availability, as well as hydrodynamic stress, both important drivers of species biomass (Heip et al., 1992; Galéron et al., 2000; Van Hoey et al., 2004). Similarly, the mineralization process rates associated with the nearshore sediments displayed a much broader range in values, simply because of the higher availability of fresh organic matter in some sites. For instance, the range in sedimentary chl *a* values, an indicator for the labile organic matter content of sediments, is $0.1 - 43$ μg g^{-1} in the nearshore, whereas along the offshore transect this was limited between $0.5 - 3.6$ μg g^{-1}.

As a potential complicating factor, the timing of both sampling campaigns should be emphasized. The NICO 10 (offshore) transect was sampled in May-June, fairly close after the spring bloom and subsequent deposition, whereas the nearshore samples were collected at the end of summer when highest mineralization rates are reached (Provoost et al., 2013; Braeckman et al., 2014). Annual variability in mineralization patterns differ in permeable and cohesive sediments. Whereas

T. 7-1: % of explained variance by axes of the PCA's. Values are not comparable between datasets, since the offshore dataset had 1/3rd of the observations of the nearshore dataset, due to averaging as a result of the biogeochemistry modelling (Chapter 3).

	% Explained variance PCA axes	
	Nearshore	Offshore
Sediment		
Axis 1	65.1	64.3
Axis 2	25.9	21.1
Axis 3	4.3	9.8
Axis 4	3.0	3.9
Biology		
Axis 1	39.0	37.2
Axis 2	15.4	19.8
Axis 3	11.3	14.8
Axis 4	9.4	7.6
Biogeochemistry		
Axis 1	47.4	63.3
Axis 2	37.3	17.1
Axis 3	11.1	14.7
Axis 4	4	4.9

permeable sediments are characterized as sites of intense, rapid organic carbon mineralization (Huettel et al., 2014; Brenner et al., 2016), mineralization in more cohesive sediments occurs predominantly through sub- to anoxic processes, which reach peak intensities much longer after bloom deposition (Soetaert et al., 1996b). Measurements of Braeckman et al. (2014) indicated that also mineralization rates between silty, and fine sandy sediments can diverge towards the end of summer, whereas they are more similar shorter after OM deposition. The relatively small differences in mineralization processes on the NICO 10 transect could well reflect a similar stage in organic matter mineralization (the oxic stage).

However, the above arguments are probably not be the only explanation for the observed differences. **In chapter 3, mineralization processes in the Central - Northern North Sea were found to be related to a depth gradient, and bottom water concentrations of certain reactants (NO$_3^-$) along the geographical range.** Total mineralization rates in the sediment decreased with increasing water depth, whereas denitrification rates were highest in sediments underlying the deepest waters. This subsequently explains why the direction of increasing denitrification is opposite to that of increasing total mineralization (Fig. 7-1 B). In the nearshore samples (Fig. 7-1 A), total denitrification related more to total mineralization (but also the activities of macrofauna in the sediment, see **Chapter 2**).

When observing distributions of species communities at a local scale, as done for the BPNS (**Chapter 2**), communities are structured along the habitat templet theory (Southwood, 1977; Townsend et al., 1997), which states that the functional composition of communities reflects habitat characteristics to which species have to cope with in order to successfully thrive in a given habitat. This is why sediment characteristics can so easily be linked to the species communities that inhabit them (Vanaverbeke et al. 2011). Similar findings were documented, e.g. for the Dogger Bank by (Kröncke, 2011). When considering distribution changes in the 670 km long offshore transect, i.e. on the "macro scale", (**Chapter 3**), bathymetric and hydrodynamic factors (e.g. stratification, current patterns) become additional drivers affecting species community structure (Becker et al., 1992; Neumann et al., 2016). For example, the dispersal of larvae of many species to potentially suitable habitats is regulated by dominant current patterns (Etter and Bower, 2015; Molen et al., 2018; Savina et al., 2010). So, the connectedness between the samples from the long transect may not be as pronounced as in the BPNS (see Fig. 1-1, Introduction).

Lastly, biogeographical patterns are also revealed over larger spatial scales. The rising sea level after the last glacial period (~ 115000 - 11700 ya) caused a gradual flooding, and deepening of the Northern and Central North Sea, starting from ±11000 ya. The Southern North Sea was filled first through the Channel, forming a narrow stream towards the North that slowly widened over the years. However, both water bodies remained separated until about 8500 ya by the Dogger Bank, which was then a much larger land mass called Doggerland (Sturt et al., 2013). This means that in the Central and Northern North Sea, species communities developed by species colonizing the waters from the North, whereas a different species community colonized the Southern North Sea from the South, until increasing sea level rise widened the Channel, flooded Doggerland completely, and connected both regions. It is likely that the observed latitudinal gradient is a remnant of these differential colonization events (Heip et al., 1992).

7.3.   Anthropogenic impacts

7.3.1.   Are sediments of the North Sea biologically and biogeochemically depleted?

Almost the entire North Sea benthic ecosystem has been shaped by several 100s of years of human activity in the marine environment (Gilbert et al., 2014). Before that time, flat oysters (Ostrea edulis) were the dominant suspension feeding organism throughout the Southern North Sea, with oyster reefs estimated to have occurred over 25500 km^2 (de Vooys et al., 2004). These bivalves used to filter suspended material from the water column, trapping organic material (i.e. carbon and nutrients) in biomass, and eventually the dead reef matrix underneath. The reef structure, both live organisms and the "dead" matrix, supports a complex food-web, and provides other functions such as sediment trapping and stabilization, nursery, and increase habitat complexity (Cloern, 1982; Gilbert et al., 2014). Indeed, biogenic reefs provide habitat for a multitude of species, increasing benthic functionality through an increase of species diversity (Holt et al., 1998). In a food web dominated by large organisms, as opposed to a microbial food web, nutrients are retained much longer within the benthic component, thereby exerting a stronger control on primary productivity (Gilbert et al., 2014).

This has changed with the onset of bottom trawling in medieval times, with a full expansion of this fishing technique throughout the North Sea since the 1900s (Wimpenny, 1953; Lenz, 1992). Earliest recorded concerns about the detrimental effects of bottom trawling on the seabed integrity stem from the 14th century, as illustrated by this anonymous quote preserved in the Rolls of Parliament (the official records of the parliament of England, later the United Kingdom; De Groot (1984)):

"…And besides this [depletion of fish in overfished areas], the great long iron [leer] of the Wondyrchoun presses so hard on the ground when fishing that it destroys the living slime and the plants growing on the bottom under the water, and also the spat of oysters, mussels, and of other fish, by which the large fish are accustomed to live and be nourished."

Nowadays, bottom trawling is widespread throughout the North Sea (Fig. 7-2 A), and large swaths of seafloor are trawled between 1 and 10 times per year, with even higher frequencies in the most productive areas (Eigaard et al., 2017). Because of the consequences of chronic trawling on the benthic ecosystem (e.g. sediment and organic matter resuspension, mortality of benthos, homogenization of sediment topography, see **Chapter 5**), this has led to the current state that *O. edulis* is virtually extinct in the Southern North Sea, so that detritivores and scavengers are the dominant benthic organisms now, and that truly long-lived species are scarce (Kaiser et al., 2006; Tillin et al., 2006; Callaway et al., 2007).

The large chronic fishing pressure may also provide an additional explanation for the fact that the bulk of mineralization occurs through oxic processes, and the rather low concentrations of nutrients in the sediment along the substantial transect sampled across the Central – Northern North Sea (Chapter 3). Results of the dynamic modelling exercise performed in **Chapter 5** illustrate how trawling may have changed sediments over time: **chronic bottom trawling leads to low organic matter contents and reaction products in the sediment, due to a direct removal of fresh organic material from the sediment surface, as well as a removal of bioturbators that normally bury organic matter in deeper sediment layers.**

It is interesting to consider how species communities are shaped by these long-term changes to sedimentary functioning in turn. The biomass of organisms, as well as the type of organisms that occur at a certain location are strongly determined by the amount, and palatability of available organic matter In general, fauna prefer organic matter of higher reactivity as this is more easily digestible and contains more accessible nutrients (Dauwe et al., 1998; Dauwe and Middelburg, 1998; LaRowe et al., 2020; Paulmier et al., 2009), but there is a range of reactivities that species exploit, and adapt their lifestyle to (Dauwe et al., 1998). However, it is difficult to separate this from the depletion effect (the physical removal / culling). Tillin et al. (2006) showed that trawling significantly reduced the biomass of permanently attached species, filter feeding species, long lived and large animals, whether there was no significant effect on the biomass of scavengers, burrowers, and short-lived or small animals, across 4 tested areas.

This leads to a conundrum, that stems from a drawback of using steady state models, or similarly, to not sample repeatedly over timescales at which such changes might be expected (10s of years). Whereas sediments (and species communities) have been subjected to changes that accumulate in time, we used

the current situation as the "background" situation which was analysed using a steady-state assumption. In lack of knowledge of the perturbations to which the sediments were subjected, we necessarily neglected such long term changes which were already induced by the fisheries. Besides modelling evidence that fisheries may impoverish and alter biogeochemistry, this is partly supported by ^{210}Pb profiles constructed from deep sediment cores collected in the North Sea between 1994 and 1996 (De Haas et al., 1997). ^{210}Pb is a radioactive isotope that has its origin in the atmosphere, and enters the aquatic environment through precipitation, and that is used to estimate sedimentation rates in aquatic sediments. Since ^{210}Pb adsorbs onto silicate particles (i.e. clay - silt), ^{210}Pb concentrations are expected to be highest on the sediment surface in undisturbed sediments, where 'fresh' silicates are deposited. Further downwards in the sediment, the tracer decays along a known half-life (22.3 y), allowing the time since deposition of a certain sediment layer to be calculated (Kirchner, 2011). In 17 of 27 locations sampled by De Haas et al. (1997), ^{210}Pb profiles displayed no significant downcore decrease in activity. This was attributed to the dynamic nature of the North Sea (De Haas et al., 1997; van Raaphorst et al., 1998), but similar looking ^{210}Pb profiles were used to indicate persistent erosion in chronically trawled seafloors in more fisheries-focused work (Martín et al., 2014; Oberle et al., 2016; Paradis et al., 2019).

Unfortunately, observations of organic carbon content and biogeochemical functioning of sediments from the 1900's do not exist, and recent data is not of sufficient spatio-temporal resolution to be linked for example to VMS data (Vessel Monitoring System), which in contrast is available for EU waters since the early-mid 2000's for EU waters and accurately tracks the activities of fishing vessels. However, a more detailed look at the sediment cores such as those collected by De Haas et al. (1997) may offer an interesting research venture when combined with historic estimates of fishing activities.
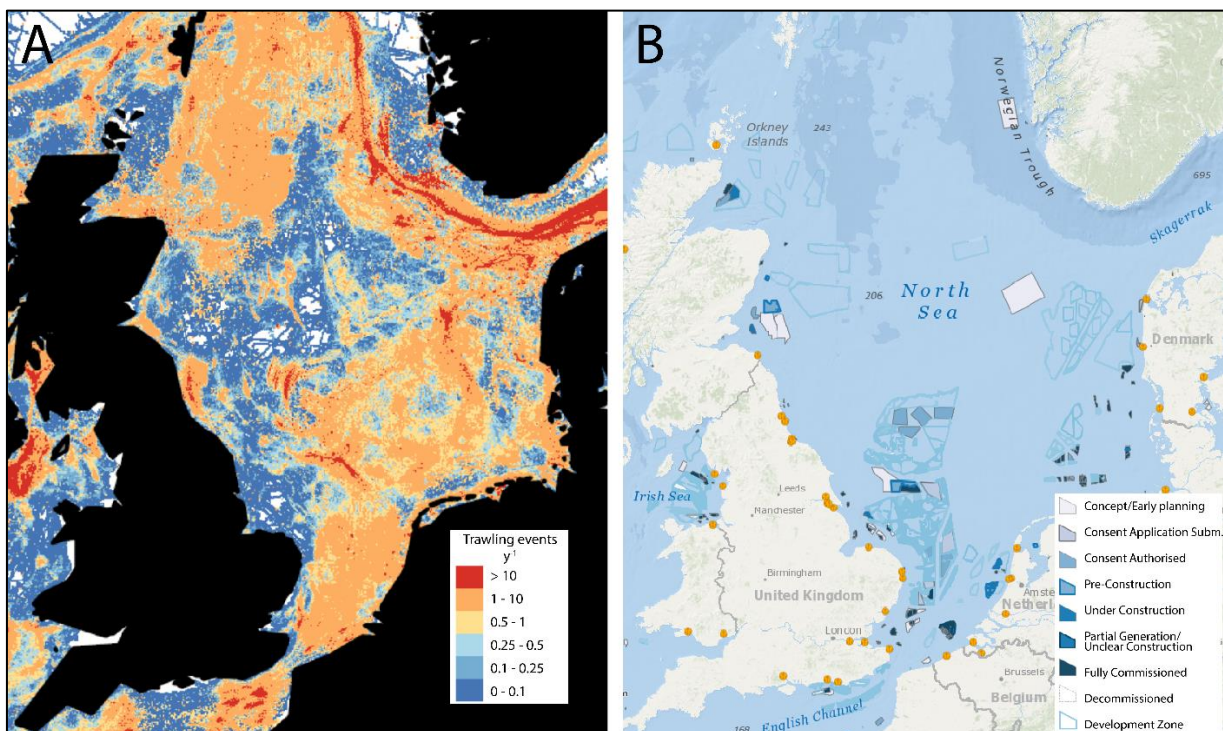
Fig. 7-2: (A) Bottom trawling intensity (events y-1) from 2010 to 2012, and (B) current and future OWF development in the North Sea. Figure A adapted from Eigaard et al., 2017, figure (B) from 4C offshore (4C offshore, last accessed 24/08/2020).

7.3.2. OWFs support new ecosystem services

The view of a North Sea ecosystem negatively affected by human pressures also offers an interesting perspective to look at the effects of OWF construction in the North Sea. In the near future, OWFs will cover a substantial area of the North Sea (Fig. 7-2 B), each containing tens to hundreds of turbines overgrown with suspension feeding fouling fauna. Our model results of **Chapter 6** and the associated work by Ivanov et al. (in prep.) showed that **filtration by the blue mussel (*M. edulis*) can cause a significant transfer of organic matter and silt from the water column to nearby sediments in the form of faecal pellets. This can lead to an increased build-up of organic material in the sediment, as high organic matter deposition increases the proportion of anoxic mineralization processes deeper in the sediment.** This, combined with the prohibition or reduction of fishing, may cause an increase in the biogeochemical complexity in North sea sediments.

Additionally, OWFs are associated with more complex food webs when compared to the natural soft sediments they are placed on. This increases the amount of nutrients assimilated (and temporarily retained) in living tissue (Mavraki et al., 2020a, 2020b). At least in terms of organic matter storage, it appears that OWFs partly replace this ecosystem function that was once provided by the vast beds of *O. edulis*.

National management decisions will determine to which extent this increased carbon storage will either persist or be of temporary nature. Whereas bottom trawling, and thus resuspension of organic material (or any commercial fishing) is prohibited within OWFs in Belgium, the Netherlands, and Germany, it is permitted in France and in the UK, albeit outside a 50 m exclusion zone around each turbine. Either way, assuming that these measures imposed on fisheries will be maintained in the future, OWFs will store more carbon in their surrounding sediments. Evidence from continuous monitoring of sediments surrounding wind turbines confirms that concentrations of fine sediments and TOC in these locations are indeed increasing, for example in Belgian and U.S. based OWFs (e.g. Coates et al., 2014; Lefaible et al., 2018, 2019; HDR, 2020), though there are exceptions to this trend (e.g. Prinses Amalia wind farm, the Netherlands; Leewis et al. (2018)). There is also the decommissioning question to consider, for OWFs as well as for oil and gas installations in the North Sea (Fowler et al., 2020; Sommer et al., 2019). The decision to fully remove these structures once their end-of-life is reached, will mostly result in the release of stored carbon and nutrients over time, as there will be much less influx of material. What research in this thesis has shown, is that modifications of mineralization processes induced by OWFs may be of significant value from an ecosystem service perspective. **For this reason, benthic functionality should be included in the process of deciding whether partial decommissioning, instead of full decommissioning should be pursued.**

There are still many unknowns concerning OWF – ecosystem and OWF – biogeochemistry interactions. In addition, we know even less about how these OWF-induced effects interact with the multitude of other pressures acting on shelf seas (e.g. bottom trawling, pollution, climate change; for a summary of these applied to the North Sea see Emeis et al. (2015)). These knowledge gaps are steadily being addressed by research performed throughout the world, and it is clear that it will take an

interdisciplinary approach, from observations of the smallest organisms attached to turbine foundations to basin-wide ecosystem models, to evaluate which new state the North Sea is heading towards. With ecosystem models, the complex interactions and feed-back loops between biological and physical processes can be evaluated in the context of compounding anthropogenic disturbances (Griffiths et al., 2017). The challenge is to make these models then sufficiently approximate reality.

7.4.   Considerations for the future

While we have developed and used diagenetic models to provide a glimpse into the future (**Chapter 6**) or to better understand the present (**Chapters 3, 5**), there are still several steps that would need to be taken in future modelling exercises. These involve to better include faunal activities in models of sediment biogeochemistry by improving the coordinating of biological and biogeochemical studies, and to keep acquiring high quality data with the intent to calibrate, and fit those models.

7.4.1.   Improving the biology – biogeochemistry interaction

It remains challenging to incorporate biological processes in detailed biogeochemical models. Species communities often display high variability in terms of biomass and abundance, both on an intra-and interannual scale (**Chapter 2;** Frid et al. (1996); Ysebaert and Herman (2002)). In addition, the same species do not necessarily exhibit the same behaviors across a habitat gradient as this may depend on the species community composition in which they occur (**Chapter 4,** Hale et al., (2014); Murray et al. (2014)). As clearly shown in the variance partitioning in **Chapter 2** for example, biology can be an important factor explaining the magnitude of certain mineralization processes, but at the same time research points towards a large amount of context dependency concerning the role of macrofauna.

Mechanistically, it is also difficult to couple species presences to behavioral processes, even with the use of their functional traits. Biological traits (characteristics or features exhibited by organisms) are of great value in ecology, i.e. to understand the occurrence of species in certain habitats, and assess their resilience to disturbances (Beauchard et al., 2017), but it is important that the attribution of certain traits or trait scores is grounded by observations (Hale et al., 2014). In our work for instance, we showed that the bioirrigation index (IP_c), was not correlated to measurements of bioirrigation rates (**Chapter 2, Chapter 4**). Whereas this does not mean that the IP_c is a useless measure, we (**Chapter 2**), and others (Wrede et al. (2019) found it to be a predictor of certain process rates or fluxes. Nevertheless, more work needs to be done to see if the IP_c could be reformulated to better represent what it aims to indicate (e.g. Queirios et al., 2015). The Bioturbation Potential index (BP_c, Solan et al., 2004) has been around for much longer than the IP_c (Wrede et al. 2018). The BP_c index was found to be most of all a predictor for the average 'jump length' of a particle during a bioturbation event, and not of biodiffusivity Db, which could be used in a model description (Queirós et al., 2015). **We showed for the first time that also the IP_c provides only a partial link to effective irrigation: IP_c was related to the depth of the irrigated layer (Chapter 4) and not to the irrigation intensity.**

Also, there needs to be a combined effort of biologists and biogeochemists to link the biologically-based and mainly qualitative indices to the quantitative measures that are needed in biogeochemical models.

For this, the techniques for measuring rates of faunal activities should be more standardized. In a recent compilation of bioturbation and bioirrigation rates by Solan et al. (2019), 15 different measurement techniques were listed for bioturbation, producing rates spanning 6 orders of magnitude. The same is true for bioirrigation (17 techniques), of which the units had to be expressed as ml h^{-1} ind.$^{-1}$ to allow for a comparison between sources. Unfortunately, this unit is quite difficult to work with in a model, which requires rates expressed per surface area or volume. Ideally one would wish to arrive at one measurement technique, providing a consistent activity rate and in a unit expressed with the same rigor as an SI unit. The relative homogeneity in the way nutrient fluxes are measured and reported in various research articles for example, shows that this is feasible.

There is also a danger in *a priori* selecting a limited set of traits to generate an index, as this implies that the mechanistic causes of a process are close to fully known. In this sense, it should be mentioned that the original intent of the BP$_c$ to study how bioturbation might be affected by species extinctions (Solan et al., 2004), and was composed of traits previously linked to bioturbation, but also to vulnerability to extinction. It was later used as a functional, quantitative measure to calculate the impacts of biology on contemporary sediment biogeochemistry, with mixed results. The IP$_c$ in turn, was heavily based on the BP$_c$ to make the link between species communities and solute exchange rates (Wrede et al., 2018). Better indices may be obtained with a multivariate inverse approach where all possible (functional) traits are considered when trying to link benthic species biomass and abundances to measured process rates or other relevant aspects of the ecosystem (e.g. Hevia et al., 2017). For this approach initially no new samples should be collected. For example, numerous studies have already been performed in which the species community, bioturbation rates, and some aspect of sediment biogeochemistry have been sampled simultaneously (e.g. **Chapters 2** and **3** in this work, Braeckman et al., 2010, Wrede et al., 2018). Since the collection of species traits can be done *a-posteriori*, all these experiments can be used in the search for improved functional indices.

7.4.2. Models go together with data

Mechanistic models require high quality data for ground-truthing, in model jargon called calibration and validation. Our estimate of the small area of the North Sea surface that has so far been sampled to quantify exchange fluxes or nutrient profiles is not much larger than 100 m^2. This is virtually nothing, considering the heterogeneity displayed by sediments in some regions. In addition, we lack information on the seasonal dynamics of benthic processes. Peaks in mineralization rates may easily be missed in discrete sampling, resulting in an underestimation of the total mineralization that occurs in a certain location. A useful dataset to fuel ecosystem models that operate on a large scale would contain consistent measurements of relevant water column parameters and benthic exchange fluxes, replicated during a period long enough to capture the strong seasonal dynamics that shape benthic-pelagic coupling. Whereas this is very much a modelers' dream, in this period of drastic changes to the seascape, data that can fuel predictive models throughout the coming generation is more welcome than ever.

For instance, it would be highly valuable to characterize sediment biogeochemistry of sites that are designated for OWF development in the Southern-Central North Sea (Mostly in U.K. waters, Fig. 7-2 B). Firstly, in this area of the North Sea, highest primary production rates are observed each year as a

result of high nutrient inputs and continuous mixing of the water column (see Introduction). Furthermore, the shallow depth of this area (< 50 m) emphasizes the role of sediments in recycling of this primary production. Secondly, the main transport direction in the North Sea is northward (see Fig. 1-1, Introduction), meaning that a significant amount of organic matter from the Southern North Sea is transported in successive deposition-resuspension events, finally to the Skagerrak, providing an important input of (increasingly degraded) organic material to food-webs along the way (Dauwe et al., 1998; Dauwe and Middelburg, 1998). Our results of **Chapter 6**, and other modelling studies of OWFs imply a redistribution of primary production (Slavik et al., 2019) and a local retention of organic matter in OWFs, with possible feed-back effects between benthic and pelagic compartments that still need to be investigated. It is likely that the placement of a considerable amount of wind turbines will have a massive effect on the entire North Sea ecosystem. Investigations should best follow a BACI sampling design (before-after-control-impact), in which mineralization processes are characterized before the placement of OWFs, on representative sampling points that include areas that will and will not be transformed to OWFs, and where sediment maps may be used to estimate spatial heterogeneity. After implementation of the OWFs, sampling of sediment biogeochemistry has to be included in monitoring designs, ideally coupled to permanent in-situ sensors for monitoring water characteristics (nutrient and chl *a* content) within and outside of the OWFs. This would clarify whether enhanced mineralization in sediments leads to equally enhanced nutrient concentrations in the water column, and how this links to changes or local concentrations of primary productivity. With this information, the direct effects of OWFs on benthic-pelagic coupling can be monitored, and mechanistic models may be calibrated to extrapolate effects to the future and to larger areas.

Ideally, the local environment around the turbines should also be characterized, through high-resolution sampling around individual turbines. In the model presented in **Chapter 6**, assumptions had to be made about the amount, and characteristics of the faecal pellets that are deposited around a turbine, a crucial step in the model description for which few sources were found. Though experimental work (e.g. in the Persuade project (Vanaverbeke et al., 2020) and in the FaCE-It project) is increasing our knowledge about the biogeochemical effects of fauna living on wind turbines, it was found difficult to couple this information to the observations of changing organic matter content in close proximity of wind turbines (Ivanov, pers. comm.). Sampling so close to offshore wind turbines however is difficult for practical and safety reasons, and can only be performed with the help of divers. However, measurements of the organic carbon and chl *a* content, and basic observations of the sediment biogeochemistry (O_2 fluxes, porewater nutrient profiles) sampled on concentric circles around turbines, together with modelling techniques illustrated in this work, could pinpoint the specific effects of individual turbines on their surroundings. This would again provide spatial mechanistic models with the ground-truthing data, moderating the large uncertainty that now surrounds our knowledge on this topic.

Cited literature

4C offshore: Global offshore windfarms, [online] Available from: https://www.4coffshore.com/offshorewind/ (Accessed 24 August 2020), 2020.

Ahmerkamp, S., Marchant, H. K., Peng, C., Probandt, D., Littmann, S., Kuypers, M. M. M. and Holtappels, M.: The effect of sediment grain properties and porewater flow on microbial abundance and respiration in permeable sediments, Sci. Rep., 10(1), 1–12, doi:10.1038/s41598-020-60557-7, 2020.

Ait Ballagh, F. E., Rabouille, C., Andrieux-Loyer, F., Soetaert, K., Elkalay, K. and Khalil, K.: Spatio-temporal dynamics of sedimentary phosphorus along two temperate eutrophic estuaries: A data-modelling approach, Cont. Shelf Res., 193(March 2019), 104037, doi:10.1016/j.csr.2019.104037, 2020.

Akaike, H.: A new look at the statistical model identification, IEEE Trans. Automat. Contr., 19(6), 716–723, doi:10.1109/TAC.1974.1100705, 1974.

Al-Raei, A. M., Bosselmann, K., Böttcher, M. E., Hespenheide, B. and Tauber, F.: Seasonal dynamics of microbial sulfate reduction in temperate intertidal surface sediments: controls by temperature and organic matter, Ocean Dyn., 59(2), 351–370, doi:10.1007/s10236-009-0186-5, 2009.

Aller, R. C.: Quantifying solute distributions in the bioturbated zone of marine sediments by defining an average microenvironment, Geochim. Cosmochim. Acta, 44(12), 1955–1965, doi:10.1016/0016-7037(80)90195-7, 1980.

Aller, R. C. and Aller, J. Y.: Meiofauna and solute transport in marine muds, Limnol. Oceanogr., 37(5), 1018–1033, doi:10.4319/lo.1992.37.5.1018, 1992.

Aller, R. C. and Aller, J. Y.: The effect of biogenic irrigation intensity and solute exchange on diagenetic reaction rates in marine sediments, J. Mar. Res., 56(4), 905–936, doi:10.1357/002224098321667413, 1998.

Aller, R. C. and Yingst, J. Y.: Effects of the marine deposit-feeders Heteromastus filiformis (Polychaeta), Macoma balthica (Bivalvia), and Tellina texana (Bivalvia) on averaged sedimentary solute transport, reaction rates, and microbial distributions, J. Mar. Res., 43(3), 615–645, doi:10.1357/002224085788440349, 1985.

Almroth, E., Tengberg, A., Andersson, J. H., Pakhomova, S. and Hall, P. O. J.: Effects of resuspension on benthic fluxes of oxygen, nutrients, dissolved inorganic carbon, iron and manganese in the Gulf of Finland, Baltic Sea, Cont. Shelf Res., 29(5–6), 807–818, doi:10.1016/j.csr.2008.12.011, 2009.

Amoroso, R. O., Pitcher, C. R., Rijnsdorp, A. D., McConnaughey, R. A., Parma, A. M., Suuronen, P., Eigaard, O. R., Bastardie, F., Hintzen, N. T., Althaus, F., Baird, S. J., Black, J., Buhl-Mortensen, L., Campbell, A. B., Catarino, R., Collie, J., Cowan, J. H., Durholtz, D., Engstrom, N., Fairweather, T. P., Fock, H. O., Ford, R., Gálvez, P. A., Gerritsen, H., Góngora, M. E., González, J. A., Hiddink, J. G., Hughes, K. M., Intelmann, S. S., Jenkins, C., Jonsson, P., Kainge, P., Kangas, M., Kathena, J. N., Kavadas, S., Leslie, R. W., Lewise, S. G., Lundy, M., Makin, D., Martin, J., Mazor, T., Gonzalez-Mirelis, G., Newman, S. J., Papadopoulou, N., Posen, P. E., Rochester, W., Russok, T., Salal, A., Semmens, J. M., Silvan, C., Tsoloso, A., Vanelslander, B., Wakefield, C. B., Wood, B. A., Hilborn, R., Kaiser, M. J. and Jennings, S.: Bottom trawl fishing footprints on the world's continental shelves, Proc. Natl. Acad. Sci. U. S. A., 115(43), E10275–E10282, doi:10.1073/pnas.1802379115, 2018.

Andersson, J. H., Middelburg, J. J. and Soetaert, K.: Identifiability and uncertainty analysis of bio-irrigation rates, J. Mar. Res., 64(3), 407–429, doi:10.1357/002224006778189590, 2006.

Azzalini, A.: The R package sn: The Skew-Normal and Related Distributions such as the Skew (version 1.6-0), [online] Available from: http://azzalini.stat.unipd.it/SN, 2020.

De Backer, A., van Ael, E., Vincx, M. and Degraer, S.: Behaviour and time allocation of the mud shrimp, Corophium volutator, during the tidal cycle: A laboratory study, Helgol. Mar. Res., 64(1), 63–67, doi:10.1007/s10152-009-0167-6, 2010.

De Backer, A., Van Hoey, G., Coates, D., Vanaverbeke, J. and Hostens, K.: Similar diversity-disturbance responses to different physical impacts: Three cases of small-scale biodiversity increase in the Belgian part of the North Sea, Mar. Pollut. Bull., 84(1–2), 251–262, doi:10.1016/j.marpolbul.2014.05.006, 2014.

Baeye, M. and Fettweis, M.: In situ observations of suspended particulate matter plumes at an offshore wind farm, southern North Sea, Geo-Marine Lett., 35(4), 247–255, doi:10.1007/s00367-015-0404-8, 2015.

Bale, N. J., Villanueva, L., Fan, H., Stal, L. J., Hopmans, E. C., Schouten, S. and Sinninghe Damsté, J. S.: Occurrence and activity of anammox bacteria in surface sediments of the southern North Sea, FEMS Microbiol. Ecol., 89(1), 99–110, doi:10.1111/1574-6941.12338, 2014.

Bannister, R. J., Valdemarsen, T., Hansen, P. K., Holmer, M. and Ervik, A.: Changes in benthic sediment conditions under an atlantic salmon farm at a deep, well-flushed coastal site, Aquac. Environ. Interact., 5(1), 29–47, doi:10.3354/aei00092, 2014.

Banta, G. T., Holmer, M., Jensen, M. H. and Kristensen, E.: Effects of two polychaete worms, Nereis diversicolor and Arenicola marina, on aerobic and anaerobic decomposition in a sandy marine sediment, Aquat. Microb. Ecol., 19(2), 189–204, doi:10.3354/ame019189, 1999.

Baptist, M. J., van Dalfsen, J., Weber, A., Passchier, S. and van Heteren, S.: The distribution of macrozoobenthos in the southern North Sea in relation to meso-scale bedforms, Estuar. Coast. Shelf Sci., 68(3–4), 538–546, doi:10.1016/j.ecss.2006.02.023, 2006.

Baretta, J. W., Ebenhöh, W. and Ruardij, P.: The European regional seas ecosystem model, a complex marine ecosystem model, Netherlands J. Sea Res., 33(3–4), 233–246, doi:10.1016/0077-7579(95)90047-0, 1995.

Baselga, A.: Partitioning the turnover and nestedness components of beta diversity, Glob. Ecol. Biogeogr., 19(1), 134–143, doi:10.1111/j.1466-8238.2009.00490.x, 2010.

Baselga, A., Orme, D., Villeger, S., De Bortoli, J. and Leprieur, F.: betapart: Partitioning Beta Diversity into Turnover and Nestedness Components, [online] Available from: https://cran.r-project.org/package=betapart, 2018.

Bayne, B. L., Iglesias, J. I. P., Hawkins, A. J. S., Navarro, E., Heral, M. and Deslous-Paoli, J. M.: Feeding behaviour of the mussel, Mytilus edulis: responses to variations in quantity and organic content of the seston, J. Mar. Biol. Assoc. United Kingdom, 73(4), 813–829, doi:10.1017/S0025315400034743, 1993.

Beauchard, O., Veríssimo, H., Queirós, A. M. and Herman, P. M. J.: The use of multiple biological traits in marine community ecology and its potential in ecological indicator development, Ecol. Indic., 76, 81–96, doi:10.1016/j.ecolind.2017.01.011, 2017.

Becker, G. A., Dick, S. and Dippner, J. W.: Hydrography of the German Bight, Mar. Ecol. Prog. Ser., 91(1–3), 9–18, doi:10.3354/meps091009, 1992.

De Beer, D., Wenzhöfer, F., Ferdelman, T. G., Boehme, S. E., Huettel, M., Van Beusekom, J. E. E., Böttcher, M. E., Musat, N. and Dubilier, N.: Transport and mineralization rates in North Sea sandy intertidal sediments, Sylt-Rømø Basin, Wadden Sea, Limnol. Oceanogr., 50(1), 113–127, doi:10.4319/lo.2005.50.1.0113, 2005.

Behrendt, A., De Beer, D. and Stief, P.: Vertical activity distribution of dissimilatory nitrate reduction in coastal marine sediments, Biogeosciences, 10(11), 7509–7523, doi:10.5194/bg-10-7509-2013, 2013.

Belley, R. and Snelgrove, P. V. R.: Relative Contributions of Biodiversity and Environment to Benthic Ecosystem Functioning, Front. Mar. Sci., 3, 242, doi:10.3389/fmars.2016.00242, 2016.

Berelson, W. M., Heggie, D., Longmore, a, Kilgore, T., Nicholson, G. and Skyring, G.: Benthic Nutrient Recycling in Port Phillip Bay, Australia, Estuar. coast. shelf Sci, 46, 917–934, doi:DOI: 10.1006/ecss.1998.0328, 1998.

Berg, P.: Dynamic Modeling of Early Diagenesis and Nutrient Cycling. A Case Study in an Artic Marine Sediment, Am. J. Sci., 303(10), 905–955, doi:10.2475/ajs.303.10.905, 2003.

Berg, P., Rysgaard, S., Funch, P. and Sejr, M. K.: Effects of bioturbation on solutes and solids in marine sediments,

Aquat. Microb. Ecol., 26(1), 81–94, doi:DOI 10.3354/ame026081, 2001.

Bergman, M. J. N. and Hup, M.: Direct effects of beamtrawling on macrofauna in a sandy sediment in the southern north sea, ICES J. Mar. Sci., 49(1), 5–11, doi:10.1093/icesjms/49.1.5, 1992.

Bergman, M. J. N. and Van Santbrink, J. W.: Mortality in megafaunal benthic populations caused by trawl fisheries on the Dutch continental shelf in the North Sea in 1994, ICES J. Mar. Sci., 57(5), 1321–1331, doi:10.1006/jmsc.2000.0917, 2000.

Bergström, L., Kautsky, L., Malm, T., Ohlsson, H., Wahlberg, M., Rosenberg, R. and Capetillo, N. Å.: The effects of wind power on marine life - A Synthesis, Bromma., 2012.

Bergström, L., Kautsky, L., Malm, T., Rosenberg, R., Wahlberg, M., Åstrand Capetillo, N. and Wilhelmsson, D.: Effects of offshore wind farms on marine wildlife - A generalized impact assessment, Environ. Res. Lett., 9(3), doi:10.1088/1748-9326/9/3/034012, 2014.

Bertics, V., Sohm, J., Treude, T., Chow, C., Capone, D., Fuhrman, J. and Ziebis, W.: Burrowing deeper into benthic nitrogen cycling: the impact of bioturbation on nitrogen fixation coupled to sulfate reduction, Mar. Ecol. Prog. Ser., 409, 1–15, doi:10.3354/meps08639, 2010.

Besio, G., Blondeaux, P., Brocchini, M. and Vittori, G.: On the modeling of sand wave migration, J. Geophys. Res. C Ocean., 109(4), doi:10.1029/2002JC001622, 2004.

van Beusekom, J. E. E., Brockmann, U. H., Hesse, K.-J., Hickel, W., Poremba, K. and Tillmann, U.: The importance of sediments in the transformation and turnover of nutrients and organic matter in the Wadden Sea and German Bight, Dtsch. Hydrogr. Zeitschrift, 51(2–3), 245–266, doi:10.1007/BF02764176, 1999.

Billen, G.: A budget of nitrogen recycling in North Sea sediments off the Belgian coast, Estuar. Coast. Mar. Sci., 7(2), 127–146, doi:10.1016/0302-3524(78)90070-1, 1978.

Billen, G., Garnier, J. and Rousseau, V.: Nutrient fluxes and water quality in the drainage network of the Scheldt basin over the last 50 years, Hydrobiologia, 540(1–3), 47–67, doi:10.1007/s10750-004-7103-1, 2005.

Bishop, M. J., Mayer-Pinto, M., Airoldi, L., Firth, L. B., Morris, R. L., Loke, L. H. L., Hawkins, S. J., Naylor, L. A., Coleman, R. A., Chee, S. Y. and Dafforn, K. A.: Effects of ocean sprawl on ecological connectivity: impacts and solutions, J. Exp. Mar. Bio. Ecol., 492, 7–30, doi:10.1016/j.jembe.2017.01.021, 2017.

Blanchet, F. G., Legendre, P. and Borcard, D.: Forward selection of explanatory variables, Ecology, 89(9), 2623–2632, doi:10.1890/07-0986.1, 2008.

Bockelmann, F. D., Puls, W., Kleeberg, U., Müller, D. and Emeis, K. C.: Mapping mud content and median grain-size of North Sea sediments – A geostatistical approach, Mar. Geol., 397(March 2017), 60–71, doi:10.1016/j.margeo.2017.11.003, 2018.

Bolam, S. G. and Eggleton, J. D.: Macrofaunal production and biological traits: Spatial relationships along the UK continental shelf, J. Sea Res., 88, 47–58, doi:10.1016/j.seares.2014.01.001, 2014.

Boon, A. and Duineveld, G.: Chlorophyll a as a marker for bioturbation and carbon flux in southern and central North Sea sediments, Mar. Ecol. Prog. Ser., 162, 33–43, doi:10.3354/meps162033, 1998.

Boon, A. R., Duineveld, G. C. A., Berghuis, E. M. and Van Der Weele, J. A.: Relationships between Benthic Activity and the Annual Phytopigment Cycle in Near-bottom Water and Sediments in the Southern North Sea, Estuar. Coast. Shelf Sci., 46, 1–13, doi:10.1006/ecss.1997.0264, 1998.

Borcard, D., Gillet, F. and Legendre, P.: Numerical Ecology with R, Springer New York, New York, NY., 2011.

De Borger, E., Tiano, J., Braeckman, U., Ysebaert, T. and Soetaert, K.: Biological and biogeochemical methods for estimating bio-irrigation: a case study in the Oosterschelde estuary, Biogeosciences, 17(April), 1701–1715, doi:10.5194/bg-2019-413, 2020.

Le Bot, S., Lafite, R., Fournier, M., Baltzer, A. and Desprez, M.: Morphological and sedimentary impacts and

recovery on a mixed sandy to pebbly seabed exposed to marine aggregate extraction (Eastern English Channel, France), Estuar. Coast. Shelf Sci., 89(3), 221–233, doi:https://doi.org/10.1016/j.ecss.2010.06.012, 2010.

Böttcher, M. E., Hespenheide, B., Llobet-Brossa, E., Beardsley, C., Larsen, O., Schramm, A., Wieland, A., Böttcher, G., Berninger, U. G. and Amann, R.: The biogeochemistry, stable isotope geochemistry, and microbial community structure of a temperate intertidal mudflat: An integrated study, Cont. Shelf Res., 20(12–13), 1749–1769, doi:10.1016/S0278-4343(00)00046-7, 2000.

Boudreau, B. P.: Mathematics of tracer mixing in sediments: II. Nonlocal mixing and biological conveyor-belt phenomena., Am. J. Sci., 286(3), 199–238, doi:10.2475/ajs.286.3.199, 1986.

Boudreau, B. P.: The diffusive tortuosity of fine-grained unlithified sediments, Geochim. Cosmochim. Acta, 60(16), 3139–3142, doi:10.1016/0016-7037(96)00158-5, 1996.

Boudreau, B. P.: Diagenetic models and their implementation: modelling transport and reactions in aquatic sediments, Springer-Verlag, Berlin., 1997.

Boudreau, B. P.: The Mathematics of Early Diagenesis: From Worms to Waves, Rev. Geophys., 38(3), 389–416, doi:10.1029/2000RG000081, 2000.

Boudreau, B. P. and Ruddick, B. R.: On a Reactive Continuum Representation of Organic-Matter Diagenesis, Am. J. Sci., 291(5), 507–538, doi:10.2475/ajs.292.1.79, 1991.

Braeckman, U., Provoost, P., Gribsholt, B., Van Gansbeke, D., Middelburg, J. J., Soetaert, K., Vincx, M. and Vanaverbeke, J.: Role of macrofauna functional traits and density in biogeochemical fluxes and bioturbation, Mar. Ecol. Prog. Ser., 399(2010), 173–186, doi:10.3354/meps08336, 2010.

Braeckman, U., Van Colen, C., Soetaert, K., Vincx, M. and Vanaverbeke, J.: Contrasting macrobenthic activities differentially affect nematode density and diversity in a shallow subtidal marine sediment, Mar. Ecol. Prog. Ser., 422, 179–191, doi:10.3354/meps08910, 2011.

Braeckman, U., Foshtomi, M. Y., Van Gansbeke, D., Meysman, F., Soetaert, K., Vincx, M. and Vanaverbeke, J.: Variable Importance of Macrofaunal Functional Biodiversity for Biogeochemical Cycling in Temperate Coastal Sediments, Ecosystems, 17(4), 720–737, doi:10.1007/s10021-014-9755-7, 2014.

Bratek, A., Van, Beusekom, J. E. E., Neumann, A., Sanders, T., Friedrich, J., Emeis, K.-C. and Dähnke, K.: Spatial variations in sedimentary N-transformation rates in the North Sea (German Bight), Biogeosciences, 17(10), 2839–2851, doi:10.5194/bg-17-2839-2020, 2020.

Breine, N. T., De Backer, A., Van Colen, C., Moens, T., Hostens, K. and Van Hoey, G.: Structural and functional diversity of soft-bottom macrobenthic communities in the Southern North Sea, Estuar. Coast. Shelf Sci., 214(September), 173–184, doi:10.1016/j.ecss.2018.09.012, 2018.

Bremner, J., Rogers, S. and Frid, C.: Assessing functional diversity in marine benthic ecosystems: a comparison of approaches, Mar. Ecol. Prog. Ser., 254, 11–25, doi:10.3354/meps254011, 2003.

Brenner, H., Braeckman, U., Le Guitton, M. and Meysman, F. J. R.: The impact of sedimentary alkalinity release on the water column CO2 system in the North Sea, Biogeosciences, 13(3), 841–863, doi:10.5194/bg-13-841-2016, 2016.

Brey, T.: An empirical model for estimating aquatic invertebrate respiration, Methods Ecol. Evol., 1(1), 92–101, doi:10.1111/j.2041-210x.2009.00008.x, 2010.

Brion, N., Jans, S., Chou, L. and Rousseau, V.: Nutrient loads to the Belgian Coastal Zone, in Current Status of Eutrophication in the Belgian Coastal Zone, edited by V. Rousseau, C. Lancelot, and D. Cox, pp. 17–43, Presse Universitaire de Bruxelles, Brussels., 2006.

Brylinsky, M., Gibson, J. and Gordon Jr., D. C.: Impacts of Flounder Trawls on the Intertidal Habitat and Community of the Minas Basin, Bay of Fundy, Can. J. Fish. Aquat. Sci., 51(3), 650–661, doi:10.1139/f94-066, 1994.

Buchanan, J. B.: Sediment Analysis, 2nd ed., edited by N. A. Holmes and A. D. McIntyre, Blackwell Scientific

Publications, Oxford., 1984.

Buhr, K.-J.: Suspension-feeding and assimilation efficiency in Lanice conchilega (Polychaeta), Mar. Biol., 38(4), 373–383, doi:10.1007/BF00391377, 1976.

Buhr, K.-J. and Winter, J. E.: Distribution and maintenance of a Lanice Conchilega association in the Weser estuary (FRG), with special reference to the suspension-feeding behaviour of Lanice Conchilega, in Biology of Benthic Organisms, pp. 101–113, Elsevier., 1977.

Burson, A., Stomp, M., Akil, L., Brussaard, C. P. D. and Huisman, J.: Unbalanced reduction of nutrient loads has created an offshore gradient from phosphorus to nitrogen limitation in the North Sea, Limnol. Oceanogr., 61(3), 869–888, doi:10.1002/lno.10257, 2016.

Butenschön, M., Clark, J., Aldridge, J. N., Icarus Allen, J., Artioli, Y., Blackford, J., Bruggeman, J., Cazenave, P., Ciavatta, S., Kay, S., Lessin, G., Van Leeuwen, S., Van Der Molen, J., De Mora, L., Polimene, L., Sailley, S., Stephens, N. and Torres, R.: ERSEM 15.06: A generic model for marine biogeochemistry and the ecosystem dynamics of the lower trophic levels, Geosci. Model Dev., 9(4), 1293–1339, doi:10.5194/gmd-9-1293-2016, 2016.

De Cáceres, M. and Legendre, P.: Associations between species and groups of sites: Indices and statistical inference, Ecology, 90(12), 3566–3574, doi:10.1890/08-1823.1, 2009.

Callaway, R., Engelhard, G. H., Dann, J., Cotter, J. and Rumohr, H.: A century of North Sea epibenthos and trawling: Comparison between 1902-1912, 1982-1985 and 2000, Mar. Ecol. Prog. Ser., 346(May 2014), 27–43, doi:10.3354/meps07038, 2007.

Callier, M. D., Weise, A. M., McKindsey, C. W. and Desrosiers, G.: Sedimentation rates in a suspended mussel farm (Great-Entry Lagoon, Canada): Biodeposit production and dispersion, Mar. Ecol. Prog. Ser., 322(Hargrave 2005), 129–141, doi:10.3354/meps322129, 2006.

Canfield, D. ., Jørgensen, B. ., Fossing, H., Glud, R., Gundersen, J., Ramsing, N. ., Thamdrup, B., Hansen, J. ., Nielsen, L. . and Hall, P. O. .: Pathways of organic carbon oxidation in three continental margin sediments, Mar. Geol., 113(1–2), 27–40, doi:10.1016/0025-3227(93)90147-N, 1993.

Capuzzo, E., Lynam, C. P., Barry, J., Stephens, D., Forster, R. M., Greenwood, N., McQuatters-Gollop, A., Silva, T., van Leeuwen, S. M. and Engelhard, G. H.: A decline in primary production in the North Sea over 25 years, associated with reductions in zooplankton abundance and fish stock recruitment, Glob. Chang. Biol., 24(1), e352–e364, doi:10.1111/gcb.13916, 2018.

Cardenas, M. B., Cook, P. L. M., Jiang, H. and Traykovski, P.: Constraining denitrification in permeable wave-influenced marine sediment using linked hydrodynamic and biogeochemical modeling, Earth Planet. Sci. Lett., 275(1–2), 127–137, doi:10.1016/j.epsl.2008.08.016, 2008.

Cashion, T., Al-Abdulrazzak, D., Belhabib, D., Derrick, B., Divovich, E., Moutopoulos, D. K., Noël, S. L., Palomares, M. L. D., Teh, L. C. L., Zeller, D. and Pauly, D.: Reconstructing global marine fishing gear use: Catches and landed values by gear type and sector, Fish. Res., 206(October), 57–64, doi:10.1016/j.fishres.2018.04.010, 2018.

Cataño-Lopera, Y. A. and García, M. H.: Geometry and migration characteristics of bedforms under waves and currents. Part 2: Ripples superimposed on sandwaves, Coast. Eng., 53(9), 781–792, doi:10.1016/j.coastaleng.2006.03.008, 2006.

Cheng, C. H., Soetaert, K. and Borsje, B. W.: Sediment characteristics over asymmetrical tidal sand waves in the Dutch north sea, J. Mar. Sci. Eng., 8(6), 409, doi:10.3390/JMSE8060409, 2020.

Christensen, B., Vedel, A. and Kristensen, E.: Carbon and nitrogen fluxes in sediment inhabited by suspension-feeding (Nereis diversicolor) and non-suspension-feeding (N. virens) polychaetes, Mar. Ecol. Prog. Ser., 192, 203–217, doi:10.3354/meps192203, 2000.

Clavero, V., Niell, F. X. and Fernandez, J. A.: Effects of Nereis diversicolor O. F. Muller abundance on the dissolved phosphate exchange between sediment and overlying water in Palmones River estuary (southern Spain), Estuar. Coast. Shelf Sci., 33(2), 193–202, doi:10.1016/0272-7714(91)90006-W, 1991.

Cloern, J.: Does the Benthos Control Phytoplankton Biomass in South San Francisco Bay?, Mar. Ecol. Prog. Ser., 9, 191–202, doi:10.3354/meps009191, 1982.

Coates, D. A., Deschutter, Y., Vincx, M. and Vanaverbeke, J.: Enrichment and shifts in macrobenthic assemblages in an offshore wind farm area in the Belgian part of the North Sea wind farm area in the Belgian part of the North Sea, Mar. Environ. Res., (December), 1–12, doi:10.1016/j.marenvres.2013.12.008, 2013.

Coates, D. A., Deschutter, Y., Vincx, M. and Vanaverbeke, J.: Enrichment and shifts in macrobenthic assemblages in an offshore wind farm area in the Belgian part of the North Sea, Mar. Environ. Res., 95, 1–12, doi:10.1016/j.marenvres.2013.12.008, 2014.

Colman, A. S. and Holland, H. D.: The global diagenetic flux of phosphorus from marine sediments to the oceans: redox sensitivity and the control of atmospheric oxygen levels, in Marine Authigenesis: From Global to Microbial, pp. 53–75, SEPM (Society for Sedimentary Geology)., 2000.

Copernicus Marine Service Information, E. U.: Atlantic- European North West Shelf- Ocean Biogeochemistry Reanalysis, [online] Available from: http://marine.copernicus.eu/services-portfolio/access-to-products/?option=com_csw&view=details&product_id=NORTHWESTSHELF_REANALYSIS_BIO_004_011 (Accessed 4 April 2020), 2020.

Couceiro, F., Fones, G. R., Thompson, C. E. L., Statham, P. J., Sivyer, D. B., Parker, R., Kelly-Gerreyn, B. A. and Amos, C. L.: Impact of resuspension of cohesive sediments at the Oyster Grounds (North Sea) on nutrient exchange across the sediment-water interface, Biogeochemistry, 113(1–3), 37–52, doi:10.1007/s10533-012-9710-7, 2013.

Craeymeersch, J., P, Kingston, P., Rachor, E., Duineveld, G., Heip, C. and Vanden Berghe, E.: North Sea Benthos Survey., 1986.

D'Andrea, A. F. and DeWitt, T. H.: Geochemical ecosystem engineering by the mud shrimp Upogebia pugettensis (Crustacea: Thalassinidae) in Yaquina Bay, Oregon: Density-dependent effects on organic matter remineralization and nutrient cycling, Limnol. Oceanogr., 54(6), 1911–1932, doi:10.4319/lo.2009.54.6.1911, 2009.

Dauwe, B. and Middelburg, J. J.: Amino acids and hexosamines as indicators of organic matter degradation state in North Sea sediments, Limnol. Oceanogr., 43(5), 782–798, doi:10.4319/lo.1998.43.5.0782, 1998.

Dauwe, B., Herman, P. M. J. and Heip, C. H. R.: Community structure and bioturbation potential of macrofauna at four North Sea stations with contrasting food supply, Mar. Ecol. Prog. Ser., 173(November 1998), 67–83, doi:10.3354/meps173067, 1998.

Davis, M. and McIntire, C.: Effects of physical gradients on the production dynamics of sediment-associated algae, Mar. Ecol. Prog. Ser., 13, 103–114, doi:10.3354/meps013103, 1983.

Deek, A., Emeis, K. and van Beusekom, J.: Nitrogen removal in coastal sediments of the German Wadden Sea, Biogeochemistry, 108(1–3), 467–483, doi:10.1007/s10533-011-9611-1, 2012.

Degraer, S., Vincx, M., Meire, P. and Offringa, H.: The macrozoobenthos of an important wintering area of the common scoter (Melanitta nigra), J. Mar. Biol. Assoc. United Kingdom, 79(2), 243–251, doi:10.1017/S0025315498000277, 1999.

Degraer, S., Van Lancker, V., Moerkerke, G., Van Hoey, G., Vanstaen, K., Vincx, M. and Henriet, J.-P.: Evaluation of the ecological value of the foreshore: habitatmodel and macrobenthic side-scan sonar interpretation: extension along the Belgian Coastal Zone. Final report., 2003.

Degraer, S., Wittoeck, J., Appeltans, W., Cooreman, K., Deprez, T., Hillewaert, H., Hostens, K., Mees, J., Vanden Berghe, E. and Vincx, M.: Macrobel: Long term trends in the macrobenthos of the Belgian Continental Shelf. Oostende, Belgium., [online] Available from: http://www.vliz.be/vmdcdata/macrobel/, 2006.

Degraer, S., Verfaillie, E., Willems, W., Adriaens, E., Vincx, M. and Van Lancker, V.: Habitat suitability modelling as a mapping tool for macrobenthic communities: An example from the Belgian part of the North Sea, Cont. Shelf Res., 28(3), 369–379, doi:10.1016/j.csr.2007.09.001, 2008.

Degraer, S., Braeckman, U., Haelters, J., Hostens, K., Jacques, T., Kerckhof, F., Merckx, B., Rabaut, M., Stienen, E. W. M., Van Hoey, G., Van Lancker, V. and Vincx, M.: Studie betreffende het opstellen van een lijst van potentiële Habitatrichtlijngebieden in het Belgische deel van de Noordzee., Brussel, België., 2009.

Degrendele, K. and Vandenreyken, H.: Belgian marine sand : a scarce resource ?, in Study day, 9 June 2017, Hotel Andromeda, Ostend, edited by K. Degrendele and H. Vandenreyken, p. 164, FPS Economy, S.M.E.s, Self-employed and Energy, Brussels., 2017.

Depestele, J., Ivanović, A., Degrendele, K., Esmaeili, M., Polet, H., Roche, M., Summerbell, K., Teal, L. R., Vanelslander, B. and O'Neill, F. G.: Measuring and assessing the physical impact of beam trawling, ICES J. Mar. Sci., 73(suppl_1), i15–i26, doi:10.1093/icesjms/fsv056, 2016.

Depestele, J., Degrendele, K., Esmaeili, M., Ivanovic, A., Kröger, S., O'Neill, F. G., Parker, R., Polet, H., Roche, M., Teal, L. R., Vanelslander, B. and Rijnsdorp, A. D.: Comparison of mechanical disturbance in soft sediments due to tickler-chain SumWing trawl vs. Electro-fitted PulseWing trawl, ICES J. Mar. Sci., 76(1), 312–329, doi:10.1093/icesjms/fsy124, 2019.

Desmit, X., Nohe, A., Borges, A. V., Prins, T., De Cauwer, K., Lagring, R., Van der Zande, D. and Sabbe, K.: Changes in chlorophyll concentration and phenology in the North Sea in relation to de-eutrophication and sea surface warming, Limnol. Oceanogr., (2016), 1–20, doi:10.1002/lno.11351, 2019.

Díaz, S. and Cabido, M.: Vive la différence: Plant functional diversity matters to ecosystem processes, Trends Ecol. Evol., 16(11), 646–655, doi:10.1016/S0169-5347(01)02283-2, 2001.

Dickens, G. R., Koelling, M., Smith, D. C. and Schnieders, L.: Rhizon sampling of pore waters on scientific drilling expeditions: An example from the IODP expedition 302, Arctic Coring Expedition (ACEX), Sci. Drill., (4), 22–25, doi:10.2204/iodp.sd.4.08.2007, 2007.

Dornhoffer, T., Waldbusser, G. G. and Meile, C.: Burrow patchiness and oxygen fluxes in bioirrigated sediments, J. Exp. Mar. Bio. Ecol., 412, 81–86, doi:10.1016/j.jembe.2011.11.004, 2012.

Dornhoffer, T. M., Waldbusser, G. G. and Meile, C.: Modeling lugworm irrigation behavior effects on sediment nitrogen cycling, Mar. Ecol. Prog. Ser., 534, 121–134, doi:10.3354/meps11381, 2015.

Dounas, C. G., Davies, I. M., Hayes, P. J., Arvanitidis, C. D. and Koulouri, P. T.: The effect of different types of otter trawl ground rope on benthic nutrient releases and sediment biogeochemistry, Benthic Habitats Eff. Fish., 41(January), 539–544, 2005.

Dray, S. and Dufour, A.-B.: The ade4 Package: Implementing the Duality Diagram for Ecologists, J. Stat. Softw., 22(4), 1–20, doi:10.18637/jss.v022.i04, 2007.

Dray, S., Chessel, D. and Thioulouse, J.: Co-inertia analysis and the linking of ecological data tables, Ecology, 84(11), 3078–3089, doi:10.1890/03-0178, 2003.

Duarte, C. M., Pitt, K. A., Lucas, C. H., Purcell, J. E., Uye, S., Robinson, K., Brotz, L., Decker, M. B., Sutherland, K. R., Malej, A., Madin, L., Mianzan, H., Gili, J.-M., Fuentes, V., Atienza, D., Pagés, F., Breitburg, D., Malek, J., Graham, W. M. and Condon, R. H.: Is global ocean sprawl a cause of jellyfish blooms?, Front. Ecol. Environ., 11(2), 91–97, doi:10.1890/110246, 2013.

Dufrêne, M. and Legendre, P.: Species assemblages and indicator species: The need for a flexible asymmetrical approach, Ecol. Monogr., 67(3), 345–366, doi:10.2307/2963459, 1997.

Duncan, C., Thompson, J. R. and Pettorelli, N.: The quest for a mechanistic understanding of biodiversity–Ecosystem services relationships, Proc. R. Soc. B Biol. Sci., 282(1817), doi:10.1098/rspb.2015.1348, 2015.

Duplisea, D. E., Jennings, S., Malcolm, S. J., Parker, R. and Sivyer, D. B.: Modelling potential impacts of bottom trawl fisheries on soft sediment biogeochemistry in the North Sea, Geochem. Trans., 2, 112–117, doi:10.1039/b108342b, 2001.

Van Duyl, F. C., Van Raaphorst, W. and Kop, A. J.: Benthic bacterial production and nutrient sediment-water

exchange in sandy North Sea sediments, Mar. Ecol. Prog. Ser., 100(1–2), 85–95, doi:10.3354/meps100085, 1993.

E.U. Copernicus Marine Service Information: Atlantic Iberian Biscay Irish Ocean biogeochamical analysis and forecast, [online] Available from: https://resources.marine.copernicus.eu/?option=com_csw&task=results?option=com_csw&view=details&produ ct_id=IBI_ANALYSIS_FORECAST_BIO_005_004 (Accessed 17 August 2020), 2020.

EC: Assessment of plans and projects significantly affecting Natura 2000 sites: Methodological guidance on the provisions of Article 6(3) and (4) of the Habitats Directive 92/43/EEC. [online] Available from: http://europa.eu.int/comm/environment/pubs/home.htm, 2001.

Eggleston, J. and Rojstaczer, S.: Inferring spatial correlation of hydraulic conductivity from sediment cores and outcrops, Geophys. Res. Lett., 25(13), 2321–2324, doi:10.1029/98GL01773, 1998.

Ehrenhauss, S., Witte, U., Janssen, F. and Huettel, M.: Decomposition of diatoms and nutrient dynamics in permeable North Sea sediments, Cont. Shelf Res., 24(6), 721–737, doi:10.1016/j.csr.2004.01.002, 2004a.

Ehrenhauss, S., Witte, U., Janssen, F. and Huettel, M.: Decomposition of diatoms and nutrient dynamics in permeable North Sea sediments, Cont. Shelf Res., 24, 721–737, doi:10.1016/j.csr.2004.01.002, 2004b.

Ehrhold, A., Blanchard, M., Auffret, J.-P. and Garlan, T.: Conséquences de la prolifération de la crépidule (Crepidula fornicata) sur l'évolution sédimentaire de la baie du Mont-Saint-Michel (Manche, France), Comptes Rendus l'Académie des Sci. - Ser. IIA - Earth Planet. Sci., 327(9), 583–588, doi:https://doi.org/10.1016/S1251-8050(99)80111-6, 1998.

Eiane, K. and Ohman, M. D.: Stage-specific mortality of Calanus finmarchicus, Pseudocalanus elongatus and Oithona similis on Fladen Ground, North Sea, during a spring bloom, Mar. Ecol. Prog. Ser., 268(Flex 1976), 183–193, doi:10.3354/meps268183, 2004.

Eigaard, O. R., Bastardie, F., Hintzen, N. T., Buhl-Mortensen, L., Buhl-Mortensen, P., Catarino, R., Dinesen, G. E., Egekvist, J., Fock, H. O., Geitner, K., Gerritsen, H. D., González, M. M., Jonsson, P., Kavadas, S., Laffargue, P., Lundy, M., Gonzalez-Mirelis, G., Nielsen, J. R., Papadopoulou, N., Posen, P. E., Pulcinella, J., Russo, T., Sala, A., Silva, C., Smith, C. J., Vanelslander, B. and Rijnsdorp, A. D.: The footprint of bottom trawling in European waters: Distribution, intensity, and seabed integrity, ICES J. Mar. Sci., 74(3), 847–865, doi:10.1093/icesjms/fsw194, 2017.

Eisma, D. and Kalf, J.: Dispersal, concentration and deposition of suspended matter in the North Sea., J. - Geol. Soc., 144(1), 161–178, doi:10.1144/gsjgs.144.1.0161, 1987.

Elliott, M., Nedwell, S., Jones, N. V., Read, S. J., Cutts, N. D. and Hemingway, K. L.: Intertidal Sand and Mudflats & Subtidal Mobile Sandbanks (Volume II). An overview of dynamic and sensitivity characteristics for conservation management of marine SAC's., Scottish Assoc. Mar. Sci. (UK Mar. SACs Proj., II(August), 151 [online] Available from: http://scholar.google.com/scholar?hl=en&btnG=Search&q=intitle:INTERTIDAL+SAND+AND+MUDFLATS+ &+SUBTIDAL+MOBILE+SANDBANKS+An+overview+of+dynamic+and+sensitivity+characteristics+for+cons ervation+management+of+marine+SACs#1, 1998.

Emeis, K. C., van Beusekom, J., Callies, U., Ebinghaus, R., Kannen, A., Kraus, G., Kröncke, I., Lenhart, H., Lorkowski, I., Matthias, V., Möllmann, C., Pätsch, J., Scharfe, M., Thomas, H., Weisse, R. and Zorita, E.: The North Sea - A shelf sea in the Anthropocene, J. Mar. Syst., 141, 18–33, doi:10.1016/j.jmarsys.2014.03.012, 2015.

Escofier, B. and Pagès, J.: Multiple factor analysis (AFMULT package), Comput. Stat. Data Anal., 18(1), 121–140, doi:10.1016/0167-9473(94)90135-X, 1994.

Essink, K.: Ecological effects of dumping of dredged sediments; options for management, J. Coast. Conserv., 5(1), 69–80, doi:10.1007/BF02802741, 1999.

Etter, R. J. and Bower, A. S.: Dispersal and population connectivity in the deep North Atlantic estimated from physical transport processes, Deep. Res. Part I Oceanogr. Res. Pap., 104, 159–172, doi:10.1016/j.dsr.2015.06.009, 2015.

European Commission: An EU Strategy to harness the potential of offshore renewable energy for a climate neutral future, Brussels., 2020a.

European Commission: European Climate Law, COM(2020) 80 Final, 0036, 25, doi:10.1017/CBO9781107415324.004, 2020b.

European Commission: The Blue Economy Report. 2020, Publications office of the European Union, Luxembourg., 2020c.

European MSP platform: Projects, [online] Available from: https://www.msp-platform.eu/msp-practice/msp-projects (Accessed 20 August 2020), 2020.

Fan, H., Bolhuis, H. and Stal, L. J.: Drivers of the dynamics of diazotrophs and denitrifiers in North Sea bottom waters and sediments, Front. Microbiol., 6(JUL), 738, doi:10.3389/fmicb.2015.00738, 2015.

Ferguson, A. J. P., Oakes, J. and Eyre, B. D.: Bottom trawling reduces benthic denitrification and has the potential to influence the global nitrogen cycle, Limnol. Oceanogr. Lett., doi:10.1002/lol2.10150, 2020.

Fettweis, M., Houziaux, J. S., Du Four, I., Van Lancker, V., Baeteman, C., Mathys, M., Van den Eynde, D., Francken, F. and Wartel, S.: Long-term influence of maritime access works on the distribution of cohesive sediments: Analysis of historical and recent data from the Belgian nearshore area (southern North Sea), Geo-Marine Lett., 29(5), 321–330, doi:10.1007/s00367-009-0161-7, 2009.

Fettweis, M., Francken, F., Van den Eynde, D., Verwaest, T., Janssens, J. and Van Lancker, V.: Storm influence on SPM concentrations in a coastal turbidity maximum area with high anthropogenic impact (southern North Sea), Cont. Shelf Res., 30(13), 1417–1427, doi:10.1016/j.csr.2010.05.001, 2010.

Fettweis, M., Baeye, M., Francken, F., Lauwaert, B., Van den Eynde, D., Van Lancker, V., Martens, C. and Michielsen, T.: Monitoring the effects of disposal of fine sediments from maintenance dredging on suspended particulate matter concentration in the Belgian nearshore area (southern North Sea), Mar. Pollut. Bull., 62(2), 258–269, doi:10.1016/j.marpolbul.2010.11.002, 2011.

Fick, A.: Ueber Diffusion, Ann. der Phys. und Chemie, 170(1), 59–86, doi:10.1002/andp.18551700105, 1855.

Flanders Marine Institute: Soil, [online] Available from: http://www.vliz.be/en/soilspecial (Accessed 18 June 2020), 2020.

Floeter, J., van Beusekom, J. E. E., Auch, D., Callies, U., Carpenter, J., Dudeck, T., Eberle, S., Eckhardt, A., Gloe, D., Hänselmann, K., Hufnagl, M., Janßen, S., Lenhart, H., Möller, K. O., North, R. P., Pohlmann, T., Riethmüller, R., Schulz, S., Spreizenbarth, S., Temming, A., Walter, B., Zielinski, O. and Möllmann, C.: Pelagic effects of offshore wind farm foundations in the stratified North Sea, Prog. Oceanogr., 156, 154–173, doi:10.1016/j.pocean.2017.07.003, 2017.

Forster, R. M.: The effect of monopile-induced turbulence on local suspended sediment pattern around UK wind farms The effect of monopile-induced turbulence on local suspended sediment pattern around UK wind farms: field survey report., 2018.

Forster, S. and Graf, G.: Impact of irrigation on oxygen flux into the sediment: intermittent pumping by Callianassa subterranea and ?piston-pumping? by Lanice conchilega, Mar. Biol., 123(2), 335–346, doi:10.1007/BF00353625, 1995.

Forster, S., Glud, R. N., Gundersen, J. K. and Huettel, M.: In situ Study of Bromide Tracer and Oxygen Flux in Coastal Sediments, Estuar. Coast. Shelf Sci., 49(6), 813–827, doi:10.1006/ecss.1999.0557, 1999.

Forster, S., Bobertz, B. and Bohling, B.: Permeability of sands in the coastal areas of the southern Baltic Sea: Mapping a grain-size related sediment property, Aquat. Geochemistry, 9(3), 171–190, doi:10.1023/B:AQUA.0000022953.52275.8b, 2003a.

Forster, S., Khalili, A. and Kitlar, J.: Variation of nonlocal irrigation in a subtidal benthic community, J. Mar. Res., 61(3), 335–357, doi:10.1357/002224003322201223, 2003b.

Fowler, A. M., Jørgensen, A.-M., Coolen, J. W. P., Jones, D. O. B., Svendsen, J. C., Brabant, R., Rumes, B. and Degraer, S.: The ecology of infrastructure decommissioning in the North Sea: what we need to know and how to achieve it, edited by M. Kaiser, ICES J. Mar. Sci., 77(3), 1109–1126, doi:10.1093/icesjms/fsz143, 2020.

Franco, M. de A., Vanaverbeke, J., Van Oevelen, D., Soetaert, K., Costa, M. J., Vincx, M. and Moens, T.: Respiration partitioning in contrasting subtidal sediments: seasonality and response to a spring phytoplankton deposition, Mar. Ecol., 31(2), 276–290, doi:10.1111/j.1439-0485.2009.00319.x, 2010.

François, F., Poggiale, J.-C., Durbec, J.-P. and Stora, G.: A new approach for the modelling of sediment reworking induced by a macrobenthic community, Acta Biotheor., 45(3–4), 295–319, doi:10.1023/A:1000636109604, 1997.

Frid, C. L. J., Buchanan, J. B. and Garwood, P. R.: Variability and stability in benthos: Twenty-two years of monitoring off Northumberland, ICES J. Mar. Sci., 53(6), 978–980, doi:10.1006/jmsc.1996.0121, 1996.

Froelich, P. N., Klinkhammer, G. P., Bender, M. L., Luedtke, N. A., Heath, G. R., Cullen, D., Dauphin, P., Hammond, D., Hartman, B. and Maynard, V.: Early oxidation of organic matter in pelagic sediments of the eastern equatorial Atlantic: suboxic diagenesis, Geochim. Cosmochim. Acta, 43(7), 1075–1090, doi:10.1016/0016-7037(79)90095-4, 1979.

Furukawa, Y., Bentley, S. J. and Lavoie, D. L.: Bioirrigation modeling in experimental benthic mesocosms, J. Mar. Res., 59, 417–452, doi:10.1357/002224001762842262, 2001.

Galéron, J., Sibuet, M., Mahaut, M. L. and Dinet, A.: Variation in structure and biomass of the benthic communities at three contrasting sites in the tropical Northeast Atlantic, Mar. Ecol. Prog. Ser., 197, 121–137, doi:10.3354/meps197121, 2000.

Galloway, J. N., Dentener, F. J., Capone, D. G., Boyer, E. W., Howarth, R. W., Seitzinger, S. P., Asner, G. P., Cleveland, C. C., Green, P. A., Holland, E. A., Karl, D. M., Michaels, A. F., Porter, J. H., Townsend, A. R. and Vorosmarty, C. J.: Nitrogen Cycles: Past, Present, and Future, Biogeochemistry, 70(2), 153–226, doi:10.1007/s10533-004-0370-0, 2004.

Gao, H., Schreiber, F., Collins, G., Jensen, M. M., Kostka, J. E., Lavik, G., De Beer, D., Zhou, H. Y. and Kuypers, M. M. M.: Aerobic denitrification in permeable Wadden Sea sediments, ISME J., 4(3), 417–426, doi:10.1038/ismej.2009.127, 2010.

Gao, Y., Lesven, L., Gillan, D., Sabbe, K., Billon, G., De Galan, S., Elskens, M., Baeyens, W. and Leermakers, M.: Geochemical behavior of trace elements in sub-tidal marine sediments of the Belgian coast, Mar. Chem., 117(1–4), 88–96, doi:10.1016/j.marchem.2009.05.002, 2009.

Gaston, G. R., Bartlett, J. H. W., Mcallister, A. P. and Heard, R. W.: Biomass variations of estuarine macrobenthos preserved in ethanol and formalin, Estuaries, 19(3), 674–679, doi:10.2307/1352527, 1996.

GEBCO Compilation Group: GEBCO 2020 Grid, , doi:10.5285/a29c5465-b138-234d-e053-6c86abc040b9, 2020.

Gehlen, M., Malschaert, H. and Van Raaphorst, W. R.: Spatial and temporal variability of benthic silica fluxes in the southeastern North Sea, Cont. Shelf Res., 15(13), 1675–1696, doi:10.1016/0278-4343(95)00012-P, 1995.

Gerke, K. M., Sidle, R. C. and Mallants, D.: Criteria for selecting fluorescent dye tracers for soil hydrological applications using Uranine as an example, J. Hydrol. Hydromechanics, 61(4), 313–325, doi:10.2478/johh-2013-0040, 2013.

Gieskes, W. W. C. and Kraay, G. W.: Phytoplankton, its pigments, and primary production at a central north sea station in May, July and September 1981, Netherlands J. Sea Res., 18(1–2), 51–70, doi:10.1016/0077-7579(84)90024-3, 1984.

Gilbert, A. J., McQuatters-Gollop, A., Langmead, O., Mee, L. and Vermaat, J.: Visions for the North Sea: The Societal Dilemma Behind Specifying Good Environmental Status, Ambio, 44(2), 142–153, doi:10.1007/s13280-014-0536-5, 2014.

Glud, R., Forster, S. and Huettel, M.: Influence of radial pressure gradients on solute exchange in stirred benthic

chambers, Mar. Ecol. Prog. Ser., 141, 303–311, doi:10.3354/meps141303, 1996.

Glud, R. N.: Oxygen dynamics of marine sediments, Mar. Biol. Res., 4(4), 243–289, doi:Doi 10.1080/17451000801888726, 2008.

Godbold, J. A. and Solan, M.: Relative importance of biodiversity and the abiotic environment in mediating an ecosystem process, Mar. Ecol. Prog. Ser., 396, 273–282, doi:10.3354/meps08401, 2009a.

Godbold, J. A. and Solan, M.: Relative importance of biodiversity and the environment in mediating ecosystem process, Mar. Ecol. Prog. Ser., (December), doi:10.3354/meps08401, 2009b.

Gogina, M., Morys, C., Forster, S., Gräwe, U., Friedland, R. and Zettler, M. L.: Towards benthic ecosystem functioning maps: Quantifying bioturbation potential in the German part of the Baltic Sea, Ecol. Indic., 73, 574–588, doi:10.1016/j.ecolind.2016.10.025, 2017.

Gogina, M., Lipka, M., Woelfel, J., Liu, B., Morys, C., Böttcher, M. E. and Zettler, M. L.: In search of a field-based relationship between benthic macrofauna and biogeochemistry in a modern brackish coastal sea, Front. Mar. Sci., 5(DEC), 1–18, doi:10.3389/fmars.2018.00489, 2018.

Green, M. O., Vincent, C. ., McCave, I. N., Dickson, R. R., Rees, J. M. and Pearsons, N. D.: Storm sediment transport: observations from the British North Sea shelf, Cont. Shelf Res., 15(8), 889–912, doi:10.1016/0278-4343(95)80001-T, 1995.

Greenwood, N., Parker, E. R., Fernand, L., Sivyer, D. B., Weston, K., Painting, S. J., Kröger, S., Forster, R. M., Lees, H. E., Mills, D. K. and Laane, R. W. P. M.: Detection of low bottom water oxygen concentrations in the North Sea; Implications for monitoring and assessment of ecosystem health, Biogeosciences, 7(4), 1357–1373, doi:10.5194/bg-7-1357-2010, 2010.

Griffiths, J. R., Kadin, M., Nascimento, F. J. A., Tamelander, T., Törnroos, A., Bonaglia, S., Bonsdorff, E., Brüchert, V., Gårdmark, A., Järnström, M., Kotta, J., Lindegren, M., Nordström, M. C., Norkko, A., Olsson, J., Weigel, B., Žydelis, R., Blenckner, T., Niiranen, S. and Winder, M.: The importance of benthic–pelagic coupling for marine ecosystem functioning in a changing world, Glob. Chang. Biol., 23(6), 2179–2196, doi:10.1111/gcb.13642, 2017.

Groot, S. J. De: The impact of bottom trawling on benthic fauna of the North Sea, Ocean Manag., 9(3–4), 177–190 [online] Available from: http://linkinghub.elsevier.com/retrieve/pii/0302184X84900027, 1984.

Gust, G. and Harrison, J. T.: Biological pumps at the sediment-water interface: Mechanistic evaluation of the alpheid shrimp Alpheus mackayi and its irrigation pattern, Mar. Biol., 64(1), 71–78, doi:10.1007/BF00394082, 1981.

De Haas, H., Boer, W. and Van Weering, T. C. E.: Recent sedimentation and organic carbon burial in a shelf sea: The North Sea, Mar. Geol., 144(1–3), 131–146, doi:10.1016/S0025-3227(97)00082-0, 1997.

Hale, R., Mavrogordato, M. N., Tolhurst, T. J. and Solan, M.: Characterizations of how species mediate ecosystem properties require more comprehensive functional effect descriptors, Sci. Rep., 4, 6463, doi:10.1038/srep06463, 2014.

Van Haren, H., Howarth, M. J., Jones, K. and Ezzi, I.: Autumnal reduction of stratification in the northern North Sea and its impact, Cont. Shelf Res., 23(2), 177–191, doi:10.1016/S0278-4343(02)00171-1, 2003.

Harrison, J. A., Bouwman, A. F., Mayorga, E. and Seitzinger, S.: Magnitudes and sources of dissolved inorganic phosphorus inputs to surface fresh waters and the coastal zone: A new global model, Global Biogeochem. Cycles, 24(1), n/a-n/a, doi:10.1029/2009GB003590, 2010.

HDR: Benthic and Epifaunal Monitoring During Wind Turbine Installation and Operation at the Block Island Wind Farm, Rhode Island. Project Report (Draft). Final Report to the U.S. Department of the Interior, Bureau of Ocean Energy Management, Office of Renewabl., 2020.

Hedman, J. E., Gunnarsson, J. S., Samuelsson, G. and Gilbert, F.: Particle reworking and solute transport by the sediment-living polychaetes Marenzelleria neglecta and Hediste diversicolor, J. Exp. Mar. Bio. Ecol., 407(2), 294–

301, doi:10.1016/j.jembe.2011.06.026, 2011.

Heip, C., Basford, D., Craeymeersch, J. A., Dewarumez, J. M., Dorjes, J., De Wilde, P., Duineveld, G., Eleftheriou, A., Herman, P. M. J., Niermann, U., Kingston, P., Kiinitzer, A., Rachor, E., Rumohr, H., Soetaert, K. and Soltwede, T.: Trends in biomass, density and diversity of north sea macrofauna, ICES J. Mar. Sci., 49(1), 13–22, doi:10.1093/icesjms/49.1.13, 1992.

Heip, C. H. R., Goosen, N. K., Herman, P. M. J., Kromkamp, J., Middelburg, J. J. and Soetaert, K.: Production and consumption of biological particles in temperate tidal estuaries, Oceanogr. Mar. Biol., 33, 1–149, 1995.

Hellemann, D., Tallberg, P., Aalto, S., Bartoli, M. and Hietanen, S.: Seasonal cycle of benthic denitrification and DNRA in the aphotic coastal zone, northern Baltic Sea, Mar. Ecol. Prog. Ser., 637, 15–28, doi:10.3354/meps13259, 2020.

Heo, M. and Gabriel, K. R.: A permutation test of association between configurations by means of the RV coefficient, Commun. Stat. Part B Simul. Comput., 27(3), 843–856, doi:10.1080/03610919808813512, 1998.

Hevia, V., Martín-López, B., Palomo, S., García-Llorente, M., de Bello, F. and González, J. A.: Trait-based approaches to analyze links between the drivers of change and ecosystem services: Synthesizing existing evidence and future challenges, Ecol. Evol., 7(3), 831–844, doi:10.1002/ece3.2692, 2017.

Hiddink, J. G., Jennings, S., Sciberras, M., Szostek, C. L., Hughes, K. M., Ellis, N., Rijnsdorp, A. D., McConnaughey, R. A., Mazor, T., Hilborn, R., Collie, J. S., Pitcher, C. R., Amoroso, R. O., Parma, A. M., Suuronen, P. and Kaiser, M. J.: Global analysis of depletion and recovery of seabed biota after bottom trawling disturbance, Proc. Natl. Acad. Sci. U. S. A., 114(31), 8301–8306, doi:10.1073/pnas.1618858114, 2017.

Hiddink, J. G., Jennings, S., Sciberras, M., Bolam, S. G., Cambiè, G., McConnaughey, R. A., Mazor, T., Hilborn, R., Collie, J. S., Pitcher, C. R., Parma, A. M., Suuronen, P., Kaiser, M. J. and Rijnsdorp, A. D.: Assessing bottom trawling impacts based on the longevity of benthic invertebrates, J. Appl. Ecol., 56(5), 1075–1084, doi:10.1111/1365-2664.13278, 2019.

Hillman, J. R., Stephenson, F., Thrush, S. F. and Lundquist, C. J.: Investigating changes in estuarine ecosystem functioning under future scenarios, Ecol. Appl., 30(4), 1–12, doi:10.1002/eap.2090, 2020.

Van Hoey, G., Degraer, S. and Vincx, M.: Macrobenthic community structure of soft-bottom sediments at the Belgian Continental Shelf, Estuar. Coast. Shelf Sci., 59(4), 599–613, doi:10.1016/j.ecss.2003.11.005, 2004.

Holland, K. T. and Elmore, P. A.: A review of heterogeneous sediments in coastal environments, Earth-Science Rev., 89(3–4), 116–134, doi:10.1016/j.earscirev.2008.03.003, 2008.

Holt, J., Butenschön, M., Wakelin, S. L., Artioli, Y. and Allen, J. I.: Oceanic controls on the primary production of the northwest European continental shelf: model experiments under recent past conditions and a potential future scenario, Biogeosciences, 9(1), 97–117, doi:10.5194/bg-9-97-2012, 2012.

Holt, J., Schrum, C., Cannaby, H., Daewel, U., Allen, I., Artioli, Y., Bopp, L., Butenschon, M., Fach, B. A., Harle, J., Pushpadas, D., Salihoglu, B. and Wakelin, S.: Potential impacts of climate change on the primary production of regional seas: A comparative analysis of five European seas, Prog. Oceanogr., 140, 91–115, doi:10.1016/j.pocean.2015.11.004, 2016.

Holt, T. J. ., Rees, E. I., Hawkins, S. J. and Seed, R.: Vol. IX. Biogenic reefs 1, Science (80-.)., IX(August), 1–169, doi:10.1080/09538250903090424, 1998.

Holtmann, S. E., Groenewold, A., Schrader, K. H. M., Asjes, J., Craeymeersch, J. A., Duineveld, G. C. A., van Bostelen, A. J. and van der Meer, J.: Atlas of the zoobenthos of the Dutch continental shelf, Ministry of Transport, Public Works and Water Management, Rijswijk. [online] Available from: http://www.marinespecies.org/aphia.php?p=taxdetails&id=130644, 1996.

Huettel, M.: Influence of the lugworm Arenicola marina on porewater nutrient profiles of sand flat sediments, Mar. Ecol. Prog. Ser., 62, 241–248, doi:10.3354/meps062241, 1990.

Huettel, M. and Gust, G.: Impact of bioroughness on interfacial solute exchange in permeable sediments, Mar. Ecol. Prog. Ser., 89(2–3), 253–267, doi:10.3354/meps089253, 1992.

Huettel, M. and Rusch, A.: Transport and degradation of phytoplankton in permeable sediment, Limnol. Oceanogr., 45(3), 534–549, doi:10.4319/lo.2000.45.3.0534, 2000.

Huettel, M., Røy, H., Precht, E. and Ehrenhauss, S.: Hydrodynamical impact on biogeochemical processes in aquatic sediments, in The Interactions between Sediments and Water, pp. 231–236, Springer Netherlands, Dordrecht., 2003a.

Huettel, M., Røy, H., Precht, E. and Ehrenhauss, S.: Hydrodynamical impact on biogeochemical processes in aquatic sediments, in The Interactions between Sediments and Water, vol. 494, pp. 231–236, Springer Netherlands, Dordrecht., 2003b.

Huettel, M., Berg, P. and Kostka, J. E.: Benthic exchange and biogeochemical cycling in permeable sediments., Ann. Rev. Mar. Sci., 6, 23–51, doi:10.1146/annurev-marine-051413-012706, 2014.

ICES: Working Group on Electrical Trawling (WGELECTRA), ICES Sci. Reports / Rapp. Sci. du Ciem, 1(71), 87, doi:10.17895/ices.pub.5619, 2020.

Ingall, E. and Jahnke, R.: Evidence for enhanced phosphorus regeneration from marine sediments overlain by oxygen depleted waters, Geochim. Cosmochim. Acta, 58(11), 2571–2575, doi:10.1016/0016-7037(94)90033-7, 1994.

Inger, R., Attrill, M. J., Bearhop, S., Broderick, A. C., James Grecian, W., Hodgson, D. J., Mills, C., Sheehan, E., Votier, S. C., Witt, M. J. and Godley, B. J.: Marine renewable energy: Potential benefits to biodiversity? An urgent call for research, J. Appl. Ecol., 46(6), 1145–1153, doi:10.1111/j.1365-2664.2009.01697.x, 2009.

Ivanov, E., Capet, A., Barth, A., Delhez, E. J. M., Soetaert, K. and Grégoire, M.: Hydrodynamic variability in the Southern Bight of the North Sea in response to typical atmospheric and tidal regimes. Benefit of using a high resolution model, Ocean Model., 154, 101682, doi:10.1016/j.ocemod.2020.101682, 2020.

Jansen, H. M., Strand, Ø., Verdegem, M. and Smaal, A.: Accumulation, release and turnover of nutrients (C-N-P-Si) by the blue mussel Mytilus edulis under oligotrophic conditions, J. Exp. Mar. Bio. Ecol., 416–417, 185–195, doi:10.1016/j.jembe.2011.11.009, 2012.

Jodo, M., Kawamoto, K., Tochimoto, M. and Coverly, S. C.: Determination of nutrients in seawater by segmented-flow analysis with higher analysis rate and reduced interference on ammonia, J. Automat. Chem., 14(5), 163–167, doi:10.1155/S1463924692000300, 1992.

Joint, I. and Pomroy, A.: Phytoplankton biomass and production in the southern North Sea, Mar. Ecol. Prog. Ser., 99(1–2), 169–182, doi:10.3354/meps099169, 1993.

Jørgensen, B. B.: Mineralization of organic matter in the sea bed—the role of sulphate reduction, Nature, 296(5858), 643–645, doi:10.1038/296643a0, 1982.

Jørgensen, B. B.: Bacteria and Marine Biogeochemistry, in Marine Geochemistry, edited by H. D. Schulz and M. Zabel, pp. 173–207, Springer Berlin Heidelberg, Berlin, Heidelberg., 2000.

Joschko, T. J., Buck, B. H., Gutow, L. and Schröder, A.: Colonization of an artificial hard substrate by Mytilus edulis in the German Bight, Mar. Biol. Res., 4(5), 350–360, doi:10.1080/17451000801947043, 2008.

Jouffray, J.-B., Blasiak, R., Norström, A. V., Österblom, H. and Nyström, M.: The Blue Acceleration: The Trajectory of Human Expansion into the Ocean, One Earth, 2(1), 43–54, doi:10.1016/j.oneear.2019.12.016, 2020.

Kaiser, M. J., Clarke, K. R., Hinz, H., Austen, M. C. V., Somerfield, P. J. and Karakassis, I.: Global analysis of response and recovery of benthic biota to fishing, Mar. Ecol. Prog. Ser., 311(May 2014), 1–14, doi:10.3354/meps311001, 2006.

Kalantzi, I. and Karakassis, I.: Benthic impacts of fish farming: Meta-analysis of community and geochemical data, Mar. Pollut. Bull., 52(5), 484–493, doi:10.1016/j.marpolbul.2005.09.034, 2006.

Kamp, A., De Beer, D., Nitsch, J. L., Lavik, G. and Stief, P.: Diatoms respire nitrate to survive dark and anoxic conditions, Proc. Natl. Acad. Sci. U. S. A., 108(14), 5649–5654, doi:10.1073/pnas.1015744108, 2011.

Kamp, A., Høgslund, S., Risgaard-Petersen, N. and Stief, P.: Nitrate Storage and Dissimilatory Nitrate Reduction by Eukaryotic Microbes, Front. Microbiol., 6, doi:10.3389/fmicb.2015.01492, 2015.

Kikuchi, E.: Effects of the brackish deposit-feeding polychaetes Notomastus sp. (Capitellidae) and Neanthes japonica (Izuka) (Nereidae) on sedimentary O_2 consumption and CO_2 production rates, J. Exp. Mar. Bio. Ecol., 114(1), 15–25, doi:10.1016/0022-0981(87)90136-5, 1987.

Kirchner, G.: 210Pb as a tool for establishing sediment chronologies: Examples of potentials and limitations of conventional dating models, J. Environ. Radioact., 102(5), 490–494, doi:10.1016/j.jenvrad.2010.11.010, 2011.

Klump, J. V. and Martens, C. S.: The seasonality of nutrient regeneration in an organic-rich coastal sediment: Kinetic modeling of changing pore-water nutrient and sulfate distributions, Limnol. Oceanogr., 34(3), 559–577, doi:10.4319/lo.1989.34.3.0559, 1989.

Koo, B. J., Kwon, K. K. and Hyun, J. H.: Effect of environmental conditions on variation in the sediment-water interface created by complex macrofaunal burrows on a tidal flat, J. Sea Res., 58(4), 302–312, doi:10.1016/j.seares.2007.07.002, 2007.

Kristensen, E.: Impact of polychaetes (Nereis spp. and Arenicola marina) on carbon biogeochemistry in coastal marine sediments, Geochem. Trans., 2, 92–103, doi:10.1039/b108114d, 2001.

Kristensen, E. and Kostka, J. E.: Macrofaunal Burrows and Irrigation in Marine Sediment: Microbiological and Biogeochemical Interactions, Interact. Between Macro- Microorg. Mar. Sediments, (January), 125–157, doi:10.1029/CE060p0125, 2013.

Kristensen, E., Penha-Lopes, G., Delefosse, M., Valdemarsen, T., Quintana, C. and Banta, G.: What is bioturbation? The need for a precise definition for fauna in aquatic sciences, Mar. Ecol. Prog. Ser., 446, 285–302, doi:10.3354/meps09506, 2012.

Kröncke, I.: Changes in Dogger Bank macrofauna communities in the 20th century caused by fishing and climate, Estuar. Coast. Shelf Sci., 94(3), 234–245, doi:10.1016/j.ecss.2011.06.015, 2011.

Kröncke, I., Reiss, H., Eggleton, J. D., Aldridge, J., Bergman, M. J. N., Cochrane, S., Craeymeersch, J. A., Degraer, S., Desroy, N., Dewarumez, J. M., Duineveld, G. C. A., Essink, K., Hillewaert, H., Lavaleye, M. S. S., Moll, A., Nehring, S., Newell, R., Oug, E., Pohlmann, T., Rachor, E., Robertson, M., Rumohr, H., Schratzberger, M., Smith, R., Berghe, E. Vanden, van Dalfsen, J., van Hoey, G., Vincx, M., Willems, W. and Rees, H. L.: Changes in North Sea macrofauna communities and species distribution between 1986 and 2000, Estuar. Coast. Shelf Sci., 94(1), 1–15, doi:10.1016/j.ecss.2011.04.008, 2011.

Krone, R., Gutow, L., Joschko, T. J. and Schröder, A.: Epifauna dynamics at an offshore foundation - Implications of future wind power farming in the North Sea, Mar. Environ. Res., 85, 1–12, doi:10.1016/j.marenvres.2012.12.004, 2013.

Kruse, M., Lindaas, J. C., Olivares, A., Korporaal, H., Keijzer, D. de, Ring, H., Kotzur, S., Bentin, M., Askari, H., Rasmussen, M., Skyt, P., Larsen, J., Bie, J. K., Stubbe, W., Motmans, S., de Pauw, B., Sunner, I., Kallio, N., Maheri, A., Ivanovic, A., Klinge, I., Stensgaard, S. and Carstensen, H.: Market analysis Decom Tools 2019., 2019.

Langhamer, O.: Artificial reef effect in relation to offshore renewable energy conversion: State of the art, Sci. World J., 2012, doi:10.1100/2012/386713, 2012.

LaRowe, D. E., Arndt, S., Bradley, J. A., Estes, E. R., Hoarfrost, A., Lang, S. Q., Lloyd, K. G., Mahmoudi, N., Orsi, W. D., Shah Walter, S. R., Steen, A. D. and Zhao, R.: The fate of organic carbon in marine sediments - New insights from recent data and analysis, Earth-Science Rev., 204(August 2019), 103146, doi:10.1016/j.earscirev.2020.103146, 2020.

Lavorel, S. and Garnier, E.: Predicting changes in community composition and ecosystem functioning from plant traits: revisiting the Holy Grail, Funct. Ecol., 16, 545–556, 2002.

Laxton, J. L.: A particle-size classification of sand and gravel deposits as a basis for end-use assessment, Eng. Geol., 32(1–2), 29–37, doi:10.1016/0013-7952(92)90015-Q, 1992.

van Leeuwen, S. M., van der Molen, J., Ruardij, P., Fernand, L. and Jickells, T.: Modelling the contribution of deep chlorophyll maxima to annual primary production in the North Sea, Biogeochemistry, 113(1–3), 137–152, doi:10.1007/s10533-012-9704-5, 2013.

van Leeuwen, S. M., Tett, P., Mills, D. K. and van der Molen, J.: Stratified and nonstratified areas in the North Sea: Long-term variability and biological and policy implications, J. Geophys. Res. Ocean., 2121–2128, doi:10.1002/jgrc.20224, 2015.

Leewis, L., Klink, A. D. and Verduin, E. C.: Benthic development in and around offshore wind farm Prinses Amalia Wind Park near the Dutch coastal zone before and after construction (2003-2017), Amsterdam., 2018.

Lefaible, N., Braeckman, U. and Moens, T.: Effects of wind turbine foundations on surrounding macrobenthic communities, in Environmental Impacts of Offshore Wind Farms in the Belgian Part of the North Sea: Assessing and Managing Effect Spheres of Influence, edited by S. Degraer, R. Brabant, B. Rumes, and L. Vigin, p. 136, Brussels., 2018.

Lefaible, N., Braeckman, U. and Moens, T.: Evaluation of turbine-related impacts on macrobenthic communities within two offshore wind farms during operational phase, in Environmental Impacts of Offshore Winid Farms in the Belgian Part of the North Sea: Marking a Decade of Monitoring, Research and Innovation, edited by S. Degraer, R. Brabant, B. Rumes, and L. Vigin, pp. 65–71, Brussels., 2019.

Legendre, P. and Legendre, L. F. J.: Numerical Ecology, 2nd ed., Elsevier Science, Amsterdam., 1998.

Legge, O., Johnson, M., Hicks, N., Jickells, T., Diesing, M., Aldridge, J., Andrews, J., Artioli, Y., Bakker, D. C. E., Burrows, M. T., Carr, N., Cripps, G., Felgate, S. L., Fernand, L., Greenwood, N., Hartman, S., Kröger, S., Lessin, G., Mahaffey, C., Mayor, D. J., Parker, R., Queirós, A. M., Shutler, J. D., Silva, T., Stahl, H., Tinker, J., Underwood, G. J. C., Van Der Molen, J., Wakelin, S., Weston, K. and Williamson, P.: Carbon on the Northwest European Shelf: Contemporary Budget and Future Influences, Front. Mar. Sci., 7(March), doi:10.3389/fmars.2020.00143, 2020.

Legrand, S., de la Vallée, P., Fettweis, M. and Van Den Eynde, D.: Permanente en significante wijzigingen van de hydrografische eigenschappen, Brussel, België., 2018.

Lenhart, H. J., Mills, D. K., Baretta-Bekker, H., van Leeuwen, S. M., der Molen, J. van, Baretta, J. W., Blaas, M., Desmit, X., Kühn, W., Lacroix, G., Los, H. J., Ménesguen, A., Neves, R., Proctor, R., Ruardij, P., Skogen, M. D., Vanhoutte-Brunier, A., Villars, M. T. and Wakelin, S. L.: Predicting the consequences of nutrient reduction on the eutrophication status of the North Sea, J. Mar. Syst., 81(1–2), 148–170, doi:10.1016/j.jmarsys.2009.12.014, 2010.

Lenz, W.: Die Überfischung der Nordsee – ein historischer Überblick des Konfliktes zwischen Politik und Wissenschaft, Hist. Meereskundliches Jahrb., 1(1), 87–108, 1992.

Lessin, G., Artioli, Y., Almroth-Rosell, E., Blackford, J. C., Dale, A. W., Glud, R. N., Middelburg, J. J., Pastres, R., Queirós, A. M., Rabouille, C., Regnier, P., Soetaert, K., Solidoro, C., Stephens, N. and Yakushev, E.: Modelling Marine Sediment Biogeochemistry: Current Knowledge Gaps, Challenges, and Some Methodological Advice for Advancement, Front. Mar. Sci., 5(February), 1–8, doi:10.3389/fmars.2018.00019, 2018.

Li, S. and Jay, S.: Transboundary marine spatial planning across Europe: Trends and priorities in nearly two decades of project work, Mar. Policy, 118(February), 104012, doi:10.1016/j.marpol.2020.104012, 2020.

Lipsewers, Y. A., Bale, N. J., Hopmans, E. C., Schouten, S., Sinninghe Damsté, J. S. and Villanueva, L.: Seasonality and depth distribution of the abundance and activity of ammonia oxidizing microorganisms in marine coastal sediments (North Sea), Front. Microbiol., 5(SEP), 472, doi:10.3389/fmicb.2014.00472, 2014.

Llobet-Brossa, E., Rosselló-Mora, R. and Amann, R.: Microbial Community Composition of Wadden Sea Sediments as Revealed by Fluorescence In Situ Hybridization, Appl. Environ. Microbiol., 64(7), 2691–2696, doi:10.1128/AEM.64.7.2691-2696.1998, 1998.

Llobet-Brossa, E., Rabus, R., Böttcher, M. E., Könneke, M., Finke, N., Schramm, A., Meyer, R. L., Grötzschel, S.,

Rosselló-Mora, R. and Amann, R.: Community structure and activity of sulfate-reducing bacteria in an intertidal surface sediment: A multi-method approach, Aquat. Microb. Ecol., 29(3), 211–226, doi:10.3354/ame029211, 2002.

Lohse, L., Malschaert, J. F. P., Slomp, C. P., Helder, W. and van Raaphorst, W.: Sediment-water fluxes of inorganic nitrogen compounds along the transport route of organic matter in the North Sea, Ophelia, 41(1), 173–197, doi:10.1080/00785236.1995.10422043, 1995.

Lucchetti, A. and Sala, A.: Impact and performance of mediterranean fishing gear by side-scan sonar technology, Can. J. Fish. Aquat. Sci., 69(11), 1806–1816, doi:10.1139/f2012-107, 2012.

Luff, R. and Moll, A.: Seasonal dynamics of the North Sea sediments using a three-dimensional coupled sediment-water model system, Cont. Shelf Res., 24(10), 1099–1127, doi:10.1016/j.csr.2004.03.010, 2004.

MacDonald, E. C., Frost, E. H., MacNeil, S. M., Hamilton, D. J. and Barbeau, M. A.: Behavioral response of Corophium volutator to shorebird predation in the upper bay of Fundy, Canada, PLoS One, 9(10), doi:10.1371/journal.pone.0110633, 2014.

Magni, P. and Montani, S.: Seasonal patterns of pore-water nutrients, benthic chlorophyll a and sedimentary AVS in a macrobenthos-rich tidal flat, Hydrobiologia, 571(1), 297–311, doi:10.1007/s10750-006-0242-9, 2006.

Maire, O., Lecroart, P., Meysman, F., Rosenberg, R., Duchêne, J. and Grémare, A.: Quantification of sediment reworking rates in bioturbation research: a review, Aquat. Biol., 2(3), 219–238, doi:10.3354/ab00053, 2008.

Maire, O., Merchant, J. N., Bulling, M., Teal, L. R., Grémare, A., Duchêne, J. C. and Solan, M.: Indirect effects of non-lethal predation on bivalve activity and sediment reworking, J. Exp. Mar. Bio. Ecol., 395(1–2), 30–36, doi:10.1016/j.jembe.2010.08.004, 2010.

Marchant, H. K., Holtappels, M., Lavik, G., Ahmerkamp, S., Winter, C. and Kuypers, M. M. M.: Coupled nitrification-denitrification leads to extensive N loss in subtidal permeable sediments, Limnol. Oceanogr., 61(3), 1033–1048, doi:10.1002/lno.10271, 2016.

van Marlen, B., de Haan, D., van Gool, A. and Burggraaf, D.: The effect of pulse stimulation on marine biota – Research in relation to ICES advice – Progress report on the effects on benthic invertebrates, , 53, 2009.

Van Marlen, B., Wiegerinck, J. A. M., van Os-Koomen, E. and van Barneveld, E.: Catch comparison of flatfish pulse trawls and a tickler chain beam trawl, Fish. Res., 151, 57–69, doi:10.1016/j.fishres.2013.11.007, 2014.

Martín, J., Puig, P., Masqué, P., Palanques, A. and Sánchez-Gómez, A.: Impact of bottom trawling on deep-sea sediment properties along the flanks of a submarine canyon, PLoS One, 9(8), doi:10.1371/journal.pone.0104536, 2014.

Martin, W. R. and Banta, G. T.: The measurement of sediment irrigation rates: A comparison of the Br- tracer and 222Rn/ 226Ra disequilibrum techniques, J. Mar. Res., 50, 125–154, doi:10.1357/002224092784797737, 1992.

Mavraki, N., Degraer, S., Vanaverbeke, J. and Braeckman, U.: Organic matter assimilation by hard substrate fauna in an offshore wind farm area: a pulse-chase study, edited by J. Norkko, ICES J. Mar. Sci., doi:10.1093/icesjms/fsaa133, 2020a.

Mavraki, N., De Mesel, I., Degraer, S., Moens, T. and Vanaverbeke, J.: Resource Niches of Co-occurring Invertebrate Species at an Offshore Wind Turbine Indicate a Substantial Degree of Trophic Plasticity, Front. Mar. Sci., 7(June), 1–17, doi:10.3389/fmars.2020.00379, 2020b.

Mayer, L. M.: Surface area control of organic carbon accumulation in continental shelf sediments, Geochim. Cosmochim. Acta, 58(4), 1271–1284, doi:10.1016/0016-7037(94)90381-6, 1994.

Mayer, L. M., Schick, D. F., Findlay, R. H. and Rice, D. L.: Effects of commercial dragging on sedimentary organic matter, Mar. Environ. Res., 31(4), 249–261, doi:10.1016/0141-1136(91)90015-Z, 1991.

McCave, I. N., Bryant, R. J., Cook, H. F. and Coughanowr, C. A.: Evaluation of a laser-diffraction-size analyzer for use with natural sediments, J. Sediment. Res., 56, 561–564, doi:10.1306/212f89cc-2b24-11d7- 8648000102c1865d, 1986.

McConnaughey, R. A., Hiddink, J. G., Jennings, S., Pitcher, C. R., Kaiser, M. J., Suuronen, P., Sciberras, M., Rijnsdorp, A. D., Collie, J. S., Mazor, T., Amoroso, R. O., Parma, A. M. and Hilborn, R.: Choosing best practices for managing impacts of trawl fishing on seabed habitats and biota, Fish Fish., 21(2), 319–337, doi:10.1111/faf.12431, 2020.

McCurdy, D. G., Boates, J. S. and Forbes, M. R.: Reproductive synchrony in the intertidal amphipod Corophium volutator, Oikos, 88(2), 301–308, doi:10.1034/j.1600-0706.2000.880208.x, 2000.

van den Meersche, K., Soetaert, K. and van Oevelen, D.: xsample(): An R function for Sampling Linear Inverse Problems, J. Stat. Softw., 30, doi:10.1002/wics.10, 2009.

Mengual, B., Cayocca, F., Le Hir, P., Draye, R., Laffargue, P., Vincent, B. and Garlan, T.: Influence of bottom trawling on sediment resuspension in the 'Grande-Vasière' area (Bay of Biscay, France), Ocean Dyn., 66(9), 1181–1207, doi:10.1007/s10236-016-0974-7, 2016.

Mengual, B., Le Hir, P., Cayocca, F. and Garlan, T.: Bottom trawling contribution to the spatio-temporal variability of sediment fluxes on the continental shelf of the Bay of Biscay (France), Mar. Geol., 414(May), 77–91, doi:10.1016/j.margeo.2019.05.009, 2019.

Mermillod-Blondin, F., Rosenberg, R., François-Carcaillet, F., Norling, K. and Mauclaire, L.: Influence of bioturbation by three benthic infaunal species on microbial communities and biogeochemical processes in marine sediment, Aquat. Microb. Ecol., 36(3), 271–284, doi:10.3354/ame036271, 2004.

De Mesel, I., Kerckhof, F., Norro, A., Rumes, B. and Degraer, S.: Succession and seasonal dynamics of the epifauna community on offshore wind farm foundations and their role as stepping stones for non-indigenous species, Hydrobiologia, 756(1), 37–50, doi:10.1007/s10750-014-2157-1, 2015.

Mestdagh, S., Bagaço, L., Ysebaert, T., Braeckman, U., De Smet, B., Moens, T. and Van Colen, C.: Functional trait responses to sediment deposition reduce macrofauna-mediated ecosystem functioning in an estuarine mudflat, Biogeosciences, 15(9), 2587–2599, doi:10.5194/bg-15-2587-2018, 2018.

Mestdagh, S., Fang, X., Soetaert, K., Ysebaert, T., Moens, T. and Van Colen, C.: Seasonal variability in ecosystem functioning across estuarine gradients: The role of sediment communities and ecosystem processes, Mar. Environ. Res., 162, 105096, doi:10.1016/j.marenvres.2020.105096, 2020.

Meysman, F. J. R., Galaktionov, O. S. and Middelburg, J. J.: Irrigation patterns in permeable sediments induced by burrow ventilation: A case study of Arenicola marina, Mar. Ecol. Prog. Ser., 303(November), 195–212, doi:10.3354/meps303195, 2005a.

Meysman, F. J. R., Boudreau, B. P. and Middelburg, J. J.: Modeling reactive transport in sediments subject to bioturbation and compaction, Geochim. Cosmochim. Acta, 69(14), 3601–3617, doi:10.1016/j.gca.2005.01.004, 2005b.

Meysman, F. J. R., Galaktionov, O. S., Gribsholt, B. and Middelburg, J. J.: Bio-irrigation in permeable sediments: An assessment of model complexity, J. Mar. Res., 64(4), 589–627, doi:10.1357/002224006778715757, 2006a.

Meysman, F. J. R., Galaktionov, O. S., Gribsholt, B. and Middelburg, J. J.: Bioirrigation in permeable sediments: Advective pore-water transport induced by burrow ventilation, Limnol. Oceanogr., 51(1), 142–156, doi:10.4319/lo.2006.51.1.0142, 2006b.

Middelburg, J. J. and Soetaert, K.: Chapter 11 . The role of sediments in shelf ecosystem dynamics, in The Sea, vol. 13, edited by A. R. Robinson, J. McCarthy, and B. J. Rothschild, pp. 353–373, Harvard University Press, Cambridge., 2004.

Middelburg, J. J., Soetaert, K., Herman, P. M. J. and Heip, C. H. R.: Denitrification in marine sediments: A model study, Global Biogeochem. Cycles, 10(4), 661–673, doi:10.1029/96GB02562, 1996.

Middelburg, J. J., Soetaert, K. and Herman, P. M. J.: Empirical relationships for use in global diagenetic models, Deep Sea Res. Part I Oceanogr. Res. Pap., 44(2), 327–344, doi:10.1016/S0967-0637(96)00101-X, 1997.

van der Molen, J., Aldridge, J. N., Coughlan, C., Parker, E. R., Stephens, D. and Ruardij, P.: Modelling marine ecosystem response to climate change and trawling in the North Sea, Biogeochemistry, 113(1–3), 213–236, doi:10.1007/s10533-012-9763-7, 2013.

Molen, J. van der, García-García, L. M., Whomersley, P., Callaway, A., Posen, P. E. and Hyder, K.: Connectivity of larval stages of sedentary marine communities between hard substrates and offshore structures in the North Sea, Sci. Rep., 8(1), 1–14, doi:10.1038/s41598-018-32912-2, 2018.

Moll, A.: Assessment of three-dimensional physical-biological ECOHAM1 simulations by quantified validation for the North Sea with ICES and ERSEM data, ICES J. Mar. Sci., 57(4), 1060–1068, doi:10.1006/jmsc.2000.0590, 2000.

Morato, T., Watson, R., Pitcher, T. J. and Pauly, D.: Fishing down the deep, Fish Fish., 7(1), 24–34, doi:10.1111/j.1467-2979.2006.00205.x, 2006.

Mortimer, C. H.: The Exchange of Dissolved Substances between Mud and Water in Lakes, J. Ecol., 30(1), 147, doi:10.2307/2256691, 1942.

Morys, C., Powilleit, M. and Forster, S.: Bioturbation in relation to the depth distribution of macrozoobenthos in the southwestern Baltic Sea, Mar. Ecol. Prog. Ser., 579, 19–36, doi:10.3354/meps12236, 2017.

Mouret, A., Anschutz, P., Lecroart, P., Chaillou, G., Hyacinthe, C., Deborde, J., Jorissen, F. J., Deflandre, B., Schmidt, S. and Jouanneau, J. M.: Benthic geochemistry of manganese in the Bay of Biscay, and sediment mass accumulation rate, Geo-Marine Lett., 29(3), 133–149, doi:10.1007/s00367-008-0130-6, 2009.

Murray, F., Douglas, A. and Solan, M.: Species that share traits do not necessarily form distinct and universally applicable functional effect groups, Mar. Ecol. Prog. Ser., 516, 23–34, doi:10.3354/meps11020, 2014.

Murray, F., Copland, P., Boulcott, P., Robertson, M. and Bailey, N.: Impacts of electrofishing for razor clams (Ensis spp.) on benthic fauna, Fish. Res., 174, 40–46, doi:10.1016/j.fishres.2015.08.028, 2016.

Na, T., Gribsholt, B., Galaktionov, O. S., Lee, T. and Meysman, F. J. R.: Influence of advective bio-irrigation on carbon and nitrogen cycling in sandy sediments, J. Mar. Res., 66, 691–722, doi:10.1357/002224008787536826, 2008.

Navel, S., Sauvage, S., Delmotte, S., Gerino, M., Marmonier, P. and Mermillod-Blondin, F.: A modelling approach to quantify the influence of fine sediment deposition on biogeochemical processes occurring in the hyporheic zone, Ann. Limnol. - Int. J. Limnol., 48(3), 279–287, doi:10.1051/limn/2012017, 2012.

Nedwell, D. B., Parkes, R. J., Upton, A. C. and Assinder, D. J.: Seasonal fluxes across the sediment—water interface, and processes within sediments, in Understanding the North Sea System, pp. 141–151, Springer Netherlands, Dordrecht., 1994.

Németh, A. A., Hulscher, S. J. M. H. and De Vriend, H. J.: Modelling sand wave migration in shallow shelf seas, Cont. Shelf Res., 22(18–19), 2795–2806, doi:10.1016/S0278-4343(02)00127-9, 2002.

Neubacher, E. C., Parker, R. E. and Trimmer, M.: Short-term hypoxia alters the balance of the nitrogen cycle in coastal sediments, Limnol. Oceanogr., 56(2), 651–665, doi:10.4319/lo.2011.56.2.0651, 2011.

Neumann, A., van Beusekom, J. E. E., Holtappels, M. and Emeis, K. C.: Nitrate consumption in sediments of the German Bight (North Sea), J. Sea Res., 127(February 2016), 26–35, doi:10.1016/j.seares.2017.06.012, 2017.

Neumann, H., Diekmann, R. and Kröncke, I.: Functional composition of epifauna in the south-eastern North Sea in relation to habitat characteristics and fishing effort, Estuar. Coast. Shelf Sci., 169, 182–194, doi:10.1016/j.ecss.2015.12.011, 2016.

Newell, S. E., McCarthy, M. J., Gardner, W. S. and Fulweiler, R. W.: Sediment Nitrogen Fixation: a Call for Re-evaluating Coastal N Budgets, Estuaries and Coasts, 39(6), 1626–1638, doi:10.1007/s12237-016-0116-y, 2016a.

Newell, S. E., McCarthy, M. J., Gardner, W. S. and Fulweiler, R. W.: Sediment Nitrogen Fixation: a Call for Re-evaluating Coastal N Budgets, Estuaries and Coasts, 39(6), 1626–1638, doi:10.1007/s12237-016-0116-y, 2016b.

Nghiem, A. and Pineda, I.: Wind energy in Europe: Scenarios for 2030, Brussels. [online] Available from: https://windeurope.org/wp-content/uploads/files/about-wind/reports/Wind-energy-in-Europe-Scenarios-for-2030.pdf%0Ahttp://www.ewea.org/fileadmin/files/library/publications/reports/EWEA-Wind-energy-scenarios-2030.pdf, 2017.

Nielsen, O. I., Gribsholt, B., Kristensen, E. and Revsbech, N. P.: Microscale distribution of oxygen and nitrate in sediment inhabited by Nereis diversicolor: Spatial patterns and estimated reaction rates, Aquat. Microb. Ecol., 34(1), 23–32, doi:10.3354/ame034023, 2004.

Nizzoli, D., Welsh, D. T., Bartoli, M. and Viaroli, P.: Impacts of mussel (Mytilus galloprovincialis) farming on oxygen consumption and nutrient recycling in a eutrophic coastal lagoon, Hydrobiologia, 550(1), 183–198, doi:10.1007/s10750-005-4378-9, 2005.

Nohe, A.: Long-term trends in phytoplankton biomass , composition and dynamics in the Belgian part of the North Sea, Ghent University., 2019.

Nohe, A., Goffin, A., Tyberghein, L., Lagring, R., De Cauwer, K., Vyverman, W. and Sabbe, K.: Marked changes in diatom and dinoflagellate biomass, composition and seasonality in the Belgian Part of the North Sea between the 1970s and 2000s, Sci. Total Environ., 716, doi:10.1016/j.scitotenv.2019.136316, 2020.

Norse, E. A., Brooke, S., Cheung, W. W. L., Clark, M. R., Ekeland, I., Froese, R., Gjerde, K. M., Haedrich, R. L., Heppell, S. S., Morato, T., Morgan, L. E., Pauly, D., Sumaila, R. and Watson, R.: Sustainability of deep-sea fisheries, Mar. Policy, 36(2), 307–320, doi:10.1016/j.marpol.2011.06.008, 2012.

Northeast Fisheries Science Center: Benthic Habitat Database, [online] Available from: https://catalog.data.gov/dataset/benthic-habitat-database, 2018.

van Nugteren, P., Moodley, L., Brummer, G. J., Heip, C. H. R., Herman, P. M. J. and Middelburg, J. J.: Seafloor ecosystem functioning: The importance of organic matter priming, Mar. Biol., 156(11), 2277–2287, doi:10.1007/s00227-009-1255-5, 2009.

NWO: NICO-Expeditie Netherlands Initiative Changing Oceans, [online] Available from: https://nico-expeditie.nl/ (Accessed 13 August 2020), 2019.

O'Neill, F. G. and Ivanović, A.: The physical impact of towed demersal fishing gears on soft sediments, ICES J. Mar. Sci., 73(suppl_1), i5–i14, doi:10.1093/icesjms/fsv125, 2016.

O'Neill, F. G. and Summerbell, K.: The mobilisation of sediment by demersal otter trawls, Mar. Pollut. Bull., 62(5), 1088–1097, doi:https://doi.org/10.1016/j.marpolbul.2011.01.038, 2011a.

O'Neill, F. G. and Summerbell, K.: The mobilisation of sediment by demersal otter trawls, Mar. Pollut. Bull., 62(5), 1088–1097, doi:10.1016/j.marpolbul.2011.01.038, 2011b.

Oberle, F. K. J., Swarzenski, P. W., Reddy, C. M., Nelson, R. K., Baasch, B. and Hanebuth, T. J. J.: Deciphering the lithological consequences of bottom trawling to sedimentary habitats on the shelf, J. Mar. Syst., 159, 120–131, doi:10.1016/j.jmarsys.2015.12.008, 2016.

Oehler, T., Martinez, R., Schückel, U., Winter, C., Kröncke, I. and Schlüter, M.: Seasonal and spatial variations of benthic oxygen and nitrogen fluxes in the Helgoland Mud Area (southern North Sea), Cont. Shelf Res., 106, 118–129, doi:10.1016/j.csr.2015.06.009, 2015.

Oksanen, J., Blanchet, F. G., Friendly, M., Kindt, R., Legendre, P., McGlinn, D., Minchin, P. R., O'Hara, R. B., Simpson, G. L., Solymos, P., Stevens, M. H. H., Szoecs, E. and Wagner, H.: vegan: Community Ecology Package, [online] Available from: https://cran.r-project.org/package=vegan, 2019.

Olaffson, E.: Do Macrofauna Structure Meiofauna Assemblages in Marine Soft-Bottoms? A review of Experimental Studies, Vie Milieu, 53(4), 249–265, 2003.

Oldham, C., Ivey, G. and Pullin, C.: Estimation of a characteristic friction velocity in stirred benthic chambers, Mar. Ecol. Prog. Ser., 279, 291–295, doi:10.3354/meps279291, 2004.

Osinga, R., Kop, A. J., Duineveld, G. C. A., Prins, R. A. and Van Duyl, F. C.: Benthic mineralization rates at two locations in the southern North Sea, J. Sea Res., 36(3–4), 181–191, doi:10.1016/s1385-1101(96)90788-1, 1996.

OSPAR: PARCOM recommendation 88/2: On the reduction in nutrients to the Paris convention area., Paris Comission., 1988.

Palanques, A., Guillén, J. and Puig, P.: Impact of bottom trawling on water turbidity and muddy sediment of an unfished continental shelf, Limnol. Oceanogr., 46(5), 1100–1110, doi:10.4319/lo.2001.46.5.1100, 2001.

Palanques, A., Puig, P., Guillén, J., Demestre, M. and Martín, J.: Effects of bottom trawling on the Ebro continental shelf sedimentary system (NW Mediterranean), Cont. Shelf Res., 72, 83–98, doi:10.1016/j.csr.2013.10.008, 2014.

Paradis, S., Pusceddu, A., Masqué, P., Puig, P., Moccia, D., Russo, T. and Iacono, C. Lo: Organic matter contents and degradation in a highly trawled area during fresh particle inputs (Gulf of Castellammare, southwestern Mediterranean), Biogeosciences, 16(21), 4307–4320, doi:10.5194/bg-16-4307-2019, 2019.

Paschen, M., Richter, U. and Köpnick, W.: Trawl Penetration in the Seabed (TRAPESE). Final report Contract No. 96-006., 2000.

Passy, P., Gypens, N., Billen, G., Garnier, J., Thieu, V., Rousseau, V., Callens, J., Parent, J.-Y. and Lancelot, C.: A model reconstruction of riverine nutrient fluxes and eutrophication in the Belgian Coastal Zone since 1984, J. Mar. Syst., 128, 106–122, doi:10.1016/j.jmarsys.2013.05.005, 2013.

Paulmier, A., Kriest, I. and Oschlies, A.: Stoichiometries of remineralisation and denitrification in global biogeochemical ocean models, Biogeosciences, 6(5), 923–935, doi:10.5194/bg-6-923-2009, 2009.

Pearson, T. H. and Rosenberg, R.: Macrobenthic succession in relation to organic enrichment and pollution of the marine environment, Oceanogr. Mar. Biol. An Annu. Rev., 16(1), 229–311, doi:10.2983/035.034.01211u110, 1978.

Pinheiro, J., Bates, D., DebRoy, S., Sarkar, D. and R Core Team: {nlme}: Linear and Nonlinear Mixed Effects Models, [online] Available from: https://cran.r-project.org/package=nlme, 2019.

Pinheiro, J., Bates, D., DebRoy, S. and Sarkar, D.: nlme: Linear and Nonlinear Mixed Effects Models, 2020.

Pinheiro, J. C. and Bates, D. M.: Mixed-Effects Models in S and S-PLUS, edited by J. Chambers, W. Eddy, W. Hardle, S. Sheater, and L. Tierney, Springer-Verlag, New York., 2000.

Pitcher, C. R., Ellis, N., Jennings, S., Hiddink, J. G., Mazor, T., Kaiser, M. J., Kangas, M. I., McConnaughey, R. A., Parma, A. M., Rijnsdorp, A. D., Suuronen, P., Collie, J. S., Amoroso, R., Hughes, K. M. and Hilborn, R.: Estimating the sustainability of towed fishing-gear impacts on seabed habitats: a simple quantitative risk assessment method applicable to data-limited fisheries, Methods Ecol. Evol., 8(4), 472–480, doi:10.1111/2041-210X.12705, 2017.

Polerecky, L., Volkenborn, N. and Stief, P.: High temporal resolution oxygen imaging in bioirrigated sediments, Environ. Sci. Technol., 40(18), 5763–5769, doi:10.1021/es060494l, 2006.

Polymenakou, P. N., Pusceddu, A., Tselepides, A., Polychronaki, T., Giannakourou, A., Fiordelmondo, C., Hatziyanni, E. and Danovaro, R.: Benthic microbial abundance and activities in an intensively trawled ecosystem (Thermaikos Gulf, Aegean Sea), Cont. Shelf Res., 25(19–20), 2570–2584, doi:10.1016/j.csr.2005.08.018, 2005.

Poos, J.-J., Hintzen, N. T., van Rijssel, J. C. and Rijnsdorp, A. D.: Efficiency changes in bottom trawling for flatfish species as a result of the replacement of mechanical stimulation by electric stimulation, edited by M. Pol, ICES J. Mar. Sci., doi:10.1093/icesjms/fsaa126, 2020.

Precht, E. and Huettel, M.: Advective pore-water exchange driven by surface gravity waves and its ecological implications, Limnol. Oceanogr., 48(4), 1674–1684, doi:10.4319/lo.2003.48.4.1674, 2003.

Price, W. L.: A controlled random search procedure for global optimisation, Comput. J., 20(4), 367–370, doi:10.1093/comjnl/20.4.367, 1977.

Probandt, D., Knittel, K., Tegetmeyer, H. E., Ahmerkamp, S., Holtappels, M. and Amann, R.: Permeability shapes bacterial communities in sublittoral surface sediments, Environ. Microbiol., 19(4), 1584–1599, doi:10.1111/1462-

2920.13676, 2017.

Provoost, P., Braeckman, U., Van Gansbeke, D., Moodley, L., Soetaert, K., Middelburg, J. J. and Vanaverbeke, J.: Modelling benthic oxygen consumption and benthic-pelagic coupling at a shallow station in the southern North Sea, Estuar. Coast. Shelf Sci., 120, 1–11, doi:10.1016/j.ecss.2013.01.008, 2013.

Puig, P., Canals, M., Company, J. B., Martín, J., Amblas, D., Lastras, G., Palanques, A. and Calafat, A. M.: Ploughing the deep sea floor, Nature, 489(7415), 286–289, doi:10.1038/nature11410, 2012.

Pusceddu, A., Fiordelmondo, C., Polymenakou, P., Polychronaki, T., Tselepides, A. and Danovaro, R.: Effects of bottom trawling on the quantity and biochemical composition of organic matter in coastal marine sediments (Thermaikos Gulf, northwestern Aegean Sea), Cont. Shelf Res., 25(19–20), 2491–2505, doi:10.1016/j.csr.2005.08.013, 2005.

Pusceddu, A., Bianchelli, S., Martín, J., Puig, P., Palanques, A., Masqué, P. and Danovaro, R.: Chronic and intensive bottom trawling impairs deep-sea biodiversity and ecosystem functioning, Proc. Natl. Acad. Sci. U. S. A., 111(24), 8861–8866, doi:10.1073/pnas.1405454111, 2014.

Qian, H., Ricklefs, R. E. and White, P. S.: Beta diversity of angiosperms in temperate floras of eastern Asia and eastern North America, Ecol. Lett., 8(1), 15–22, doi:10.1111/j.1461-0248.2004.00682.x, 2005.

Quante, M., Colijn, F., Bakker, J. P., Härdtle, W., Heinrich, H., Lefebvre, C., Nöhren, I., Olesen, J. E., Pohlmann, T., Sterr, H., Sündermann, J. and Tölle, M. H.: North Sea Region Climate Change Assessment., 2016.

Queirós, A. M., Birchenough, S. N. R., Bremner, J., Godbold, J. A., Parker, R. E., Romero-Ramirez, A., Reiss, H., Solan, M., Somerfield, P. J., Van Colen, C., Van Hoey, G. and Widdicombe, S.: A bioturbation classification of European marine infaunal invertebrates, Ecol. Evol., 3(11), 3958–3985, doi:10.1002/ece3.769, 2013.

Queirós, A. M., Stephens, N., Cook, R., Ravaglioli, C., Nunes, J., Dashfield, S., Harris, C., Tilstone, G. H., Fishwick, J., Braeckman, U., Somerfield, P. J. and Widdicombe, S.: Can benthic community structure be used to predict the process of bioturbation in real ecosystems?, Prog. Oceanogr., 137(April), 559–569, doi:10.1016/j.pocean.2015.04.027, 2015.

Quintana, C. O., Tang, M. and Kristensen, E.: Simultaneous study of particle reworking, irrigation transport and reaction rates in sediment bioturbated by the polychaetes Heteromastus and Marenzelleria, J. Exp. Mar. Bio. Ecol., 352(2), 392–406, doi:10.1016/j.jembe.2007.08.015, 2007.

R Core Team: R: A language and environment for statistical computing, [online] Available from: http://www.r-project.org/, 2020.

Raaphorst, W. Van and Malschaert, J. F. P.: Ammonium adsorption in superficial North Sea sediments, Cont. Shelf Res., 16(11), 1415–1435, doi:10.1016/0278-4343(95)00081-X, 1996.

Raaphorst, W. Van, Kloosterhuis, H. T., Cramer, A. and Bakker, K. J. M.: Nutrient early diagenesis in the sandy sediments of the dogger bank area, north sea: Pore water results, Netherlands J. Sea Res., 26(1), 25–52, doi:10.1016/0077-7579(90)90054-K, 1990.

Van Raaphorst, W., Kloosterhuis, H. T., Berghuis, E. M., Gieles, A. J. M., Malschaert, J. F. P. and Van Noort, G. J.: Nitrogen cycling in two types of sediments of the Southern North sea (Frisian front, broad fourteens): field data and mesocosm results, Netherlands J. Sea Res., 28(4), 293–316, doi:10.1016/0077-7579(92)90033-B, 1992.

Ragueneau, O., Chauvaud, L., Moriceau, B., Leynaert, A., Thouzeau, G., Donval, A., Le Loc'h, F. and Jean, F.: Biodeposition by an invasive suspension feeder impacts the biogeochemical cycle of Si in a coastal ecosystem (Bay of Brest, France), Biogeochemistry, 75(1), 19–41, doi:10.1007/s10533-004-5677-3, 2005.

Raitsos, D. E., Pradhan, Y., Lavender, S. J., Hoteit, I., Mcquatters-Gollop, A., Reid, P. C. and Richardson, A. J.: From silk to satellite: Half a century of ocean colour anomalies in the Northeast Atlantic, Glob. Chang. Biol., 20(7), 2117–2123, doi:10.1111/gcb.12457, 2014.

Ramirez, L., Fraile, D. and Brindley, G.: Offshore wind in Europe: Key trends and statistics 2019, edited by C.

Walsh, Brussels. [online] Available from: https://windeurope.org/wp-content/uploads/files/about-wind/statistics/WindEurope-Annual-Offshore-Statistics-2019.pdf, 2020.

Rampazzo, F., Berto, D., Giani, M., Brigolin, D., Covelli, S., Cacciatore, F., Brusà, R. B., Bellucci, L. G. and Pastres, R.: Impact of mussel farming on sedimentary geochemical properties of a Northern Adriatic area influenced by freshwater inflows, Estuar. Coast. Shelf Sci., 129, 49–58, doi:10.1016/j.ecss.2013.06.001, 2013.

Rao, A. M. F., Malkin, S. Y., Montserrat, F. and Meysman, F. J. R.: Alkalinity production in intertidal sands intensified by lugworm bioirrigation, Estuar. Coast. Shelf Sci., 148, 36–47, doi:10.1016/j.ecss.2014.06.006, 2014.

Rao, A. M. F., Malkin, S. Y. and Hidalgo-martinez, S.: The impact of electrogenic sulfide oxidation on elemental cycling and solute fluxes in coastal sediment ScienceDirect The impact of electrogenic sulfide oxidation on elemental cycling and solute fluxes in coastal sediment, Geochim. Cosmochim. Acta, 172(January), 265–286, doi:10.1016/j.gca.2015.09.014, 2016.

Rasheed, M., Badran, M. I. and Huettel, M.: Influence of sediment permeability and mineral composition on organic matter degradation in three sediments from the Gulf of Aqaba, Red Sea, Estuar. Coast. Shelf Sci., 57(1–2), 369–384, doi:10.1016/S0272-7714(02)00362-1, 2003.

Redfield, A. C.: The biological control of chemical factors in the environment., Sci. Prog., 11, 150–70 [online] Available from: http://www.ncbi.nlm.nih.gov/pubmed/24545739, 1960.

Reid, P. C., Lancelot, C., Gieskes, W. W. C., Hagmeier, E. and Weichart, G.: Phytoplankton of the North Sea and its dynamics: A review, Netherlands J. Sea Res., 26(2–4), 295–331, doi:10.1016/0077-7579(90)90094-W, 1990.

Renz, J. R., Powilleit, M., Gogina, M., Zettler, M. L., Morys, C. and Forster, S.: Community bioirrigation potential (BIP c), an index to quantify the potential for solute exchange at the sediment-water interface, Mar. Environ. Res., (July), 0–1, doi:10.1016/j.marenvres.2018.09.013, 2018.

Reubens, J. T., Degraer, S. and Vincx, M.: Aggregation and feeding behaviour of pouting (Trisopterus luscus) at wind turbines in the Belgian part of the North Sea, Fish. Res., 108(1), 223–227, doi:10.1016/j.fishres.2010.11.025, 2011.

Revsbech, N. P.: An oxygen microsensor with a guard cathode, Limnol. Oceanogr., 34(2), 474–478, doi:10.4319/lo.1989.34.2.0474, 1989.

Richardson, K.: Subsurface phytoplankton blooms fuel pelagic production in the North Sea, J. Plankton Res., 22(9), 1663–1671, doi:10.1093/plankt/22.9.1663, 2000.

Riemann, B. and Hoffmann, E.: Ecological consequences of dredging and bottom trawling in the Limfjord, Denmark, Mar. Ecol. Prog. Ser., 69(1–2), 171–178, doi:10.3354/meps069171, 1991.

Riisgård, H. U., Kittner, C. and Seerup, D. F.: Regulation of opening state and filtration rate in filter-feeding bivalves (Cardium edule, Mytilus edulis, Mya arenaria) in response to low algal concentration, J. Exp. Mar. Bio. Ecol., 284(1–2), 105–127, doi:10.1016/S0022-0981(02)00496-3, 2003.

Rijnsdorp, A.: Micro-scale distribution of beam trawl effort in the southern North Sea between 1993 and 1996 in relation to the trawling frequency of the sea bed and the impact on benthic organisms, ICES J. Mar. Sci., 55(3), 403–419, doi:10.1006/jmsc.1997.0326, 1998.

Rijnsdorp, A. A. D., Boute, P., Tiano, J., Lankheet, M., Soetaert, K., Beier, U., De Borger, E. and Hintzen, N.: The implications of a transition from tickler chain beam trawl to electric pulse trawl on the sustainability and ecosystem effects of the fishery for North Sea sole : an impact assessment, IJmuiden., 2020a.

Rijnsdorp, A. D., Bastardie, F., Bolam, S. G., Buhl-Mortensen, L., Eigaard, O. R., Hamon, K. G., Hiddink, J. G., Hintzen, N. T., Ivanović, A., Kenny, A., Laffargue, P., Nielsen, J. R., O'Neill, F. G., Piet, G. J., Polet, H., Sala, A., Smith, C., van Denderen, P. D., van Kooten, T. and Zengin, M.: Towards a framework for the quantitative assessment of trawling impact on the seabed and benthic ecosystem, ICES J. Mar. Sci., 73(suppl_1), i127–i138, doi:10.1093/icesjms/fsv207, 2016.

Rijnsdorp, A. D., Bolam, S. G., Garcia, C., Hiddink, J. G., Hintzen, N. T., van Denderen, P. D. and van Kooten, T.: Estimating sensitivity of seabed habitats to disturbance by bottom trawling based on the longevity of benthic fauna, Ecol. Appl., 28(5), 1302–1312, doi:10.1002/eap.1731, 2018.

Rijnsdorp, A. D., Depestele, J., Eigaard, O. R., Hintzen, N. T., Ivanović, A., Molenaar, P., O'Neill, F. G., Polet, H., Poos, J. J. and Kooten, T. van: Mitigating seafloor disturbance of bottom trawl fisheries for North Sea sole Solea solea by replacing mechanical with electrical stimulation. (in press), PLoS One, doi:10.1371/journal.pone.0228528, 2020b.

Ripley, B., Venables, B., Bates, D. M., Hornik, K., Gebhardt, A. and Firth, D.: Support Functions and Datasets for Venables and Ripley's MASS, 2020.

Ritchie, R. J.: Consistent sets of spectrophotometric chlorophyll equations for acetone, methanol and ethanol solvents, Photosynth. Res., 89(1), 27–41, doi:10.1007/s11120-006-9065-9, 2006.

Rivier, A., Bennis, A. C., Pinon, G., Magar, V. and Gross, M.: Parameterization of wind turbine impacts on hydrodynamics and sediment transport, Ocean Dyn., 66(10), 1285–1299, doi:10.1007/s10236-016-0983-6, 2016.

Roberts, K. L., Kessler, A. J., Grace, M. R. and Cook, P. L. M.: Increased rates of dissimilatory nitrate reduction to ammonium (DNRA) under oxic conditions in a periodically hypoxic estuary, Geochim. Cosmochim. Acta, 133, 313–324, doi:10.1016/j.gca.2014.02.042, 2014.

Robinson, J. E., Newell, R. C., Seiderer, L. J. and Simpson, N. M.: Impacts of aggregate dredging on sediment composition and associated benthic fauna at an offshore dredge site in the southern North Sea, Mar. Environ. Res., 60(1), 51–68, doi:https://doi.org/10.1016/j.marenvres.2004.09.001, 2005.

Rosales Villa, A. R., Jickells, T. D., Sivyer, D. B., Parker, E. R. and Thamdrup, B.: Benthic nitrogen cycling in the North Sea, Cont. Shelf Res., 185(May 2018), 31–36, doi:10.1016/j.csr.2018.05.005, 2019.

Rousseau, V., Lancelot, C. and Cox, D.: Current Status of Eutrophication in the Belgian Coastal Zone, edited by V. Rousseau, C. Lancelot, and D. Cox, Presse Universitaire de Bruxelles, Brussels., 2006.

Ruardij, P. and Van Raaphorst, W.: Benthic nutrient regeneration in the ERSEM ecosystem model of the North Sea, Netherlands J. Sea Res., 33(3–4), 453–483, doi:10.1016/0077-7579(95)90057-8, 1995.

Ruttenberg, K. C. and Berner, R. A.: Authigenic apatite formation and burial in sediments from non-upwelling, continental margin environments, Geochim. Cosmochim. Acta, 57(5), 991–1007, doi:10.1016/0016-7037(93)90035-U, 1993.

Rysgaard, S., Christensen, P. B. and Nielsen, L. P.: Seasonal variation in nitrification and denitrification in estuarine sediment colonized by benthic microalgae and bioturbation infauna, Mar. Ecol. Prog. Ser., 126, 111–121, doi:10.1007/BF01873045, 1995.

Rysgaard, S., Christensen, P. B., Sørensen, M. V., Funch, P. and Berg, P.: Marine meiofauna, carbon and nitrogen mineralization in sandy and soft sediments of Disko Bay, West Greenland, Aquat. Microb. Ecol., 21, 59–71, doi:10.3354/ame021059, 2000.

Savina, M., Lacroix, G. and Ruddick, K.: Modelling the transport of common sole larvae in the southern North Sea: Influence of hydrodynamics and larval vertical movements, J. Mar. Syst., 81(1–2), 86–98, doi:10.1016/j.jmarsys.2009.12.008, 2010.

Schlüter, M., Sauter, E., Hansen, H. P. and Suess, E.: Seasonal variations of bioirrigation in coastal sediments: Modelling of field data, Geochim. Cosmochim. Acta, 64(5), 821–834, doi:10.1016/S0016-7037(99)00375-0, 2000.

Sciberras, M., Parker, R., Powell, C., Robertson, C., Kröger, S., Bolam, S. and Geert Hiddink, J.: Impacts of bottom fishing on the sediment infaunal community and biogeochemistry of cohesive and non-cohesive sediments, Limnol. Oceanogr., 61(6), 2076–2089, doi:10.1002/lno.10354, 2016.

Sciberras, M., Hiddink, J. G., Jennings, S., Szostek, C. L., Hughes, K. M., Kneafsey, B., Clarke, L. J., Ellis, N., Rijnsdorp, A. D., McConnaughey, R. A., Hilborn, R., Collie, J. S., Pitcher, C. R., Amoroso, R. O., Parma, A. M.,

Suuronen, P. and Kaiser, M. J.: Response of benthic fauna to experimental bottom fishing: A global meta-analysis, Fish Fish., 19(4), 698–715, doi:10.1111/faf.12283, 2018.

Seeberg-Elverfeldt, J., Schluter, M., Feseker, T. and Kolling, M.: Rhizon sampling of porewaters near the sediment-water interface of aquatic systems, Limnol. Oceanogr., 3, 361–371, doi:Pii S0012-821x(02)01064-6 Doi 10.1016/S0012-821x(02)01064-6, 2005.

Seitzinger, S., Harrison, J. A., Böhlke, J. K., Bouwman, A. F., Lowrance, R., Peterson, B., Tobias, C. and Van Drecht, G.: Denitrification across landscapes and waterscapes: A synthesis, Ecol. Appl., 16(6), 2064–2090, doi:10.1890/1051-0761(2006)016[2064:DALAWA]2.0.CO;2, 2006.

Seitzinger, S. P.: Denitrification in freshwater and coastal marine ecosystems: Ecological and geochemical significance, Limnol. Oceanogr., 33(4part2), 702–724, doi:10.4319/lo.1988.33.4part2.0702, 1988.

Selot, F., Fraile, D. and Brindley, G.: Offshore wind in Europe: Key trends and statistics 2018., 2019.

Serpetti, N., Heath, M., Rose, M. and Witte, U.: High resolution mapping of sediment organic matter from acoustic reflectance data, Hydrobiologia, 680(1), 265–284, doi:10.1007/s10750-011-0937-4, 2012.

Shotbolt, L.: Pore water sampling from lake and estuary sediments using Rhizon samplers, J. Paleolimnol., 44(2), 695–700, doi:10.1007/s10933-008-9301-8, 2010.

Sistermans, W. C. H., Hummel, H., Dekker, A. and Dek, L. A.: Inventarisatie macrofauna Westerschelde Najaar 2005, Yerseke., 2006.

Slavik, K., Lemmen, C., Zhang, W., Kerimoglu, O., Klingbeil, K. and Wirtz, K. W.: The large-scale impact of offshore wind farm structures on pelagic primary productivity in the southern North Sea, Hydrobiologia, 845(1), 35–53, doi:10.1007/s10750-018-3653-5, 2019.

Slomp, C. P.: Phosphorus Cycling in the Estuarine and Coastal Zones, in Treatise on Estuarine and Coastal Science, vol. 5, pp. 201–229, Elsevier., 2011.

Slomp, C. P., Epping, E. H. G., Helder, W. and Raaphorst, W. Van: A key role for iron-bound phosphorus in authigenic apatite formation in North Atlantic continental platform sediments, J. Mar. Res., 54(6), 1179–1205, doi:10.1357/0022240963213745, 1996a.

Slomp, C. P., Van der Gaast, S. J. and Van Raaphorst, W.: Phosphorus binding by poorly crystalline iron oxides in North Sea sediments, Mar. Chem., 52(1), 55–73, doi:10.1016/0304-4203(95)00078-X, 1996b.

De Smet, B., Braeckman, U., Soetaert, K., Vincx, M. and Vanaverbeke, J.: Predator effects on the feeding and bioirrigation activity of ecosystem-engineered Lanice conchilega reefs, J. Exp. Mar. Bio. Ecol., 475, 31–37, doi:10.1016/j.jembe.2015.11.005, 2016.

Snelgrove, P. and Butman, C. A.: Animal-sediment relationships revisited: cause versus effect, Oceanogr. Mar. Biol. An Annu. Rev., 32, 111–1777, 1994.

Snelgrove, P. V. R., Thrush, S. F., Wall, D. H. and Norkko, A.: Real world biodiversity-ecosystem functioning: A seafloor perspective, Trends Ecol. Evol., 29(7), 398–405, doi:10.1016/j.tree.2014.05.002, 2014.

Soetaert, K.: rootSolve: Nonlinear root finding, equilibrium and steady-state analysis of ordinary differential equations, 2009.

Soetaert, K. and Herman, P. M. J.: A practical guide to ecological modelling: Using R as a simulation platform, edited by K. Soetaert and P. M. J. Herman, Springer Netherlands, Dordrecht., 2009.

Soetaert, K. and Meysman, F.: Reactive transport in aquatic ecosystems: Rapid model prototyping in the open source software R, Environ. Model. Softw., 32, 49–60, doi:10.1016/j.envsoft.2011.08.011, 2012.

Soetaert, K. and Middelburg, J. J.: Modeling eutrophication and oligotrophication of shallow-water marine systems: The importance of sediments under stratified and well-mixed conditions, Hydrobiologia, 629(1), 239–254, doi:10.1007/s10750-009-9777-x, 2009.

Soetaert, K. and Petzoldt, T.: Inverse Modelling, Sensitivity and Monte Carlo analysis in R Using PAckage FME, J. Stat. Softw., 33(3), 1–28, doi:10.18637/jss.v033.i03, 2010.

Soetaert, K. and Petzoldt, T.: marelac: Tools for Aquatic Sciences, [online] Available from: https://cran.r-project.org/package=marelac, 2018.

Soetaert, K., Herman, P. M. J. and Middelburg, J. J.: A model of early diagenetic processes from the shelf to abyssal depths, Geochim. Cosmochim. Acta, 60(6), 1019–1040, doi:10.1016/0016-7037(96)00013-0, 1996a.

Soetaert, K., Herman, P. M. J. and Middelburg, J. J.: Dynamic response of deep-sea sediments to seasonal variations: A model, Limnol. Oceanogr., 41(8), 1651–1668, doi:10.4319/lo.1996.41.8.1651, 1996b.

Soetaert, K., Middelburg, J. J., Herman, P. M. J. and Buis, K.: On the coupling of benthic and pelagic biogeochemical models, Earth-Science Rev., 51(1–4), 173–201, doi:10.1016/S0012-8252(00)00004-0, 2000.

Soetaert, K., Herman, P. M. ., Middelburg, J. J., Heip, C., Smith, C. L., Tett, P. and Wild-Allen, K.: Numerical modelling of the shelf break ecosystem: reproducing benthic and pelagic measurements, Deep Sea Res. Part II Top. Stud. Oceanogr., 48(14), 3141–3177, doi:10.1016/S0967-0645(01)00035-2, 2001.

Soetaert, K., Van den Meersche, K. and van Oevelen, D.: limSolve: Solving Linear Inverse Models. R package 1.5.1., 2009.

Soetaert, K., Petzoldt, T. and Setzer, R. W.: Solving Differential Equations in R: Package deSolve, J. Stat. Softw., 33(9), 1–25, doi:10.18637/jss.v033.i09, 2010.

Soetaert, M., Chiers, K., Duchateau, L., Polet, H., Verschueren, B. and Decostere, A.: Determining the safety range of electrical pulses for two benthic invertebrates: brown shrimp (Crangon crangon L.) and ragworm (Alitta virens S.), ICES J. Mar. Sci., 72(3), 973–980, doi:10.1093/icesjms/fsu176, 2015a.

Soetaert, M., Decostere, A., Polet, H., Verschueren, B. and Chiers, K.: Electrotrawling: a promising alternative fishing technique warranting further exploration, Fish Fish., 16(1), 104–124, doi:10.1111/faf.12047, 2015b.

Soetaert, M., Verschueren, B., Chiers, K., Duchateau, L., Polet, H. and Decostere, A.: Laboratory Study of the Impact of Repetitive Electrical and Mechanical Stimulation on Brown Shrimp Crangon crangon, Mar. Coast. Fish., 8(1), 404–411, doi:10.1080/19425120.2016.1180333, 2016.

Solan, M.: Extinction and Ecosystem Function in the Marine Benthos, Science (80-.)., 306(5699), 1177–1180, doi:10.1126/science.1103960, 2004a.

Solan, M.: Extinction and Ecosystem Function in the Marine Benthos, Science (80-.)., 306(5699), 1177–1180, doi:10.1126/science.1103960, 2004b.

Solan, M., Wigham, B. D., Hudson, I. R., Kennedy, R., Coulon, C. H., Norling, K., Nilsson, H. C. and Rosenberg, R.: In situ quantification of bioturbation using time-lapse fluorescent sediment profile imaging (f-SPI), luminophore tracers and model simulation, Mar. Ecol. Prog. Ser., 271, 1–12, doi:10.3354/meps271001, 2004.

Solan, M., Ward, E. R., White, E. L., Hibberd, E. E., Cassidy, C., Schuster, J. M., Hale, R. and Godbold, J. A.: Worldwide measurements of bioturbation intensity, ventilation rate, and the mixing depth of marine sediments, Sci. data, 6(1), 58, doi:10.1038/s41597-019-0069-7, 2019.

Sommer, B., Fowler, A. M., Macreadie, P. I., Palandro, D. A., Aziz, A. C. and Booth, D. J.: Decommissioning of offshore oil and gas structures – Environmental opportunities and challenges, Sci. Total Environ., 658(May 2019), 973–981, doi:10.1016/j.scitotenv.2018.12.193, 2019.

Sotillo, M. G., Cailleau, S., Lorente, P., Levier, B., Aznar, R., Reffray, G., Amo-Baladrón, A., Chanut, J., Benkiran, M. and Alvarez-Fanjul, E.: The myocean IBI ocean forecast and reanalysis systems: Operational products and roadmap to the future copernicus service, J. Oper. Oceanogr., 8(1), 63–79, doi:10.1080/1755876X.2015.1014663, 2015.

Southwood, T. R. E.: Habitat, the Templet for Ecological Strategies?, J. Anim. Ecol., 46(2), 336, doi:10.2307/3817, 1977.

Stanev, E. V., Dobrynin, M., Pleskachevsky, A., Grayek, S. and Günther, H.: Bed shear stress in the southern North Sea as an important driver for suspended sediment dynamics, Ocean Dyn., 59(2), 183–194, doi:10.1007/s10236-008-0171-4, 2009.

Stide, A. H.: Offshore Tidal Sands: Processes and deposits, 1st ed., edited by A. H. Stride, Springer Netherlands, Dordrecht., 1982.

Stoll, M. H. C., Bakker, K., Nobbe, G. H. and Haese, R. R.: Continuous-flow analysis of dissolved inorganic carbon content in seawater, Anal. Chem., 73(17), 4111–4116, doi:10.1021/ac010303r, 2001.

Sturt, F., Garrow, D. and Bradley, S.: New models of North West European Holocene palaeogeography and inundation, J. Archaeol. Sci., 40(11), 3963–3976, doi:10.1016/j.jas.2013.05.023, 2013.

Tenenhaus, M. and Young, F. W.: An analysis and synthesis of multiple correspondence analysis, optimal scaling, dual scaling, homogeneity analysis and other methods for quantifying categorical multivariate data, Psychometrika, 50(1), 91–119, doi:10.1007/BF02294151, 1985.

Therkildsen, M. S. and Lomstein, B. A.: Seasonal variation in net benthic C-mineralization in a shallow estuary, FEMS Microbiol. Ecol., 12(2), 131–142, doi:10.1111/j.1574-6941.1993.tb00025.x, 1993.

Thioulouse, J., Dray, S., Dufour, A.-B., Siberchicot, A., Jombart, T. and Pavoine, S.: Multivariate Analysis of Ecological Data, 1st ed., Springer-Verlag New York, New York., 2018.

Tiano, J. C., Witbaard, R., Bergman, M. J. N., Van Rijswijk, P., Tramper, A., Van Oevelen, D., Soetaert, K. and Degraer, S.: Acute impacts of bottom trawl gears on benthic metabolism and nutrient cycling, ICES J. Mar. Sci., 76(6), 1917–1930, doi:10.1093/icesjms/fsz060, 2019.

Tiano, J. C., van der Reijden, K. J., O'Flynn, S., Beauchard, O., van der Ree, S., van der Wees, J., Ysebaert, T. and Soetaert, K.: Experimental bottom trawling finds resilience in large-bodied infauna but vulnerability for epifauna and juveniles in the Frisian Front, Mar. Environ. Res., 159(December 2019), 104964, doi:10.1016/j.marenvres.2020.104964, 2020.

Tijssen, S. B. and Wetsteyn, F. J.: Hydrographic observations near a subsurface drifter in the oyster ground, North sea, Netherlands J. Sea Res., 18(1–2), 1–12, doi:10.1016/0077-7579(84)90021-8, 1984.

Tillin, H. M., Hiddink, J. G., Jennings, S. and Kaiser, M. J.: Chronic bottom trawling alters the functional composition of benthic invertebrate communities on a sea-basin scale, Mar. Ecol. Prog. Ser., 318(August), 31–45, doi:10.3354/meps318031, 2006.

Timmermann, K., Banta, G. T. and Glud, R. N.: Linking Arenicola marina irrigation behavior to oxygen transport and dynamics in sandy sediments, J. Mar. Res., 64(6), 915–938, doi:10.1357/002224006779698378, 2007.

Todd, V. L. G., Todd, I. B., Gardiner, J. C., Morrin, E. C. N., MacPherson, N. A., DiMarzio, N. A. and Thomsen, F.: A review of impacts of marine dredging activities on marine mammals, ICES J. Mar. Sci., 72(2), 328–340, doi:10.1093/icesjms/fsu187, 2014.

Tous Rius, A., Denis, L., Dauvin, J. C. and Spilmont, N.: Macrobenthic diversity and sediment-water exchanges of oxygen and ammonium: Example of two subtidal communities of the eastern English Channel, J. Sea Res., 136(June 2017), 15–27, doi:10.1016/j.seares.2018.02.007, 2018.

Toussaint, E., De Borger, E., Braeckman, U., De Backer, A., Soetaert, K. and Vanaverbeke, J.: Faunal and environmental drivers of carbon and nitrogen cycling along a permeability gradient in shallow North Sea sediments (in review), Sci. Total Environ., 2020.

Townsend, C. R., Dolédec, S. and Scarsbrook, M. R.: Species traits in relation to temporal and spatial heterogeneity in streams: A test of habitat templet theory, Freshw. Biol., 37(2), 367–387, doi:10.1046/j.1365-2427.1997.00166.x, 1997.

Trimmer, M., Petersen, J., Sivyer, D., Mills, C., Young, E. and Parker, E.: Impact of long-term benthic trawl disturbance on sediment sorting and biogeochemistry in the southern North Sea, Mar. Ecol. Prog. Ser., 298, 79–

94, doi:10.3354/meps298079, 2005.

United Nations: Adoption of the Paris Agreement, Proposal by the President, Draft decision, Conf. Parties, Twenty-first Sess., 21932(December), 32 [online] Available from: http://unfccc.int/resource/docs/2015/cop21/eng/l09r01.pdf, 2015.

United Nations Environment Programme Ecosystems Division: Blue Economy Concept Paper. [online] Available from: https://www.unenvironment.org/resources/report/blue-economy-concept-paper, 2014.

Upton, A. C., Nedwell, D. B., Parkes, R. J. and Harvey, S. M.: Seasonal benthic microbial activity in the southern North Sea - Oxygen uptake and sulphate reduction, Mar. Ecol. Prog. Ser., 101(3), 273–282, doi:10.3354/meps101273, 1993.

Valdemarsen, T., Kristensen, E. and Holmer, M.: Sulfur, carbon, and nitrogen cycling in faunated marine sediments impacted by repeated organic enrichment, Mar. Ecol. Prog. Ser., 400, 37–53, doi:10.3354/meps08400, 2010.

Van, W., Malschaert, H. and Van, H.: Tidal resuspension and deposition of particulate matter in the Oyster Grounds, North Sea, J. Mar. Res., 56(1), 257–291, doi:10.1357/002224098321836181, 1998.

Vanaverbeke, J., Merckx, B., Degraer, S. and Vincx, M.: Sediment-related distribution patterns of nematodes and macrofauna: Two sides of the benthic coin?, Mar. Environ. Res., 71(1), 31–40, doi:10.1016/j.marenvres.2010.09.006, 2011.

Vanaverbeke, J., Van Colen, C., Moens, T., Voet, H., Degraer, S., Soetaert, K. and Vlaminck, E.: Experimenteel onderzoek naar een toekomstig duurzaam gebruik van artificiële harde substraten in de Noordzee (PERSUADE), [online] Available from: https://www.belspo.be/belspo/fedra/proj.asp?l=nl&COD=BR%2F175%2FA1%2FPERSUADE (Accessed 8 October 2020), 2020.

Vasquez-Cardenas, D., Quintana, C. O., Meysman, F. J. R., Kristensen, E. and Boschker, H. T. S.: Species-specific effects of two bioturbating polychaetes on sediment chemoautotrophic bacteria, Mar. Ecol. Prog. Ser., 549, 55–68, doi:10.3354/meps11679, 2016.

van de Velde, S. and Meysman, F. J. R.: The Influence of Bioturbation on Iron and Sulphur Cycling in Marine Sediments: A Model Analysis, Aquat. Geochemistry, 22(5–6), 469–504, doi:10.1007/s10498-016-9301-7, 2016.

Van De Velde, S., Van Lancker, V., Hidalgo-Martinez, S., Berelson, W. M. and Meysman, F. J. R.: Anthropogenic disturbance keeps the coastal seafloor biogeochemistry in a transient state, Sci. Rep., 8(1), doi:10.1038/s41598-018-23925-y, 2018.

Vermaat, J. E., McQuatters-Gollop, A., Eleveld, M. A. and Gilbert, A. J.: Past, present and future nutrient loads of the North Sea: Causes and consequences, Estuar. Coast. Shelf Sci., 80(1), 53–59, doi:10.1016/j.ecss.2008.07.005, 2008.

Violle, C., Navas, M. L., Vile, D., Kazakou, E., Fortunel, C., Hummel, I. and Garnier, E.: Let the concept of trait be functional!, Oikos, 116(5), 882–892, doi:10.1111/j.0030-1299.2007.15559.x, 2007.

VMM, Vito, Awac, IBGE-BIM, IRCEL-CELINE and ECONOTEC: Belgium ' s greenhouse gas inventory (1990-2018) National Inventory Report., 2020.

Volkenborn, N., Hedtkamp, S. I. C., van Beusekom, J. E. E. and Reise, K.: Effects of bioturbation and bioirrigation by lugworms (Arenicola marina) on physical and chemical sediment properties and implications for intertidal habitat succession, Estuar. Coast. Shelf Sci., 74(1–2), 331–343, doi:10.1016/j.ecss.2007.05.001, 2007.

Volkenborn, N., Woodin, S., Wethey, D. and Polerecky, L.: Bioirrigation in Marine Sediments, in Reference Module in Earth Systems and Environmental Sciences, pp. 1–9, Elsevier Inc., 2016.

de Vooys, C. G. N., Dapper, R., van der Meer, J., Lavaleye, M. S. S. and Lindeboom, H. J.: Het macrobenthos op het nederlands continentale plat in de Noordzee in de periode 1870-1914 en een poging tot vergelijking met de

situatie in de periode 1970-2000, Den Burg., 2004.

Voyer, M., Quirk, G., McIlgorm, A. and Azmi, K.: Shades of blue: what do competing interpretations of the Blue Economy mean for oceans governance?, J. Environ. Policy Plan., 20(5), 595–616, doi:10.1080/1523908X.2018.1473153, 2018.

Warner, J. C., Armstrong, B., He, R. and Zambon, J. B.: Development of a Coupled Ocean-Atmosphere-Wave-Sediment Transport (COAWST) Modeling System, Ocean Model., 35(3), 230–244, doi:10.1016/j.ocemod.2010.07.010, 2010.

Warren, L. M.: The Ecology of Capitella capitata in British Waters, J. Mar. Biol. Assoc. United Kingdom, 57(1), 151–159, doi:10.1017/S0025315400021305, 1977.

Watling, L., Findlay, R. H., Mayer, L. M. and Schick, D. F.: Impact of a scallop drag on the sediment chemistry, microbiota, and faunal assemblages of a shallow subtidal marine benthic community, J. Sea Res., 46(3–4), 309–324, doi:10.1016/S1385-1101(01)00083-1, 2001.

Watson, R. A. and Morato, T.: Fishing down the deep: Accounting for within-species changes in depth of fishing, Fish. Res., 140, 63–65, doi:10.1016/j.fishres.2012.12.004, 2013.

Wentworth, C. K.: A Scale of Grade and Class Terms for Clastic Sediments, J. Geol., 30(5), 377–392, doi:www.jstor.org/stable/30063207, 1922.

West, B. T., Welch, K. B. and Galecki, A. T.: Linear Mixed Models, Chapman and Hall/CRC., 2014.

Weston, K., Fernand, L., Mills, D. K., Delahunty, R. and Brown, J.: Primary production in the deep chlorophyll maximum of the central North Sea, J. Plankton Res., 27(9), 909–922, doi:10.1093/plankt/fbi064, 2005.

Weston, K., Fernand, L., Nicholls, J., Marca-Bell, A., Mills, D., Sivyer, D. and Trimmer, M.: Sedimentary and water column processes in the Oyster Grounds: A potentially hypoxic region of the North Sea, Mar. Environ. Res., 65(3), 235–249, doi:10.1016/j.marenvres.2007.11.002, 2008.

Wetzel, M. A., Leuchs, H. and Koop, J. H. E.: Preservation effects on wet weight, dry weight, and ash-free dry weight biomass estimates of four common estuarine macro-invertebrates: No difference between ethanol and formalin, Helgol. Mar. Res., 59(3), 206–213, doi:10.1007/s10152-005-0220-z, 2005.

Wheatcroft, R. a., Jumars, P. a., Smith, C. R. and Nowell, a. R. M.: A mechanistic view of the particulate biodiffusion coefficient: Step lengths, rest periods and transport directions, J. Mar. Res., 48(1), 177–207, doi:10.1357/002224090784984560, 1990.

Wilde, P. A. W. J. D., Berghuis, E. M. and Kok, A.: Structure and energy demand of the benthic community of the oyster ground, central North Sea, Netherlands J. Sea Res., 18(1–2), 143–159, doi:10.1016/0077-7579(84)90029-2, 1984.

de Wilde, P. A. W. J., Berghuis, E. M. and Kok, A.: Biomass and activity of benthic fauna on the fladen ground (northern North Sea), Netherlands J. Sea Res., 20(2–3), 313–323, doi:10.1016/0077-7579(86)90053-0, 1986.

Wilson, A. M., Huettel, M. and Klein, S.: Grain size and depositional environment as predictors of permeability in coastal marine sands, Estuar. Coast. Shelf Sci., 80(1), 193–199, doi:10.1016/j.ecss.2008.06.011, 2008.

Wilson, R. J., Speirs, D. C., Sabatino, A. and Heath, M. R.: A synthetic map of the north-west European Shelf sedimentary environment for applications in marine science, Earth Syst. Sci. Data, 10(1), 109–130, doi:10.5194/essd-10-109-2018, 2018.

Wimpenny, R. S.: The Plaice: Being the Buckland Lectures for 1949, E. Arnold, London. [online] Available from: https://books.google.be/books?id=-lZBAAAAYAAJ, 1953.

Wollast, R.: Evaluation and comparison of the global carbon cycle in the coastal zone and in the open ocean, in The sea, vol. 10, edited by K. H. Brink and A. Robinson, pp. 213–252, John Wiley & Sons, Inc., Hoboken, New Jersey., 1998.

Wrede, A., Beermann, J., Dannheim, J., Gutow, L. and Brey, T.: Organism functional traits and ecosystem supporting services – A novel approach to predict bioirrigation, Ecol. Indic., 91(April), 737–743, doi:10.1016/j.ecolind.2018.04.026, 2018a.

Wrede, A., Beermann, J., Dannheim, J., Gutow, L. and Brey, T.: Organism functional traits and ecosystem supporting services – A novel approach to predict bioirrigation, Ecol. Indic., 91, 737–743, doi:10.1016/j.ecolind.2018.04.026, 2018b.

Wrede, A., Andresen, H., Asmus, R., Wiltshire, K. H. and Brey, T.: Macrofaunal irrigation traits enhance predictability of nutrient fluxes across the sediment-water interface, Mar. Ecol. Prog. Ser., 632(2004), 27–42, doi:10.3354/meps13165, 2019.

Wright, S. W.: Improved HPLC method for the analysis of chlorophylls and carotenoids from marine phytoplankton, Mar. Ecol. Prog. Ser., 77(2–3), 183–196, doi:10.3354/meps077183, 1991.

Ysebaert, T. and Herman, P. M. J.: Spatial and temporal variation in benthic macrofauna and relationships with environmental variables in an estuarine, intertidal soft-sediment environment, Mar. Ecol. Prog. Ser., 244(May 2016), 105–124, doi:10.3354/meps244105, 2002.

Zapata, M., Rodriquez, F. and Garrido, J.: Separation of chlorophylls and carotenoids from marine phytoplankton: a new HPLC method using a …, Mar. Ecol. Prog. Ser., 195, 29–45, doi:10.3354/meps195029, 2000.

van der Zee, C. and Chou, L.: Seasonal cycling of phosphorus in the southern bight of the North Sea, Biogeosciences Discuss., 1(1), 681–707, doi:10.5194/bgd-1-681-2004, 2004.

Zhang, W. and Wirtz, K.: Mutual Dependence Between Sedimentary Organic Carbon and Infaunal Macrobenthos Resolved by Mechanistic Modeling, J. Geophys. Res. Biogeosciences, 122(10), 2509–2526, doi:10.1002/2017JG003909, 2017.

Zuur, A. F., Ieno, E. N. and Smith, G. M.: Analysing Ecological Data, Springer, New-York., 2007.

Zuur, A. F., Ieno, E. N., Walker, N., Saveliev, A. A. and Smith, G. M.: Mixed effects models and extensions in ecology with R, Springer New York, New York, NY., 2009.

APPENDICES

Appendix A: Chapter 2

A.1. Overview of the sampling stations

Table A 1: Sampling date, coordinates, depth and bottom water temperature for each station per year.

Station	Sampling date	Latitude	Longitude	Depth (m)	Bottom water temperature (°C)	Salinity (‰)	Overlying water Incubations (mL)		
2016							Rep. A	Rep. B	Rep. C
130	6/9/2016	51°16.258	2°54.3	11	20.0	34.3	940.9	874.9	744.6
780	5/9/2016	51°28.289	3°3.501	22	20.1	32.9	801.1	805.8	702.1
BRN11	7/9/2016	51°18.518	2°36.147	24	19.4	34.4	5086.5	5086.5	5086.5
330	5/9/2016	51°26.005	2°48.519	22	19.7	33.8	5613.9	5080.8	5630.9
BBEG	6/9/2016	51°40.328	2°50.276	26	19.8	33.5	4491.1	5131.9	4564.8
2017									
130	4/9/2017	51°16.259	2°54.264	13	19.5	33.6	645.6	581.2	593.8
120	28/8/2017	51°11.106	2°42.1	11	19.8	34.8	922.1	812.1	805.8
780	7/9/2017	51°28.291	3°3.467	20	19.2	32.3	777.5	625.2	794.8
BRN11	28/8/2017	51°18.516	2°36.139	24	19.1	34.9	4394.7	4196.2	5245.3
D6N	25/8/2017	51°33.149	2°55.439	20	19.0	34.9	5557.2	5052.5	4910.7
330	4/9/2017	51°26.113	2°48.482	23	19.3	34.4	4791.6	4598.8	3918.4
D6S	25/8/2017	51°32.941	2°55.427	21	19.1	34.8	4831.3	4729.3	5528.8

A.2. Overview of fluxes and estimated rates

Table A 2: Measured sediment community oxygen consumption, fluxes of dissolved inorganic carbon, NH_x, and NO_x (mmol m^{-2} d^{-1}, average values ± sd for the three replicates per year), and modelled process rates for oxic and anoxic mineralization (Oxic Min, Anoxic Min, *mmol C m^{-2} d^{-1}*), nitrification, denitrification, DNRA, and total N mineralization (Nitr, Denitr, DNRA, Nmin, *mmol N m^{-2} d^{-1}*), and the reoxidation of reduced substances (Reoxid, *mmol O_2 m^{-2} d^{-1}*). Negative values represent fluxes into the sediment, except for SCOC, which is per definition a flux into the sediment.

Year	Station	SCOC	DIC	RQ	NH$_x$	NO$_x$	Oxic Min	Anoxic Min	Nitr	Denitr	DNRA	Nmin	Reoxid
	130	31.2 ± 19.1	213.0 ± 15.9	6.37 ± 2.21	7.6 ± 10.2	1.0 ± 0.1	5.8 ± 10	187.8 ± 23.8	15.3 ± 2.4	14.3 ± 2.6	0 ± 0	33 ± 2.5	0 ± 0
	780	48.7 ± 2.2	66.6 ± 21.4	1.38 ± 0.46	8.5 ± 1.8	0.6 ± 0.4	35.2 ± 7.5	29.7 ± 12.5	4 ± 1.8	1.5 ± 1.3	2 ± 3.5	10.4 ± 3.3	5.5 ± 5
2016	BRN11	23.5 ± 6.5	12.3 ± 28.4	0.67 ± 0.94	-1.9 ± 2.0	0.1 ± 0.3	2 ± 1.8	9.1 ± 14.6	10.5 ± 2.2	4.5 ± 5.5	6 ± 5.2	2.6 ± 3.6	0.4 ± 0.8
	330	32.4 ± 1.1	31.0 ± 4.1	0.96 ± 0.15	0.6 ± 0.4	0.5 ± 0.3	16.1 ± 1.7	10.3 ± 2.1	5.2 ± 1.2	3.7 ± 0.5	1 ± 1.7	4.8 ± 0.6	5.8 ± 0.5
	BBEG	19.7 ± 16.6	13.7 ± 10.1	1.73 ± 2.13	2.1 ± 5.4	0.7 ± 1.1	5.6 ± 7.8	7.6 ± 6.1	6.3 ± 7.7	0.4 ± 0.6	6.5 ± 8.3	2.1 ± 1.6	2.3 ± 3.1
	130	48.8 ± 9.3	123.6 ± 89.5	2.40 ± 1.54	41.5 ± 18.1	-0.1 ± 0.2	43.1 ± 19.3	82.3 ± 72.6	1.3 ± 2.2	0 ± 0	12.3 ± 7	19.6 ± 13.9	3.2 ± 5.6
	780	57.3 ± 15.1	76.2 ± 2.6	1.39 ± 0.41	4.1 ± 1.5	-0.5 ± 2.3	33.7 ± 7.5	32.2 ± 10.7	8.2 ± 1.3	8.3 ± 0.4	0.4 ± 0.6	11.9 ± 0.4	7.2 ± 10.1
	120	24.0 ± 1.0	31.2 ± 7.0	1.31 ± 0.34	0.8 ± 0.2	0.4 ± 0.5	13.2 ± 1.3	13.3 ± 5.7	4.3 ± 0.8	3.7 ± 1.2	0.2 ± 0.4	4.9 ± 1.1	2.1 ± 2.5
2017	BRN11	36.6 ± 2.4	37.6 ± 7.3	1.02 ± 0.14	0.8 ± 0.8	0.3 ± 0.2	18.8 ± 2	12.8 ± 2.8	5.9 ± 0.9	4.8 ± 2.0	0.8 ± 1.3	5.9 ± 1.1	6.1 ± 1
	D6N	23.3 ± 5.5	9.1 ± 1.4	0.41 ± 0.05	-1.4 ± 7.4	3.1 ± 6.5	3.3 ± 3.3	2.7 ± 2.4	9.5 ± 4.1	2.8 ± 4.9	5.1 ± 5.2	1.5 ± 0.2	1.1 ± 1.9
	330	28.9 ± 2.5	15.9 ± 2.7	0.56 ± 0.14	-0.7 ± 0.9	-0.4 ± 0.3	7.6 ± 1.5	3.8 ± 0.8	8.7 ± 2.1	3.5 ± 0.9	5.5 ± 2.6	2.5 ± 0.4	3.8 ± 0.7
	D6S	13.7 ± 2.5	0.2 ± 0.2	0.01 ± 0.01	1.5 ± 2.4	-0.2 ± 0.2	0.1 ± 0.1	0.1 ± 0.1	6.8 ± 1.2	0 ± 0	7.6 ± 1.6	0.03 ± 0.03	0.1 ± 0.1

A.3. Relative mineralization rates
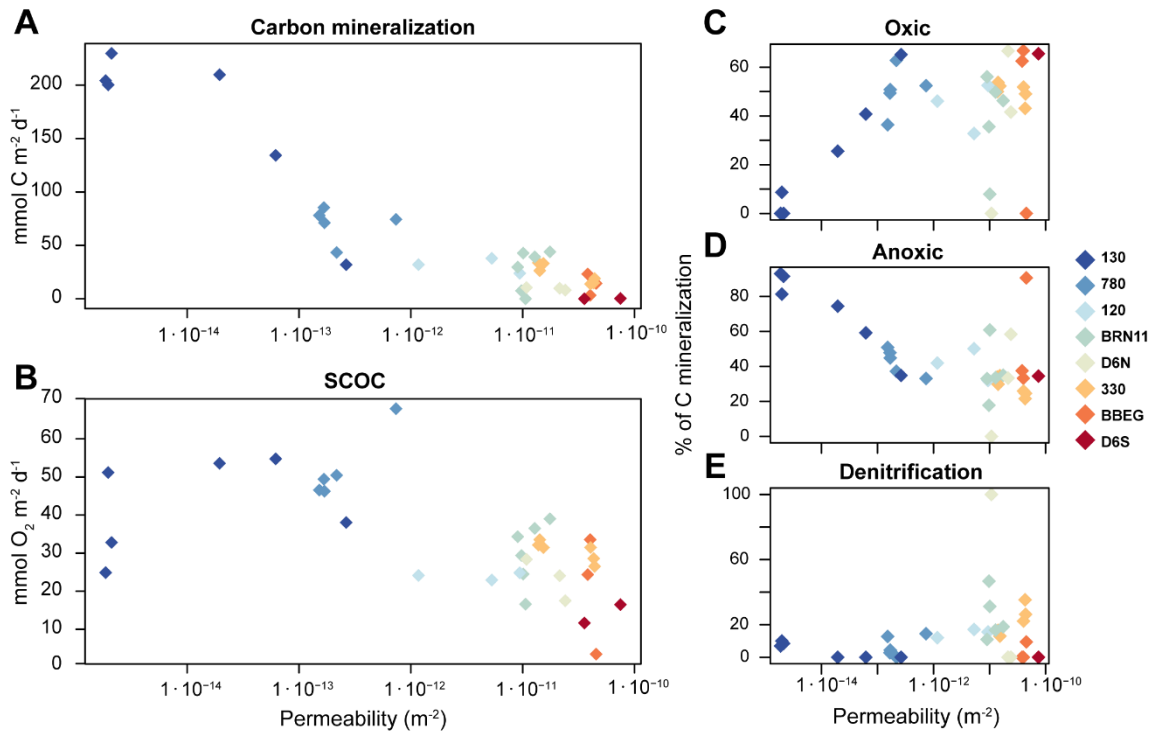
Figure A 1: Carbon mineralization processes: (A) Total organic carbon mineralization (mmol C m^{-2} d^{-1}); (B) Sediment community oxygen consumption (mmol O$_2$ m^{-2} d^{-1}); (C) - (E) Relative contribution of of carbon mineralization allocated to oxic or anoxic mineralization, or denitrification (% of total). Values represented as a function of log transformed permeability (x-axis). Permeability gradient indicated by different colors (see legend).

A.4. Correlation between the Irrigation Potential of the community and the measured irrigation rate
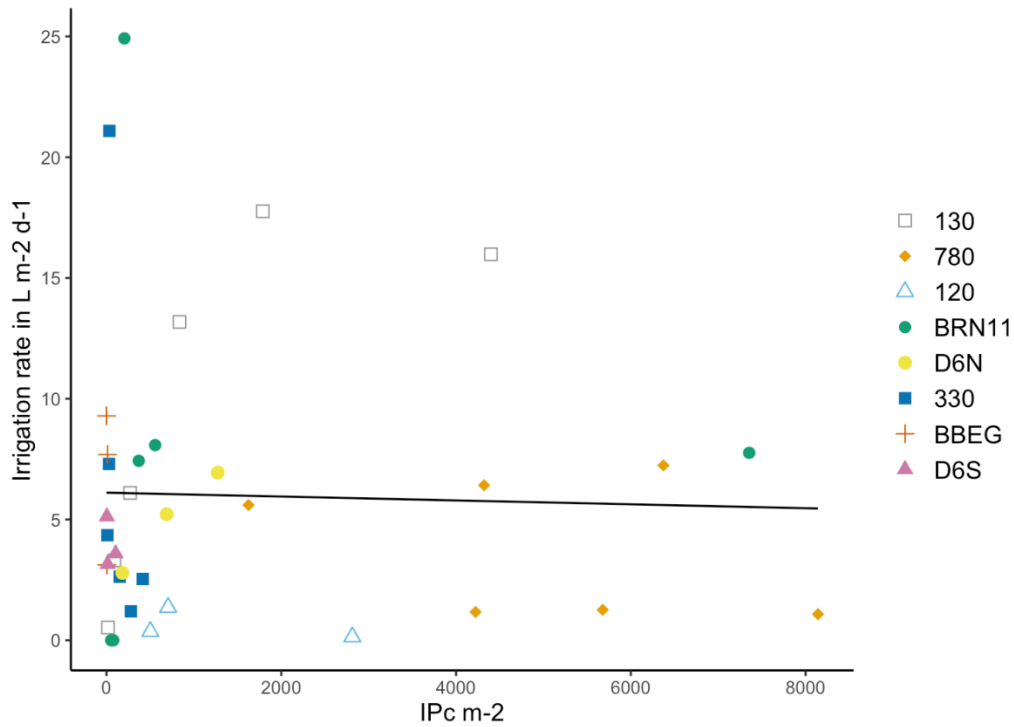
Figure A 2: Tracer derived irrigation rate as a function of the IP_c for all stations, both years combined.

Pearson correlation R = -0.03

A.5. Species table

Table A 3: Species biomass (gWW m^{-2}) and densities (ind. m^{-2}) for each station (average ± sd), per year.

Station	Species	Biomass	Density
		gWW m^{-2}	*ind. m^{-2}*
2016			
	Abra alba	0.42 ± 0.73	11.78 ± 20.4
130	*Limecola balthica*	1.31 ± 1.61	23.56 ± 20.4
	Ophiura ophiura	1.11 ± 0.81	47.11 ± 20.4
	Abra alba	170.9 ± 42.29	82.45 ± 20.4
	Amphiuridae	12.6 ± 21.83	11.78 ± 20.4
	Anthozoa	22.38 ± 38.76	11.78 ± 20.4
	Eunereis longissima	5.15 ± 8.92	11.78 ± 20.4
	Fabulina fabula	9.19 ± 7.96	23.56 ± 20.4
780	*Kurtiella bidentata*	0.18 ± 0.15	23.56 ± 20.4
	Lanice conchilega	1.16 ± 2.01	70.67 ± 122.41
	Nephtys hombergii	4.36 ± 3.77	23.56 ± 20.4
	Owenia fusiformis	44.97 ± 0	47.11 ± 20.4
	Phyllodoce mucosa	0.01 ± 0.01	11.78 ± 20.4
	Scoloplos armiger	0.01 ± 0.01	23.56 ± 20.4

	Species		
	Spiophanes bombyx	0.06 ± 0.06	47.11 ± 47.11
	Bathyporeia elegans	0.12 ± 0.11	35.34 ± 35.34
	Bathyporeia guilliamsoniana	0.47 ± 0.16	58.89 ± 40.8
	Diogenes pugilator	0.18 ± 0.32	11.78 ± 20.4
BRN11	*Lanice conchilega*	2.31 ± 4	113.54 ± 51.22
	Nephtys cirrosa	2.09 ± 2.12	47.11 ± 20.4
	Pontocrates altamarinus	0.01 ± 0.02	11.78 ± 20.4
	Urothoe brevicornis	0.58 ± 0.89	106.01 ± 127.4
	Bathyporeia elegans	0.06 ± 0.08	23.56 ± 20.4
	Gastrosaccus spinifer	0.06 ± 0.11	11.78 ± 20.4
	Nemertea	0.96 ± 1.66	11.78 ± 20.4
	Nephtys cirrosa	5.54 ± 9.19	23.56 ± 20.4
	Ophiura ophiura	0.06 ± 0.11	11.78 ± 20.4
330	*Pontocrates altamarinus*	0 ± 0	11.78 ± 20.4
	Spio sp.	0.24 ± 0.42	11.78 ± 20.4
	Spiophanes bombyx	0.1 ± 0.1	129.56 ± 129.56
	Thia scutellata	0.1 ± 0.17	11.78 ± 20.4
	Travisia forbesii	0.25 ± 0.44	11.78 ± 20.4
	Urothoe brevicornis	1.63 ± 1.44	530.04 ± 498.47
	Spiophanes bombyx	0.06 ± 0.06	47.11 ± 47.11
BBEG	*Cirratulidae*	0.61 ± 1.05	11.78 ± 20.4
	Tellina sp.	0.14 ± 0.24	11.78 ± 20.4
2017			
	Abra alba	193.03 ± 84.55	534.19 ± 185.05
	Cirratulidae	0.01 ± 0.01	85.47 ± 74.02
	Eunereis longissima	4.39 ± 7.61	42.74 ± 74.02
	Kurtiella bidentata	5.66 ± 9.46	1196.58 ± 1962.56
	Lagis koreni	10.03 ± 17.37	42.74 ± 74.02
130	*Limecola balthica*	5.34 ± 9.03	85.47 ± 74.02
	Myrianida sp.	0 ± 0	42.74 ± 74.02
	Mytilus edulis	0.05 ± 0.05	128.21 ± 128.21
	Nephtys hombergii	4.33 ± 7.51	42.74 ± 74.02
	Oligochaeta	0.04 ± 0.04	256.41 ± 222.06
	Spisula subtruncata	129.5 ± 214.85	128.21 ± 128.21
	Abludomelita obtusata	0.01 ± 0.01	64.1 ± 90.65
	Abra alba	490.65 ± 433.79	1602.56 ± 1359.82
780	*Diastylis bradyi*	0.35 ± 0.5	64.1 ± 90.65
	Fabulina fabula	82.21 ± 44.4	576.92 ± 90.65
	Glycera sp.	0.05 ± 0.06	128.21 ± 0
	Kurtiella bidentata	1.98 ± 0.38	833.33 ± 271.96

	Magelona johnstoni	0.45 ± 0.63	192.31 ± 271.96
	Myrianida sp.	0.01 ± 0	128.21 ± 0
	Nephtys hombergii	5.97 ± 8.44	64.1 ± 90.65
	Oligochaeta	0.05 ± 0.08	256.41 ± 362.62
	Ophiura sp.	1.16 ± 1.64	64.1 ± 90.65
	Owenia fusiformis	22.68 ± 1.82	128.21 ± 0
	Pariambus typicus	0.01 ± 0.02	64.1 ± 90.65
	Pholoe baltica	0.3 ± 0.43	64.1 ± 90.65
	Phyllodocidae	0.01 ± 0.01	64.1 ± 90.65
	Scoloplos armiger	0.02 ± 0.03	64.1 ± 90.65
	Sigalion mathildae	0.01 ± 0.01	64.1 ± 90.65
	Tellina sp.	0.17 ± 0.24	128.21 ± 181.31
	Abludomelita obtusata	0.16 ± 0.22	170.94 ± 195.84
	Abra alba	4.96 ± 8.3	341.88 ± 195.84
	Anthozoa	143.19 ± 128.3	85.47 ± 74.02
	Aonides oxycephala	0.3 ± 0.52	42.74 ± 74.02
	Capitella sp.	0.03 ± 0.05	85.47 ± 74.02
	Cirratulidae	0.14 ± 0.23	170.94 ± 195.84
	Crepidula fornicata	0.1 ± 0.17	42.74 ± 74.02
	Ensis directus	284.58 ± 492.9	42.74 ± 74.02
	Eumida sanguinea	0.07 ± 0.1	256.41 ± 339.2
	Eteone sp.	0.04 ± 0.03	128.21 ± 128.21
	Fabulina fabula	1.14 ± 1.98	170.94 ± 296.08
	Glycera sp.	0.19 ± 0.23	170.94 ± 74.02
	Kurtiella bidentata	1.08 ± 0.94	598.29 ± 533.76
120	*Magelona johnstoni*	0.39 ± 0.08	256.41 ± 0
	Mediomastus fragilis	0.02 ± 0.03	128.21 ± 128.21
	Megaluropus agilis	0.01 ± 0.01	42.74 ± 74.02
	Myrianida sp.	0.02 ± 0.03	213.68 ± 266.88
	Mytilus edulis	0.1 ± 0.05	256.41 ± 128.21
	Oligochaeta	0.17 ± 0.13	683.76 ± 195.84
	Owenia fusiformis	1.33 ± 1.26	85.47 ± 74.02
	Pariambus typicus	0.02 ± 0.04	128.21 ± 222.06
	Phyllodoce mucosa	0.38 ± 0.33	213.68 ± 195.84
	Sigalion mathildae	0.01 ± 0.02	42.74 ± 74.02
	Spiophanes bombyx	1.15 ± 1.15	42.74 ± 42.74
	Spirobranchus triqueter	0.04 ± 0.04	128.21 ± 128.21
	Sthenelais boa	8.92 ± 15.45	42.74 ± 74.02
	Tellina sp.	0.19 ± 0.2	128.21 ± 128.21
	Venerupis sp.	0.14 ± 0.25	42.74 ± 74.02

	Acrocnida brachiata	5.17 ± 8.95	11.78 ± 20.4
	Anthozoa	0.05 ± 0.08	11.78 ± 20.4
	Bathyporeia guilliamsoniana	0.1 ± 0.18	23.56 ± 40.8
	Callianassidae	6.65 ± 11.52	11.78 ± 20.4
	Cirratulidae	0.01 ± 0.02	23.56 ± 40.8
	Echinocardium cordatum	106.55 ± 184.55	11.78 ± 20.4
	Eteone sp.	0.05 ± 0.05	35.34 ± 35.34
	Euspira sp.	0.37 ± 0.64	11.78 ± 20.4
	Iphinoe trispinosa	0.04 ± 0.07	23.56 ± 40.8
	Kurtiella bidentata	0.01 ± 0.01	23.56 ± 40.8
	Lagis koreni	1.47 ± 2.54	11.78 ± 20.4
	Leucothoe incisa	0.04 ± 0.07	23.56 ± 40.8
	Magelona johnstoni	0.02 ± 0.03	11.78 ± 20.4
BRN11	*Mytilus edulis*	0 ± 0.01	11.78 ± 20.4
	Nephtys cirrosa	6.68 ± 11.26	47.11 ± 53.98
	Nephtys sp.	0.02 ± 0.02	23.56 ± 20.4
	Phoronis pallida	0.21 ± 0.36	23.56 ± 40.8
	Phyllodoce mucosa	0.48 ± 0.83	11.78 ± 20.4
	Poecilochaetus serpens	0.76 ± 1.32	82.45 ± 142.81
	Processa modica	1.38 ± 2.38	23.56 ± 40.8
	Pseudocuma simile	0 ± 0	11.78 ± 20.4
	Spirobranchus triqueter	0 ± 0	11.78 ± 20.4
	Thracia phaseolina	8.9 ± 12.64	35.34 ± 35.34
	Tornus subcarinatus	0.01 ± 0.02	23.56 ± 40.8
	Tritia reticulata	17.4 ± 30.13	11.78 ± 20.4
	Urothoe brevicornis	0.47 ± 0.72	117.79 ± 102.01
	Urothoe poseidonis	0.17 ± 0.14	47.11 ± 40.8
	Urothoe sp.	0.02 ± 0.01	70.67 ± 0
	Aricidea minuta	0 ± 0	11.78 ± 20.4
	Bathyporeia elegans	0.22 ± 0.37	106.01 ± 183.61
	Bathyporeia sp.	0 ± 0	23.56 ± 40.8
	Branchiostoma lanceolatum	0 ± 0.01	11.78 ± 20.4
	Crangon crangon	0.03 ± 0.05	11.78 ± 20.4
	Diastylis bradyi	0.01 ± 0.02	11.78 ± 20.4
D6N	*Diogenes pugilator*	1.9 ± 2.45	82.45 ± 81.6
	Echinocardium cordatum	9.5 ± 11.26	35.34 ± 35.34
	Eteone sp.	0.13 ± 0.08	129.56 ± 73.56
	Euspira nitida	0.05 ± 0.08	11.78 ± 20.4
	Glycera lapidum	0.04 ± 0.07	11.78 ± 20.4
	Megaluropus agilis	0.02 ± 0.02	117.79 ± 102.01

	Species		
	Mytilus edulis	0 ± 0.01	11.78 ± 20.4
	Nephtys cirrosa	5.66 ± 2.04	70.67 ± 35.34
	Nephtys sp.	0.1 ± 0.1	58.89 ± 53.98
	Nototropis falcatus	0 ± 0	11.78 ± 20.4
	Ophelia sp.	0 ± 0.01	11.78 ± 20.4
	Ophiura sp.	0.42 ± 0.5	58.89 ± 53.98
	Processa sp.	0.05 ± 0.09	11.78 ± 20.4
	Pseudocuma simile	0.02 ± 0.02	35.34 ± 35.34
	Scolelepis bonnieri	0.2 ± 0.35	11.78 ± 20.4
	Spiophanes bombyx	0.25 ± 0.25	11.78 ± 11.78
	Spisula elliptica	3.1 ± 4.2	23.56 ± 20.4
	Tellimya ferruginosa	0.02 ± 0.04	23.56 ± 40.8
	Urothoe brevicornis	0.6 ± 0.22	223.79 ± 142.81
	Urothoe sp.	0.08 ± 0.06	153.12 ± 73.56
330	*Gastrosaccus spinifer*	0.51 ± 0.45	70.67 ± 35.34
	Glycera lapidum	0.04 ± 0.07	11.78 ± 20.4
	Jassa herdmani	0.01 ± 0.02	11.78 ± 20.4
	Liocarcinus sp.	0.4 ± 0.69	11.78 ± 20.4
	Mytilus edulis	0 ± 0.01	11.78 ± 20.4
	Nephtys cirrosa	0.76 ± 1.32	11.78 ± 20.4
	Nephtys sp.	0.24 ± 0.38	47.11 ± 53.98
	Pontocrates altamarinus	0.01 ± 0.02	23.56 ± 40.8
D6S	*Bivalvia*	0.01 ± 0.02	8.83 ± 17.67
	Branchiostoma lanceolatum	0 ± 0.01	8.83 ± 17.67
	Gastropoda	0 ± 0.01	8.83 ± 17.67
	Gastrosaccus spinifer	0.01 ± 0.03	8.83 ± 17.67
	Glycera sp.	0.05 ± 0.07	97.17 ± 171.6
	Mytilus edulis	0.04 ± 0.05	106.01 ± 122.41
	Nephtys cirrosa	2.46 ± 4.52	26.5 ± 33.83
	Nephtys sp.	0.01 ± 0.02	8.83 ± 17.67
	Ophelia sp.	0 ± 0	17.67 ± 35.34
	Pontocrates altamarinus	0.01 ± 0.02	8.83 ± 17.67

Appendix B: Chapter 4

B.1. Calculation of equilibrium constant.

The calculation of the equilibrium constant Eq_A (mL g^{-1}) was done for sediment from incubation cores of Dortsman and Zandkreek. The Eq_A value was determined from batch adsorption experiments.

B.1.1. Sensor calibration

A fluorescence spectrophotometer (Varian Cary Eclipse fluorescence spectrophotometer) was calibrated with a dilution series of uranine. Uranine solutions of 0 µg/L, 2 µg/L, 5 µg/L, 10 µg/L, 15 µg/L and 20 µg/L were prepared by diluting a starting concentration of 1 mg L^{-1} of uranine salts (sodium fluoresceine - $C_{20}H_{10}NaO_5^-$) in 0.2 µm filtered Oosterschelde water. The fluorescence (RFUB) of each concentration was determined in 10 mm × 10 mm cuvettes, for an excitation wavelength λ_{exc} of 494 nm, and an emission wavelength λ_{emi} of 513 nm (Gerke et al., 2013). This delivered the following calibration line (Eq. S1) with R^2 = 0.998:

$$RFUB = 0.565 + 3.085 \cdot Concentration\ (\mu g\ L^{-1}) \qquad (Eq.\ B1)$$

B.1.2. Sediment adsorption

F_w: Fluorescence of water
F_m: Fluorescence water-sediment mix

F_c: Fluorescence spike blank cores
F_e: Fluorescence spiked water-sediment mix after 24 hours (equilibrium)
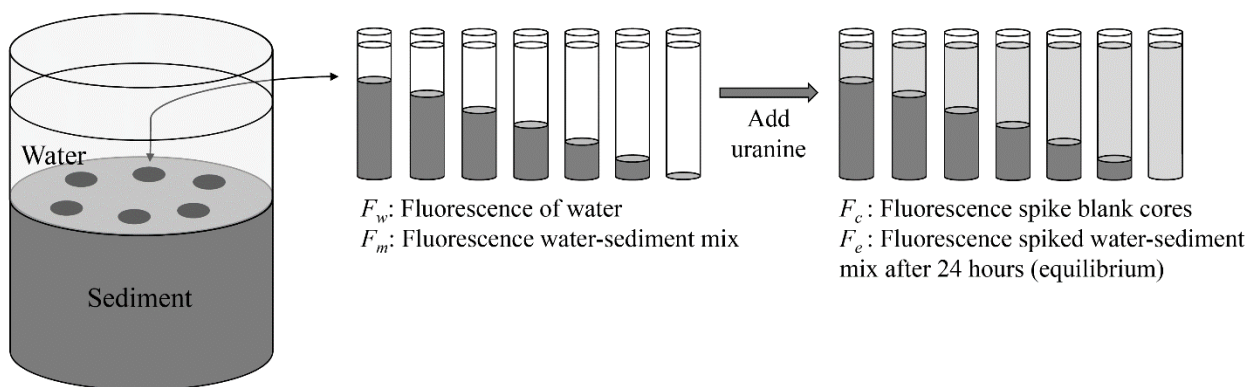
Figure B 1: Batch adsorption experiment design, and explanation of the measured fluorescence values.

Additional Ø 14 cm sediment cores were collected from Zandkreek, and Dortsman for batch adsorption experiments. These cores were left to left to equilibrate for 48 hours with the same setup as per materials and methods in the main manuscript. Subsequently 7 subcores (3.6 cm diameter) were collected with increasing amounts of sediment, starting from 0 cm of sediment (only overlying water) (Figure B1). An initial sample was taken from the overlying water and measured as the F_w (RFUB water). Subsequently the subcores were vigorously shaken for 1 minute, and left on a shaking table for 12 hours (in previous tests it became clear that substances could leech out of the sediment, thus affecting the fluorescence reading. With this step it is ensured that all substances are in equilibrium), after which a second sample was taken as the F_m value (RFUB sediment-water mixture). The overlying water in the cores was then spiked with uranine, with 3 mL of a 1 mg L^{-1} uranine stock solution, and cores were vigorously shaken for 1 minute. The F_c (RFUB

of the initial spike) was calculated afterwards, from the water volume in the core (overlying water volume + porewater volume), and the spike concentration. The cores were then placed on the shaking table, to keep the overlying water in movement, for 24 hours. After 24 hours the fluorescence was measured again to obtain F_e values (RFUB equilibrium). After the experiment, the overlying water was collected, and the volume determined. Also the sediment was collected, and freeze dried to acquire the sediment mass Msed. The difference between the wet, and the dried sediment mass was used to calculate the total volume of water (Vol) in the core.

Throughout this experiment each measurement was performed by removing a volume of 10 mL of sample, into a 15 mL centrifuge tube. The sample was then centrifuged for 6 minutes at 1500 rpm to remove colloids from suspension, which affect the fluorescence reading in a non-replicable way. The extracted sample was then added again to the core.

B.1.3. Calculations

The adsorbed equilibrium concentration (μg uranine adsorbed g^{-1} dry sediment) is calculated by dividing the initial spike concentration (F_c - F_w) minus the equilibrium concentration (F_e - F_m) by the sediment concentration in each subcore:

$$q_{ads} = \frac{((F_c - F_w) - (F_e - F_m)) \times \text{Vol}}{\text{Msed}}$$

(Eq. B2)

The water equilibrium concentration (μg uranine L^{-1}):

$$C_e = Fe - Fm$$

(Eq. B3)

The equilibrium constant (mL g^{-1}) is then the amount of uranine adsorbed by the sediment, divided by the equilibrium concentration in the water:

$$Eq_A = \frac{q_{ads}}{C_e}$$

(Eq. B4)

Eq_A in mL g^{-1}

B.1.4 Results

Table B 1: Eq_A calculated form the batch adsorption tests, with the respective sediment concentrations.

Dortsman		Zandkreek	
cSed (g L^{-1})	Eq_A (mL g^{-1})	cSed (g L^{-1})	Eq_A (mL g^{-1})
398.7	0.0161	329.4	0.0431
364.5	0.0559	309.7	0.0536
490.3	0.004	493.3	0.0416
550.3	0.0221	676.7	0.0757
744.6	0.0836	831.5	0.0211
818.3	0.0128	956.1	0.0153
Average ± sd:	0.0324 ± 0.0308	Average ± sd:	0.0417 ± 0.022

Table B1 shows the results of the batch adsorption tess. Because of the similarity between Eq_A calculated for both sediments, and the small influence this parameter has based on the sensitivity analysis, the parameter value was fixed on an average value of 0.05 mL g^{-1}.

B.2. Testing adsorption of uranine to incubation setup, and living organic matter.

To test the adsorption of uranine to the incubation setup, or living organic matter, two side-experiments were performed. In a first experiment (Figure B2 b) cores which were either aerated with a bubbling stone, or not aerated were spiked with uranine. In the second experiment (Figure B2 a) six live cockles were placed into duplicate aerated incubation cores, and then spiked with uranine. In both experiments the tracer concentrations were closely monitored for 23 – 25 hours, to check whether uranine would adsorb to a biological or artificial surface. Results of these tests indicated that there was no cause for further investigation of the adsorption properties of uranine to the experimental setup.
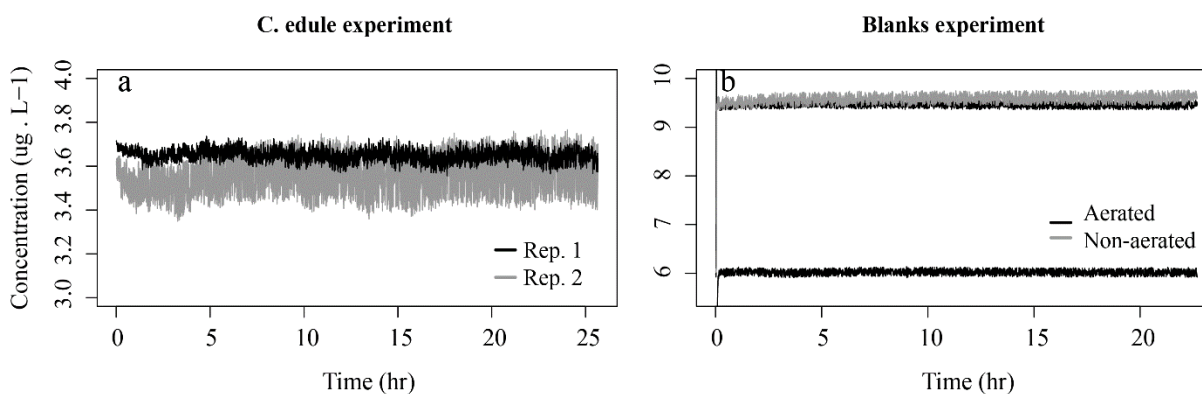
Figure B 2: a: Concentration of uranine over time in duplicate cores containing six live cockles each. b: Two cores aerated with a bubbling stone (black), and one non-aerated core (gray). For the aerated core two concentrations were tested to assess whether this would have any impact.

B.3. Species scores.

Table B 2: Scores for the BPc (BPc_R: reworking score, BPc_M: mobility score, BPc_Ft: feeding type), and for IP (IPc_Ft = feeding type, IPc_D = injection pocket depth).

Taxa	BPc_R	BPc_M	BPc_Ft	Ipc_Bt	Ipc_Ft	Ipc_D
Abra alba	2	2	S	1	1	3
Abra prismatica	2	2	S	1	1	3
Abra tenuis	2	2	S	1	1	3
Actiniaria	2	2	S	1	2	1
Ammothea hilgendorfi	2	2	S	1	3	1
Arenicola marina	3	2	UC	3	3	4
Ascidiacea	1	1	E	1	1	1
Asterias rubens	1	3	E	1	2	1
Bathyporeia sp.	2	3	S	1	3	1
Capitella capitata	3	2	UC	3	3	4

Carcinus maenas	5	4	R	1	2	1
Cerastoderma edule	2	2	S	1	1	2
Cirripedia	1	1	E	1	1	1
Corophium sp.	2	4	S	2	3	2
Crangon crangon	2	4	S	1	2	1
Crepidula fornicata	1	1	E	0	0	0
Ensis sp.	2	2	S	1	1	4
Eteone longa	4	3	B	1	2	1
Eunereis longissima	4	4	B	3	3	3
Gattyana cirrhosa	4	3	B	1	2	2
Glycera sp.	4	3	B	3	2	2
Glycera tridactyla	4	3	B	3	2	2
Hediste diversicolor	4	4	B	3	3	4
Hemigrapsus sp.	5	4	R	1	3	1
Heteromastus filiformis	3	2	UC	3	3	4
Lanice conchilega	3	1	DC	3	3	4
Limecola balthica	2	2	S	1	3	3
Malacoceros sp.	3	2	UC/DC	3	3	4
Malmgrenia darbouxi	4	3	B	1	2	4
Mediomastus fragilis	3	2	UC	3	3	3
Melinna cristata	3	1	UC/DC	3	3	2
Mya sp.	2	2	S	1	1	4
Mysta picta	4	3	B	1	2	1
Mytilus edulis	1	1	E	1	1	1
Nematoda	2	2	S	1	1	1
Nemertea	4	3	B	2	2	2
Neoamphitrite figulus	3	1	UC/DC	3	3	2
Nephtys hombergii	4	3	B	3	2	1
Nereididae	4	3	B	3	2	1
Notomastus sp.	3	2	UC	3	3	4
Ocenebra sp.	2	4	S	1	2	1
Oligochaeta	4	3	B	3	3	2
Ophiura ophiura	2	2	S	1	3	1
Peringia ulvae	2	3	S	1	3	1
Pholoe baltica	2	2	S	1	2	1
Phyllodoce mucosa	4	3	B	1	2	1
Platynereis dumerilii	4	4	B	3	3	4

Polychaeta	4	3	B	3	3	3
Polydora ciliata	3	1	UC/DC	1	1	2
Pygospio elegans	3	1	UC/DC	3	3	3
Ruditapes philippinarum	2	2	S	1	1	4
Scoloplos armiger	4	3	B	3	3	4
Scrobicularia plana	2	2	S	1	1	4
Sthenelais boa	4	3	B	1	2	1
Streblospio benedicti	3	2	UC/DC	1	2	1
Tellinoidea	2	2	S	1	1	3
Terebellidae	3	1	DC	3	3	3
Tharyx sp.	2	2	S	3	3	2
Urothoe sp.	2	3	S	3	3	3

B.4. Additional examples of fitted results/
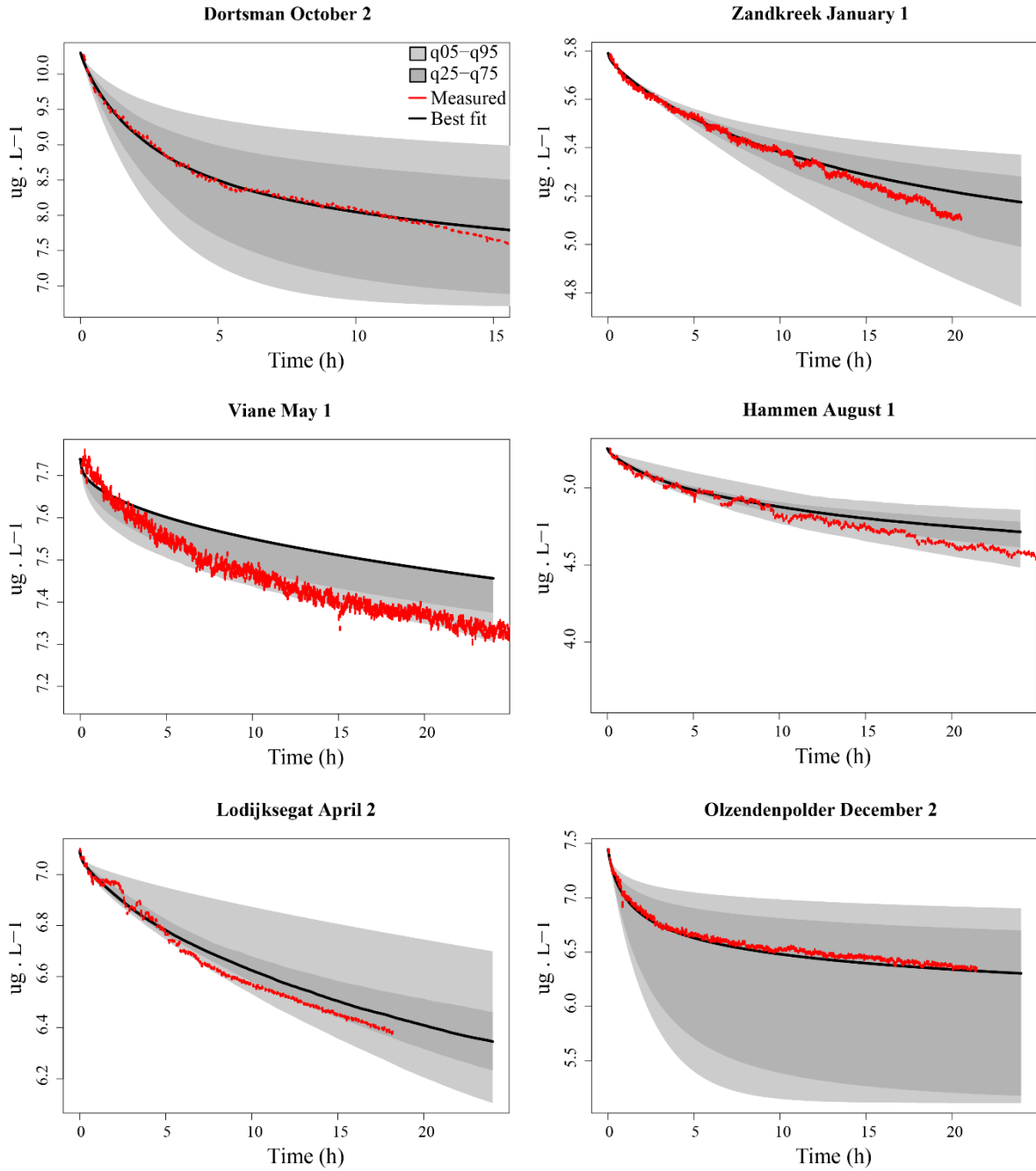
Figure B 3: Additional model fits of data (red lines) collected different sites, at different times throughout the year. The best fit tracer profile (full black line) is shown, along with the range of model results as quantiles (light and dark grey).

B.5. Correction of reported values.

Table B 3: median, Q1, and Q3 values for the pump rate and attenuation coefficient.

Season	Pump rate			Attenuation		
	Q1	Median	Q3	Q1	Median	Q3

Intertidal	Autumn	0.099	0.346	1.235	0.064	0.449	0.882
	Spring	0.1	0.4	1.316	0.183	0.26	0.401
	Summer	0.309	0.388	0.59	0.330	0.510	0.759
	Winter	0.076	0.211	1.139	0.061	0.438	0.853
Subtidal	Autumn	0.006	0.061	0.153	0.001	0.852	5.00
	Spring	0.013	0.094	0.488	0.001	0.359	0.6
	Summer	0.169	0.251	0.649	0.341	1.078	1.608
	Winter	0.536	1.143	1.787	0.04	1.290	8.106

Appendix C: Chapter 5

C.1. Data collection for parametrization

C.1.1. General sampling design

In September 2017, locations Coarse, FineH, and MudH were sampled in the Belgian Part of the North Sea (Toussaint et al., *in review*), whereas FineL and MudL were sampled in the Central-Northern North Sea in May-June of 2018 (De Borger et al., *in press*). The stations from Toussaint et al. (*in review*) have historic names as sampling stations in the Belgian Part of the North Sea: "330" for "Coarse", "780" for "FineH", and "130" for MudH (e.g. van der Zee and Chou (2004), Franco et al. (2010), Braeckman et al. (2014), Van De Velde et al. (2018)). A stainless steel NIOZ boxcorer was used to sample the sediments used to describe the different locations in this modelling study (30 cm ID, 50 cm height). At each location, triplicate intact boxcores were collected. From the September 2017 samples, a set of subcores was taken from each boxcore sample for: incubation purposes (Ø 19 Plexiglass sampling cores for coarse grained sediment to allow for a stirring mechanism for advective flows; Ø 10 cm for cohesive sediment, 10-15 cm deep + 10 cm of overlying water), to determine porewater nutrient profiles (Ø 10 cm Plexiglass sampling core), and to determine sediment characteristics (cut off syringe, upper 3 cm). Incubations were performed in the dark (to prevent photosynthetic activity), and in climate controlled laboratory conditions with disk (coarse) of teflon (cohesive) stirrers agitating the overlying water, and exchange rates of oxygen, dissolved inorganic carbon (DIC), and dissolved inorganic nitrogen (DIN) were measured.

In the May-June samples, ship-board incubations (dark) were performed using the entire boxcore sample, measuring the same parameters as previously mentioned. For this, the boxcore "bucket" containing the sediment was sealed with a Plexiglass lid containing a Teflon stirrer, and placed in a buffering vat on deck to maintain steady temperature. After this shipboard incubation, subcores were collected to measure porewater nutrient profiles (Ø 10 cm Plexiglass sampling core), oxygen microprofiles (Ø 5 cm Plexiglass sampling core), and sediment characteristics (cut off syringe, upper 2 cm).

C.1.2. Flux calculations

During incubations, the oxygen concentration in the overlying water was monitored using optode sensors (FirestingO2, Pyroscience, 2-point calibration), set at 1 Hz. At the same time, DIC and DIN concentrations were sampled from the overlying water with syringes at discreet time intervals. 5 – 10 mL were collected for DIN, and filtered through a 0.45 μm syringe filter, and stored at -20 °C until further processing. 6 - 10 mL of water were collected in headspace vials for DIC, and subsequently poisoned with 1 μL of saturated HgCl2 per mL sample for preservation and kept refrigerated at 4 °C until further processing. During incubations, O_2 concentrations did not decrease below 50 % of the initial oxygen concentration. As such, incubations in the 2017 samples lasted between 2 – 8 hours, and 24 – 36 hours in 2018.

Upon thawing, nutrient concentrations were determined by a SEAL QuAAtro segmented flow analyser (Jodo et al., 1992). DIC analysis was performed using a segmented flow analyser (San++ SKALAR) following (Stoll et al., 2001). Fluxes (in mmol m^{-2} d^{-1}) were calculated by fitting a linear regression through the concentration time series, and multiplying the regression coefficient by the height of the overlying water to convert from volumetric to surficial rates. For oxygen fluxes the same method was applied to a consistently decreasing section of the oxygen concentration data.

C.1.3. Porewater nutrient profiles

Porewater nutrients (DIN) were collected in 1-2 cm interval depth slices down to 12 cm deep, using rhizon samplers (0.15 μm pore size, Rhizosphere Research Products). The rhizons were inserted into the sediment core through pre-drilled holes in the core wall, and a maximum of 4 mL of porewater was extracted from each interval using a 5 mL syringe connected to the rhizon sampler (Dickens et al., 2007; Seeberg-Elverfeldt et al., 2005; Shotbolt, 2010). Further processing of the nutrient samples was done the same as for the nutrient flux samples.

C.1.4. Oxygen microprofiles

Oxygen-depth profiles in the sediment were measured using Clark-type O_2 micro-electrodes (50 μm tip diameter, Unisense) (Revsbech, 1989). Readings were taken at 100 μm intervals, starting 2000 μm (2 mm) above the sediment-water interface (water aerated to 100% O_2 saturation before the experiment) down to the depth in the sediment at which all oxygen was depleted. A two-point calibration was conducted prior to measurements using 100 and 0 % oxygen saturated seawater to represent water column and anoxic O_2 concentrations, respectively. In each sediment core, up to three replicate profiles were taken from different areas of the sediment (except in Coarse, where the risk of damage to the sensor due to coarseness of the sediment was determined too great).

C.1.5. Sediment characteristics

Sediment grain size was determined by laser diffraction on freeze-dried and sieved (< 1 mm) sediment samples in a Malvern Mastersizer 2000 (McCave et al., 1986). Grain size fractions were determined as volume percentages according to the Wentworth scale (Wentworth, 1922): clay/silt (< 63 μm), very fine sand (vfines: 63 – 125 μm), fine sand (fines: 125 – 250 μm), medium sand (250 – 500 μm), and coarse sand (500 μm – 1 mm). In this manuscript, the percentage of sand was calculated by summing grainsize classes between 63 and 1000 μm. The median grain size (MGS) was calculated on the fraction < 1 mm. Water content was determined as the volume of water removed by freeze drying wet sediment samples. The sediment density was determined by measuring the water displacement of a given weight of dried sediment. Sediment porosity was determined from water content and solid phase density measurements, accounting for the salt content of the pore water.

C.2. Baseline simulation porewater profiles
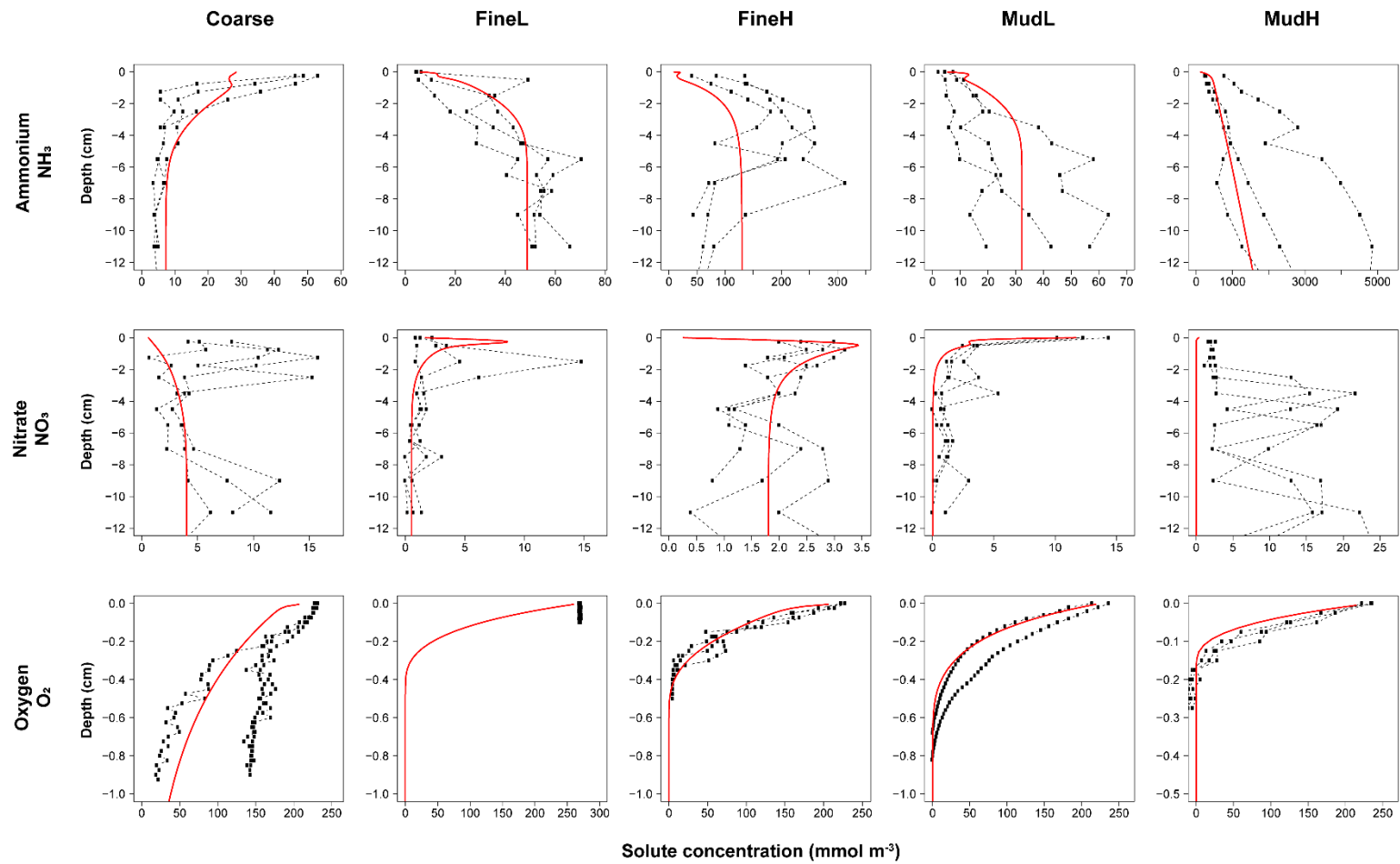
Figure C 1: Measured concentrations (black dots) and fitted profiles (red line) for ammonium, nitrate, and oxygen (mmol m^{-3}, rows) in the different types of sediment used as the basis for the disturbance simulations (columns).

C.3. Annual variability porewater concentration
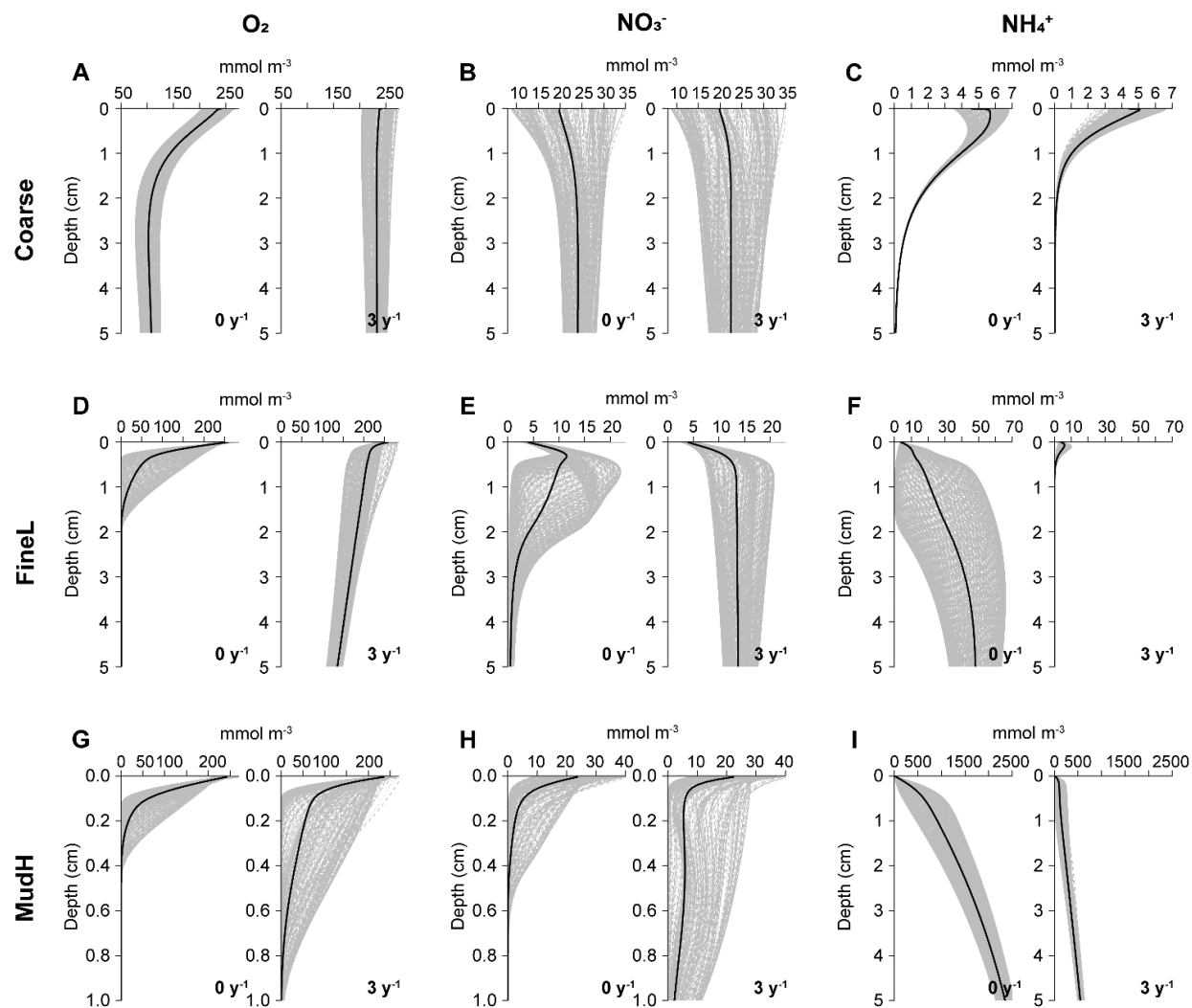
Figure C 2: Range of nutrient concentrations (gray lines) throughout the year, and average annual concentration (black line) in an untrawled sediment, and sediment trawled 3 y^{-1} of Coarse (A-C), FineL (D-F), and MudH (G-I). Nutrient concentrations in mmol m^{-3}. Note the difference in depth range (y-axis) shown for the different sediments.

C.4. Reactive carbon quality in surface sediments
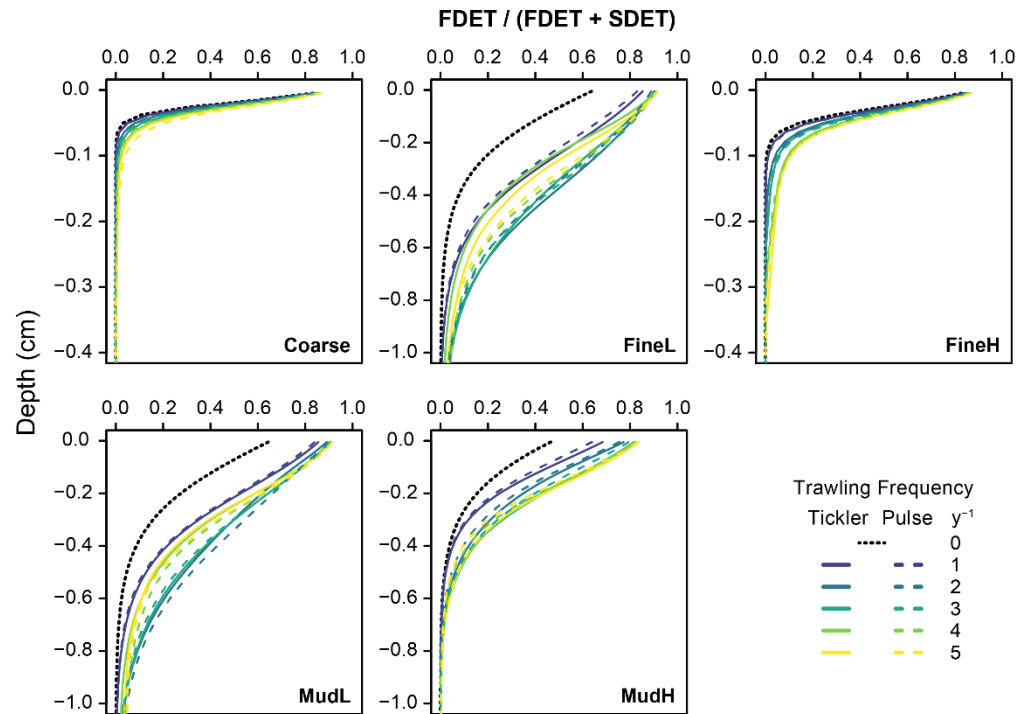
Figure C 3: Annually averaged modelled quality of the reactive organic carbon pool in the surface sediments (note different depths on y-axis between figures for visualization purposes). The carbon quality (x-axis) is represented as the proportion of fast degrading detritus (FDET, labile org. C) in the summed labile and semi-labile org. C pool (FDET + SDET). Black dotted line is the 0 trawl default, full and dotted coloured lines are tickler and pulse gear respectively, with increasing trawling frequencies as different colours.

C.5. Changes to porewater concentrations

| | | Tickler | | | | | | Pulse | | | | | |
| | | Conc. | ------- % Change ------- | | | | | Conc. | ------- % Change ------- | | | | |
	station	0	1	2	3	4	5	0	1	2	3	4	5
O₂ mmol m⁻³	Coarse	117.1	96 ± 7	97 ± 4	98 ± 3	99 ± 3	99 ± 4	117.1	98 ± 8	98 ± 3	100 ± 3	99 ± 4	97 ± 2
	FineL	8.1	239 ± 169	805 ± 280	1211 ± 387	1637 ± 270	1604 ± 347	8.1	133 ± 136	447 ± 195	1013 ± 300	1335 ± 364	1584 ± 323
	FineH	9.3	656 ± 142	1081 ± 79	1075 ± 165	1036 ± 254	965 ± 253	9.3	686 ± 322	1053 ± 202	1153 ± 158	1196 ± 217	1129 ± 212
	MudL	8.5	467.4 ± 182	1010 ± 208	1296 ± 272	1512 ± 311	1517 ± 287	8.5	296 ± 154	891 ± 169	1340 ± 392	1578 ± 351	1619 ± 264
	MudH	1.8	-28.8 ± 4	-25 ± 38	14 ± 57	27 ± 53	52 ± 57	1.8	-25 ± 4	-27 ± 21	-9 ± 44	52 ± 61	81 ± 49
NO₃⁻ mmol m⁻³	Coarse	23.5	11.3 ± 7	10 ± 8	6 ± 9	1 ± 9	0 ± 8	23.5	13 ± 7	9 ± 9	6 ± 10	4 ± 9	-4 ± 4
	FineL	2.2	991 ± 135	1038 ± 52	967 ± 90	882 ± 87	909 ± 129	2.2	866 ± 251	1044 ± 44	981 ± 53	932 ± 87	882 ± 105
	FineH	2	584 ± 88	690 ± 100	655 ± 108	585 ± 132	565 ± 132	2	559 ± 202	685 ± 115	690 ± 89	675 ± 79	626 ± 89
	MudL	1.2	1598 ± 114	1733 ± 81	1779 ± 128	1822 ± 246	1912 ± 253	1.2	1464 ± 312	1687 ± 60	1662 ± 119	1675 ± 167	1741 ± 187
	MudH	0.2	-51 ± 10	-40 ± 61	39 ± 123	70 ± 117	123 ± 125	0.2	-50 ± 11	-47 ± 31	-12 ± 85	114 ± 136	188 ± 104
NH₄⁺ mmol m⁻³	Coarse	0.9	-53 ± 2	-57 ± 3	-59 ± 2	-62 ± 2	-63 ± 2	0.9	-52 ± 4	-57 ± 3	-59 ± 2	-62 ± 2	-64 ± 2
	FineL	41	-97 ± 2	-99 ± 0	-99 ± 0	-100 ± 0	-99 ± 1	41	-94 ± 6	-99 ± 1	-99 ± 0	-99 ± 0	-100 ± 0
	FineH	125.6	-98 ± 1	-99 ± 0	-99 ± 1	-98 ± 3	-97 ± 6	125.6	-96 ± 6	-99 ± 1	-100 ± 0	-99 ± 1	-99 ± 2
	MudL	50.7	-98 ± 1	-99 ± 0	-99 ± 0	-99 ± 1	-99 ± 0	50.7	-97 ± 3	-99 ± 0	-99 ± 0	-99 ± 0	-99 ± 0
	MudH	21612	-50 ± 7	-62 ± 3	-65 ± 6	-63 ± 6	-61 ± 9	2162	-43 ± 8	-59 ± 5	-64 ± 4	-68 ± 6	-68 ± 7
Organic C mol m⁻³	Coarse	78.4	-87 ± 2	-92 ± 2	-94 ± 1	-95 ± 1	-96 ± 1	78.4	-86 ± 2	-92 ± 2	-94 ± 2	-95 ± 1	-96 ± 1
	FineL	94.9	-72 ± 7	-84 ± 3	-87 ± 3	-90 ± 2	-91 ± 1	94.9	-65 ± 12	-81 ± 6	-86 ± 2	-89 ± 2	-91 ± 1
	FineH	326.3	-86 ± 3	-93 ± 2	-95 ± 1	-96 ± 1	-96 ± 1	326.3	-84 ± 4	-93 ± 2	-94 ± 2	-96 ± 1	-96 ± 1
	MudL	92.4	-71 ± 8	-84 ± 4	-87 ± 2	-89 ± 2	-90 ± 2	92.4	-65 ± 12	-84 ± 5	-87 ± 3	-89 ± 2	-91 ± 1
	MudH	2456	-70 ± 11	-82 ± 6	-90 ± 3	-90 ± 1	-91 ± 0	2456	-63 ± 15	-75 ± 11	-83 ± 6	-85 ± 3	-90 ± 1

Table C 1: Overview of effect of increasing trawling intensities for tickler gears, and pulse gears (columns) on sedimentary concentrations of O_2, NO_3^-, NH_4^+ (top 5 cm) and organic carbon (top 10 cm). The baseline scenario (frequency = 0) is displayed as the absolute concentration (mmol m⁻³), increasing frequencies (1 – 5 y⁻¹) are shown as % change of the baseline rate (+ = increase, - = decrease). Concentrations are the average annual concentrations, in mmol m⁻³ for solutes, and mol m⁻³ for organic carbon.

C.6. Changes to process rates

	station	Tickler Rate			% Change			Pulse Rate			% Change		
		0	1	2	3	4	5	0	1	2	3	4	5
Total *mmol C m⁻² d⁻¹*	Coarse	13.6	-5 ± 0	-8 ± 13	-12 ± 10	-19 ± 9	-22 ± 10	13.6	-5 ± 0	-7 ± 7	-13 ± 11	-17 ± 7	-21 ± 5
	FineL	8.1	-5 ± 3	-13 ± 15	-20 ± 12	-21 ± 5	-27 ± 5	8.1	-6 ± 4	-8 ± 8	-18 ± 7	-22 ± 5	-24 ± 4
	FineH	30.0	-7 ± 2	-15 ± 16	-17 ± 13	-24 ± 8	-27 ± 7	30.0	-7 ± 3	-11 ± 13	-17 ± 8	-23 ± 8	-29 ± 6
	MudL	8.6	-5 ± 2	-15 ± 19	-18 ± 10	-23 ± 8	-27 ± 6	8.6	-6 ± 4	-11 ± 13	-17 ± 9	-21 ± 5	-25 ± 7
	MudH	85.0	-7 ± 2	-12 ± 12	-20 ± 10	-22 ± 5	-26 ± 6	85.0	-6 ± 3	-11 ± 9	-17 ± 8	-25 ± 8	-26 ± 5
OxicMin *mmol C m⁻² d⁻¹*	Coarse	12.0	-4 ± 1	-8 ± 13	-12 ± 10	-18 ± 9	-21 ± 10	12.0	-4 ± 1	-7 ± 7	-13 ± 10	-17 ± 7	-21 ± 5
	FineL	6.5	8 ± 4	-1 ± 17	-8 ± 14	-7 ± 6	-15 ± 6	6.5	7 ± 4	5 ± 9	-5 ± 8	-10 ± 6	-12 ± 5
	FineH	23.3	-1 ± 2	-10 ± 17	-13 ± 14	-20 ± 8	-23 ± 7	23.3	-2 ± 3	-6 ± 14	-13 ± 9	-19 ± 9	-25 ± 6
	MudL	6.1	11 ± 3	0 ± 22	-2 ± 12	-7 ± 10	-11 ± 7	6.1	10 ± 4	5 ± 15	-1 ± 10	-5 ± 6	-9 ± 8
	MudH	23.1	40 ± 10	50 ± 19	48 ± 21	54 ± 15	56 ± 12	23.1	32 ± 5	46 ± 12	45 ± 16	48 ± 22	56 ± 15
AnoxicMin *mmol C m⁻² d⁻¹*	Coarse	0.9	-20 ± 14	-24 ± 17	-20 ± 16	-23 ± 15	-24 ± 12	0.9	-23 ± 12	-20 ± 14	-18 ± 19	-25 ± 10	-24 ± 8
	FineL	1.0	-77 ± 3	-79 ± 4	-79 ± 2	-78 ± 2	-80 ± 2	1.0	-75 ± 5	-77 ± 3	-79 ± 2	-80 ± 2	-80 ± 1
	FineH	6.6	-26 ± 4	-31 ± 13	-33 ± 11	-38 ± 6	-41 ± 6	6.6	-26 ± 5	-27 ± 11	-32 ± 8	-38 ± 8	-42 ± 5
	MudL	1.5	-74 ± 1	-78 ± 5	-80 ± 3	-82 ± 3	-83 ± 2	1.5	-73 ± 2	-76 ± 4	-80 ± 3	-81 ± 2	-83 ± 2
	MudH	57.7	-27 ± 6	-39 ± 9	-49 ± 10	-54 ± 7	-61 ± 7	57.7	-22 ± 3	-36 ± 9	-43 ± 8	-57 ± 7	-60 ± 5
Denitrification *mmol C m⁻² d⁻¹*	Coarse	0.6	11 ± 14	9 ± 20	-2 ± 20	-14 ± 14	-20 ± 14	0.6	11 ± 16	8 ± 19	-6 ± 14	-8 ± 17	-19 ± 9
	FineL	0.5	-25 ± 7	-42 ± 15	-57 ± 13	-70 ± 9	-74 ± 8	0.5	-19 ± 6	-30 ± 11	-49 ± 9	-60 ± 11	-68 ± 9
	FineH	0.1	0 ± 22	-11 ± 22	-11 ± 22	-22 ± 11	-22 ± 11	0.1	0 ± 22	-11 ± 22	-11 ± 22	-22 ± 11	-33 ± 11
	MudL	0.8	1 ± 4	-13 ± 20	-22 ± 12	-31 ± 9	-35 ± 6	0.8	4 ± 5	-6 ± 15	-20 ± 12	-28 ± 9	-33 ± 6
	MudH	4.2	35 ± 15	46 ± 26	39 ± 20	48 ± 17	50 ± 9	4.2	26 ± 15	42 ± 17	41 ± 17	42 ± 19	49 ± 11

Table C 2: Overview of effect of increasing trawling intensities for tickler gears, and pulse gears (columns) on the total organic matter mineralization, and the different mineralization processes. The baseline scenario (frequency = 0) is displayed as the absolute rate (mmolC m⁻² d⁻¹), increasing frequencies (1 – 5 y⁻¹) are shown as % change of the baseline rate. Mineralization rates are the average annual concentrations.

Appendix D: Chapter 6

D.1. Bioturbation – Median grainsize

Bioturbation assumption
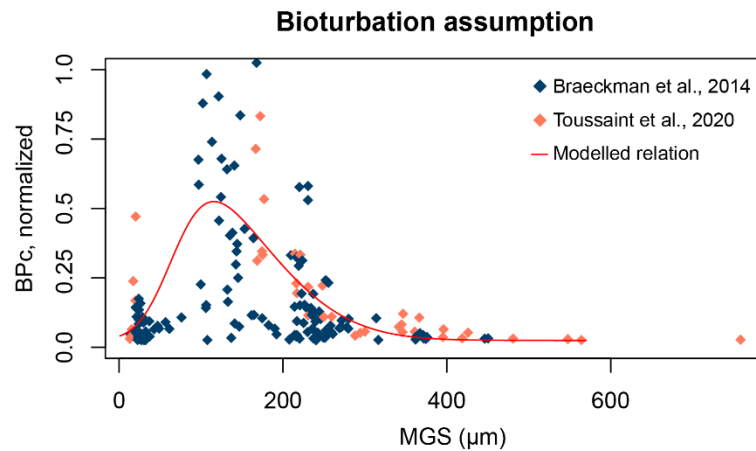
Figure D 1: Scaled BPc over median grain size (μm), with data from Braeckman et al. (2014) and Toussaint et al. (subm.).

The skewed normal distribution (dsn) was generated using the dsn function of the R package 'sn' (Azzalini, 2020), with values of 10, 105, and 3 for the location, scale, and slant parameters respectively.

D.2. Current rosette D6
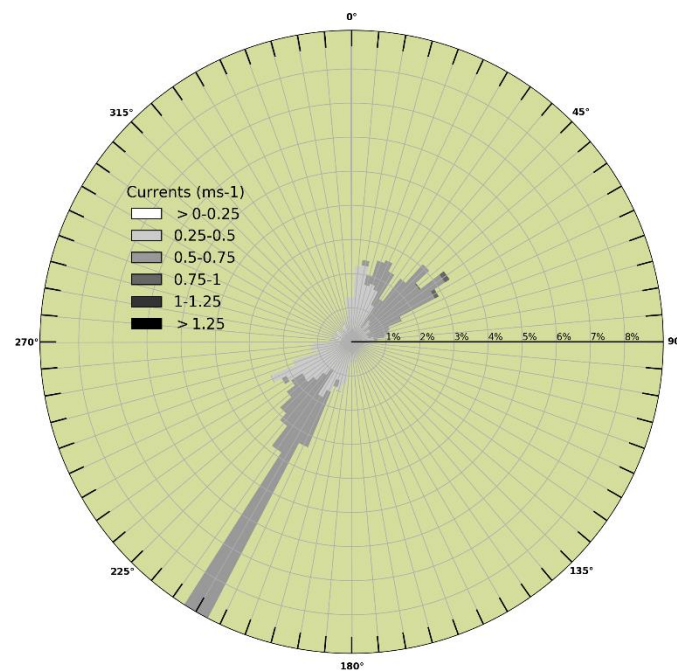
Figure D 2: Directional distribution (0° = north, 180° = south) of depth averaged currents (m s^{-1}) at the C-power windfarm, representative for the greater modelling domain.

D.3. Calculation BPNS carbon storage

Table D 1: Calculation of increased carbon storage in top 10 cm of the sediment in the BPNS.

	Current	Future
	409.3	706.5

Average increase *mmol m⁻²*		
Belgian coastal zone *km²*	3454	
Total increase in BPNS *tonnes*	16963.4	29283.4
% of Belgian 2018 GHG emissions	0.014	0.025

D.4. Comparison of modelled fluxes and reference material

Table D 2: comparison modelled fluxes, and average fluxes ± standard deviation measured by Toussaint et al. (subm.). Fluxes in mmol m⁻² d⁻¹, negative fluxes go into the sediment.

Station	O_2	O_2 model	DIC	DIC model	NH_4^+	NH_4^+ model	NO_3^-	NO_3^- model
				mmol m⁻² d⁻¹				
120	-24.0 ± 1	-30.83	31.2 ± 7.0	28.4	0.8 ± 0.2	2.6	0.4 ± 0.5	0.2
130	-48.8 ± 9.3	-36.79	123.6 ± 89.5	33.7	41.5 ± 18.1	3.1	-0.1 ± 0.2	0.2
330	-28.9 ± 2.5	-29.51	15.9 ± 2.7	27.3	-0.7 ± 0.9	2.8	-0.4 ± 0.3	0.2
780	-78.9 ± 39.0	-33.36	96.1 ± 34.6	30.4	4.1 ± 1.5	2.8	-0.5 ± 2.3	0.1
BRN11	-36.6 ± 2.4	-21.58	37.6 ± 7.3	19.7	0.8 ± 0.8	1.7	0.3 ± 0.2	0.2
D6	-23.3 ± 5.5	-26.33	9.1 ± 1.4	24.2	-1.4 ± 7.4	2.3	3.1 ± 6.5	0.2

Appendix E: Chapter 7

E.1. Observations of sediment biogeochemistry in the North Sea

The sediment surface sampled in studies reporting O_2 fluxes (derived from microprofiling or incubations), nutrient fluxes (incuding DIC), or nutrient profiles for the North Sea was estimated by multiplying the amount of samples taken, by the reported surface area of the sampling device. A sample was interpreted as the original surface taken from the seabed, not any subsamples (subcores) taken from it. E.g. if one boxcore of 31 cm ID. (inner diameter) was subsampled with one 10 cm ID. core, the sampled sediment was calculated based on the surface are of the boxcore. If this number of initial samples could not be derived (if it was not reported in the study), it was estimated based on the amount of subsamples reported. If neither the total number of initial samples, nor the amount of subsamples was reported, the amount of initial samples was estimated by assuming triplicate cores for each type of measurements, per station, per sampling event (if seasonal). If this was not possible (e.g. clearly an uneven amount of samples per factor combination), the amount of samples was estimated from a figure / table, or other information in the text. Only studies were included that analyzed or incubated undisturbed sediment samples (e.g. no slurry experiments or mesocosm experiments were included).

Table E 1: (Next page) Studies that have reported measurements of sediment O2 consumption, nutrient exchange fluxes, or nutrient profiles for the North Sea. Abbreviations for the locations are: HGMA: Helgoland mud are; BF: Broad Fourteens; FF, Frisian Front; BPNS: Belgian Part of the North Sea; FNS: Full North Sea; OG: Oster Grounds; SK: Skagerrak; GB: German Bight; ENS: Eastern North Sea; DB: Dogger Bank; OSP: Outer Silver Pit; TH: Thames, SGF; Sean Gas Field; DCZ: Dutch Coastal zone, WS: Wadden Sea.

Authors	Location	O₂ flux incl. based off profiles	Nutrient fluxes incl. DIC	Nutrient profiles	Equipment	ind.surf. (m²)	amount	total surface (m²)	seasonal dynamic	Remarks
Billen et al., 1978	BPNS, DCZ				Individual cores 7 cm ID	0.004	21	0.08		Number of cores estimated from table 3, total number not reported.
Boon et al., 1998	BF, FF	X			boxcore 31 cm ID	0.075	34	2.57		
Braeckman et al., 2014	BPNS	X	X		boxcore 31 cm ID	0.075	182	13.74	X	
Brenner et al., 2016	NS	X	X		boxcore 31 cm ID	0.075	27	2.04		Number of cores derived from figures, not reported in study.
Canfield et al., 1993	SK	X	X		multicorer 10 cm ID	0.008	15	0.12		
Couceiro et al., 2013	OG	X	X	X	boxcore 31 cm ID 50 cm boxcore	0.075 0.196	6 1	0.45 0.20		
Dauwe et al., 1998	BF, FF, GB, SK, Brouwersehaven			X	boxcore 31 cm ID	0.075	24	1.81		
De Borger et al., 2020	OG, DB, CNS, FG	X	X	X	boxcore 31 cm ID	0.075	33	2.49		
Deek et al., 2012	WS	X	X		multicorer 10 cm ID	0.008	120	0.94		Based on "at least 6 cores were collected per sampling site".
de Wilde et al., 1986	FG	X			boxcore 31 cm ID	0.075	25	1.89		
de Wilde et al., 1984	OG	X			boxcore 31 cm ID	0.075	64	4.83		Estimate based on "In 1981 96 bottles [bell jars for oxygen incubation] were measured, 27 in 1980." and "Then 1 or 2 glass incubation bottles without bottom (diameter 98 ram) were pushed 10 cm deep into the sediment. [of the boxcore]".
Ehrenhaus et al., 2004	Spiekeroog	X	X	X	multicorer 10 cm ID 19 cm diameter	0.008 0.023	10 13	0.08 0.30		

Forster et al., 1995	HGMA	X			50 cm boxcore	0.785	3	2.36		Likely number, not clearly reported.
Forster et al., 1999	HGMA, SK	X			incubation lander	0.894	6	5.36		Number of boxes could not be derived from study, assumed triplicates.
Franco et al., 2010	BPNS	X			boxcore 31 cm ID	0.075	18	1.36	X	
Gao et al., 2009	BPNS	X			cores 15 cm ID	0.018	12	0.21	X	Assumed triplicate cores.
Gao et al., 2010	WS	X	X	X	cores 9.5 cm ID	0.007	6	0.04		Assumed triplicate cores
					cores 3.5 cm ID	0.001	30	0.03		
Gehlen et al., 1995 **Lohse et al., 1995** **Lohse et al., 1993** **van Raaphorst et al., 1996**	ENS	X	X	X	boxcore 31 cm ID	0.075	96	7.25		Exact number not reported, estimated based on own methodology for similar measurements. Same set of samples for all publications.
Upton et al., 1993 **Nedwell et al., 1994**	FNS	X	X		multicorer 5.8 cm ID	0.002	960	2.20	X	Same set of samples for both publications.
Neubacher et al., 2011	OG, DB, SGF	X	X		boxcore 31 cm ID	0.075	102	7.70	X	Exact no. boxcores not derived, estimate 6 boxcores / site to retrieve samples needed.
Neumann 2017	GB	X	X	X	multicorer 10 cm ID	0.008	77	0.60		Amount of cores estimated from figure 2.
Oehler et al., 2015	HGMA	X	X		incubation box 400 cm2	0.400	18	7.20	X	
					multicorer 10 cm ID	0.007	72	0.51		
Osinga et al., 1996	OG, BF	X	X	X	boxcore 31 cm ID	0.075	48	3.62	X	Exact number of boxcores not reported, estimate 6 boxcores / site to retrieve samples needed.
Provoost et al., 2013	BPNS	X			boxcore 31 cm ID	0.075	42	3.17	X	Assumed triplicate boxcores, exact number not reported.

Raaphorst et al., 1990	OG, DB	X		X	boxcore 31 cm ID	0.075	72	5.43		Exact number not clear, assumed triplicate boxcores * 2 for profiles, and incubations.
Tiano et al., 2019	FF	X	X	X	boxcore 31 cm ID	0.075	9	0.68		Only control / T0 samples included.
					incubation lander 144 cm2	0.144	6	0.86		
Toussaint et al., subm.	BPNS	X	X		boxcore 31 cm ID	0.075	32	2.42		
Trimmer et al., 2005	OSP, TH	X	X	X	boxcore 31 cm ID	0.075	140	10.57	X	Number of cores extrapolated from "a total of 8 to 12 box cores would be sampled at any one site".
Vandevelde et al., 2018	BPNS			X	single corer 6 cm ID	0.003	84	0.24	X	Includes disturbed sediments.
van Raaphorst et al., 1992	FF, BF	X	X	X	boxcore 31 cm ID	0.075	40	3.02	X	
Van Duyl et al., 1994	DB	X	X		boxcore 31 cm ID	0.075	26	1.96		
Weston et al., 2008	OG	X	X		boxcore 31 cm ID	0.075	32	2.42		
Total (m²)								99.04		

E.2. Species collected on the NICO 10 transect

E.2.1. Methodology

During the NICO 10 research campaign (**Chapter 3**), boxcores were collected to characterize the sediment biogeochemistry on a 670 km long transect starting 100 km NW of the island of Terschelling, to the Fladen Grounds in the Northern North Sea (Table E 2, and see Fig. 3-1 for a map of the sampling sites). Triplicate boxcores were collected on each sampling station (containing 20 - 30 cm sediment), and placed into buffering tanks on deck to control the temperature. The boxcores were incubated fully, to determine nutrient exchange and oxygen consumption rates, and afterwards sediment subsamples were taken to determine profiles of porewater nutrients, oxygen, and chl *a* (see chapter 3 for a full description of the biogeochemical measurements). After these measurements were performed, the contents of all subsamples exccept the chl *a* were recombined with the contents remaining in the incubation box. The sediment was then carefully sieved over a 1 mm sieve to retrieve the macrofauna, which was subsequently stored in a 4 % buffered formalin - seawater solution until further processing. Macrofauna was identified up to the highest possible taxonomic level. Abundances (individuals per taxon) and species biomass (blotted wet weight per taxon) were recorded and used in further data analysis, after standardization to m^2 by dividing by the boxcore surface, and are reported below as mean ± sd. ($n = 3$).

Table E 2: Locations, sampling date, and depth of the stations sampled during the NICO 10 research cruise. Number coding in station names corresponds to the distance along the travelled.

Station	Region	Sampling dates, 2018	Latitude (Deg. N)	Longitude (Deg. E)	Depth (m)
O.100		June 5	54.14938	4.341914	45
O.135	Oyster Grounds	June 4	54.41973	4.046748	43
O.190		June 3	54.87539	3.686554	41
D.240	Dogger Bank	May 25	55.17374	3.161264	26
C.300	Central North Sea	June 2	55.62316	2.384164	72
C.380		June 1	56.06932	1.599237	79
C.450	Devils Hole	May 26	56.58769	0.685672	224
C.545	Central North Sea	May 31	57.36059	0.579088	84
F.640		May 27	58.20097	0.525871	148
F.695	Fladen Grounds	May 29	58.83913	0.511693	135
F.770		May 30	59.41514	0.509838	135

The structure of the macrofaunal community was investigated with a hierarchical clustering analysis based on species biomass, using the Simpson pair-wise dissimilarity as the distance matrix (Qian et al., 2005; Baselga, 2010), as this reflects spatial turnover, i.e. the replacement of species by others (Qian et

al., 2005). The resulting clusters were subsequently used as grouping factors in an indicator species analysis (Dufrêne and Legendre, 1997; De Cáceres and Legendre, 2009). In this analysis, indicator species are found for a given site or group of sites, and the significance of the group-membership is assessed through a permutation test. Since the species data contained a large amount of low/single occurrence taxa, excess variance caused by these taxa was removed by working with taxa representing the 99th percentile of taxa biomass. All analyses were performed in R (R Core Team, 2020), with the packages "ade4" for ordinations (Dray and Dufour, 2007), "vegan" to perform hierarchical clustering and variance partitioning (Oksanen et al., 2019), "betapart" to calculate the turnover component (Baselga et al., 2018), and "indicspecies" to determine the indicator species (De Cáceres and Legendre, 2009).

E.2.2. Results

The full list of taxa collected in the boxcores is shown in Table E 4. In total, 246 taxa were identified, of which 208 to species level. Species richness (no. taxa per sample) was lowest at O.100 in the Oyster Grounds (7 ± 2), with species richness otherwise ranging between 16 ± 1 at F.640, to 34 ± 9 at F.770 (Figure E 1A). O.100 samples also contained the lowest biomass (2.8 ± 3.6 gWW m^{-2}), and the lowest abundances (481 ± ind. m^{-2}). For the other stations, species biomass ranged from 37.3 ± 22.3 gWW m^{-2} in the Fladen Grounds (F.640) to 339.5 ± 512.6 gWW m^{-2} in the Central North Sea (C.380) (Figure E 1 B). Abundances ranged from 2035 ± 757 ind. m^{-2} (F.640) to 6453 ± 2864 ind. m^{-2} (F.770), with both stations sampled in the Fladen Grounds (Figure E 1C). Neither species richness, nor biomass, nor abundances display a consistent latitudinal trend.

After selecting the 99th percentile of the species biomass, 57 out of 246 taxa remained for the hierarchical clustering analysis (Figure E 1D). The clustering analysis produced three clusters at the 0.7 cut-off level, which was selected over the 0.6 level to proceed to the indicator species analysis with more evenly sized groups. The first cluster contained the Oyster Grounds, and Dogger Bank stations, and was home to species such as the molluscs *Corbula gibba*, *Euspira nitida*, and *Chamelea striatula*, and the mud shrimp *Callianassa subterranea* (Table E 3). The second cluster includes the central North Sea stations and Devils Hole, and was typified by several polychaetes: *Scoloplos armiger*, *Diplocirrus glaucus*, *Ditrupa arietina*, but also the horseshoe worm (*Phoronis muelleri*). The last cluster grouped the Fladen Grounds stations, characterized by the bivalves *Parathyasira equalis* and *Astarte sulcate*, the polychaetes *Phylo norvegicus*, *Streblosoma bairdi*, *Nephtys paradoxa*, *Rhodine gracilator*, and the brittlestar *Amphiura chiajei*. The indicator species analysis further identified species characteristic to both the Central North Sea stations, and the Fladen grounds: the echinoderm *Brissopsis lyrifera*, and the polychaete *Paramphinome jeffreysii*.

Table E 3: Indicator species for clusters identified in the hierarchical clustering procedure. Significant cluster membership is indicated by the P-values resulting from the permutation tests, assuming a significance level of $p < 0.05$.

	Species	p-value	
Oyster Ground – Dogger Bank	Corbula gibba	< 0.001	***
	Callianassa subterranea	< 0.001	***
	Euspira nitida	0.004	**
	Chamelea striatula	0.011	*
	Chaetopterus variopedatus	0.025	*
	Echinocardium cordatum	0.091	.
	Gattyana cirrhosa	0.093	.
	Sigalion mathildae	0.089	.
Central North Sea – Devils Hole	Scoloplos armiger	< 0.001	***
	Cirratulidae	0.013	*
	Diplocirrus glaucus	0.044	*
	Ditrupa arietina	0.095	.
	Phoronis muelleri	0.095	.
Fladen Grounds	Parathyasira equalis	< 0.001	***
	Phylo norvegicus	< 0.001	***
	Diastylis lucifera	0.002	**
	Amphiura chiajei	0.001	**
	Streblosoma bairdi	< 0.001	***
	Nephtys paradoxa	0.003	**
	Rhodine gracilior	0.013	*
	Maldanidae	0.018	*
	Astarte sulcata	0.068	.
Central North Sea – Fladen Grounds	Paramphinome jeffreysii	< 0.001	***
	Brissopsis lyrifera	0.068	*
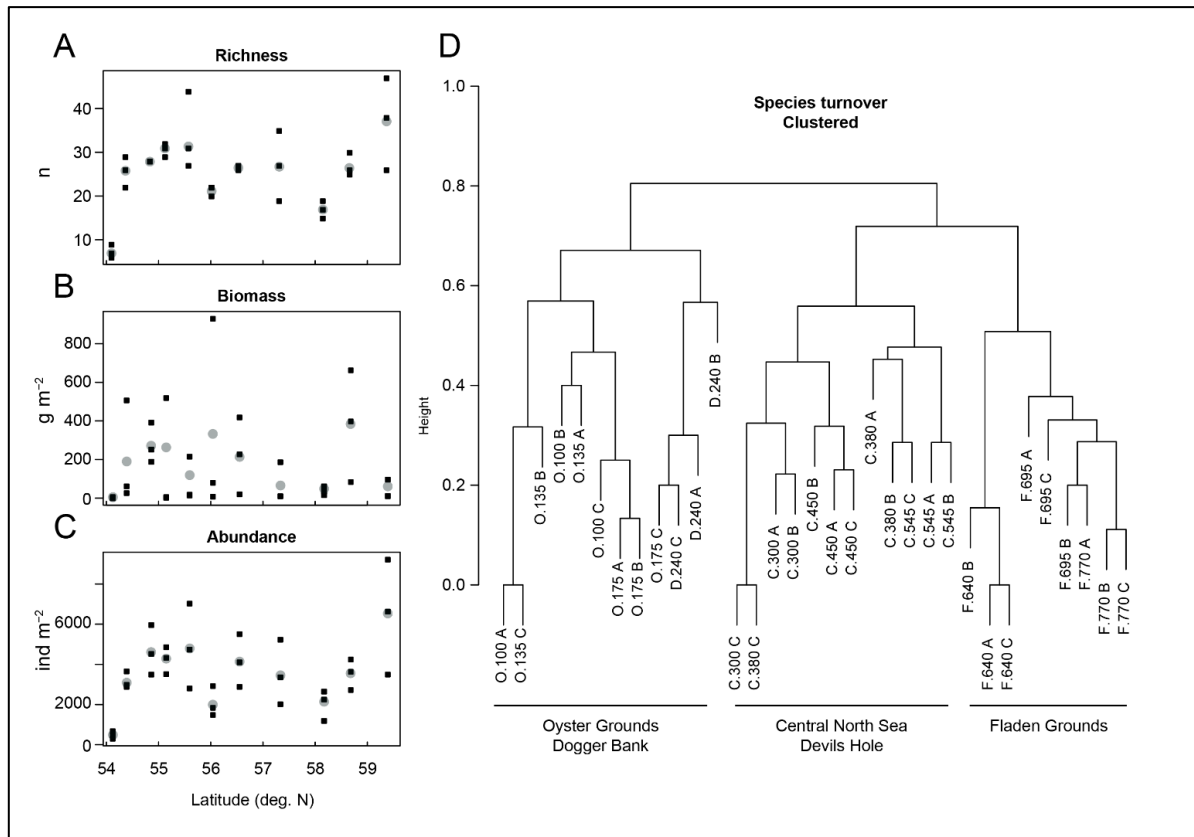
Figure E 1: (A-C) Values for species richness (n taxa per boxcore), total biomass (gWW m^{-2}), and total abundance (ind. m^{-2}) along the sampled transect. (D) Hierarchical clustering of the individual samples on the basis of the Simpson dissimilarity.

Table E 4: Species abundance and biomass collected in boxcores during the NICO 10 transect.

Taxon	Abundance m^{-2}	Biomass gWW m^{-2}	Station	Rep.	Lat. deg. N	Long. deg. E	Comment
Callianassa subterranea	12.4	0.071	O.100	1	54.1492	4.3419	
Chaetozone	12.4	0.048	O.100	1	54.1492	4.3419	
Corbula gibba	12.4	0.015	O.100	1	54.1492	4.3419	
Goniada maculata	12.4	0.013	O.100	1	54.1492	4.3419	
Hyala vitrea	24.9	0.032	O.100	1	54.1492	4.3419	
Malmgrenia ljungmani	12.4	0.042	O.100	1	54.1492	4.3419	
Spionidae	12.4	0.001	O.100	1	54.1492	4.3419	juv.
Upogebia deltaura	24.9	0.449	O.100	1	54.1492	4.3419	
Acanthocardia echinata	12.4	0.006	O.100	2	54.1492	4.3419	juv.
Ampelisca tenuicornis	12.4	0.019	O.100	2	54.1492	4.3419	
Cirratulidae	12.4	0.012	O.100	2	54.1492	4.3419	
Harpinia antennaria	24.9	0.028	O.100	2	54.1492	4.3419	
Lumbrineris	12.4	0.083	O.100	2	54.1492	4.3419	
Pectinaria belgica	24.9	0.007	O.100	2	54.1492	4.3419	
Phaxas pellucidus	24.9	0.009	O.100	2	54.1492	4.3419	spat
Spiophanes bombyx	12.4	0.006	O.100	2	54.1492	4.3419	
Sthenelais limicola	12.4	0.549	O.100	2	54.1492	4.3419	
Acanthocardia echinata	12.4	0.001	O.100	3	54.1492	4.3419	spat
Corbula gibba	12.4	0.002	O.100	3	54.1492	4.3419	

Lumbrineris	12.4	0.100	O.100	3	54.1492	4.3419	
Callianassa subterranea	12.4	0.122	O.100	4	54.1492	4.3419	
Diastyloides biplicatus	12.4	0.003	O.100	4	54.1492	4.3419	
Glycera tesselata	12.4	6.811	O.100	4	54.1492	4.3419	
Malmgrenia lunulata	12.4	0.050	O.100	4	54.1492	4.3419	
Pectinaria belgica	12.4	0.002	O.100	4	54.1492	4.3419	
Phaxas pellucidus	24.9	0.016	O.100	4	54.1492	4.3419	spat
Acanthocardia echinata	12.4	25.369	O.135	1	54.415	4.0417	
Ampelisca tenuicornis	49.7	0.170	O.135	1	54.415	4.0417	
Amphictene auricoma	37.3	1.304	O.135	1	54.415	4.0417	
Amphiura filiformis	310.8	7.556	O.135	1	54.415	4.0417	
Callianassa subterranea	24.9	4.479	O.135	1	54.415	4.0417	
Chaetopterus variopedatus	211.4	68.934	O.135	1	54.415	4.0417	
Chamelea striatula	12.4	0.003	O.135	1	54.415	4.0417	spat
Cirratulidae	62.2	0.044	O.135	1	54.415	4.0417	
Corbula gibba	24.9	0.037	O.135	1	54.415	4.0417	
Cylichna cylindracea	12.4	0.004	O.135	1	54.415	4.0417	
Diplocirrus glaucus	12.4	0.050	O.135	1	54.415	4.0417	
Ebalia tuberosa	12.4	0.062	O.135	1	54.415	4.0417	no legs
Echinocardium cordatum	12.4	274.886	O.135	1	54.415	4.0417	
Echinocardium flavescens	12.4	110.426	O.135	1	54.415	4.0417	
Eudorella truncatula	12.4	0.007	O.135	1	54.415	4.0417	
Gattyana cirrhosa	24.9	0.019	O.135	1	54.415	4.0417	
Glycera alba	12.4	11.609	O.135	1	54.415	4.0417	
Harpinia antennaria	136.8	0.197	O.135	1	54.415	4.0417	
Kurtiella bidentata	24.9	0.027	O.135	1	54.415	4.0417	
Levinsenia gracilis	12.4	0.006	O.135	1	54.415	4.0417	
Lumbrineris	12.4	0.125	O.135	1	54.415	4.0417	
Nemertea	12.4	0.006	O.135	1	54.415	4.0417	
Nucula nitidosa	12.4	0.034	O.135	1	54.415	4.0417	
Oxydromus flexuosus	12.4	0.031	O.135	1	54.415	4.0417	
Phaxas pellucidus	12.4	0.917	O.135	1	54.415	4.0417	
Pholoe assimilis	12.4	0.008	O.135	1	54.415	4.0417	
Polynoidae	12.4	0.004	O.135	1	54.415	4.0417	
Pseudione borealis	37.3	0.188	O.135	1	54.415	4.0417	2f, 1m
Spio martinensis	12.4	0.009	O.135	1	54.415	4.0417	
Spiophanes bombyx	12.4	0.081	O.135	1	54.415	4.0417	
Amphictene auricoma	12.4	0.284	O.135	2	54.415	4.0417	
Amphiura filiformis	397.9	15.408	O.135	2	54.415	4.0417	
Argissa hamatipes	12.4	0.004	O.135	2	54.415	4.0417	
Bivalvia	24.9	0.032	O.135	2	54.415	4.0417	cf. Montacutidae
Callianassa subterranea	24.9	3.309	O.135	2	54.415	4.0417	
Cirratulidae	24.9	0.040	O.135	2	54.415	4.0417	cf. Chaetozone
Corbula gibba	24.9	0.201	O.135	2	54.415	4.0417	
Cylichna cylindracea	49.7	0.271	O.135	2	54.415	4.0417	

Enipo elisabethae	12.4	0.761	O.135	2	54.415	4.0417	
Euspira nitida	12.4	1.685	O.135	2	54.415	4.0417	
Harmothoe	12.4	0.202	O.135	2	54.415	4.0417	x TBC
Harpinia antennaria	37.3	0.049	O.135	2	54.415	4.0417	
Hyala vitrea	12.4	0.022	O.135	2	54.415	4.0417	
Kurtiella bidentata	62.2	0.096	O.135	2	54.415	4.0417	
Nemertea	12.4	0.109	O.135	2	54.415	4.0417	
Nephtys	24.9	0.130	O.135	2	54.415	4.0417	juv.
Nephtys kersivalensis	24.9	1.504	O.135	2	54.415	4.0417	
Notomastus latericeus	12.4	0.220	O.135	2	54.415	4.0417	
Nucula nitidosa	12.4	1.187	O.135	2	54.415	4.0417	
Pholoe assimilis	24.9	0.020	O.135	2	54.415	4.0417	
Pseudione borealis	24.9	0.199	O.135	2	54.415	4.0417	1f, 1m
Thracia convexa	12.4	0.625	O.135	2	54.415	4.0417	
Thyasira sarsii	24.9	0.024	O.135	2	54.415	4.0417	
Abra nitida	12.4	0.174	O.135	3	54.415	4.0417	
Ampelisca tenuicornis	12.4	0.016	O.135	3	54.415	4.0417	
Amphictene auricoma	87.0	0.752	O.135	3	54.415	4.0417	
Amphiura filiformis	211.4	3.148	O.135	3	54.415	4.0417	
Brissopsis lyrifera	12.4	11.062	O.135	3	54.415	4.0417	fragments
Callianassa subterranea	74.6	3.500	O.135	3	54.415	4.0417	
Chaetopterus variopedatus	74.6	26.758	O.135	3	54.415	4.0417	
Chamelea striatula	12.4	0.102	O.135	3	54.415	4.0417	
Cirratulidae	12.4	0.012	O.135	3	54.415	4.0417	
Corbula gibba	74.6	0.907	O.135	3	54.415	4.0417	
Cylichna cylindracea	24.9	0.127	O.135	3	54.415	4.0417	
Edwardsia claparedii	12.4	0.225	O.135	3	54.415	4.0417	
Harmothoe antilopes	37.3	2.314	O.135	3	54.415	4.0417	
Harpinia antennaria	49.7	0.071	O.135	3	54.415	4.0417	
Hiatella arctica	12.4	0.009	O.135	3	54.415	4.0417	juv.
Leucothoe lilljeborgi	12.4	0.019	O.135	3	54.415	4.0417	
Montacuta substriata	24.9	0.049	O.135	3	54.415	4.0417	
Nephtys	24.9	0.197	O.135	3	54.415	4.0417	juv.
Nephtys kersivalensis	12.4	1.339	O.135	3	54.415	4.0417	
Nucula nitidosa	12.4	0.174	O.135	3	54.415	4.0417	
Ocnus lacteus	12.4	0.133	O.135	3	54.415	4.0417	
Orbinia latreillii	12.4	0.116	O.135	3	54.415	4.0417	
Pariambus typicus	12.4	0.004	O.135	3	54.415	4.0417	
Polynoidae	12.4	0.014	O.135	3	54.415	4.0417	juv.
Thracia convexa	24.9	1.688	O.135	3	54.415	4.0417	
Thyasira flexuosa	24.9	0.291	O.135	3	54.415	4.0417	
Upogebia deltaura	12.4	7.887	O.135	3	54.415	4.0417	
Abra nitida	62.2	0.440	O.190	1	54.8858	3.6918	
Bivalvia	12.4	0.004	O.190	1	54.8858	3.6918	spat
Callianassa subterranea	49.7	1.365	O.190	1	54.8858	3.6918	

Chamelea striatula	37.3	13.012	O.190	1	54.8858	3.6918	
Cirratulidae	49.7	0.068	O.190	1	54.8858	3.6918	
Corbula gibba	12.4	0.006	O.190	1	54.8858	3.6918	spat
Cylichna cylindracea	24.9	0.010	O.190	1	54.8858	3.6918	
Diplocirrus glaucus	37.3	0.143	O.190	1	54.8858	3.6918	
Echinocardium flavescens	24.9	228.884	O.190	1	54.8858	3.6918	
Ennucula tenuis	74.6	0.156	O.190	1	54.8858	3.6918	
Eudorella truncatula	12.4	0.005	O.190	1	54.8858	3.6918	
Euspira nitida	37.3	0.112	O.190	1	54.8858	3.6918	
Gattyana cirrhosa	12.4	1.114	O.190	1	54.8858	3.6918	no head
Goniada maculata	24.9	0.017	O.190	1	54.8858	3.6918	
Harpinia pectinata	74.6	0.062	O.190	1	54.8858	3.6918	
Magelona filiformis	37.3	0.043	O.190	1	54.8858	3.6918	
Nemertea	12.4	0.015	O.190	1	54.8858	3.6918	
Nephtys	12.4	0.009	O.190	1	54.8858	3.6918	juv.
Nephtys cirrosa	24.9	1.536	O.190	1	54.8858	3.6918	
Notomastus latericeus	87.0	1.857	O.190	1	54.8858	3.6918	
Ophelina acuminata	12.4	1.250	O.190	1	54.8858	3.6918	
Ophiuroidea	373.0	0.164	O.190	1	54.8858	3.6918	juv.
Pectinaria belgica	62.2	0.011	O.190	1	54.8858	3.6918	
Perioculodes longimanus	12.4	0.003	O.190	1	54.8858	3.6918	
Phaxas pellucidus	24.9	1.128	O.190	1	54.8858	3.6918	
Pholoe assimilis	12.4	0.004	O.190	1	54.8858	3.6918	
Polynoidae	12.4	0.005	O.190	1	54.8858	3.6918	no scales
Scoloplos armiger	24.9	0.159	O.190	1	54.8858	3.6918	
Streblospio benedicti	12.4	0.005	O.190	1	54.8858	3.6918	
Thyasira flexuosa	111.9	0.251	O.190	1	54.8858	3.6918	
Abra nitida	87.0	1.620	O.190	2	54.8858	3.6918	
Amphiura	49.7	0.040	O.190	2	54.8858	3.6918	juv.
Argissa hamatipes	12.4	0.008	O.190	2	54.8858	3.6918	
Asteroidea	24.9	0.026	O.190	2	54.8858	3.6918	juv.
Callianassa subterranea	12.4	0.341	O.190	2	54.8858	3.6918	
Chaetopterus variopedatus	12.4	90.603	O.190	2	54.8858	3.6918	
Chaetozone	24.9	0.031	O.190	2	54.8858	3.6918	
Chamelea striatula	12.4	51.557	O.190	2	54.8858	3.6918	
Chamelea striatula	12.4	0.046	O.190	2	54.8858	3.6918	juv.
Corbula gibba	12.4	3.722	O.190	2	54.8858	3.6918	
Diplocirrus glaucus	24.9	0.331	O.190	2	54.8858	3.6918	
Ennucula tenuis	74.6	0.074	O.190	2	54.8858	3.6918	
Euspira nitida	12.4	0.039	O.190	2	54.8858	3.6918	
Gattyana cirrhosa	24.9	18.368	O.190	2	54.8858	3.6918	
Glycera alba	12.4	0.815	O.190	2	54.8858	3.6918	
Glyphohesione klatti	24.9	0.025	O.190	2	54.8858	3.6918	
Harpinia antennaria	62.2	0.049	O.190	2	54.8858	3.6918	
Montacuta substriata	12.4	0.015	O.190	2	54.8858	3.6918	

Nemertea	12.4	0.996	O.190	2	54.8858	3.6918	
Nephtys	12.4	0.018	O.190	2	54.8858	3.6918	juv.
Notomastus latericeus	335.7	15.910	O.190	2	54.8858	3.6918	
Paranaitis wahlbergi	12.4	0.287	O.190	2	54.8858	3.6918	
Pectinaria belgica	12.4	0.005	O.190	2	54.8858	3.6918	
Phaxas pellucidus	12.4	3.228	O.190	2	54.8858	3.6918	
Sagitta	24.9	0.017	O.190	2	54.8858	3.6918	
Scoloplos armiger	62.2	0.049	O.190	2	54.8858	3.6918	
Spiophanes bombyx	87.0	0.089	O.190	2	54.8858	3.6918	
Thracia convexa	12.4	0.501	O.190	2	54.8858	3.6918	
Thyasira flexuosa	87.0	0.343	O.190	2	54.8858	3.6918	
Abra	99.5	0.040	O.190	3	54.8858	3.6918	spat
Amphiura	12.4	0.051	O.190	3	54.8858	3.6918	juv.
Argissa hamatipes	12.4	0.005	O.190	3	54.8858	3.6918	
Brissopsis lyrifera	12.4	61.352	O.190	3	54.8858	3.6918	
Callianassa subterranea	12.4	13.325	O.190	3	54.8858	3.6918	f + eggs
Chaetopterus variopedatus	12.4	6.104	O.190	3	54.8858	3.6918	
Chaetozone	12.4	0.018	O.190	3	54.8858	3.6918	
Chamelea striatula	74.6	0.113	O.190	3	54.8858	3.6918	
Cirratulidae	12.4	0.004	O.190	3	54.8858	3.6918	
Corbula gibba	12.4	0.008	O.190	3	54.8858	3.6918	juv.
Echinocardium cordatum	12.4	198.636	O.190	3	54.8858	3.6918	
Echinocardium flavescens	12.4	96.334	O.190	3	54.8858	3.6918	
Eudorella truncatula	12.4	0.008	O.190	3	54.8858	3.6918	1m
Euspira nitida	12.4	0.017	O.190	3	54.8858	3.6918	
Goniadidae	12.4	0.979	O.190	3	54.8858	3.6918	no head
Harpinia antennaria	136.8	0.197	O.190	3	54.8858	3.6918	
Lucinoma borealis	12.4	11.226	O.190	3	54.8858	3.6918	
Magelona filiformis	12.4	0.004	O.190	3	54.8858	3.6918	
Nephtys	49.7	0.066	O.190	3	54.8858	3.6918	juv.
Nephtys hombergii	12.4	3.272	O.190	3	54.8858	3.6918	
Nucula nitidosa	62.2	0.077	O.190	3	54.8858	3.6918	
Pectinaria belgica	37.3	0.007	O.190	3	54.8858	3.6918	
Perioculodes longimanus	24.9	0.015	O.190	3	54.8858	3.6918	
Phyllodoce rosea	12.4	0.006	O.190	3	54.8858	3.6918	
Scoloplos armiger	12.4	0.109	O.190	3	54.8858	3.6918	
Spiophanes bombyx	87.0	0.096	O.190	3	54.8858	3.6918	
Sthenelais limicola	12.4	0.024	O.190	3	54.8858	3.6918	
Tellimya ferruginosa	24.9	0.024	O.190	3	54.8858	3.6918	
Thracia	49.7	0.025	O.190	3	54.8858	3.6918	juv.
Thyasira sarsii	87.0	0.187	O.190	3	54.8858	3.6918	
Argissa hamatipes	12.4	0.006	O.240	1	55.171683	3.157901	
Bathyporeia	99.5	0.016	O.240	1	55.171683	3.157901	dam.
Bathyporeia elegans	74.6	0.030	O.240	1	55.171683	3.157901	
Bathyporeia guilliamsoniana	174.1	0.107	O.240	1	55.171683	3.157901	

Bathyporeia tenuipes	12.4	0.010	O.240	1	55.171683	3.157901	
Bivalvia	49.7	0.092	O.240	1	55.171683	3.157901	dam.
Chaetozone	74.6	0.218	O.240	1	55.171683	3.157901	
Corbula gibba	12.4	0.010	O.240	1	55.171683	3.157901	
Dosinia	12.4	0.249	O.240	1	55.171683	3.157901	
Ebalia tuberosa	12.4	0.053	O.240	1	55.171683	3.157901	juv.
Echinocyamus pusillus	87.0	0.024	O.240	1	55.171683	3.157901	
Edwardsia claparedii	49.7	0.167	O.240	1	55.171683	3.157901	
Eteone longa	12.4	0.015	O.240	1	55.171683	3.157901	
Euspira nitida	24.9	0.346	O.240	1	55.171683	3.157901	
Glycinde nordmanni	12.4	0.007	O.240	1	55.171683	3.157901	
Magelona alleni	24.9	0.072	O.240	1	55.171683	3.157901	
Magelona filiformis	186.5	0.001	O.240	1	55.171683	3.157901	
Maldanidae	0.0	0.834	O.240	1	55.171683	3.157901	
Megaluropus agilis	12.4	0.012	O.240	1	55.171683	3.157901	
Nephtyidae	62.2	0.562	O.240	1	55.171683	3.157901	
Pectinariidae	12.4	0.012	O.240	1	55.171683	3.157901	
Perioculodes longimanus	37.3	0.021	O.240	1	55.171683	3.157901	
Phtisica marina	24.9	0.010	O.240	1	55.171683	3.157901	
Pontocrates altamarinus	12.4	0.001	O.240	1	55.171683	3.157901	
Pseudocuma simile	12.4	0.007	O.240	1	55.171683	3.157901	
Pseudocumatidae	12.4	0.007	O.240	1	55.171683	3.157901	
Scolelepis squamata	12.4	0.399	O.240	1	55.171683	3.157901	
Scoloplos armiger	24.9	0.031	O.240	1	55.171683	3.157901	
Sigalion	12.4	0.009	O.240	1	55.171683	3.157901	
Sigalion mathildae	12.4	1.956	O.240	1	55.171683	3.157901	
Tellimya ferruginosa	12.4	0.025	O.240	1	55.171683	3.157901	
Tellinidae	24.9	0.001	O.240	1	55.171683	3.157901	juv.
Terebellidae	0.0	3.158	O.240	1	55.171683	3.157901	
Urothoe	49.7	0.025	O.240	1	55.171683	3.157901	dam.
Urothoe poseidonis	37.3	0.022	O.240	1	55.171683	3.157901	
Acrocnida brachiata	12.4	6.641	O.240	2	55.171683	3.157982	
Actiniaria	12.4	0.081	O.240	2	55.171683	3.157982	
Bathyporeia	37.3	0.010	O.240	2	55.171683	3.157982	dam.
Bathyporeia elegans	186.5	0.114	O.240	2	55.171683	3.157982	
Bathyporeia guilliamsoniana	136.8	0.144	O.240	2	55.171683	3.157982	
Bivalvia	24.9	0.262	O.240	2	55.171683	3.157982	dam.
Chaetozone	24.9	0.063	O.240	2	55.171683	3.157982	
Chamelea striatula	12.4	75.003	O.240	2	55.171683	3.157982	
Dosinia	12.4	0.387	O.240	2	55.171683	3.157982	juv.
Echinocardium cordatum	12.4	431.066	O.240	2	55.171683	3.157982	
Edwardsia claparedii	12.4	0.044	O.240	2	55.171683	3.157982	
Glycera alba	12.4	0.182	O.240	2	55.171683	3.157982	
Glycinde nordmanni	24.9	0.123	O.240	2	55.171683	3.157982	
Goniada maculata	12.4	0.030	O.240	2	55.171683	3.157982	

Hippomedon denticulatus	62.2	0.045	O.240	2	55.171683	3.157982	
Jassa sp.	261.1	0.250	O.240	2	55.171683	3.157982	
Luidia sarsii	12.4	83.750	O.240	2	55.171683	3.157982	
Lysianassidae	24.9	0.019	O.240	2	55.171683	3.157982	
Magelona alleni	24.9	0.169	O.240	2	55.171683	3.157982	
Magelona filiformis	198.9	0.068	O.240	2	55.171683	3.157982	
Perioculodes longimanus	12.4	0.001	O.240	2	55.171683	3.157982	
Pharidae	12.4	0.012	O.240	2	55.171683	3.157982	
Philine sp.	12.4	0.009	O.240	2	55.171683	3.157982	
Pisidia longicornis	12.4	0.318	O.240	2	55.171683	3.157982	
Pontocrates altamarinus	12.4	0.001	O.240	2	55.171683	3.157982	
Scoloplos armiger	24.9	0.078	O.240	2	55.171683	3.157982	
Sigalion	87.0	0.065	O.240	2	55.171683	3.157982	
Sigalion mathildae	74.6	4.874	O.240	2	55.171683	3.157982	
Sphaerodorum gracilis	12.4	0.020	O.240	2	55.171683	3.157982	
Spiophanes bombyx	12.4	0.025	O.240	2	55.171683	3.157982	
Tellimya ferruginosa	24.9	0.011	O.240	2	55.171683	3.157982	
Tellinidae	62.2	0.002	O.240	2	55.171683	3.157982	
Tharyx sp.	12.4	0.001	O.240	2	55.171683	3.157982	
Tryphosa nana	24.9	0.012	O.240	2	55.171683	3.157982	
Urothoe poseidonis	49.7	0.050	O.240	2	55.171683	3.157982	
Atylidae	12.4	0.010	O.240	3	55.171683	3.158167	dam.
Bathyporeia	111.9	0.034	O.240	3	55.171683	3.158167	dam.
Bathyporeia elegans	87.0	0.025	O.240	3	55.171683	3.158167	
Bathyporeia guilliamsoniana	49.7	0.063	O.240	3	55.171683	3.158167	
Bivalvia	49.7	0.223	O.240	3	55.171683	3.158167	dam.
Corbula gibba	12.4	0.165	O.240	3	55.171683	3.158167	
Dosinia	24.9	0.022	O.240	3	55.171683	3.158167	juv.
Echinocyamus pusillus	24.9	0.019	O.240	3	55.171683	3.158167	
Eteone longa	12.4	0.015	O.240	3	55.171683	3.158167	
Euspira nitida	12.4	0.123	O.240	3	55.171683	3.158167	
Glycinde nordmanni	12.4	0.182	O.240	3	55.171683	3.158167	
Goniada maculata	12.4	0.025	O.240	3	55.171683	3.158167	
Kurtiella bidentata	12.4	0.014	O.240	3	55.171683	3.158167	
Leiochone sp.	12.4	0.398	O.240	3	55.171683	3.158167	
Leucothoe incisa	12.4	0.015	O.240	3	55.171683	3.158167	
Magelona filiformis	261.1	0.037	O.240	3	55.171683	3.158167	
Magelona johnstoni	12.4	0.015	O.240	3	55.171683	3.158167	
Myrianida sp.	12.4	0.014	O.240	3	55.171683	3.158167	
Nephtyidae	37.3	0.116	O.240	3	55.171683	3.158167	
Ophelia borealis	12.4	0.027	O.240	3	55.171683	3.158167	
Pennatulacea	12.4	0.009	O.240	3	55.171683	3.158167	
Perioculodes longimanus	24.9	0.001	O.240	3	55.171683	3.158167	
Pseudocumatidae	12.4	0.007	O.240	3	55.171683	3.158167	
Scoloplos armiger	24.9	0.121	O.240	3	55.171683	3.158167	

Sigalion	12.4	0.014	O.240	3	55.171683	3.158167	
Sigalion mathildae	12.4	0.528	O.240	3	55.171683	3.158167	
Spiophanes bombyx	24.9	0.385	O.240	3	55.171683	3.158167	
Sthenelais limicola	12.4	0.159	O.240	3	55.171683	3.158167	
Terebellidae	12.4	0.235	O.240	3	55.171683	3.158167	
Tharyx sp.	37.3	0.004	O.240	3	55.171683	3.158167	
Urothoe	12.4	0.012	O.240	3	55.171683	3.158167	dam.
Urothoe poseidonis	24.9	0.011	O.240	3	55.171683	3.158167	
Ampelisca tenuicornis	24.9	0.021	C.300	1	55.6216	2.3865	
Amphictene auricoma	37.3	0.055	C.300	1	55.6216	2.3865	
Antalis entalis	74.6	8.102	C.300	1	55.6216	2.3865	
Argissa hamatipes	24.9	0.015	C.300	1	55.6216	2.3865	
Axinulus croulinensis	12.4	0.002	C.300	1	55.6216	2.3865	
Caprella	12.4	0.003	C.300	1	55.6216	2.3865	head and G1 only
Chamelea striatula	24.9	0.010	C.300	1	55.6216	2.3865	juv.
Cirratulidae	12.4	0.009	C.300	1	55.6216	2.3865	
Cylichna cylindracea	12.4	0.145	C.300	1	55.6216	2.3865	
Diplocirrus glaucus	37.3	0.627	C.300	1	55.6216	2.3865	
Ditrupa arietina	24.9	0.676	C.300	1	55.6216	2.3865	
Goniada	12.4	0.008	C.300	1	55.6216	2.3865	juv.
Harpinia antennaria	12.4	0.008	C.300	1	55.6216	2.3865	
Hemilamprops roseus	12.4	0.034	C.300	1	55.6216	2.3865	f
Hermania scabra	12.4	0.024	C.300	1	55.6216	2.3865	
Heteromastus filiformis	12.4	0.011	C.300	1	55.6216	2.3865	
Levinsenia gracilis	12.4	0.012	C.300	1	55.6216	2.3865	
Myriochele oculata	12.4	0.001	C.300	1	55.6216	2.3865	
Mysia undata	12.4	2.918	C.300	1	55.6216	2.3865	
Nemertea	12.4	0.035	C.300	1	55.6216	2.3865	
Ophiura affinis	12.4	0.122	C.300	1	55.6216	2.3865	
Paramphinome jeffreysii	211.4	0.116	C.300	1	55.6216	2.3865	
Rhodine gracilior	12.4	0.642	C.300	1	55.6216	2.3865	
Scoloplos armiger	37.3	0.197	C.300	1	55.6216	2.3865	
Spiophanes bombyx	12.4	0.012	C.300	1	55.6216	2.3865	
Spiophanes kroyeri	12.4	0.057	C.300	1	55.6216	2.3865	
Spisula subtruncata	12.4	0.147	C.300	1	55.6216	2.3865	juv.
Tellimya tenella	37.3	0.133	C.300	1	55.6216	2.3865	
Ampelisca tenuicornis	24.9	0.020	C.300	2	55.6216	2.3865	
Amphictene auricoma	87.0	0.655	C.300	2	55.6216	2.3865	
Amphiura filiformis	24.9	0.452	C.300	2	55.6216	2.3865	
Argissa hamatipes	37.3	0.016	C.300	2	55.6216	2.3865	
Bivalvia	12.4	0.005	C.300	2	55.6216	2.3865	spat CALC
Chaetoderma nitidulum	12.4	0.193	C.300	2	55.6216	2.3865	
Chamelea striatula	24.9	0.007	C.300	2	55.6216	2.3865	juv.
Cylichna cylindracea	12.4	0.189	C.300	2	55.6216	2.3865	
Diplocirrus glaucus	12.4	0.084	C.300	2	55.6216	2.3865	

Ditrupa arietina	161.6	4.311	C.300	2	55.6216	2.3865	with tube
Echinocardium cordatum	12.4	10.155	C.300	2	55.6216	2.3865	
Eteone longa	24.9	0.060	C.300	2	55.6216	2.3865	longa/flava complex
Eudorella truncatula	24.9	0.006	C.300	2	55.6216	2.3865	
Eudorellopsis deformis	24.9	0.011	C.300	2	55.6216	2.3865	
Goniada maculata	24.9	0.090	C.300	2	55.6216	2.3865	
Hermania scabra	49.7	0.071	C.300	2	55.6216	2.3865	
Levinsenia gracilis	87.0	0.038	C.300	2	55.6216	2.3865	
Nemertea	12.4	0.015	C.300	2	55.6216	2.3865	
Nephtys assimilis	12.4	0.473	C.300	2	55.6216	2.3865	
Nephtys cirrosa	12.4	0.170	C.300	2	55.6216	2.3865	
Ophelina modesta	24.9	0.005	C.300	2	55.6216	2.3865	
Owenia fusiformis	74.6	0.039	C.300	2	55.6216	2.3865	
Oxydromus flexuosus	37.3	0.389	C.300	2	55.6216	2.3865	
Paguridae	12.4	0.103	C.300	2	55.6216	2.3865	no chelae
Paramphinome jeffreysii	310.8	0.162	C.300	2	55.6216	2.3865	
Perioculodes longimanus	12.4	0.003	C.300	2	55.6216	2.3865	
Sagitta	12.4	0.005	C.300	2	55.6216	2.3865	
Scoloplos armiger	24.9	0.147	C.300	2	55.6216	2.3865	
Spio	49.7	0.012	C.300	2	55.6216	2.3865	
Spiophanes bombyx	12.4	0.003	C.300	2	55.6216	2.3865	
Tellimya ferruginosa	12.4	0.031	C.300	2	55.6216	2.3865	
Thelepus cincinnatus	12.4	0.020	C.300	2	55.6216	2.3865	
Ampelisca tenuicornis	24.9	0.019	C.300	3	55.6216	2.3865	
Ampharete lindstroemi	37.3	0.025	C.300	3	55.6216	2.3865	
Amphictene auricoma	111.9	0.116	C.300	3	55.6216	2.3865	
Amphiura filiformis	24.9	0.123	C.300	3	55.6216	2.3865	juv.
Antalis entalis	37.3	3.399	C.300	3	55.6216	2.3865	
Arctica islandica	12.4	176.893	C.300	3	55.6216	2.3865	
Argissa hamatipes	62.2	0.023	C.300	3	55.6216	2.3865	
Brissopsis lyrifera	12.4	32.304	C.300	3	55.6216	2.3865	
Brissopsis lyrifera	12.4	0.001	C.300	3	55.6216	2.3865	spat
Chaetoderma nitidulum	12.4	0.163	C.300	3	55.6216	2.3865	
Cirratulidae	24.9	0.022	C.300	3	55.6216	2.3865	
Crenella decussata	12.4	0.004	C.300	3	55.6216	2.3865	
Cylichna cylindracea	24.9	0.415	C.300	3	55.6216	2.3865	
Diastylis	12.4	0.050	C.300	3	55.6216	2.3865	no tail
Diplocirrus glaucus	24.9	0.247	C.300	3	55.6216	2.3865	
Ditrupa arietina	24.9	0.065	C.300	3	55.6216	2.3865	
Ennucula tenuis	24.9	0.040	C.300	3	55.6216	2.3865	
Eudorella truncatula	12.4	0.004	C.300	3	55.6216	2.3865	
Gastropoda	12.4	0.006	C.300	3	55.6216	2.3865	no shell
Glossobalanus marginatus	12.4	0.010	C.300	3	55.6216	2.3865	
Goniada maculata	12.4	0.013	C.300	3	55.6216	2.3865	
Goniadella	12.4	0.040	C.300	3	55.6216	2.3865	

Harmothoe clavigera	12.4	0.005	C.300	3	55.6216	2.3865	
Harpinia pectinata	62.2	0.030	C.300	3	55.6216	2.3865	
Hermania scabra	74.6	0.062	C.300	3	55.6216	2.3865	
Levinsenia gracilis	49.7	0.032	C.300	3	55.6216	2.3865	
Lucinoma borealis	74.6	0.049	C.300	3	55.6216	2.3865	juv.
Magelona filiformis	12.4	0.003	C.300	3	55.6216	2.3865	
Monoculodes packardi	12.4	0.001	C.300	3	55.6216	2.3865	
Montacuta substriata	49.7	0.016	C.300	3	55.6216	2.3865	with Barentsia gracilis
Myriochele oculata	12.4	0.020	C.300	3	55.6216	2.3865	
Nannastacus unguiculatus	12.4	0.005	C.300	3	55.6216	2.3865	
Nephasoma minutum	24.9	0.012	C.300	3	55.6216	2.3865	
Nephtys kersivalensis	24.9	0.736	C.300	3	55.6216	2.3865	
Ophelina modesta	74.6	0.018	C.300	3	55.6216	2.3865	
Oxydromus flexuosus	12.4	0.179	C.300	3	55.6216	2.3865	
Pagurus pubescens	12.4	0.051	C.300	3	55.6216	2.3865	
Paramphinome jeffreysii	932.5	0.558	C.300	3	55.6216	2.3865	
Retusa obtusa	12.4	0.020	C.300	3	55.6216	2.3865	juv.
Rhodine	12.4	0.046	C.300	3	55.6216	2.3865	no head, no tail
Rhodine loveni	12.4	0.306	C.300	3	55.6216	2.3865	
Scoloplos armiger	37.3	0.090	C.300	3	55.6216	2.3865	
Spio	49.7	0.030	C.300	3	55.6216	2.3865	
Spiophanes bombyx	12.4	0.004	C.300	3	55.6216	2.3865	
Spiophanes kroyeri	12.4	0.011	C.300	3	55.6216	2.3865	
Thyasiridae	49.7	0.017	C.300	3	55.6216	2.3865	juv.
Vitreolina antiflexa	12.4	0.027	C.300	3	55.6216	2.3865	
Amaeana trilobata	12.4	0.896	C.380	1	56.0649	1.5965	
Ampelisca tenuicornis	24.9	0.098	C.380	1	56.0649	1.5965	
Ampelisca typica	12.4	0.097	C.380	1	56.0649	1.5965	
Aphelochaeta marioni	124.3	12.506	C.380	1	56.0649	1.5965	
Brissopsis lyrifera	795.8	0.092	C.380	1	56.0649	1.5965	juv.
Callianassa subterranea	12.4	0.022	C.380	1	56.0649	1.5965	
Hippomedon denticulatus	12.4	0.343	C.380	1	56.0649	1.5965	
Lucinoma borealis	24.9	57.426	C.380	1	56.0649	1.5965	
Nannastacus unguiculatus	12.4	0.005	C.380	1	56.0649	1.5965	
Nephtys	12.4	0.052	C.380	1	56.0649	1.5965	juv.
Nephtys caeca	12.4	3.570	C.380	1	56.0649	1.5965	
Notomastus latericeus	12.4	1.207	C.380	1	56.0649	1.5965	no head
Oxydromus flexuosus	12.4	0.142	C.380	1	56.0649	1.5965	
Paramphinome jeffreysii	136.8	0.067	C.380	1	56.0649	1.5965	
Phoronis muelleri	24.9	2.542	C.380	1	56.0649	1.5965	
Phyllodoce maculata	12.4	0.007	C.380	1	56.0649	1.5965	
Scolelepis korsuni	12.4	0.322	C.380	1	56.0649	1.5965	
Scoloplos armiger	12.4	0.159	C.380	1	56.0649	1.5965	
Spiophanes kroyeri	37.3	0.067	C.380	1	56.0649	1.5965	
Synchelidium tenuimanum	24.9	0.004	C.380	1	56.0649	1.5965	

Terebellides shetlandica	12.4	0.110	C.380	1	56.0649	1.5965	
Timoclea ovata	12.4	0.047	C.380	1	56.0649	1.5965	
Anapagurus hyndmanni	12.4	0.270	C.380	2	56.0649	1.5965	
Aricidea suecica	12.4	0.021	C.380	2	56.0649	1.5965	
Bathyporeia elegans	12.4	0.041	C.380	2	56.0649	1.5965	
Chaetoderma nitidulum	12.4	0.624	C.380	2	56.0649	1.5965	
Cirratulidae	124.3	1.461	C.380	2	56.0649	1.5965	
Echinoidea	1715.9	0.045	C.380	2	56.0649	1.5965	juv.
Eudorellopsis deformis	12.4	0.006	C.380	2	56.0649	1.5965	
Glycera lapidum	24.9	0.614	C.380	2	56.0649	1.5965	
Lysilla loveni	12.4	0.026	C.380	2	56.0649	1.5965	
Metopa rubrovittata	12.4	0.009	C.380	2	56.0649	1.5965	
Nephtys longosetosa	12.4	0.897	C.380	2	56.0649	1.5965	
Notomastus latericeus	12.4	1.418	C.380	2	56.0649	1.5965	no head
Oedocerotidae	12.4	0.007	C.380	2	56.0649	1.5965	poor condition
Ophiuroidea	12.4	0.154	C.380	2	56.0649	1.5965	poor condition
Paramphinome jeffreysii	111.9	0.043	C.380	2	56.0649	1.5965	
Pectinaria belgica	12.4	0.007	C.380	2	56.0649	1.5965	juv.
Pennatula phosphorea	12.4	2.289	C.380	2	56.0649	1.5965	
Phyllodoce mucosa	49.7	0.027	C.380	2	56.0649	1.5965	
Polychaeta	12.4	0.814	C.380	2	56.0649	1.5965	no head
Polychaeta	12.4	0.007	C.380	2	56.0649	1.5965	fragments
Pseudocuma longicorne	12.4	0.005	C.380	2	56.0649	1.5965	
Scoloplos armiger	12.4	0.031	C.380	2	56.0649	1.5965	
Spatangoida	12.4	10.898	C.380	2	56.0649	1.5965	fragments
Spiophanes bombyx	136.8	0.049	C.380	2	56.0649	1.5965	
Sthenelais limicola	12.4	0.742	C.380	2	56.0649	1.5965	
Abra	12.4	0.015	C.380	3	56.0649	1.5965	
Ampelisca brevicornis	12.4	0.080	C.380	3	56.0649	1.5965	cf.
Ampelisca spinipes	12.4	0.065	C.380	3	56.0649	1.5965	cf.
Ampelisca tenuicornis	12.4	0.079	C.380	3	56.0649	1.5965	fem
Amphictene auricoma	24.9	0.011	C.380	3	56.0649	1.5965	
Aonides paucibranchiata	12.4	0.002	C.380	3	56.0649	1.5965	
Arctica islandica	12.4	920.385	C.380	3	56.0649	1.5965	
Asteroidea	24.9	0.026	C.380	3	56.0649	1.5965	juv.
Bivalvia	24.9	0.500	C.380	3	56.0649	1.5965	poor condition
Cirratulidae	174.1	7.035	C.380	3	56.0649	1.5965	
Diastyloides biplicatus	24.9	0.001	C.380	3	56.0649	1.5965	
Echinoidea	4327.0	5.507	C.380	3	56.0649	1.5965	juv.
Eudorellopsis deformis	49.7	0.020	C.380	3	56.0649	1.5965	
Goniada maculata	37.3	0.502	C.380	3	56.0649	1.5965	
Hemilamprops roseus	37.3	0.047	C.380	3	56.0649	1.5965	
Hydrozoa	#VALUE!	1.241	C.380	3	56.0649	1.5965	
Nephtys	12.4	0.047	C.380	3	56.0649	1.5965	juv.
Ophiuroidea	12.4	0.007	C.380	3	56.0649	1.5965	juv. (lost)

Paramphinome jeffreysii	410.3	0.163	C.380	3	56.0649	1.5965	
Parvicardium	12.4	0.021	C.380	3	56.0649	1.5965	poor condition
Phyllodoce rosea	12.4	0.024	C.380	3	56.0649	1.5965	
Polychaeta	12.4	0.969	C.380	3	56.0649	1.5965	
Scoloplos armiger	24.9	0.120	C.380	3	56.0649	1.5965	
Spiophanes bombyx	174.1	0.055	C.380	3	56.0649	1.5965	
Spiophanes kroyeri	12.4	0.001	C.380	3	56.0649	1.5965	
Terebellidae	12.4	0.157	C.380	3	56.0649	1.5965	
Tryphosites longipes	12.4	0.037	C.380	3	56.0649	1.5965	
Ampharetidae	12.4	0.001	C.450	1	56.579	0.6812	
Amphictene auricoma	37.3	0.040	C.450	1	56.579	0.6812	
Amphiura chiajei	24.9	3.414	C.450	1	56.579	0.6812	
Axinulus croulinensis	12.4	0.015	C.450	1	56.579	0.6812	
Brissopsis lyrifera	12.4	86.890	C.450	1	56.579	0.6812	
Cerianthus lloydii	12.4	118.306	C.450	1	56.579	0.6812	
Cirratulidae	87.0	0.558	C.450	1	56.579	0.6812	
Diastylis lucifera	74.6	0.193	C.450	1	56.579	0.6812	
Diplocirrus glaucus	248.7	1.682	C.450	1	56.579	0.6812	
Eunereis elitoralis	12.4	0.016	C.450	1	56.579	0.6812	
Glycera alba	12.4	0.327	C.450	1	56.579	0.6812	
Goniada maculata	12.4	0.030	C.450	1	56.579	0.6812	
Hermania scabra	12.4	0.012	C.450	1	56.579	0.6812	
Heteromastus filiformis	24.9	0.034	C.450	1	56.579	0.6812	
Laonice sarsi	12.4	0.078	C.450	1	56.579	0.6812	
Leptosynapta inhaerens	12.4	1.877	C.450	1	56.579	0.6812	
Leucon nasica	12.4	0.011	C.450	1	56.579	0.6812	
Lumbrineris tetraura	12.4	0.591	C.450	1	56.579	0.6812	
Nemertea	12.4	1.654	C.450	1	56.579	0.6812	
Notomastus latericeus	12.4	11.836	C.450	1	56.579	0.6812	no head
Owenia fusiformis	12.4	0.037	C.450	1	56.579	0.6812	
Paramphinome jeffreysii	298.4	0.175	C.450	1	56.579	0.6812	
Photis longicaudata	37.3	0.062	C.450	1	56.579	0.6812	
Phyllodoce groenlandica	12.4	0.005	C.450	1	56.579	0.6812	juv.
Scoloplos armiger	37.3	0.354	C.450	1	56.579	0.6812	
Spiophanes bombyx	12.4	0.002	C.450	1	56.579	0.6812	
Abra nitida	37.3	0.108	C.450	2	56.579	0.6812	
Abyssoninoe hibernica	12.4	0.125	C.450	2	56.579	0.6812	
Ampharete lindstroemi	12.4	0.058	C.450	2	56.579	0.6812	
Amphictene auricoma	37.3	0.063	C.450	2	56.579	0.6812	
Amphipholis squamata	49.7	0.059	C.450	2	56.579	0.6812	
Amphiura chiajei	37.3	5.049	C.450	2	56.579	0.6812	
Astacilla dilatata	24.9	0.026	C.450	2	56.579	0.6812	
Bivalvia	12.4	0.013	C.450	2	56.579	0.6812	
Cirratulidae	24.9	0.026	C.450	2	56.579	0.6812	
Crenella decussata	49.7	0.093	C.450	2	56.579	0.6812	

Diastylis lucifera	49.7	0.104	C.450	2	56.579	0.6812	
Diplocirrus glaucus	99.5	0.477	C.450	2	56.579	0.6812	
Edwardsia claparedii	12.4	0.502	C.450	2	56.579	0.6812	
Euspira montagui	12.4	0.359	C.450	2	56.579	0.6812	
Glycera	12.4	0.028	C.450	2	56.579	0.6812	juv.
Glycera unicornis	37.3	10.339	C.450	2	56.579	0.6812	
Glycinde nordmanni	24.9	0.067	C.450	2	56.579	0.6812	
Hermania scabra	74.6	0.083	C.450	2	56.579	0.6812	
Leucon nasica	37.3	0.084	C.450	2	56.579	0.6812	
Nemertea	12.4	0.456	C.450	2	56.579	0.6812	
Nephtys kersivalensis	12.4	1.164	C.450	2	56.579	0.6812	
Notomastus latericeus	24.9	0.106	C.450	2	56.579	0.6812	
Nuculana minuta	12.4	0.116	C.450	2	56.579	0.6812	
Odostomia turrita	12.4	0.011	C.450	2	56.579	0.6812	
Ophelina modesta	62.2	0.016	C.450	2	56.579	0.6812	
Paramphinome jeffreysii	609.3	0.373	C.450	2	56.579	0.6812	
Sphaerodorum gracilis	87.0	0.176	C.450	2	56.579	0.6812	
Virgularia mirabilis	12.4	0.162	C.450	2	56.579	0.6812	
Amphictene auricoma	24.9	0.127	C.450	3	56.579	0.6812	
Amphipholis squamata	12.4	0.003	C.450	3	56.579	0.6812	
Amphiura chiajei	87.0	8.445	C.450	3	56.579	0.6812	
Bivalvia	12.4	0.014	C.450	3	56.579	0.6812	
Brissopsis lyrifera	12.4	356.981	C.450	3	56.579	0.6812	
Cirratulidae	24.9	0.063	C.450	3	56.579	0.6812	
Crenella decussata	12.4	0.002	C.450	3	56.579	0.6812	
Diastylis lucifera	24.9	0.024	C.450	3	56.579	0.6812	
Diplocirrus glaucus	174.1	0.983	C.450	3	56.579	0.6812	
Eulalia mustela	12.4	0.041	C.450	3	56.579	0.6812	
Glycera alba	12.4	7.836	C.450	3	56.579	0.6812	
Hermania scabra	12.4	0.004	C.450	3	56.579	0.6812	
Heteromastus filiformis	37.3	0.185	C.450	3	56.579	0.6812	
Kurtiella bidentata	74.6	0.089	C.450	3	56.579	0.6812	
Leptosynapta inhaerens	87.0	16.501	C.450	3	56.579	0.6812	
Leucon nasica	24.9	0.022	C.450	3	56.579	0.6812	
Montacuta substriata	12.4	0.026	C.450	3	56.579	0.6812	
Nephtys kersivalensis	12.4	0.534	C.450	3	56.579	0.6812	
Odostomia turrita	12.4	0.012	C.450	3	56.579	0.6812	
Oestergrenia thomsonii	62.2	11.476	C.450	3	56.579	0.6812	
Ophryotrocha longidentata	12.4	0.002	C.450	3	56.579	0.6812	
Oxydromus flexuosus	12.4	0.070	C.450	3	56.579	0.6812	
Panthalis oerstedi	12.4	14.691	C.450	3	56.579	0.6812	
Paramphinome jeffreysii	795.8	0.406	C.450	3	56.579	0.6812	
Scoloplos armiger	24.9	0.161	C.450	3	56.579	0.6812	
Sphaerodorum gracilis	62.2	0.138	C.450	3	56.579	0.6812	
Sthenelais limicola	12.4	0.204	C.450	3	56.579	0.6812	

Westwoodilla caecula	12.4	0.023	C.450	3	56.579	0.6812	
Abra nitida	49.7	0.011	C.545	1	57.361	0.578	spat
Ampelisca tenuicornis	12.4	0.073	C.545	1	57.361	0.578	no head
Arctica islandica	24.9	185.418	C.545	1	57.361	0.578	
Aricidea suecica	12.4	0.041	C.545	1	57.361	0.578	
Brissopsis lyrifera	497.4	0.063	C.545	1	57.361	0.578	spat
Crangon crangon	12.4	0.113	C.545	1	57.361	0.578	
Eudorellopsis deformis	12.4	0.008	C.545	1	57.361	0.578	
Glycera	12.4	0.037	C.545	1	57.361	0.578	juv.
Glyphohesione klatti	12.4	0.009	C.545	1	57.361	0.578	
Goniada maculata	24.9	0.089	C.545	1	57.361	0.578	
Harpinia pectinata	24.9	0.020	C.545	1	57.361	0.578	
Heteromastus filiformis	12.4	0.012	C.545	1	57.361	0.578	
Kurtiella bidentata	12.4	0.015	C.545	1	57.361	0.578	
Nephtys kersivalensis	12.4	0.471	C.545	1	57.361	0.578	
Paramphinome jeffreysii	12.4	0.007	C.545	1	57.361	0.578	
Prionospio steenstrupi	12.4	0.004	C.545	1	57.361	0.578	
Pseudocuma simile	12.4	0.005	C.545	1	57.361	0.578	
Scoloplos armiger	24.9	0.212	C.545	1	57.361	0.578	
Scoloplos armiger	37.3	0.007	C.545	1	57.361	0.578	
Thyasira flexuosa	12.4	0.139	C.545	1	57.361	0.578	
Ampelisca typica	12.4	0.100	C.545	2	57.361	0.578	f, length A1/A2
Anapagurus laevis	12.4	0.399	C.545	2	57.361	0.578	
Aphelochaeta marioni	12.4	0.498	C.545	2	57.361	0.578	
Bathyporeia elegans	37.3	0.071	C.545	2	57.361	0.578	
Bivalvia	12.4	0.003	C.545	2	57.361	0.578	spat
Brissopsis lyrifera	62.2	0.005	C.545	2	57.361	0.578	juv.
Cirratulidae	24.9	0.034	C.545	2	57.361	0.578	
Cylichna cylindracea	24.9	0.032	C.545	2	57.361	0.578	
Diastyloides biplicatus	12.4	0.005	C.545	2	57.361	0.578	
Echinocyamus pusillus	24.9	0.056	C.545	2	57.361	0.578	
Ennucula tenuis	12.4	1.061	C.545	2	57.361	0.578	
Glycera alba	24.9	0.987	C.545	2	57.361	0.578	
Goniada maculata	12.4	0.032	C.545	2	57.361	0.578	
Harpinia antennaria	12.4	0.010	C.545	2	57.361	0.578	
Myriochele oculata	12.4	0.015	C.545	2	57.361	0.578	
Nemertea	12.4	0.065	C.545	2	57.361	0.578	
Nephtys kersivalensis	12.4	4.947	C.545	2	57.361	0.578	
Ophiuroidea	37.3	0.005	C.545	2	57.361	0.578	juv.
Paramphinome jeffreysii	12.4	0.007	C.545	2	57.361	0.578	
Phaxas pellucidus	24.9	0.092	C.545	2	57.361	0.578	
Phoronis muelleri	12.4	0.691	C.545	2	57.361	0.578	
Phyllodocidae	12.4	0.020	C.545	2	57.361	0.578	no head
Poecilochaetus serpens	24.9	0.007	C.545	2	57.361	0.578	
Scoloplos armiger	74.6	0.420	C.545	2	57.361	0.578	

Spiophanes bombyx	62.2	0.018	C.545	2	57.361	0.578	
Spiophanes kroyeri	12.4	0.069	C.545	2	57.361	0.578	
Sthenelais limicola	12.4	1.018	C.545	2	57.361	0.578	
Synchelidium tenuimanum	24.9	0.019	C.545	2	57.361	0.578	
Thyasira flexuosa	12.4	0.316	C.545	2	57.361	0.578	
Abra nitida	49.7	0.011	C.545	3	57.361	0.578	spat
Ampharetidae	24.9	0.013	C.545	3	57.361	0.578	juv.
Amphiura filiformis	37.3	0.661	C.545	3	57.361	0.578	
Aricidea suecica	12.4	0.009	C.545	3	57.361	0.578	
Bathyporeia elegans	24.9	0.034	C.545	3	57.361	0.578	
Brissopsis lyrifera	12.4	0.128	C.545	3	57.361	0.578	
Brissopsis lyrifera	410.3	0.050	C.545	3	57.361	0.578	juv.
Cirratulidae	49.7	0.162	C.545	3	57.361	0.578	
Diplocirrus glaucus	12.4	0.573	C.545	3	57.361	0.578	
Echinocyamus pusillus	12.4	0.002	C.545	3	57.361	0.578	
Edwardsia claparedii	62.2	0.333	C.545	3	57.361	0.578	
Eudorellopsis deformis	12.4	0.004	C.545	3	57.361	0.578	
Glycera	12.4	0.052	C.545	3	57.361	0.578	juv.
Glyphohesione klatti	12.4	0.022	C.545	3	57.361	0.578	
Gnathia oxyuraea	12.4	0.009	C.545	3	57.361	0.578	m
Goniada maculata	49.7	0.161	C.545	3	57.361	0.578	
Harmothoe	12.4	0.009	C.545	3	57.361	0.578	
Harpinia antennaria	12.4	0.043	C.545	3	57.361	0.578	
Harpinia pectinata	87.0	0.107	C.545	3	57.361	0.578	
Laonome kroyeri	12.4	0.002	C.545	3	57.361	0.578	
Nephtys	24.9	0.223	C.545	3	57.361	0.578	juv.
Nephtys caeca	12.4	0.842	C.545	3	57.361	0.578	
Notomastus latericeus	12.4	2.577	C.545	3	57.361	0.578	
Paramphinome jeffreysii	62.2	0.026	C.545	3	57.361	0.578	
Parvicardium pinnulatum	12.4	0.047	C.545	3	57.361	0.578	
Phoronis muelleri	37.3	1.075	C.545	3	57.361	0.578	with tube
Phyllodoce rosea	12.4	0.009	C.545	3	57.361	0.578	
Prionospio steenstrupi	12.4	0.007	C.545	3	57.361	0.578	
Pseudocuma simile	12.4	0.008	C.545	3	57.361	0.578	f
Rhodine	12.4	1.605	C.545	3	57.361	0.578	no head, no tail
Scoloplos armiger	24.9	0.286	C.545	3	57.361	0.578	
Spiophanes bombyx	74.6	0.085	C.545	3	57.361	0.578	
Spiophanes kroyeri	37.3	0.145	C.545	3	57.361	0.578	
Sthenelais limicola	12.4	0.054	C.545	3	57.361	0.578	
Synchelidium tenuimanum	24.9	0.009	C.545	3	57.361	0.578	
Thyasira flexuosa	12.4	1.303	C.545	3	57.361	0.578	
Amphiura chiajei	74.6	13.173	F.640	1	58.1966	0.5102	
Brissopsis lyrifera	12.4	0.360	F.640	1	58.1966	0.5102	
Calocaris macandreae	12.4	9.276	F.640	1	58.1966	0.5102	
Eudorella emarginata	12.4	0.025	F.640	1	58.1966	0.5102	

Heteromastus filiformis	99.5	0.398	F.640	1	58.1966	0.5102	
Leucothoe lilljeborgi	24.9	0.054	F.640	1	58.1966	0.5102	
Maldanidae	12.4	0.010	F.640	1	58.1966	0.5102	no head
Mendicula ferruginosa	24.9	0.019	F.640	1	58.1966	0.5102	
Nemertea	12.4	0.140	F.640	1	58.1966	0.5102	
Nephtys ciliata	12.4	0.771	F.640	1	58.1966	0.5102	
Ophiuroidea	12.4	0.002	F.640	1	58.1966	0.5102	
Parathyasira equalis	74.6	0.182	F.640	1	58.1966	0.5102	
Phoxocephalus holbolli	12.4	0.009	F.640	1	58.1966	0.5102	
Phylo norvegicus	24.9	1.773	F.640	1	58.1966	0.5102	
Pista cristata	12.4	0.124	F.640	1	58.1966	0.5102	
Rhodine gracilior	12.4	0.001	F.640	1	58.1966	0.5102	juv.
Spio	12.4	0.020	F.640	1	58.1966	0.5102	
Streblosoma bairdi	37.3	8.550	F.640	1	58.1966	0.5102	
Virgularia mirabilis	37.3	0.070	F.640	1	58.1966	0.5102	
Amphiura chiajei	37.3	6.549	F.640	2	58.1966	0.5102	
Axinulus croulinensis	24.9	0.020	F.640	2	58.1966	0.5102	
Brissopsis lyrifera	12.4	1.850	F.640	2	58.1966	0.5102	
Campylaspis rubicunda	12.4	0.007	F.640	2	58.1966	0.5102	
Ceratocephale loveni	12.4	1.080	F.640	2	58.1966	0.5102	
Gastropoda	12.4	0.014	F.640	2	58.1966	0.5102	no shell
Heteromastus filiformis	49.7	0.134	F.640	2	58.1966	0.5102	
Leucon nasica	12.4	0.033	F.640	2	58.1966	0.5102	
Montacuta substriata	12.4	0.006	F.640	2	58.1966	0.5102	
Nemertea	12.4	1.771	F.640	2	58.1966	0.5102	
Oxydromus flexuosus	12.4	0.299	F.640	2	58.1966	0.5102	
Parathyasira equalis	74.6	0.471	F.640	2	58.1966	0.5102	
Polychaeta	12.4	0.027	F.640	2	58.1966	0.5102	
Rhodine gracilior	24.9	1.614	F.640	2	58.1966	0.5102	
Sipuncula	12.4	0.046	F.640	2	58.1966	0.5102	
Streblosoma bairdi	24.9	8.069	F.640	2	58.1966	0.5102	
Terebellides shetlandica	24.9	1.020	F.640	2	58.1966	0.5102	
Thracia convexa	12.4	37.740	F.640	2	58.1966	0.5102	
Virgularia mirabilis	37.3	0.036	F.640	2	58.1966	0.5102	
Brissopsis lyrifera	12.4	6.769	F.640	3	58.1966	0.5102	
Capitella	12.4	0.064	F.640	3	58.1966	0.5102	
Cuspidaria obesa	12.4	0.115	F.640	3	58.1966	0.5102	
Gastropoda	12.4	0.024	F.640	3	58.1966	0.5102	no shell
Heteromastus filiformis	12.4	0.043	F.640	3	58.1966	0.5102	
Lumbrineris tetraura	12.4	0.351	F.640	3	58.1966	0.5102	
Mendicula ferruginosa	12.4	0.034	F.640	3	58.1966	0.5102	
Nemertea	12.4	0.309	F.640	3	58.1966	0.5102	
Nephtys	12.4	0.008	F.640	3	58.1966	0.5102	juv.
Parathyasira equalis	12.4	0.055	F.640	3	58.1966	0.5102	
Phylo norvegicus	12.4	0.944	F.640	3	58.1966	0.5102	

Pista cristata	24.9	1.629	F.640	3	58.1966	0.5102	
Rhodine gracilior	24.9	2.182	F.640	3	58.1966	0.5102	
Streblosoma bairdi	24.9	3.717	F.640	3	58.1966	0.5102	
Virgularia mirabilis	62.2	0.110	F.640	3	58.1966	0.5102	
Amphiura chiajei	24.9	0.654	F.695	1	58.7084	0.5	
Argissa hamatipes	12.4	0.005	F.695	1	58.7084	0.5	
Astarte sulcata	12.4	53.887	F.695	1	58.7084	0.5	
Brissopsis lyrifera	12.4	23.244	F.695	1	58.7084	0.5	
Cirratulidae	24.9	0.189	F.695	1	58.7084	0.5	
Crenella decussata	24.9	0.010	F.695	1	58.7084	0.5	
Diastylis lucifera	286.0	0.294	F.695	1	58.7084	0.5	
Harpinia antennaria	12.4	0.006	F.695	1	58.7084	0.5	
Harpinia pectinata	12.4	0.010	F.695	1	58.7084	0.5	
Heteromastus filiformis	24.9	0.034	F.695	1	58.7084	0.5	
Laonice sarsi	12.4	0.056	F.695	1	58.7084	0.5	
Leucon nasica	24.9	0.047	F.695	1	58.7084	0.5	
Levinsenia gracilis	24.9	0.008	F.695	1	58.7084	0.5	
Lumbrineris tetraura	12.4	0.165	F.695	1	58.7084	0.5	
Mendicula ferruginosa	12.4	0.063	F.695	1	58.7084	0.5	
Nuculana minuta	37.3	1.181	F.695	1	58.7084	0.5	
Ophiuroidea	37.3	0.005	F.695	1	58.7084	0.5	juv.
Paramphinome jeffreysii	49.7	0.045	F.695	1	58.7084	0.5	
Parathyasira equalis	124.3	0.249	F.695	1	58.7084	0.5	
Peachia cylindrica	12.4	0.070	F.695	1	58.7084	0.5	
Phylo norvegicus	12.4	0.760	F.695	1	58.7084	0.5	
Scolelepis korsuni	24.9	0.097	F.695	1	58.7084	0.5	
Spio	12.4	0.003	F.695	1	58.7084	0.5	
Spiophanes kroyeri	12.4	0.016	F.695	1	58.7084	0.5	
Streblosoma bairdi	12.4	2.553	F.695	1	58.7084	0.5	
Tellimya ferruginosa	12.4	0.131	F.695	1	58.7084	0.5	
Ampelisca gibba	12.4	0.021	F.695	2	58.7084	0.5	
Amphiura chiajei	37.3	1.681	F.695	2	58.7084	0.5	
Arctica islandica	12.4	218.820	F.695	2	58.7084	0.5	
Axinulus croulinensis	37.3	0.012	F.695	2	58.7084	0.5	
Brissopsis lyrifera	12.4	118.563	F.695	2	58.7084	0.5	
Diastylis lucifera	223.8	2.336	F.695	2	58.7084	0.5	
Eudorella emarginata	12.4	0.017	F.695	2	58.7084	0.5	
Gracilechinus acutus	24.9	55.761	F.695	2	58.7084	0.5	
Harpinia pectinata	24.9	0.036	F.695	2	58.7084	0.5	
Heteromastus filiformis	74.6	0.231	F.695	2	58.7084	0.5	
Laonice sarsi	24.9	0.160	F.695	2	58.7084	0.5	
Levinsenia gracilis	24.9	0.013	F.695	2	58.7084	0.5	
Lumbrineris tetraura	12.4	0.022	F.695	2	58.7084	0.5	
Maldanidae	24.9	0.121	F.695	2	58.7084	0.5	no tail
Mendicula ferruginosa	24.9	0.030	F.695	2	58.7084	0.5	

Montacuta substriata	24.9	0.003	F.695	2	58.7084	0.5	
Nephtys paradoxa	12.4	0.093	F.695	2	58.7084	0.5	
Notomastus latericeus	12.4	0.298	F.695	2	58.7084	0.5	no head
Nuculana minuta	12.4	0.037	F.695	2	58.7084	0.5	
Ophiuroidea	87.0	0.056	F.695	2	58.7084	0.5	juv.
Oweniidae	12.4	0.102	F.695	2	58.7084	0.5	
Paramphinome jeffreysii	37.3	0.027	F.695	2	58.7084	0.5	
Parathyasira equalis	37.3	0.209	F.695	2	58.7084	0.5	
Pista cristata	12.4	0.104	F.695	2	58.7084	0.5	
Westwoodilla caecula	12.4	0.030	F.695	2	58.7084	0.5	
Amphictene auricoma	12.4	0.353	F.695	3	58.7084	0.5	
Amphipholis squamata	24.9	0.006	F.695	3	58.7084	0.5	
Amphiura chiajei	24.9	2.371	F.695	3	58.7084	0.5	
Arctica islandica	12.4	539.390	F.695	3	58.7084	0.5	
Astarte sulcata	37.3	109.375	F.695	3	58.7084	0.5	
Axinulus croulinensis	24.9	0.038	F.695	3	58.7084	0.5	
Bivalvia	24.9	0.034	F.695	3	58.7084	0.5	sp1
Bivalvia	12.4	0.002	F.695	3	58.7084	0.5	no shell
Bradabyssa villosa	24.9	0.314	F.695	3	58.7084	0.5	
Byblis gaimardi	12.4	0.336	F.695	3	58.7084	0.5	
Campylaspis rubicunda	12.4	0.004	F.695	3	58.7084	0.5	
Diastylis lucifera	360.6	0.379	F.695	3	58.7084	0.5	
Glycera	12.4	0.011	F.695	3	58.7084	0.5	juv.
Harpinia pectinata	49.7	0.057	F.695	3	58.7084	0.5	
Heteromastus filiformis	37.3	0.062	F.695	3	58.7084	0.5	
Levinsenia gracilis	111.9	0.036	F.695	3	58.7084	0.5	
Lumbrineris tetraura	24.9	0.065	F.695	3	58.7084	0.5	
Maldanidae	12.4	0.525	F.695	3	58.7084	0.5	
Mendicula ferruginosa	12.4	0.019	F.695	3	58.7084	0.5	
Notomastus latericeus	12.4	1.112	F.695	3	58.7084	0.5	
Nuculana minuta	12.4	0.019	F.695	3	58.7084	0.5	
Nudibranchia	12.4	0.003	F.695	3	58.7084	0.5	
Oweniidae	161.6	0.289	F.695	3	58.7084	0.5	juv.
Paramphinome jeffreysii	49.7	0.047	F.695	3	58.7084	0.5	
Parathyasira equalis	24.9	0.075	F.695	3	58.7084	0.5	
Pectinaria belgica	37.3	3.578	F.695	3	58.7084	0.5	
Phaxas pellucidus	24.9	1.918	F.695	3	58.7084	0.5	
Phylo norvegicus	12.4	2.506	F.695	3	58.7084	0.5	
Rhodine gracilior	12.4	0.316	F.695	3	58.7084	0.5	
Spio	37.3	0.253	F.695	3	58.7084	0.5	
Sthenelais limicola	12.4	0.151	F.695	3	58.7084	0.5	
Timoclea ovata	12.4	0.017	F.695	3	58.7084	0.5	
Amphipoda	12.4	0.002	F.770	1	59.4166	0.4997	
Amphiura	74.6	0.152	F.770	1	59.4166	0.4997	juv.
Amphiura chiajei	87.0	1.185	F.770	1	59.4166	0.4997	

Arrhis phyllonyx	37.3	0.025	F.770	1	59.4166	0.4997	
Astacilla dilatata	111.9	0.052	F.770	1	59.4166	0.4997	
Axinulus croulinensis	99.5	0.044	F.770	1	59.4166	0.4997	
Brissopsis lyrifera	932.5	0.168	F.770	1	59.4166	0.4997	juv.
Diastylis echinata	12.4	0.016	F.770	1	59.4166	0.4997	
Diastylis lucifera	62.2	0.048	F.770	1	59.4166	0.4997	
Diplocirrus glaucus	124.3	0.101	F.770	1	59.4166	0.4997	
Eriopisa elongata	24.9	0.040	F.770	1	59.4166	0.4997	
Eudorella emarginata	87.0	0.220	F.770	1	59.4166	0.4997	
Gastropoda	124.3	0.166	F.770	1	59.4166	0.4997	no shell
Glycera	12.4	0.005	F.770	1	59.4166	0.4997	juv.
Harpinia pectinata	12.4	0.008	F.770	1	59.4166	0.4997	
Heteromastus filiformis	24.9	0.037	F.770	1	59.4166	0.4997	
Iphinoe serrata	24.9	0.033	F.770	1	59.4166	0.4997	
Laonice sarsi	12.4	0.331	F.770	1	59.4166	0.4997	
Laonome kroyeri	12.4	0.005	F.770	1	59.4166	0.4997	
Leucon nasica	286.0	0.267	F.770	1	59.4166	0.4997	
Levinsenia gracilis	111.9	0.060	F.770	1	59.4166	0.4997	
Lumbrineris fragilis	62.2	0.684	F.770	1	59.4166	0.4997	
Lumbrineris tetraura	24.9	0.014	F.770	1	59.4166	0.4997	
Macrostylis spinifera	12.4	0.003	F.770	1	59.4166	0.4997	
Maldanidae	12.4	1.730	F.770	1	59.4166	0.4997	no head, no tail
Mendicula ferruginosa	37.3	0.047	F.770	1	59.4166	0.4997	
Montacuta substriata	12.4	0.008	F.770	1	59.4166	0.4997	
Nemertea	12.4	0.060	F.770	1	59.4166	0.4997	
Nephasoma minutum	74.6	0.011	F.770	1	59.4166	0.4997	
Nephtys	37.3	0.098	F.770	1	59.4166	0.4997	juv.
Nephtys kersivalensis	12.4	2.842	F.770	1	59.4166	0.4997	
Nephtys paradoxa	12.4	0.455	F.770	1	59.4166	0.4997	
Notomastus latericeus	12.4	0.046	F.770	1	59.4166	0.4997	
Ophelina modesta	12.4	0.003	F.770	1	59.4166	0.4997	
Ophiuroidea	12.4	0.000	F.770	1	59.4166	0.4997	juv.
Orbiniidae	12.4	0.007	F.770	1	59.4166	0.4997	no head, no tail
Ostracoda	12.4	0.019	F.770	1	59.4166	0.4997	
Oxydromus flexuosus	12.4	0.006	F.770	1	59.4166	0.4997	
Paramphinome jeffreysii	907.7	1.075	F.770	1	59.4166	0.4997	
Parathyasira equalis	111.9	0.703	F.770	1	59.4166	0.4997	
Peachia cylindrica	49.7	0.155	F.770	1	59.4166	0.4997	
Pectinaria belgica	87.0	0.191	F.770	1	59.4166	0.4997	
Perioculodes longimanus	12.4	0.002	F.770	1	59.4166	0.4997	
Pholoe	12.4	0.001	F.770	1	59.4166	0.4997	
Polychaeta	12.4	0.331	F.770	1	59.4166	0.4997	
Polynoidae	12.4	0.006	F.770	1	59.4166	0.4997	
Praxillella affinis	12.4	0.149	F.770	1	59.4166	0.4997	
Spio	87.0	0.418	F.770	1	59.4166	0.4997	

Spiophanes kroyeri	37.3	0.576	F.770	1	59.4166	0.4997	
Synchelidium tenuimanum	12.4	0.006	F.770	1	59.4166	0.4997	
Typhlotanais aequiremis	12.4	0.008	F.770	1	59.4166	0.4997	
Virgularia mirabilis	12.4	0.564	F.770	1	59.4166	0.4997	
Ampharete lindstroemi	12.4	0.029	F.770	2	59.4166	0.4997	
Amphiglena mediterranea	12.4	0.009	F.770	2	59.4166	0.4997	
Amphiura chiajei	37.3	1.339	F.770	2	59.4166	0.4997	
Astacilla dilatata	62.2	0.073	F.770	2	59.4166	0.4997	
Axinulus croulinensis	124.3	0.063	F.770	2	59.4166	0.4997	
Brissopsis lyrifera	12.4	86.150	F.770	2	59.4166	0.4997	
Brissopsis lyrifera	509.8	0.004	F.770	2	59.4166	0.4997	juv.
Campylaspis rubicunda	24.9	0.014	F.770	2	59.4166	0.4997	
Diastylis lucifera	49.7	0.074	F.770	2	59.4166	0.4997	
Diplocirrus glaucus	12.4	0.032	F.770	2	59.4166	0.4997	
Eriopisa elongata	24.9	0.090	F.770	2	59.4166	0.4997	
Eudorella emarginata	37.3	0.060	F.770	2	59.4166	0.4997	
Gastropoda	87.0	0.162	F.770	2	59.4166	0.4997	no shell
Hemilamprops roseus	12.4	0.013	F.770	2	59.4166	0.4997	
Heteromastus filiformis	111.9	0.620	F.770	2	59.4166	0.4997	
Iphinoe serrata	24.9	0.036	F.770	2	59.4166	0.4997	
Laetmonice filicornis	12.4	0.012	F.770	2	59.4166	0.4997	
Laonice sarsi	12.4	0.212	F.770	2	59.4166	0.4997	
Leucon nasica	198.9	0.166	F.770	2	59.4166	0.4997	
Levinsenia gracilis	174.1	0.209	F.770	2	59.4166	0.4997	
Luidia sarsi	12.4	0.032	F.770	2	59.4166	0.4997	juv.
Lumbrineris tetraura	99.5	0.548	F.770	2	59.4166	0.4997	
Macrostylis spinifera	24.9	0.003	F.770	2	59.4166	0.4997	
Mendicula ferruginosa	12.4	0.009	F.770	2	59.4166	0.4997	
Nephtys	12.4	0.062	F.770	2	59.4166	0.4997	juv.
Nephtys paradoxa	24.9	0.642	F.770	2	59.4166	0.4997	
Notomastus latericeus	12.4	1.594	F.770	2	59.4166	0.4997	
Ophiuroidea	74.6	0.007	F.770	2	59.4166	0.4997	juv.
Oxydromus flexuosus	24.9	0.037	F.770	2	59.4166	0.4997	
Paramphinome jeffreysii	1106.6	1.377	F.770	2	59.4166	0.4997	
Parathyasira equalis	174.1	0.549	F.770	2	59.4166	0.4997	
Pectinaria belgica	74.6	0.028	F.770	2	59.4166	0.4997	
Philinidae	12.4	0.028	F.770	2	59.4166	0.4997	no shell
Phylo norvegicus	12.4	0.959	F.770	2	59.4166	0.4997	
Spio	62.2	0.120	F.770	2	59.4166	0.4997	
Spiophanes kroyeri	12.4	0.265	F.770	2	59.4166	0.4997	
Sthenelais limicola	12.4	0.026	F.770	2	59.4166	0.4997	
Terebellides shetlandica	12.4	0.317	F.770	2	59.4166	0.4997	
Vitreolina antiflexa	12.4	0.009	F.770	2	59.4166	0.4997	
Ampharete lindstroemi	12.4	0.011	F.770	3	59.4166	0.4997	
Amphiura chiajei	62.2	0.692	F.770	3	59.4166	0.4997	

Axinulus croulinensis	49.7	0.018	F.770	3	59.4166	0.4997	
Byblis gaimardi	12.4	0.049	F.770	3	59.4166	0.4997	
Diastylis lucifera	37.3	0.059	F.770	3	59.4166	0.4997	
Diplocirrus glaucus	12.4	0.010	F.770	3	59.4166	0.4997	
Eudorella emarginata	12.4	0.009	F.770	3	59.4166	0.4997	
Glycera	12.4	0.007	F.770	3	59.4166	0.4997	juv.
Heteromastus filiformis	37.3	0.143	F.770	3	59.4166	0.4997	
Leucon nasica	12.4	0.031	F.770	3	59.4166	0.4997	
Leucothoe lilljeborgi	12.4	0.008	F.770	3	59.4166	0.4997	
Levinsenia gracilis	111.9	0.134	F.770	3	59.4166	0.4997	
Lumbrineris tetraura	24.9	0.437	F.770	3	59.4166	0.4997	
Mendicula ferruginosa	12.4	0.030	F.770	3	59.4166	0.4997	
Nephasoma minutum	12.4	0.052	F.770	3	59.4166	0.4997	
Nephtys	12.4	0.025	F.770	3	59.4166	0.4997	juv.
Nephtys paradoxa	12.4	1.099	F.770	3	59.4166	0.4997	
Oxydromus flexuosus	12.4	0.203	F.770	3	59.4166	0.4997	
Paramphinome jeffreysii	360.6	0.467	F.770	3	59.4166	0.4997	
Parathyasira equalis	49.7	0.096	F.770	3	59.4166	0.4997	
Pectinaria belgica	12.4	0.003	F.770	3	59.4166	0.4997	
Phylo norvegicus	24.9	5.039	F.770	3	59.4166	0.4997	
Praxillella gracilis	12.4	0.273	F.770	3	59.4166	0.4997	
Spio	24.9	0.021	F.770	3	59.4166	0.4997	
Spiophanes kroyeri	24.9	0.102	F.770	3	59.4166	0.4997	
Streblosoma bairdi	12.4	1.707	F.770	3	59.4166	0.4997	

SUMMARY

In sediments of shelf seas, organic material of marine or terrestrial origin is recycled to free nutrients, available to processes in the water column (= mineralization). Thus, these sediments provide valuable ecosystem services in terms of nutrient cycling, eutrophication buffering and climate regulation. The intense human activities in these regions, bring sediments in an altered state, changing their nutrient recycling and storage capacity.

Sediment biogeochemistry is controlled by environmental conditions, such as the sediment type and hydrodynamics that determine deposition and retention of organic material. Likewise, benthic fauna play a pivotal role in the regulation of mineralization processes through various activities. The balance of these drivers, as well as the spatial variation they exhibit remain difficult to understand, and this hampers our capability to anticipate or predict the effects of anthropogenic activities on the workings of sediments.

This PhD thesis aimed to characterize sediment biogeochemistry in the North Sea, a heavily impacted shelf sea. Two studies, performed in a coastal area (the Belgian Part) and offshore (the Central and Northern North Sea) looked at the current biogeochemical functioning in relation to biology and environmental drivers. Models were developed based on these data and used to describe the effects of two anthropogenic activities on mineralization of organic matter (OM) in sediments: bottom trawling and offshore windfarm construction. Finally we tested in how far biological information can be used to derive biogeochemical characteristics, using a crucial faunal activity, bio-irrigation.

Fundamental work was discussed in **Chapters 2** and **3**. In **Chapter 2**, sediment characteristics and the benthic species community were determined in the Belgian Part of the North Sea (BPNS), along with the characterization of mineralization processes. Using variance partitioning, we found that anoxic mineralization processes were predominantly related to physical environmental parameters, whereas oxic mineralization processes were more strongly linked to the faunal component. Based on these data, we constructed linear models relating mineralization process rates to biotic and/or abiotic variables. Such models can increase our capacity to estimate how mineralization processes will change as a result of alterations to the biotic or abiotic environment.

An investigation of the greater North Sea was performed on a 670 km long transect spanning from Terschelling, 100 km from the coast, to the Fladen Grounds in the Northern North Sea (**Chapter 3**). Mineralization process rates were derived from on on-board core incubations and solute profiles through early diagenetic modelling. In contrast to the work performed in **Chapter 2**, mineralization processes correlated less to sediment characteristics, but were more related to water depth and bottom water concentrations of certain nutrients (NO_3^-). An offshore gradient of increased removal of nitrogen and decreased removal of phosphorus by the sediments was found.

In **Chapter 4** we describe a novel technique to quantify bioirrigation rates, the exchange of solutes between the sediment and the water column through organismal activities. Measurements from core incubations were combined with a mechanistic model of solute exchange. This improved on current measurements, by separating the bioirrigation process in an exchange rate, and a depth over which this exchange occurs. This technique was applied on field measurements collected in several sites in the Oosterscheldt estuary over the course of a year. We found similar pumping rates in subtidal and intertidal habitats, but shallower irrigation in the subtidal, linked to differences in species composition between both.

The effects of specific anthropogenic impacts (bottom trawl fisheries, offshore windfarm development) were investigated in **Chapters 5** and **6** using dynamic models of sediment diagenesis. In **Chapter 5**, bottom trawling impacts were implemented in the dynamic model as a combined erosion and mixing event. This affected the upper few centimeters of the sediment matrix, and also reduced faunal activity. By evaluating the effects of continuous trawling events on mineralization pathways over a period of 15 years, our main results were that sediments became depleted in organic carbon and nutrients, regardless of the trawling frequency they were subjected to ($1 - 5$ trawls y^{-1}). By simultaneously reducing the amount of bioturbating fauna, these effects were exacerbated. This has negative consequences for the buffering and eutrophication countering functions that sediments provide.

The effects of offshore windfarms (OWFs) on benthic processes (**Chapter 6**) were assessed by coupling our diagenetic model with an extended hydrodynamic model (in cooperation with Liege University). The redistribution of OM to sediments as a result of current and future OWF developments was calculated using a 3D hydrodynamic model of the Southern Bight of the North Sea. By coupling this output to a model of early diagenesis, changes to sedimentary carbon and nutrient cycling were assessed. This showed that sediments in OWFs can become sites of enhanced OM mineralization, where more carbon is stored in sediments as a result of an increased importance of anoxic mineralization processes. When integrated over the full area of the BPNS, alterations to C and N cycling were small, but of sufficient magnitude to be relevant in national greenhouse gas budgeting.

In the discussion (**Chapter 7**), we highlight that drivers of sediment biogeochemistry may vary strongly. Sometimes this relates to causes that are not currently observable, e.g. the historic context (e.g. biogeography, chronic bottom trawling) and connectivity of different habitats. We also point to ways in which more biology can be included in models of sediment biogeochemistry. Our novel measurement technique for bioirrigation is a first step, that may allow us to link species traits with faunal activity and biogeochemical consequences. Lastly, there remain understudied regions in the North Sea in which economic developments are being planned. In light of likely impacts, these are locations where the functioning of sediments needs to be described in order to anticipate future changes to the North Sea ecosystem.

SAMENVATTING

In sedimenten van kustzeeën wordt organisch materiaal (OM) van mariene of terrestrische oorsprong gerecycleerd tot vrije nutriënten, beschikbaar voor processen in de water kolom (= mineralisatie). Hierdoor voorzien deze sedimenten in waardevolle ecosysteemdiensten zoals nutriëntencyclering, bufferen van eutrofiëring, en klimaatregulatie. Intense menselijke activiteiten in deze regio's wijzigen de toestand van sedimenten, waardoor hun werking wijzigt.

De biogeochemie van sedimenten wordt gestuurd door omgevingsfactoren, zoals het sedimenttype en hydrodynamiek, die de depositie en retentie van OM mee bepalen. Ook bodemfauna speelt een centrale rol in de regulering van mineralisatieprocessen, door het uitoefenen van verschillende activiteiten. De balans tussen deze sturingsfactoren, en hoe deze in de ruimte variëren blijft moeilijk te achterhalen, wat het ingewikkeld maakt om de effecten van antropogene activiteiten op de werking van sedimenten te interpreteren of voorspellen.

In dit proefschrift is getracht om de biogeochemie van sedimenten te karakteriseren in een kustzee onderhevig aan intense verstoringen, de Noordzee. In twee studies, uitgevoerd dicht bij de kust (Belgisch deel), en in open zee (het centraal een noordelijke deel van de Noordzee), is de huidige biogeochemie en de koppeling met biologie en omgevingsfactoren bestudeerd. Gebaseerd op deze data zijn vervolgens modellen ontwikkeld om de effecten van twee antropogene activiteiten op de mineralisatie van OM in het sediment te beschrijven: vissen met bodemsleepnetten, en de bouw van offshore windparken. Als laatste is bestudeerd in hoeverre informatie over bodemfauna gebruikt kan worden om aspecten van biogeochemie te onderzoeken, via een cruciale activiteit van bodemfauna: bioirrigatie.

Het fundamentele werk werd besproken in **Hoofdstuk 2** en **3**. In **Hoofdstuk 2** werden sedimenteigenschappen en de soortengemeenschap van het Belgische Deel van de Noordzee onderzocht, samen met de mineralisatieprocessen. Uit de resultaten van een variantieanalyse is gebleken dat anoxische mineralisatieprocessen vooral gerelateerd waren aan fysieke omgevingsfactoren, terwijl oxische mineralisatieprocessen sterker aan de biologie gelinkt waren. Gebaseerd op deze data zijn vervolgens lineaire modellen ontwikkeld om mineralisatieprocessen aan biologische en/of abiotische factoren te relateren. Dit soort modellen verhoogt onze capaciteit om te voorspellen hoe mineralisatieprocessen veranderen als gevolg van wijzigingen aan de biotische of abiotische omgeving.

De Noordzee werd meer uitgebreid onderzocht op een transect van 670 km, dat van 100 km voor de kust van Terschelling tot de Fladen Grounds in het noordelijke deel van de Noordzee liep. Mineralisatieprocessen werden afgeleid uit metingen die aan boord werden uitgevoerd, met behulp van diagenetische modellering. In tegenstelling tot het werk van **Hoofdstuk 2**, waren de mineralisatieprocessen minder gelinkt aan het sedimenttype, maar eerder aan de waterdiepte en concentraties van bepaalde nutriënten (NO_3^-). Richting het noordelijke deel van het transect nam stikstofverwijdering vanuit sedimenten toe, terwijl fosfor eerder behouden bleef.

In **Hoofdstuk 4** werd een nieuwe techniek beschreven voor het kwantificeren van bioirrigatie, het uitwisselen van water tussen het sediment en de waterkolom door de activiteiten van bodemfauna. Hiervoor werden metingen uit core incubaties gecombineerd met een mechanistisch model van wateruitwisseling. Dit was een verbetering t.o.v. gangbare technieken omdat het bioirrigatieproces opgesplitst wordt in een pompsnelheid, en een diepte waarover dit gebeurt. Deze techniek werd toegepast op veldmetingen die verzameld werden op verschillende locaties in de Oosterschelde doorheen een jaar. We vonden gelijkaardige pompsnelheden in subtidale en intertidale habitats, maar bioirrigatie was minder diep in het subtidaal, wat wellicht gelinkt was aan verschillen in de soortencompositie.

De effecten van specifieke antropogene activiteiten (vissen met bodemsleepnetten, bouw van offshore windparken) werden onderzocht in **Hoofdstuk 5** en **6** met behulp van dynamische diagenetische modellen. In **Hoofdstuk 5** werd het effect van bodemsleepnetten in het dynamisch model geïmplementeerd als een simultane erosie en omwoeling van de bovenste sedimentlaag, die ook de activiteit van bodemfauna verminderde. Het voornaamste consistente gevolg van 15 jaar lang $1 - 5$ j^{-1} vissen met bodemsleepnetten was een drastische afname in zowel het OM gehalte, als de nutriënten in het sediment. De afname in de activiteit van fauna versnelde dit effect. Dit heeft negatieve gevolgen voor de buffercapaciteit van sedimenten, en hun rol in de regulatie van eutrofiëring.

De gevolgen van offshore windparken (OWP) op bodemprocessen (**Hoofdstuk 6**) werden onderzocht door een diagenetisch model te kopellen aan een hydrodynamisch model (in samenwerking met Université de Liège). De herverdeling van OM naar sedimenten als gevolg van de huidige en toekomstige ontwikkeling van OWP werd berekend met een 3D hydrodynamisch model van de Zuidelijke Bocht van de Noordzee. Door de output van dit model te gebruiken in een diagenetisch model, werden veranderingen in nutriëntencyclering onderzocht. Dit toonde aan dat sedimenten binnen OWP zones kunnen worden met verhoogde OM mineralisatie, waar meer koolstof in het sediment wordt opgeslagen doordat het belang van anoxische mineralisatie toeneemt. Over het gehele Belgisch Deel van de Noordzee waren de veranderingen klein, maar wel nog van mogelijk belang voor de budgettering van broeikasgassen van België.

In de discussie (**Hoofdstuk 7**) benadrukten we dat sturingsfactoren van de biogeochemie in sedimenten sterk kunnen verschillen. Soms heeft dit te maken met moeilijk te observeren factoren, zoals de historische context (biogeografie, chronische bodembevissing), of verschillen in de connectiviteit van habitats. We duidden ook hoe biologie beter in biogeochemische modellen gebruikt kan worden. Onze nieuwe meettechniek voor bioirrigatie is een eerste stap waarmee de activiteiten van fauna via soorteigenschappen gelinkt kunnen worden aan biogeochemische effecten. Als laatste is het zo dat er economische ontwikkelingen gepland worden in gebieden van de Noordzee die nog niet goed bestudeerd zijn. Gezien de mogelijke gevolgen zijn dit locaties waar het functioneren van sedimenten beschreven moet worden om te kunnen anticiperen op veranderingen in het ecosysteem van de Noordzee.

Acknowledgements

For almost five years I have been lucky enough to receive practical help, advice, and encouragement of many colleagues, family members, and friends, all of which I am very grateful for.

First of all, I'd like to thank my promotors Karline Soetaert and Ulrike Braeckman, for giving me this opportunity. Karline, you've taught me a lot about all things modelling, the workings of R, academic writing, and biogeochemistry, but if I ever know half as much as you do about any of these things I will consider myself an expert. Ulrike, your insightful comments, knowledge of all possible literature, and most of all your ever positive feedback have consistently lifted the quality of my research, as well as my spirits.

I was lucky to have been part the FaCE-It project, with colleagues who made fieldwork and meetings something to look forward to every time. Elise, Evgeny and Ninon, good luck with all your future undertakings. With this I also want to thank the coordinators of this project: Jan, Steven, and Tom.

No research without data of course, and no data of the seafloor without ships. I've always enjoyed my time on board, thanks to the captains and crews of the Pelagia, the Simon Stevin, the Belgica, and the Navicula.

I have also had two analytical labs at my disposal to have samples analysed. Jan Peene, Jan Sinke, Jurian Brasser, Peter van Breugel and Yvonne van der Maes at NIOZ must have processed about 2500 water and sediment samples for me, with the only errors caused by own mislabeling of vials. To Dirk Van Gansbeke and Bruno Vlaeminck from the chemical lab at the Sterre also a big thank you.

These last years I was able to work in two supportive environments: the NIOZ in Yerseke, and Marbiol in Ghent. In these places I am grateful for everyone who facilitates the life of (spoilt) PhD students, of which I mention a few by name here. Jan Megens: master of the coffee maker and office management, Pieter and Anton: field technicians and lab responsibles, i.e. those who actually make sure that measurements are successful, and Annick and Isolde: who know how to navigate all the confusing administrative procedures that can be thrown at you.

It's easier when you have friends in the workplace. Justin and Chiu, thanks for sharing this adventure with me, who needs a tidy office right? Carpooling to and from Antwerp also taught me a lot of things: career planning, anger management, multivariate statistics, and the art of relativizing. Sandra, Olivier, Tom, and Lorenz, thank you for this, I'm happy to have shared all these rides and discussions with you.

En dan de vrienden en familie aan het thuisfront uiteraard. Of het nu de Baggenstraat, Sciencetime, hier thuis, of ergens anders was, met veel interesse en nieuwsgierigheid hebben jullie steeds proberen begrijpen waarom ik nu juist het zand in de Noordzee moest onderzoeken. Soms wist ik het ook niet zo goed meer, maar door er tegen jullie over te vertellen kon ik de draad gewoonlijk weer terug oppikken.

Mama, bedankt om me van jongs af aan te omringen met boeken over fantasie en wetenschap, en me steeds te stimuleren om de kansen te grijpen die me gegeven werden.

Acknowledgements

Hanne, aan jou ben ik eigenlijk een apart boek verschuldigd, een hele dikke waarin ik je bedank voor bijna 5 jaar steun. Je haalt steeds het beste in mij naar boven, en onze toekomstplannen zijn mijn grootste motivatie. Met jou wordt elke onderneming een avontuur, en elke kamer een thuis.